NORTHWESTERN UNIVERSITY

EXPERIMENTAL VERIFICATION OF FLEXURAL GUIDED WAVES IN CONCRETE CYLINDRICAL PILES

A DISSERTATION

SUBMITTED TO THE GRADUATE SCHOOL
IN PARTIAL FULFILLMENT OF THE REQUIREMENTS

for the degree

DOCTOR OF PHILOSOPHY

Field of Civil Engineering

By
James J. Lynch, Jr.

EVANSTON ILLINOIS

December, 2007

UMI Number: 3284190

ProQuest Information and Learning Company
300 North Zeeb Road
P.O. Box 1346
Ann Arbor, MI 48106-1346

ABSTRACT

EXPERIMENTAL VERIFICATION OF FLEXURAL GUIDED WAVES IN CONCRETE CYLINDRICAL PILES

James J. Lynch, Jr.

Two experimental methods have been developed to induce flexural waves in concrete piles for which a portion of the shaft is accessible, and the test results were compared to theoretical solutions of flexural guided wave propagation. The pile response is measured and the results are analyzed to compute the group velocity – frequency relationship or the phase velocity – frequency relationship. The experimentally-determined velocity – frequency values are compared to theoretical values of velocity for the flexural branches. Three prototype piles were evaluated nondestructively by both methods. One prototype pile was evaluated under traction-free and embedded conditions, and the other piles were evaluated under embedded conditions.

One of the test methods uses an impact on the side of the pile by a modal hammer to induce a low frequency flexural wave. The other test method uses a piezoelectric shaker mounted to the side of the pile to induce a high frequency wave. The pile response is measured with triaxial accelerometers mounted to the side of the pile. The piezoelectric shaker is computer-controlled to generate a force of specified amplitude, frequency, and duration.

The impact tests are analyzed to determine the phase velocity – frequency relationship, and to determine the group velocity and its frequency. The phase velocity is computed from the resonant frequencies identified on the acceleration spectrum of the recorded pile response. The group velocity is computed from the travel distance of the flexural wave and the return time between successive returns of the flexural wave. The frequency of the group is identified as the peak with the largest magnitude on the acceleration spectrum. The impact test generates waves that fall on the F(1,1) branch.

The controlled frequency results are analyzed to determine the group velocity and its frequency. One new prototype pile was tested under traction-free and embedded conditions and two existing prototype piles were tested under embedded conditions. The results were analyzed in the time domain and the frequency domain because the waves are dispersive. The analysis of the test results indicate that modes were excited on the F(1,1), F(1,2), F(1,3), and F(1,5) branches.

Acknowledgements

I would like to thank all of the faculty and staff at Northwestern Univeristy and the professionals in private practice who assisted me in the course of my research. First and foremost, I would like to thank my advisor, Dr. Richard J. Finno for his support and guidance during the course of my studies and research at Northwestern Univeristy, as well as Drs. Charles H. Dowding and Raymond J. Krizek, my other committee members, for their comments and suggestions on this project. I would also like to thank Dr. Surendra Shah for his input and assistance regarding NDE of concrete. I also recognize the contributions of the late Dr. Allen G. Davis to this project, to the field of NDE of deep foundations, and to the field of NDE of concrete.

Thanks to my colleagues at Northwestern Univeristy who assisted me in my research, especially Hsiao-Chou Chao and Helsin Wang who worked directly with me on other aspects of this project.

Finally, I would like to thank my family and friends who supported and encouraged me before coming to Northwestern Univeristy, during my time at Northwestern Univeristy, and as I enter the next phase of my career. I would especially like to thank my parents, James J. and the late Donna M. Lynch, my sisters, Michelle and Heather, and their families. I would also like to thank the staff at Testing Engineers and Consultants, Inc., my former employer, and the faculty, staff, and students at the University of Detroit Mercy, my current employer.

List of Symbols

a	Pile radius
A	Unknown constant
c_B	Bar wave velocity (m/s)
c_G	Group velocity (m/s)
$c_{G(ND)}$	Nondimensional group velocity
c_L	Compression wave velocity (m/s)
c_P	Phase velocity (m/s)
$c_{P(ND)}$	Nondimensional phase velocity
c_T	Shear wave velocity (m/s)
c_{Tc}	Shear wave velocity (m/s) of concrete
c_{Ts}	Shear wave velocity (m/s) of soil
f	Frequency (Hz) or Function of r associated with scalar potential
f_c	Cutoff frequency (Hz)
f_n	Frequency (Hz) at harmonic number n
f_{UMF}	Frequency (Hz) or universal mode
g	Normalizing constant
G_C	Shear modulus of concrete
G_S	Shear modulus of soil
H	Hankel function

h	Vector function of r associated with vector potential
i	Imaginary number
J	Bessel function
K	Bessel function
L	Pile length or travel distance
m	Shear modulus ratio
n	Index
r	Radius Radial coordinate direction or Density ratio
u	Vector of displacements
u_1	Amplitude at point 1
u_2	Amplitude at point 2
x_{ij}	Entries in coefficient matrix
z	Position along pile or Longitudinal coordinate direction
α	Substitution
β	Substitution
ξ	Wavenumber
ξ_a	Nondimensional wavenumber
θ	Angle or Angular coordinate direction
Θ	Scalar potential
ω	Frequency (rad/sec)

λ	Lame's constant or Wavelength
Δt	Time difference
ΔL	Spacing
ρ	Density
ρ_c	Density of concrete
ρ_s	Density of soil
ν	Poisson's ratio
ν_c	Poisson's ratio of concrete
ν_s	Poisson's ratio of soil
σ	Standard deviation
σ_{ij}	Component of stress tensor
Ω	Nondimensional frequency
Ω_c	Nondimensional cutoff frequency
$\boldsymbol{\Phi}$	Scalar potential
$\boldsymbol{\Psi}$	Vector potential
$\boldsymbol{\nabla}$	Divergence operator (on vector functions) Gradient operator (on scalar functions)

Table of Contents

List of Tables

List of Figures

Chapter 1: Introduction

The defects that occur in deep foundations can affect their load-carrying capacity and, if the load-carrying capacity is sufficiently reduced, the structure may need to be repaired or replaced. The defects that occur in drilled shafts typically occur during construction, e.g., necking and caving, or in service from excessive lateral loads. The defects that occur in driven precast concrete piles can occur during installation from overstressing the pile or in service from excessive lateral load or corrosion of the reinforcing steel that results in cracks in the concrete. Nondestructive testing can be used as part of the evaluation of a deep foundation containing suspected defects. If defects are identified, then the foundation is analyzed to determine its load-carrying capacity.

Conventional methods for NDE of deep foundations are based on the propagation of low frequency stress waves, and the results are analyzed by one-dimensional theory. The low frequencies imply that the stress waves have long wavelengths and, as such, they are limited in their ability to identify small defects or to accurately identify the location of defects. The use of high frequency energies can improve this situation. Higher frequencies imply shorter wavelengths, theoretically allowing identification of smaller defects or more accurate identification of the location of defects; however, the assumptions of one-dimensional wave propagation are no longer valid when frequencies

become relatively high (Hannifah, 1999). Another limitation of common methods for NDE of deep foundations occurs when the top of the structure to be evaluated is not accessible due to the presence of an intervening structure, as in the case of a cap or grade beam over piles or drilled shafts. If the intervening structure is contiguous with the deep foundation element, some energy from the stress wave passes through the intervening structure and into the pile, but not all of it (Finno and Gassman, 1998). If the structure is not contiguous with the deep foundation element, for example, in the case of a precast concrete beam or slab placed on the structure, the energy from the stress wave that passes into the portion of the structure to be evaluated is negligible.

Two new methods are presented in this thesis to overcome some limitations of the existing methods for NDE of deep foundations, provided at least part of the side of the structure is accessible. One method uses a hammer impact on the side of the pile to generate a low frequency flexural stress wave (the lateral impact method). Another method uses a piezoelectric shaker mounted to the side of the structure to generate a higher frequency stress wave than the impact method (the controlled frequency method). In both cases, the responses of the structure are measured with accelerometers mounted to the side of the pile.

The lateral impact method is a modification of the flexural wave identification (FWI) method (Finno et al. 2001), which has been used to evaluate a full-size structure in service but has not been compared to theoretical results. Other methods using a lateral impact to generate a

stress wave have been proposed as well, but they have not been compared to theoretical results either.

The results of both the lateral impact and controlled frequency methods must be analyzed by three-dimensional theory, as the waves are dispersive. The governing equation for three-dimensional guided wave propagation within an embedded cylinder was derived and solved for the symmetric (longitudinal) branches by Hannifah (1999). The controlled frequency method has been verified for the longitudinal modes (Chao 2002) but not for the flexural branches. The governing equation proposed by Hannifah (1998) has subsequently been solved for the flexural branches by Wang (2004), thus allowing theoretical verification of the lateral impact and controlled frequency methods.

The work presented herein focuses on the verification of flexural waves induced by lateral impacts and flexural controlled frequency method. Test results are presented for prototype piles under traction-free and embedded conditions, and those test results are compared to numerical solutions of the governing equation.

This dissertation encompasses eight chapters. Chapter 2 summarizes the conventional sonic echo (SE) and impulse response (IR) methods for NDE of deep foundations, presents details of the structures by which the lateral impact method and flexural controlled frequency method are to be verified, presents the governing equation for three dimensional wave

propagation within a cylindrical waveguide and solutions of the flexural modes. The assumptions, test equipment, analytical procedures and limitations of the SE and IR methods are presented. The prototype piles at the national geotechnical experimentation site (NGES) at Northwestern Univeristy, in Evanston, Illinois, have been evaluated nondestructively by existing methods and new methods. The new methods are based on three-dimensional wave propagation in a waveguide.

The governing equation for three-dimensional wave propagation within a cylinder was numerically solved by Wang (2004). The frequency equation was developed from the boundary / compatibility conditions, and solved in nondimensional form with the concrete properties and soil properties. The nondimensional frequency – nondimensional wavenumber results from the solution of the frequency equation are converted to nondimensional group velocity – nondimensional frequency relationships and nondimensional phase velocity – nondimensional frequency relationships to allow comparison with test results for NDE of deep foundations. The equations for computing the displacement profiles and the equation for normalizing the displacements are presented along with an example of the displacement profile at one value of nondimensional frequency. The displacement values are used to help identify the reflection of a wave comprised of modes on more than one branch. The displacements are functions of the unknown constants determined from the solution of the frequency equation, but they are non-unique, i.e., any scalar multiple of the unknown constants provides a solution. The displacements are normalized by the power flux.

Chapter 3 describes the test procedures, test equipment, and analytical procedures used in the experimental program. In the lateral impact method, a stress wave is generated with an impact from a modal hammer. In the flexural controlled frequency method, the stress wave is generated with a computer-controlled piezoelectric shaker. In both cases, the responses are measured with accelerometers. For both the impact method and flexural controlled frequency method, the input and response are recorded with a virtual oscilloscope coded in the LabVIEW ™ programming language. For the flexural controlled frequency method, the vibrations imparted by the shaker are controlled with a virtual pulse generator coded in the LabVIEW ™ programming language. The generator sends a digital pulse to a digital to analog converter that sends the signal to a power amplifier and step-up transformer that drive the piezoelectric shaker. The measured results are filtered to remove portions of the signal for which the frequency content lies outside the frequency range of the input. The time-varying frequency content of the flexural controlled frequency method is analyzed by the joint time frequency analysis (JTFA) method, and the time ordinate of the JTFA array is converted to velocity in the joint velocity frequency analysis (JVFA) method.

Chapter 4 describes the prototype pile (herein designated C355-2430) evaluated by the impact and shaker methods. The mix design and construction practices are summarized and the results of standard concrete compressive strength and density tests are presented. The results of the dynamic characterization of the concrete are presented, including the Poisson's ratio from impact tests performed on the test cylinders from which the compressive strength was

determined, the bar wave velocity, shear wave velocity, and Poisson's ratio of the prototype pile. The dynamic properties of the prototype pile were determined from SE results analyzed by one-dimensional and three-dimensional theory. The frequency equation presented in Chapter 2 was solved numerically for with the properties of the new prototype pile and the properties for traction-free conditions. A procedure to convert from nondimensional form to dimensional form is presented and applied to the nondimensional data from the new prototype pile.

Chapter 5 presents the results of lateral impact tests performed on the new prototype pile under traction-free conditions and embedded conditions, as well as the results of lateral impact tests performed on two existing prototype piles under embedded conditions to verify the guided wave theory presented in Chapter 2. A flexural wave was induced by a hammer impact to the side of the pile, and the response was measured with a triaxial accelerometer. The accelerometer was mounted to the side of the pile and tests were performed with impacts oriented at 90-degree intervals around the pile. The results were analyzed to determine the phase velocity – frequency relationship and the group velocity – frequency relationship. For the tests performed on prototype pile C355-2430 under traction-free conditions, the experimental results were compared to the numerically-determined phase velocity – frequency relationships and numerically-determined group velocity – frequency relationships, presented in Chapter 4. The tests performed on prototype pile C355-2430 under traction-free conditions were repeated for three piles under embedded conditions. Numerically-determined group velocity – frequency curves and phase velocity – frequency curves were developed for each embedded pile by solving the

frequency equation presented in Chapter 2 in nondimensional form for the pile – soil system, and converting to dimensional form by the procedures presented in Chapter 4.

Chapter 6 presents the flexural controlled frequency results for prototype pile C355-2430 under traction-free conditions to verify the guided wave theory presented in Chapter 2 for the higher frequencies generated in the flexural controlled frequency tests. The tests were performed at three different frequencies and the results were analyzed to determine the group velocity. The experimentally-determined group velocity was compared to the numerically-determined group velocity – frequency curves for various flexural branches to identify the branch on which the stress wave was propagating. The numerically-determined group velocity – frequency curves were presented in Chapter 4.

Chapter 7 presents the flexural controlled frequency results for prototype pile C355-2430 and two existing prototype piles embedded in the very loose sand at the NGES at Northwestern Univeristy to verify the guided wave theory presented in Chapter 2. The new prototype pile was evaluated at three different frequencies and the existing prototype piles were evaluated at two different frequencies. The results were analyzed to determine the group velocity, and the experimentally-determined group velocity was compared to the numerically-determined group velocity.

Chapter 8 summarizes the work presented in this thesis and presents conclusions regarding the applicability of guided wave theory for NDE of deep foundations, and provides recommended test procedures and analytical methods.

Chapter 2: Technical Background

Experimental results for NDE of deep foundations can be analyzed by either one-dimensional or three-dimensional theories. One-dimensional theory assumes that the propagation velocity of the longitudinal wave does not depend on frequency, which allows easy interpretation of the test results. The low frequency stress waves generated in the one-dimensional tests have long wavelengths, which limits the size of the defect that can be identified and the accuracy with which defects can be identified. Higher frequency tests can generate stress waves with shorter wavelengths than the one-dimensional tests, but the assumptions of one-dimensional wave propagation will no longer be valid (Hannifah, 1999).

A summary and the limitations of the one-dimensional methods along with a method for analyzing three-dimensional wave propagation in a cylindrical waveguide are presented herein. The method for analyzing three-dimensional wave propagation includes formulation of the governing equation and a method for numerically solving that governing equation. Based on this numerical solution, results will be presented for the flexural branches (Wang, 2004) in terms of nondimensional frequency – nondimensional wavenumber relationships, and these results will be used to compute nondimensional frequency – nondimensional group velocity relationships, nondimensional frequency –

nondimensional phase velocity relationships. Waves propagating in a cylindrical waveguide that is embedded in soil attenuate as energy leaks into the surrounding soil, and as such, the method

of computing attenuation will be presented. As an example of the mode shape calculations, the displacement profiles will be presented for one value of nondimensional frequency.

2.1 Experimental Methods for Nondestructive Evaluation of Deep Foundations

Various methods are potentially available for nondestructive evaluation of deep foundations. Each method uses equipment to generate a dynamic force and to record the response of the deep foundation, and each method requires certain assumptions about the type of wave and the behavior of the material so that the data can be analyzed.

The traditional methods for nondestructive evaluation of deep foundations are the sonic echo (SE) and impulse response method. Two methods that have been developed to overcome some of the limitations of the traditional methods are the controlled frequency method and the lateral impact method. Each method, including the newer methods require assumptions about the type of wave and have limitations to their applicability for nondestructive evaluation of deep foundations.

2.1.1 One-Dimensional Methods for Nondestructive Evaluation of Deep Foundations

In methods for NDE of deep foundations based on one-dimensional wave propagation, one measures the response of a structure due to an impact that induces a low-frequency, long-

wavelength stress waves. The key properties of the one-dimensional methods are that the wavelengths are large compared to the size of the structure, the mode shapes are uniform across the section, the propagation velocity is constant, and attenuation occurs as energy leaks into the surrounding soil.

In the one-dimensional methods, a stress wave is generated by a hammer impact and the response is measured with an accelerometer or geophone (velocity transducer). The propagating stress wave reflects off changes in mechanical impedance, and the returning stress wave causes an increase in measured response when it passes the transducer. Reflections are identified as increases in response of the acceleration – time history (or velocity – time history) or as peaks in the acceleration spectrum (or velocity spectrum). The commonly-used one-dimensional methods for NDE of deep foundations are the sonic echo (SE) and impulse-response (IR) methods. The SE and IR methods are well-understood and have been in use for over 30 years (Davis, 1975; Finno & Gassman, 1998; Gassman & Finno, 2000).

Figure 2-1 schematically shows the equipment setup for a sonic echo or impulse response test.

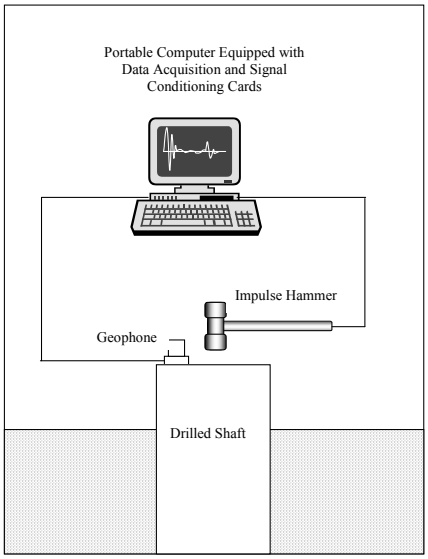

Figure 2-1: Schematic of impulse – response test configuration
(After Finno & Gassman, 1998)

The hammer strikes the top of the structure and the geophone is mounted atop the structure. Measuring the response at a geophone atop the structure precludes direct measurement of the propagation velocity unless the exact location of a reflection source is known. As such, the propagation velocity must be estimated based on the assumed properties of the concrete, typically from published data or operator experience.

The hammer impact produces a stress wave with a range of frequencies, with a maximum frequency equal to the inverse of the duration of the impact (Sansalone and Carino, 1986). The maximum frequency is defined as the highest frequency with significant energy.

2.1.2 Controlled Frequency Method

The controlled frequency method (Chao, 2002) was developed to induce a higher-frequency stress wave than can be generated in a conventional impact test, and, theoretically, identify smaller defects than can be identified in conventional impact tests or to identify the location of defects more accurately than can be identified in conventional impact tests. The stress wave is generated with a piezoelectric shaker mounted to the top of the deep foundation and the response is measured with one or more accelerometers mounted to the top of the deep foundation. The results are interpreted to identify the first pass of the wave and one or more returns of the reflected wave and to compute the group velocity from the travel distance and travel time.

2.1.3 Lateral Impact Methods

Deep foundation-supported structures in which the top of the deep foundation is not accessible but part of its side is accessible could potentially be evaluated nondestructively with a dynamic force applied to the side of a deep foundation. A lateral impact applied to the side of a deep foundation will transmit energy directly into the deep foundation to be evaluated and transducers mounted to the side of the deep foundation will measure the response of the deep foundation. Two test procedures, the flexural wave identification (FWI) method (Finno et al., 2001) and the bending wave method (Holt et al., 1994; Holt, 1995; Hughes et al, 2000) have

been developed to impart energy into a deep foundation by a lateral impact, measure the response of the structure, and identify returns of reflected waves from the measured response.

In the FWI method, the response is measured with two accelerometers mounted along the side of the pile. The group velocity is computed from the spacing between the accelerometers and time lag between first arrivals at the two accelerometers. Reflections are identified from the first pass and return to both accelerometers.

In the bending wave method as proposed by Holt et al. (1994, 1995), the response is measured with two accelerometers, and the data are interpreted by isolating one phase of the wave, i.e., one frequency, and identifying the return of the reflected phase. Jalinoos et al. (1995) evaluated structures by several methods, including the sonic echo and bending wave methods, and contrasted the results.

In the bending wave method proposed by Hughes et al. (2000), one evaluation of a deep foundation consisted of multiple tests in which the response was measured with one accelerometer, but the accelerometer was placed in a different position for each test. The results were analyzed to determine the natural frequencies and mode shapes at each position, and were compared to theoretical values computed by structural dynamics software.

2.2 Test Site at Northwestern University

The experimental procedures to be presented in this document have been verified on prototype piles in the laboratory, and on prototype piles installed in soil. The prototype piles and one set of full-sized drilled shafts have been constructed at the National Geotechnical Experimentation Site (NGES) at Northwestern University.

The general site stratigraphy is granular fill placed on soft to medium clay over hard silt. The hard silt is underlain by dolomite bedrock (Finno & Gassman, 1998). The drilled shafts are 0.61 to 0.91 meters in diameter and are 12.19 to 27.48 meters long and two of the drilled shafts have planned defect (Finno & Gassman, 1998). The prototype piles are 254 to 305 mm in diameter, and are 2.22 to 2.40 mm long (Chao, 2002).

The site has been characterized with conventional soil borings and CPT soundings. As part of the conventional soil borings, in-situ tests were performed and Shelby tube samples were collected. The in-situ tests performed as part of the soil borings included standard penetration tests (SPT), field vane tests, Menard Pressuremeter tests (PMT), dilatometer tests (DMT), and cross-hole seismic tests. The Shelby tube samples were collected for laboratory testing, including moisture content, bulk density, Atterberg Limits, consolidation properties, unconfined compressive strength, and traxial compressive strength (drained and undrained). See Osborn (1997) for details of the investigation and a summary of the experimental results. The dynamic properties of the soil of primary interest to this work are summarized in Table 2-1.

Table 2-1: Summary of dynamic properties of soil at NGES, Northwestern University

Soil Layer	Terminal Depth (m)[1]	P-Wave Velocity (m/s) [1]	Shear Wave Velocity (m/s)	
			Measured[1]	Best Fit[2]
Sand Fill Partially Saturated	4	1500	180	100 to 115
Sand Fill Saturated	9	1500	180	110 to 115
Soft to Medium Clay	19	2000	200	170 to 200
Clay with Gravel	20	2000	200	320
Soft to Medium Clay	21	2000	200	220
Glacial Till	27	2000 to 2500	300 to 500	375

Notes: 1 Osborn, 1997
2 Finno & Gassman, 1998

The soil layers and terminal depth of each layer were identified during the geotechnical investigation performed between 1987 and 1996 (Osborn, 1997). The propagation velocity values were determined through cross-hole seismic tests performed by STS Consultants, Ltd., in December, 1994. The best-fit value of shear wave velocity was determined from the simulation of impulse – response results as the value that provided the best qualitative fit between the simulated results and measured results. Construction of the drilled shafts disturbed the soil in the area of the shaft, and caused the differences in the shear wave velocity.

Five drilled shafts have been constructed at the NGES and three prototype piles have been embedded into the soil, as shown on Figure 2-2. The drilled shafts are 0.61 m to 0.91 m in diameter and 12.19 m to 27.59 m long. The prototype piles are 254 mm to 355 mm in diameter and 2.22 m to 2.43 m long. The group B prototype piles were installed by Chao (2002). The group C pile was installed a part of this work.

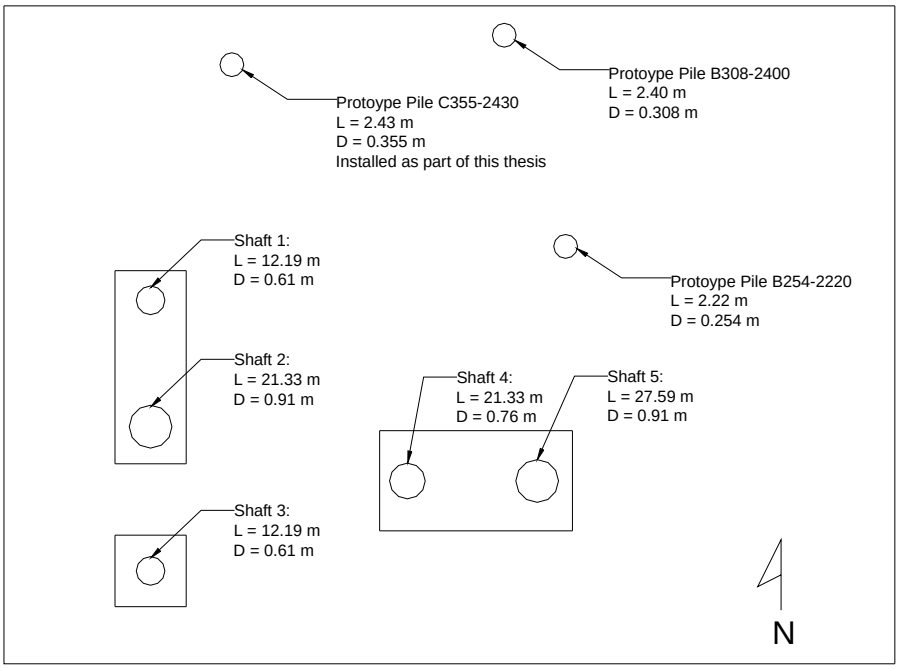

Figure 2-2: Locations of drilled pier caps and prototype piles at NGES Northwestern University

Shafts 1 and 2 have planned defects. The drilled shafts at the NGES at Northwestern University were evaluated nondestructively before and after construction of the caps to identify limits of the IR method, such as the cutoff frequencies caused by the presence of intervening structures (Gassman & Finno, 2000), and resolution as a function of length to diameter ratio (L/D) and soil type (Finno & Gassman, 1998). Improvements to the IR method such as the multiple geophone approach (Gassman & Finno, 1999) were also applied to the drilled shafts. Details of the evaluation of the drilled shafts and caps will not be provided; rather, they are shown on Figure 2-2 to provide a reference from which to locate the prototype piles.

The Group B prototype piles shown on Figure 2-2 have been evaluated nondestructively by Chao (2002) to determine their dynamic properties and to nondestructively evaluate deep foundations with symmetric three-dimensional waves in a wave guide. The flexural wave evaluation of B and C prototype piles will be presented in Chapter 5 for the impact tests and in Chapter 7 for the controlled frequency method. The relevant properties of the embedded Group B prototype piles are presented in Table 2-2.

Table 2-2: Group B Prototype Piles – Dynamic Properties
(After Chao, 2002)

Pile Id	Bar Wave Velocity (m/s)[1]	Shear Wave Velocity (m/s)[2]	Poisson's Ratio[3]
B254-2220	4150	2730	0.18
B308-2400	4050	2720	0.28

Notes: 1: Determined from Sonic Echo Test
2: Determined from Sonic Echo Test and UMF Identification (Chao, 2002)
3: Calculated from Bar Wave Velocity and Shear Wave Velocity

The prototype piles are founded entirely in the sand fill above the water table. The shear wave velocity was assumed to be 100 m/s, which is the lower end of the best-fit values presented in Table 2-1. The assumed bulk density was assumed to be 1600 kg/m^3, which is within the expected range for loose, granular soil.

2.3 Three-dimensional Methods for NDE of Deep Foundation Elements

The maximum frequency generated by a hammer impact and, consequently, the shortest wavelength, is a function of the mass and stiffness of the hammer and the stiffness of the surface struck by the hammer. If a stress wave with shorter wavelengths is required, a vibration generating system that can generate higher frequencies than a hammer impact is needed. At higher frequencies, the assumptions of one-dimensional wave propagation will no longer be valid because the wave propagation is dispersive, i.e., the propagation velocity depends on the frequency (Chao, 2002). The following sections summarize the theoretical background needed to analyze the results of higher frequency tests. The results to be presented will also allow theoretical verification of the lateral impact methods described in Section 2.3.

For the traction-free case, guided wave theory has been experimentally verified on metal rods (Zemanek, 1971), metal wires (Nicholson et al., 1989), and hollow metal tubes (Nicholson et al., 1991). For the embedded case, guided wave theory has been experimentally verified for the longitudinal modes (Chao, 2002).

2.3.1 Guided Wave Propagation

Three-dimensional wave propagation within a cylindrical waveguide could follow the path shown on Figure 2-3. Because the waveguide is cylindrical, the equations will be formulated in cylindrical coordinates.

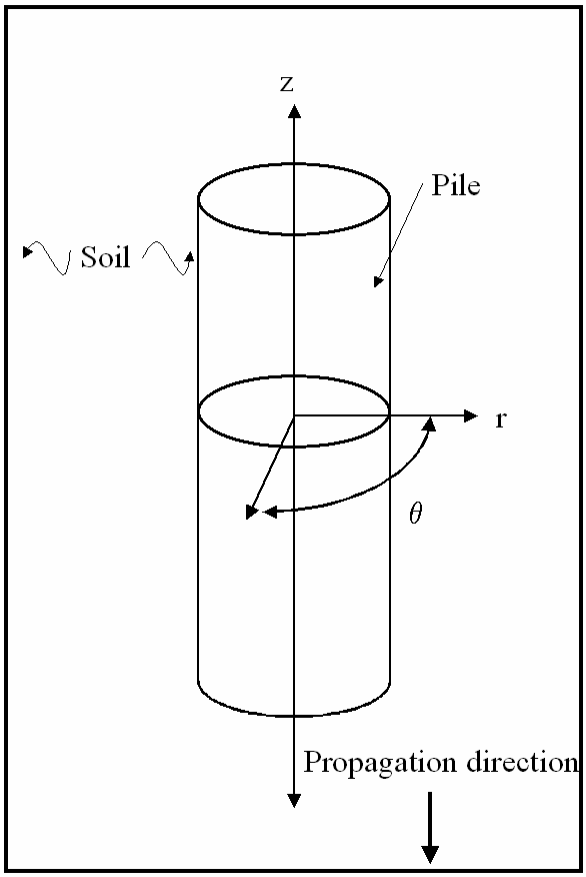

Figure 2-3: Guided wave propagation and coordinate directions for cylindrical waveguide

The propagation of waves in a three-dimensional medium is governed by the three-dimensional wave equation. In scalar form, this equation is

$$(\lambda + \mu)u_{j,ji} + \mu u_{i,jj} = \rho \ddot{u}_i \qquad (2\text{-}1)$$

and in vector form one can write

$$(\lambda + \mu)\nabla\nabla \bullet \mathbf{u} + \mu\nabla^2\mathbf{u} = \rho\ddot{\mathbf{u}} \qquad (2\text{-}2)$$

where **u** is the vector of coordinates of displacements, ρ is the density of the concrete, and λ and μ are Lame's constant and the shear modulus, respectively. The del operator, ∇, is the derivative with respect to the spatial coordinates, and the two dots over **u** on the right hand side of equation 2-2 represents the second derivative with respect to time.

The displacement field, **u**, can each be expressed by the Helmholtz equation, in which **u** is the sum of the gradient of a scalar potential, Φ, and the curl of a vector potential, **Ψ** (Graff, 1975).

$$\mathbf{u} = \nabla \mathbf{\Phi} + \nabla \times \Psi, \quad \nabla \bullet \Psi = 0 \tag{2-3}$$

The Helmholtz equation allows compression, or dilation, waves to be separated from the shear, or distortion, waves, i.e., the wave equation is decoupled. If the body force is zero, the decoupled equations become

$$\nabla^2 \Phi = \frac{1}{c_L^2} \frac{\partial^2 \Phi}{\partial t^2}, \quad \nabla^2 \Psi = \frac{1}{c_T^2} \frac{\partial^2 \Psi}{\partial t^2} \tag{2-4}$$

where c_L is the compression wave velocity and c_T is the shear wave velocity.

The scalar potential and each component of the vector potential defined in equation 2-3, and expressed in the cylindrical coordinates shown on Figure 2-3, are the product of individual functions of r, θ, and z

$$\Phi = f(r)\Theta_\phi(\theta)e^{i(\omega t - \xi z)} \tag{2-5}$$

$$\Psi_r = h_r(r)\Theta_r(\theta)e^{i(\omega t-\xi z)} \tag{2-6}$$

$$\Psi_\theta = h_\theta(r)\Theta_\theta(\theta)e^{i(\omega t-\xi z)} \tag{2-7}$$

$$\Psi_z = h_z(r)\Theta_z(\theta)e^{i(\omega t-\xi z)} \tag{2-8}$$

The solution of equation 2-1 requires the definition of a domain, the application of boundary conditions, and the application of initial conditions. The assumed geometry is a circular pile of finite diameter and infinite length for the traction-free case or a circular pile of finite diameter and infinite length embedded in a soil medium of infinite extent for the embedded case.

The three displacement components, expressed in cylindrical coordinates are

$$u_r = \frac{\partial \Phi_j}{\partial r} + \frac{1}{r}\frac{\partial \Psi_{z_j}}{\partial \theta} - \frac{\partial \Psi_{\theta_j}}{\partial z} \tag{2-9}$$

$$u_\theta = \frac{1}{r}\frac{\partial \Phi_j}{\partial r} + \frac{\partial \Psi_{r_j}}{\partial \theta} + \frac{\partial \Psi_{z_j}}{\partial z} \tag{2-10}$$

$$u_z = \frac{\partial \Phi_j}{\partial z} + \frac{1}{r}\frac{\partial \left(r\Psi_{\theta_j}\right)}{\partial r} - \frac{1}{r}\frac{\partial \Psi_{r_j}}{\partial \theta} \tag{2-11}$$

and six stress components in cylindrical coordinates are

$$\sigma_{rr_j} = \lambda_j \nabla^2 \Phi_j + 2\mu_j \frac{\partial u_{r_j}}{\partial r} \tag{2-12}$$

$$\sigma_{\theta\theta_j} = \lambda_j \nabla^2 \Phi_j + 2\mu_j \left(\frac{u_{r_j}}{r} + \frac{1}{r}\frac{\partial u_{\theta_j}}{\partial \theta} \right) \tag{2-13}$$

$$\sigma_{rr_j} = \lambda_j \nabla^2 \Phi_j + 2\mu_j \frac{\partial u_{z_j}}{\partial z} \tag{2-14}$$

$$\sigma_{r\theta_j} = \mu_j \left(\frac{1}{r} \frac{\partial u_{r_j}}{\partial \theta} + \frac{\partial u_{\theta_j}}{\partial r} - \frac{u_{\theta_j}}{r} \right) \tag{2-15}$$

$$\sigma_{rz_j} = \mu_j \left(\frac{\partial u_{r_j}}{\partial z} + \frac{\partial u_{z_j}}{\partial r} \right) \tag{2-16}$$

$$\sigma_{\theta z_j} = \mu_j \left(\frac{\partial u_{\theta_j}}{\partial z} + \frac{1}{r} \frac{\partial u_{z_j}}{\partial \theta} \right) \tag{2-17}$$

where *j* can equal *c* for the displacement and stress components in the concrete or *s* for the displacement and stress components in the soil.

The solution of the governing equation in cylindrical coordinates produces Bessel functions in the pile and Hankel functions (Bessel functions of the third kind) in the soil. The argument of each Bessel Function or Hankel Function is a function of the frequency, ω, and wavenumber, ξ, which are simplified as

$$\alpha_j = \sqrt{\frac{\omega^2}{c_{L_k}^2} - \xi^2} \tag{2-18}$$

$$\beta_j = \sqrt{\frac{\omega^2}{c_{T_k}^2} - \xi^2} \tag{2-19}$$

The term *j* can be *p* for propagation of waves in the pile or *s* for propagation of waves in the soil. When *j* is set to *p*, *k* is *c* for the properties of the concrete of which the pile is constructed, and when *j* is set to *s*, *k* is *s* for the soil.

The boundary conditions require that the stresses are zero at the outer edge of the pile for the traction-free case (Graff, 1975), or that the stresses in the pile equal the stresses in the soil at the soil-pile interface and that the displacements in the pile equal the displacements in the soil at the soil-pile interface (Hannifah, 1999). The initial conditions considered herein are that the input is harmonic.

The governing equation with application of the boundary conditions and initial conditions produces a system of 3 equations with 3 unknowns or 6 equations with 6 unknowns for the traction-free and embedded conditions, respectively. In both case, the right hand side of the equations is zero, i.e., the system is homogeneous.

2.3.2 Matrix – Vector Formulation of Governing Equation for Embedded Conditions

The set of six equations with six unknowns produced by application of the compatibility conditions for an embedded cylinder can be rewritten as a coefficient matrix multiplied by a vector of unknown constants defined by

$$\begin{bmatrix} x_{11} & x_{12} & x_{13} & x_{14} & x_{15} & x_{16} \\ x_{21} & x_{22} & x_{23} & x_{24} & x_{25} & x_{26} \\ x_{31} & x_{32} & x_{33} & x_{34} & x_{35} & x_{36} \\ x_{41} & x_{42} & x_{43} & x_{44} & x_{45} & x_{46} \\ x_{51} & x_{52} & x_{53} & x_{54} & x_{55} & x_{56} \\ x_{61} & x_{62} & x_{63} & x_{64} & x_{65} & x_{66} \end{bmatrix} \begin{Bmatrix} A_{1_p} \\ A_{4_p} \\ A_{6_p} \\ A_{1_s} \\ A_{4_p} \\ A_{4_s} \end{Bmatrix} = \begin{Bmatrix} 0 \\ 0 \\ 0 \\ 0 \\ 0 \\ 0 \end{Bmatrix} \qquad (2\text{-}20)$$

The matrix of entries x_{ij} of equation 2-20 is called the coefficient matrix and the vector of A_{1p}, A_{4p}, A_{6p}, A_{1s}, A_{4s}, and A_{6s} are called the vector of unknown constants in which *p* corresponds to the pile and *s* corresponds to the soil.

The terms in x_{ij} are

$$
\begin{aligned}
x_{11} &= |\alpha_p| J_n'(|\alpha_p| a) \\
x_{12} &= -\xi J_n'(|\beta_p| a) \\
x_{13} &= \frac{n}{a} J_n(|\beta_p| a) \\
x_{14} &= -|\alpha_p| H_n'^{(2)}(|\alpha_s| a) \\
x_{15} &= \xi H_n'^{(2)}(|\beta_s| a) \\
x_{16} &= -\frac{n}{a} H_n^{(2)}(|\beta_s| a)
\end{aligned}
\qquad (2\text{-}21)
$$

$$
\begin{aligned}
x_{21} &= -\frac{n}{a} J_n(|\alpha_p| a) \\
x_{22} &= \frac{n\xi}{|\beta_p| a} J_n(|\beta_p| a) \\
x_{23} &= -|\beta_p| J_n'(|\beta_p| a) \\
x_{24} &= \frac{n}{a} H_n^{(2)}(|\alpha_s| a) \\
x_{25} &= \frac{n\xi}{|\beta_s| a} H_n^{(2)}(|\beta_s| a) \\
x_{26} &= |\beta_s| H_n'^{(2)}(|\beta_s| a)
\end{aligned}
\qquad (2\text{-}22)
$$

$$
\begin{aligned}
x_{31} &= -i\xi J_n\left(|\alpha_p|a\right) \\
x_{32} &= -i|\beta_p| J_n\left(|\beta_p|a\right) \\
x_{33} &= 0 \\
x_{34} &= i\xi H_n^{(2)}\left(|\alpha_s|a\right) \\
x_{35} &= i|\beta_s| H_n^{(2)}\left(|\beta_s|a\right) \\
x_{36} &= 0
\end{aligned}
\tag{2-23}
$$

$$
\begin{aligned}
x_{41} &= \left[-\lambda_c\left(|\alpha_p|^2+\xi^2\right)+2\mu_p\left(\frac{n^2}{a^2}-|\alpha_p|^2\right)\right]J_n\left(|\alpha_p|a\right)- \\
&\quad 2\mu_p\frac{|\alpha_p|}{a}J_n'\left(|\alpha_p|a\right) \\
x_{42} &= 2\mu_c\xi\left[\left(|\beta_p|-\frac{n^2}{|\beta_p|a^2}\right)\right]J_n\left(|\beta_p|a\right)+\frac{1}{r}J_n'\left(|\beta_p|a\right) \\
x_{43} &= 2\mu_c\frac{n}{a}\left[|\beta_p|J_n'\left(|\beta_p|a\right)-\frac{1}{r}J_n\left(|\beta_p|a\right)\right] \\
x_{44} &= -\left[-\lambda_s\left(|\alpha_s|^2+\xi^2\right)+2\mu_s\left(\frac{n^2}{a^2}-|\alpha_s|^2\right)\right]H_n^{(2)}\left(|\alpha_s|a\right)- \\
&\quad 2\mu_s\frac{|\alpha_s|}{a}H_n'^{(2)}\left(|\alpha_s|a\right) \\
x_{45} &= -2\mu_s\xi\left[\left(|\beta_s|-\frac{n^2}{|\beta_s|a^2}\right)\right]H_n^{(2)}\left(|\beta_s|a\right)+\frac{1}{r}H_n'^{(2)}\left(|\beta_s|a\right) \\
x_{46} &= -2\mu_s\frac{n}{a}\left[|\beta_s|H_n'^{(2)}\left(|\beta_s|a\right)-\frac{1}{r}H_n^{(2)}\left(|\beta_s|a\right)\right]
\end{aligned}
\tag{2-24}
$$

$$
\begin{aligned}
x_{51} &= \mu_c \frac{2n}{a}\left[\frac{1}{a} J_n\left(|\alpha_p| a\right) - |\alpha_p| J_n'\left(|\alpha_p| a\right)\right] \\
x_{52} &= \mu_c \frac{2n\xi}{a}\left[J_n'\left(|\beta_p| a\right) - \frac{1}{|\beta_p| a} J_n\left(|\beta_p| a\right)\right] \\
x_{53} &= \mu_c\left[\frac{2|\beta_p|}{a} J_n'\left(|\beta_p| a\right) - \left(\frac{2n^2}{a^2} - |\beta_p|^2\right) J_n\left(|\beta_p| a\right)\right] \\
x_{54} &= -\mu_s \frac{2n}{a}\left[\frac{1}{a} H_n^{(2)}\left(|\alpha_s| a\right) - |\alpha_s| H_n'^{(2)}\left(|\alpha_s| a\right)\right] \\
x_{55} &= -\mu_s \frac{2n\xi}{a}\left[H_n'^{(2)}\left(|\beta_s| a\right) - \frac{1}{|\beta_s| a} H_n^{(2)}\left(|\beta_s| a\right)\right] \\
x_{56} &= -\mu_s\left[\frac{2|\beta_s|}{a} H_n'^{(2)}\left(|\beta_s| a\right) - \left(\frac{2n^2}{a^2} - |\beta_s|^2\right) H_n^{(2)}\left(|\beta_s| a\right)\right]
\end{aligned}
\qquad (2\text{-}25)
$$

$$
\begin{aligned}
x_{61} &= -i\mu_c 2\xi|\alpha_p| J_n'\left(|\alpha_p| a\right) \\
x_{62} &= i\mu_c\left(\xi^2 - |\beta_p|^2\right) J_n'\left(|\beta_p| a\right) \\
x_{63} &= -i\mu_c \frac{n\xi}{a} J_n\left(|\beta_p| a\right) \\
x_{64} &= i\mu_s 2\xi|\alpha_s| H_n'^{(2)}\left(|\alpha_s| a\right) \\
x_{65} &= -i\mu_s\left(\xi^2 - |\beta_s|^2\right) H_n'^{(2)}\left(|\beta_s| a\right) \\
x_{66} &= i\mu_s \frac{n\xi}{a} H_n^{(2)}\left(|\beta_s| a\right)
\end{aligned}
\qquad (2\text{-}26)
$$

where *J* and *H* are Bessel and Hankel functions, respectively, *n* is the order of the Bessel or Hankel function, *i* is the square root of –1, *a* is the pile radius, ξ is the complex-valued wavenumber, μ_c is the shear modulus of the concrete, μ_s is the shear modulus of the soil, λ_c is Lame's constant for the concrete, λ_s is Lame's constant for the soil, and α and β are terms defined by equations 2-18 and 2-19 with *p* representing the pile and *s* representing the soil. The terms α and β are complex-valued and the terms $|\alpha|$ and $|\beta|$ represent the magnitude of the complex number.

In general, the system defined by equation 2-20 has only a trivial solution, i.e., all entries in the vector of unknown constants are zero. When the determinant of the coefficient matrix is zero, a nontrivial solution will exist, but the solution will not be unique. A non-unique solution implies that one vector of nonzero constants multiplied by the coefficient matrix will produce a null vector, but so will any scalar multiple of the vector of nonzero constants.

Several mathematical statements of the existence of a nontrivial solution can be made, including

- The determinant of the matrix is zero (Hanifah 1999),
- the rank of the matrix is less than the size of the matrix (O'Neill 1991),
- one of the eigenvalues is zero,
- one of the equations is a linear combination of the other equations, and,
- all entries of one row or column of the matrix are zero

The equation produced by expanding the determinant of the coefficient matrix is called the frequency equation, and it relates the real-valued frequency to the complex-valued wavenumber. The solution method is any method that finds values of frequency and wavenumber that satisfy the conditions under which a nontrivial solution exists.

The coefficient matrix contains longitudinal, flexural, and torsional modes of wave propagation. If the frequency equation is to be solved and applied to a pile, the desired mode of wave propagation must be extracted from the equation.

2.3.3 Conversion of the Frequency Equation to Nondimensional Form

The concrete properties needed to solve the frequency equation are the Poisson's ratio, density and shear modulus; the same properties are needed for the soil to consider the embedded pile case. A nondimensional form of the governing equation is created from the ratios of the soil properties to the concrete properties.

The density ratio, r, is expressed in terms of the concrete density, ρ_c, and the soil density, ρ_s, as

$$r = \frac{\rho_c}{\rho_s} \tag{2-27}$$

and the shear modulus ratio, *m*, is expressed in terms of the concrete shear modulus, G_c, and the soil shear modulus, G_s, as

$$m = \frac{G_c}{G_s} = \frac{c_{Tc}^2 \rho_c}{c_{Ts}^2 \rho_s} \tag{2-28}$$

By converting to nondimensional form, the nondimensional frequency, Ω, and nondimensional wavenumber, ξ_a, are expressed as

$$\Omega = \frac{\omega a}{c_T} \tag{2-29}$$

$$\xi_a = \xi a \tag{2-30}$$

where, ω is the frequency, ξ, is the wavenumber, c_T is the shear wave velocity, and *a* is the pile radius.

Once the frequency equation has been solved in nondimensional form, the results can be applied to any size concrete pile in terms of the six required parameters.

The following sections summarize a method developed by Wang (2004) for solving the frequency equation in nondimensional form and subsequently computing nondimensional phase velocities, nondimensional group velocities, nondimensional attenuation, and mode shapes for the flexural branches and modes.

2.3.4 Numerical Solution of Frequency Equation for Flexural Branches

The first flexural branches, i.e., F(1,m), are defined by setting *n* of equations 2-21 through 2-26 equal to one. Because the frequency equation is the product of Bessel Functions and Hankel functions, each of which has an infinite number of solutions, the frequency equation will have an infinite number of solutions. Furthermore, the argument of each Bessel or Hankel function is α or β as defined in equations 2-18 and 2-19, and there are infinite combinations of nondimensional frequency and nondimensional wavenumber that will produce the same value of α or β. The solution to the frequency equation then takes the form of an infinite number of branches with an infinite number of points on each branch.

For a given wavenumber, the lowest frequency that solves the frequency equation belongs to the first branch, the second lowest frequency belongs to the second branch, etc.

The approach to numerically solve the frequency equation is

1. Determine the concrete properties (G_c, ν_c and ρ_c) and the soil properties (G_c, ν_c and ρ_c).
2. Compute the density ratio, r, and the modulus ratio, m, by equations 2-27 and 2-28, respectively.
3. Select the branch of interest.
4. Select the range of nondimensional frequency values or nondimensional wavenumber values to be included in the solution.
5. Find one point on the branch within the desired range of values.
   a. Select the nondimensional frequency and real part of the nondimensional wavenumber corresponding to the existing solutions for the traction-free case.
   b. The imaginary part must be determined uniquely for the embedded case. Finding the first value may require some experimentation.
6. Find an approximate value for the next point.
7. Iterate over values of nondimensional frequency and nondimensional wavenumber, in the vicinity of the approximate value computed in Step 6, until the value of the frequency equation is less than a prescribed tolerance.
8. Repeat Steps 6 and 7 to find the remaining points on the branch within the desired range of values.

The initial value of nondimensional frequency depends on the branch under consideration, and was generally selected near the cutoff frequency for the branch. Dispersion curves for both the longitudinal branches and flexural branches with traction-free conditions have been published by Zemanek (1971). For the traction-free case, the wavenumber will be single-valued, i.e., real or imaginary; for the embedded case, the wavenumber will be complex-valued. The real part of the numerically-determined wavenumber for the traction free case (Zemanek, 1971) is close enough to the numerically-determined real part of the wavenumber for the embedded case (Hannifah, 1999; and Wang, 2004) that the nondimensional frequency – nondimensional wavenumber results of the traction-free case can be used as the first guess for nondimensional frequency – real part of the nondimensional wavenumber for the embedded case.

The algorithm for solving the frequency equation has been coded into Maple ®. The program is called "Flexural_Disperion.mws" and included in the appendix. The code has been written so that the shear modulus of the concrete and soil are expressed in terms of the shear modulus ratio, and the density for the concrete and soil are expressed in terms of the density ratio.

When solving the entire dispersion curve, one must provide the initial value of nondimensional frequency and a range of values for the real and imaginary parts of the nondimensional wavenumber in which the solution lies. The initial value of nondimensional frequency and nondimensional wavenumber are taken from existing solutions for the traction-free case. The exact value of the wavenumber is found with the "fsolve" function preprogrammed with Maple ®. The values of the next point are estimated by the following algorithm

1. Define a step size
2. Compute the derivative of the frequency equation with respect to the nondimensional frequency.
3. Evaluate the derivative computed in Steps 2 at the current point.
4. Compute the approximate value of the next nondimensional frequency as the step size multiplied by the value from Step 3.
5. Compute the derivative of the frequency equation with respect to the nondimensional wavenumber.
6. Evaluate the derivative computed in Step 5 at the current point.
7. Compute the approximate value of the next nondimensional wavenumber as the step size multiplied by the value from Step 6.

If the step size is too large, the next point may be too far from the solution for the algorithm to find the point or, worse yet, it could fall close enough to the solution on another branch that the point identified belongs to the wrong branch. A smaller step size will produce a

smoother curve and decrease the chances of not finding a solution or of jumping to another branch, but the analysis will require more time.

When solving for one point on a branch, for example, when computing the mode shape for one nondimensional frequency, the following procedure is used

1. Select the nondimensional frequency at which the frequency equation is to be solved.
2. Determine the range of values in which the real part of the nondimensional wavenumber and imaginary part of the nondimensional wavenumber will fall. These values can be determined from the data for the entire dispersion curve.
3. Find the exact value of nondimensional wavenumber by running the portion of "Flexural_Dispersion.mws" designed to find the first point on a dispersion curve using the value of nondimensional frequency from Step 1 and the values of nondimensional wavenumber from Step 2.

These procedures are applicable to any branch. The experimental verification to be presented later in this document will focus on the flexural branches. The following sections will present numerical results for the flexural branches.

2.3.5 Nondimensional Frequency – Nondimensional Wavenumber Results

Once the frequency equation has been formulated in matrix-vector form, the portions of the overall equation pertaining to the flexural modes can be isolated and the frequency equation can be solved by the procedure presented in Section 2.3.4. The frequency equation has been solved for several branches with a range of concrete properties and soil properties (Wang, 2004). As an example, the results of the numerical solution for the first five flexural branches is presented on Figure 2-4.

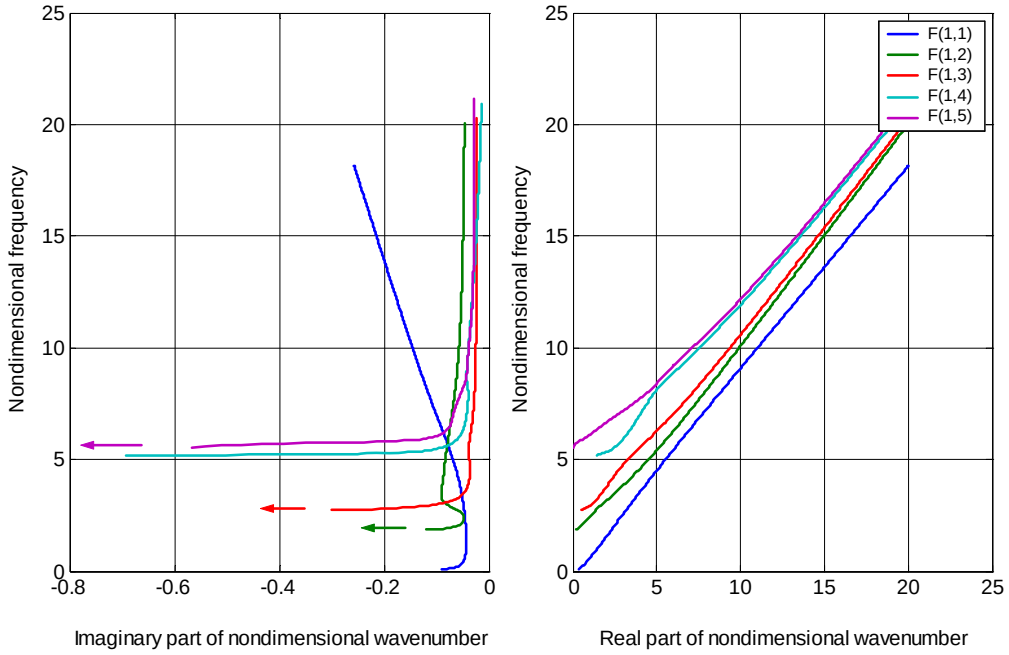

Figure 2-4: Nondimensional frequency and nondimensional wavenumber for first five flexural branches of concrete with $\nu_c = 0.20$

For three-dimensional guided wave propagation in traction-free cylinders, the real part of the nondimensional wavenumber goes to zero for all branches presented (Achenbach, 1975; Nicholson et al. 1989). For the embedded case, the numerically-computed real part of the F(1,1) branch passes through the origin so the cutoff frequency occurs when the real part of the wavenumber goes to zero. The real part of the numerically-computed wavenumber does not go to zero for the F(1,2) branch, the F(1,3) branch and the F(1,4) branch, rather the imaginary part of the numerically-computed wavenumber becomes very large and the curves shown in Figure 2-4 approach the cutoff frequencies. The real part of the numerically-computed wavenumber for the F(1,5) branch goes to zero as the curve shown in Figure 2-4 approaches the cutoff frequency.

Wang (2004) performed parametric studies for the flexural branches to determine the effects of variations in concrete and soil properties on the dispersion curves. The real part of the nondimensional wavenumber is unaffected by variations in the shear modulus ratio or density ratio, but the imaginary part of the nondimensional wavenumber is affected by variations in these quantities. As the shear modulus ratio increases and the soil becomes softer, the imaginary part of the nondimensional wavenumber decreases. The limit would be an infinite shear modulus ratio, which corresponds to traction-free conditions.

2.3.6 Determination of Nondimensional Phase and Group Velocity Values

The propagation of three-dimensional waves within a waveguide will be dispersive, i.e., each phase moves with its own distinct velocity. As the waves propagate, alternating constructive and destructive interference will cause the appearance of the waves traveling in groups. The nondimensional phase velocity, $c_{p(ND)}$, is defined in terms of the nondimensional frequency and nondimensional wavenumber:

$$c_{p(ND)} = \frac{\Omega}{\mathrm{Re}(\xi_a)} \qquad (2\text{-}31)$$

In the above equation, Ω is the nondimensional frequency, and $\mathrm{Re}(\xi_a)$ is the real part of the nondimensional wavenumber determined from the procedures presented in Section 2.3.4.

The phase velocity for the first five flexural branches has been computed from the data presented on Figure 2-4, and the results are shown on Figure 2-5.

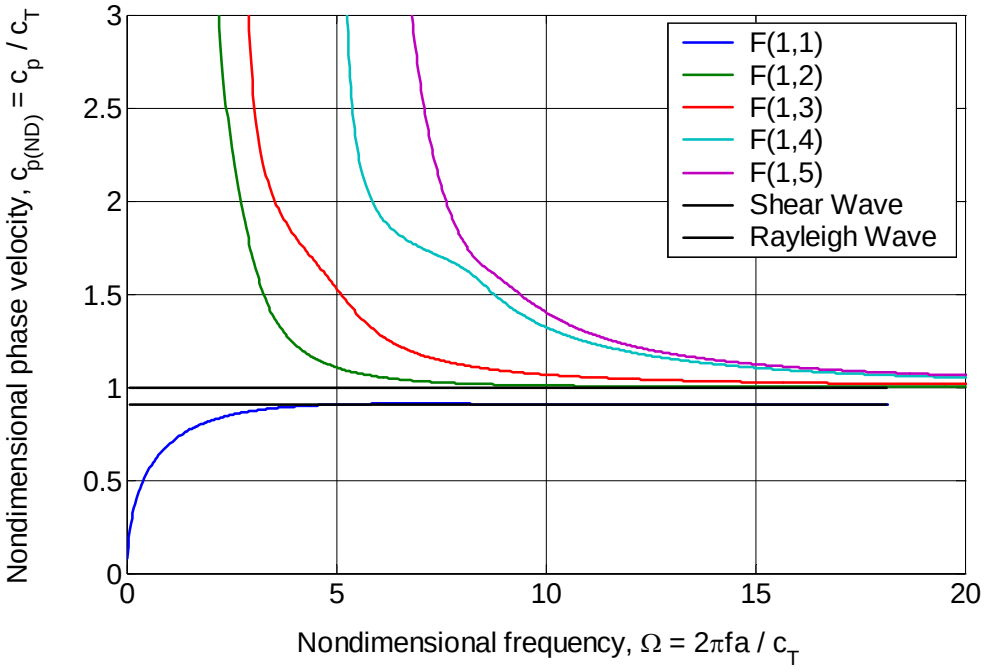

Figure 2-5: Nondimesnional phase velocity – nondimensional frequency relationship for first five flexural branches of concrete with $\nu_c = 0.20$

The nondimensional phase velocity for the F(1,1) branch approaches zero as the nondimensional frequency approaches zero and becomes asymptotic to the Rayleigh wave velocity at high values of nondimensional frequency. For concrete with a Poisson's ratio of 0.20, the ratio of the Rayleigh wave velocity to the shear wave velocity is 0.908. The nondimensional phase velocity values for the remaining branches approach infinity as the nondimensional frequency approaches their respective cutoff frequency values, and the nondimensional phase velocity values become asymptotic to the shear wave velocity at high values of nondimensional frequency.

The nondimensional group velocity, $c_{g(ND)}$, is the derivative of the nondimensional frequency, Ω, with respect to the real part of the nondimensional wavenumber, $\mathrm{Re}(\xi_a)$, and is calculated by

$$c_{g(ND)} = \frac{\partial \Omega}{\partial \mathrm{Re}(\xi_a)} \qquad (2\text{-}32)$$

The nondimensional group velocity – nondimensional frequency curves for the first five flexural branches are shown on Figure 2-6.

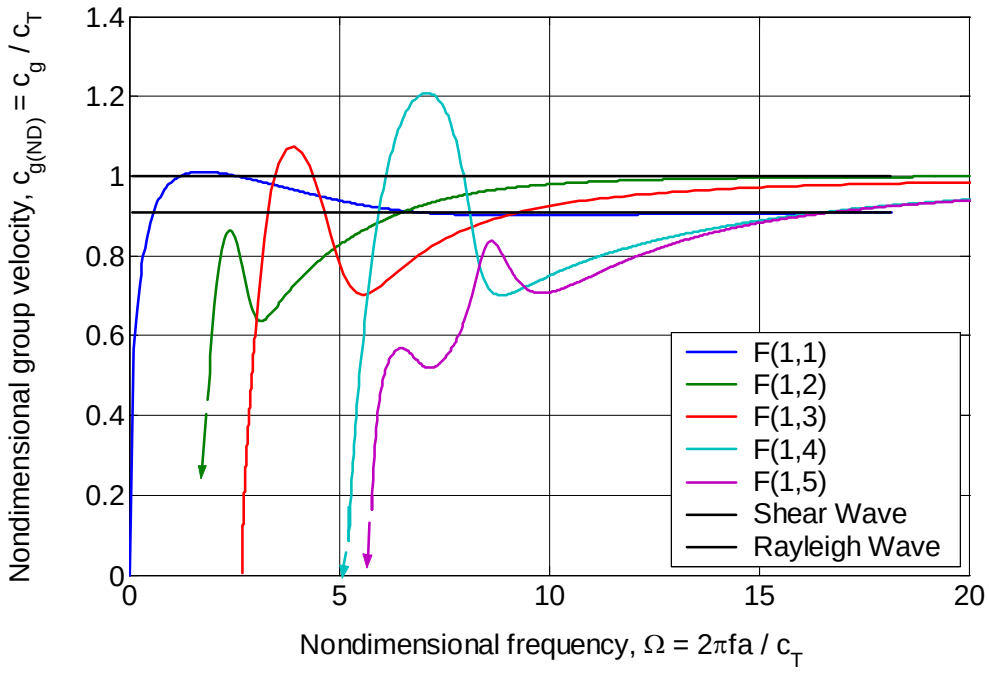

Figure 2-6: Nondimensional group velocity – nondimensional frequency relationship for first five flexural branches of concrete with $\nu_c = 0.20$

For the F(1,1) branch, the nondimensional group velocity is zero at zero nondimensional frequency, reaches a maximum value that is slightly higher than the shear wave velocity, then

decreases as the nondimensional frequency increases. At high values of nondimensional frequency, the nondimensional group velocity for the F(1,1) branch approaches 0.908, which is the Rayleigh wave velocity value., For the remaining branches, the nondimensional group velocities approach zero at their respective cutoff frequencies and approach the shear wave velocity at high values of nondimensional frequency. The arrows are drawn on the nondimensional group velocity – nondimensional frequency curves for the F(1,2), F(1,4) and F(1,5) branches to indicate that the nondimensional group velocity would go to zero if the nondimensional wavenumber had gone to zero, as shown on Figure 2-4. For the branches in which the real part of the nondimensional wavenumber goes to zero, i.e., the F(1,1) branch and F(1,3) branch, the group velocities are zero at the respective nondimensional cutoff frequencies. Between the two sets of asymptotic nondimensional group velocity values, the nondimensional group velocity – nondimensional frequency relationship for each branch has a local maximum and minimum, except for the F(1,5) branch which has two local maxima and two local minima.

2.3.7 Attenuation

The frequency equation was solved based on the assumption that energy leaks from the pile into the surrounding soil but no energy loss occurs through damping and scattering within the pile itself, i.e., geometrical attenuation is the only source of energy loss considered in this analysis (Hanifah, 1999). Diffraction and scattering are neglected because the wavelengths for the frequencies typically employed in these tests are large compared to the size of the aggregate (Hannifah, 1999).

The procedure for determining attenuation based on energy loss into the surrounding soil was proposed by Hanifah (1999), and will be used in this analysis.

The attenuation coefficient, ϑ, may be expressed in nepers as

$$\vartheta = \log_e\left(\frac{u_2}{u_1}\right) \quad nepers \tag{2-33}$$

where u_1 and u_2 are the amplitude of the signals at the two different positions, and (u_2/u_1) is the amplitude ratio. Equation 2-33 is expressed in natural log but can be converted to common log if the right hand side of equation 2-33 is multiplied by 2.3062.

$$\vartheta = 2.3062\log\left(\frac{u_2}{u_1}\right) \quad nepers \tag{2-34}$$

The nondimensional attenuation is the imaginary part of the wavenumber as determined through numerical solution of the frequency equation.

$$\vartheta = \mathrm{Im}(\xi)\Delta L \quad nepers \tag{2-35}$$

where ΔL is the travel distance of the wave.

The attenuation coefficient in terms of nondimensional wavenumber is

$$\vartheta = -\mathrm{Im}(\xi_a)\frac{\Delta L}{a} \quad nepers \tag{2-36}$$

By equating the right hand side of equation 2-18 with the right hand side of equation 2-20, the amplitude ratio can be expressed in terms of the nondimensional wavenumber, travel distance, and pile radius

$$2.3062 \log\left(\frac{u_2}{u_1}\right) = -\mathrm{Im}(\xi_a)\frac{\Delta L}{a} \qquad (2\text{-}37)$$

Rearranging equation 2-37 and taking the antilog of the rearranged equation, one can compute the expected attenuation for a pile

$$\frac{u_2}{u_1} = 10^{-\left(\frac{\mathrm{Im}(\xi_a)\Delta L}{2.3062a}\right)} \qquad (2\text{-}38)$$

Equation 2-36 can be used to predict the amplitude ratio of an incident and reflected wave measured at the same location or the same pass of the wave measured at two different locations.

2.3.8 Normalized Displacement Profiles

The radial, longitudinal and tangential displacement profiles are illustrated for the response of a pile at 0-degree and 90-degree orientations to the impact location for all modes active at one frequency. The sign convention for the relationship between the impact location and the measurement location is presented on Figure 2-7.

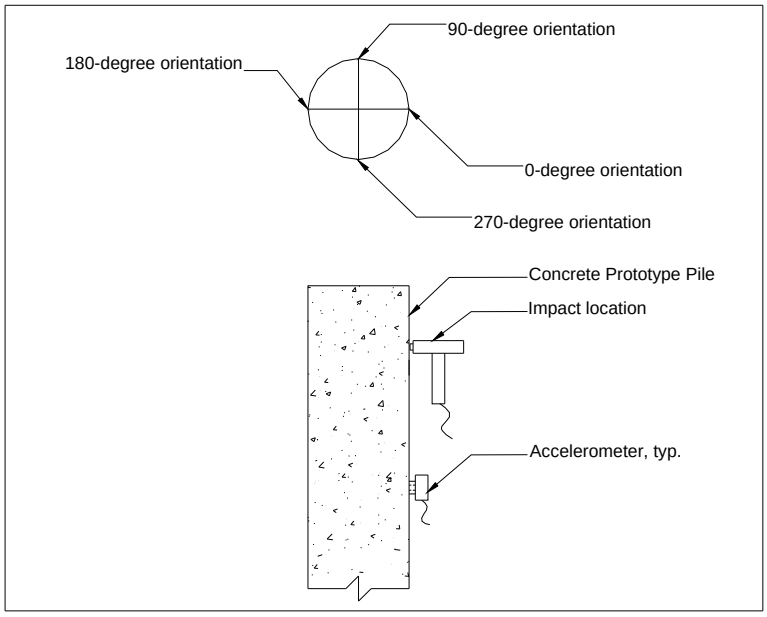

Figure 2-7: Orientation convention for input and response for flexural modes

Figure 2-7 shows that 0-degree orientation is defined such that the accelerometer is mounted on the pile directly below where the force is applied. The remaining angles are defined with counterclockwise as positive. When the stress wave passes a point, the displacement vector, **u**, will have radial, longitudinal and tangential components. The displacement components were computed by Hannifah (1998).

$$u_r = \left(\frac{1}{a}\right)\left\{\begin{array}{l} \dfrac{A_{1p}}{R}[\alpha a J_0(\alpha a R) - J_1(\alpha a R)] \\ -\dfrac{A_{4p}}{R}\left(\dfrac{\xi a}{\beta a}\right)[\beta a J_0(\beta a R) - J_1(\beta a R)] \\ +\dfrac{A_{6p}}{R} J_1(\beta a R) \end{array}\right\} \cos(n\theta) e^{i(\xi z - \omega t)} \qquad (2\text{-}39)$$

$$u_z = \frac{i}{a}[-A_{1p}\xi a J_0(\alpha a R) - A_{4p}\beta a J_0(\beta a R)]\cos(n\theta) e^{i(\xi z - \omega t)} \qquad (2\text{-}40)$$

$$u_\theta = \left(\frac{1}{a}\right)\begin{Bmatrix} -\frac{A_{1p}}{R}J_1(\alpha aR) + \frac{A_{4p}}{R}\left(\frac{\xi a}{\beta a}\right)J_1(\beta aR) \\ -\frac{A_{6p}}{R}[\beta a J_0(\beta aR) - J_1(\beta aR)] \end{Bmatrix} \sin(n\theta)e^{i(\xi z - \omega t)} \qquad (2\text{-}41)$$

where A_{1p}, A_{4p}, and A_{6p} are the unknown coefficients as discussed in Section 2.3.1. The terms α, β ω, and ξ were defined in Section 2.3.1. The displacement values were divided by the radius, a, so that the domain is the normalized radius [0, 1]. The angle, θ, refers to the angle between the impact and the measurement location, as shown on Figure 2-7. Equations 2-39 through 2-41 apply to the displacements for any mode on any branch. The longitudinal modes are solved by setting *n* equal to zero (Hannifah, 1998); the flexural modes are solved by setting *n* equal to or greater than one (Wang, 2004).

For a given mode the displacement is computed numerically by determining the unknown constants and substituting the unknown constants into the expression for displacement. The unknown constants represent non-unique solutions to the system of equations, which precludes direct comparison of displacements for different modes. The computed displacements are rescaled by the power flux distribution to allow direct comparison of different modes (Hanifah, 1999). The equation for normalizing constant has a different form for the flexural modes than for the longitudinal modes. The normalizing constant for modes on the antisymmetric branches is (Wang, 2004)

$$g = \sqrt{\left| \frac{4\xi_i a}{\pi\Omega C_s a \times \left[\mathrm{Im}\left[\sigma_{rr}(r) \times u_r^*(r)\right] + \mathrm{Im}\left[\sigma_{\theta r}(r) \times u_\theta^*(r)\right] + \mathrm{Im}\left[\sigma_{zr}(r) \times u_z^*(r)\right]\right] n_r \Big|_{r=+a}} \right|}. \qquad (2\text{-}42)$$

where Ω is the nondimensional frequency, ξ_i is the imaginary part of the nondimensional wavenumber. The terms u_r, u_θ, and u_z, are the displacements defined by equations 2-9 through 2-11, and the * indicates that they are the complex conjugate of the displacements. The terms σ_{rr}, $\sigma_{\theta r}$, and σ_{zr} are the stress components defined by equations 2-12 through 2-17.

2.3.8.1 Determination of Unknown Constants

The wave equation presented in Section 2.3.1 with application of the boundary conditions and initial conditions can be expressed in matrix-vector form (Wang, 2004) that represents compatibility at the pile-soil interface. The entries in the vector are the coefficients for the displacement components and stress components in the concrete and soil.

One method of determining the unknown constant is to assign an arbitrary value to one constant and to solve for the other constants in terms of the constant with the assigned value. Another method is to find the null space vector through numerical analysis software, as was done herein. The two methods provide the same vector, although the values of the constants may be scaled with respect to each other.

Once the frequency and wavenumber have been selected and the unknown constants have been determined for that ordered pair, the mode shapes can be determined.

The mode shapes were calculated in either Maple ® (Wang, 2004) or Matlab ®, the codes for both programs are presented in the appendix. For either program, the input values are nondimensional frequency, nondimensional wavenumber, soil properties, and concrete properties. The coefficient matrix is evaluated with the input properties and the nullspace vector is calculated. The input values are selected to solve the frequency equation, i.e., the matrix should be singular. Given the precision of the arithmetic and the tolerance on the nullspace algorithms in the software, the program may not be able to find a nullspace vector. To circumvent the problems associated with the matrix not being close enough to singular, the following procedure was implemented to ensure that a nullspace vector exists

1. Evaluate the coefficient matrix with the input values.
2. Decompose the evaluated matrix from Step 1 into an upper and lower triangular matrix.
3. Set the bottom right-hand entry of the upper triangular matrix from Step 2 to zero.
4. Find the nullspace vector of the modified matrix from Step 3

The upper triangular matrix has the same determinant as the original matrix. Setting the bottom right-hand entry of the upper triangular matrix produces a row of all zeros, which ensures that the matrix has a nullspace vector. The original matrix multiplied by the nullspace vector of the modified matrix produces a vector that is very close to zero.

2.3.8.2 Displacement Profile Calculation and Normalization

To measure the response of a pile to transient flexural waves, one must determine the locations of the accelerometers and the applied force, which then defines the angle for that test. The displacement profile and normalization coefficient are computed by the following procedure

1. Determine the angle between the input and accelerometer position.
2. Obtain the concrete and soil properties for the pile.
3. Compute the nondimensional frequency of the input.
4. Compute the nondimensional wavenumber of the input by the procedure defined in Section 2.3.4.
5. Compute the unknown constants by the procedure in Section 2.3.8.1, using the values from Steps 2, 3, and 4 as inputs.
6. Compute the displacement profiles by Equations 2-39, 2-40, and 2-41 using the results of Steps 2 through 5 as inputs.
7. Compute the normalizing constant, g, by Equation 2-42 using the results of Steps 2 through 6 as inputs.
8. Rescale the displacement profiles computed in Step 6 by the normalizing constant computed in Step 7.

2.3.8.3 Example Displacement Profiles

The normalized displacement profiles are presented for the 0-degree and 90-degree orientations for one value on nondimensional frequency. The normalized displacement profile in the 180-degree orientation will be the same as the normalized displacement profile for the 0-degree direction, except that the sign will be opposite. Likewise, the normalized displacement profile for the 270-degree direction will be the same as the normalized displacement profile for the 90-degree direction, except that the sign will be opposite.

The nondimensional frequency selected is 3.527 and the Poisson's ratio of the concrete is 0.20. The material properties for traction-free conditions are

- Shear Modulus Ratio: 32500
- Density Ratio: 133
- Poisson's Ratio of Soil: 0.30

The nondimensional wavenumber values, rounded to four significant digits, are presented on Table 2-3 for each of the active branches.

Table 2-3: Nondimensional wavenumber values for flexural branches at nondimensional frequency of 3.527 with traction-free conditions and concrete with a Poisson's ratio of 0.20

Branch	Nondimensional wavenumber	
	Real part	Imaginary part
F(1,1)	3.978	0.001316
F(1,2)	2.575	0.0005600
F(1,3)	1.760	0.0009242

For the selected nondimensional frequency, modes will be active on the first three flexural branches, as shown on Table 2-3. The nondimensional frequency value, material properties, and values presented on Table 2-3 are the inputs for the normalized displacement profile calculations. The nondimensional wavenumber values were rounded to four significant digits.

The real part and imaginary part of the displacement profile, as well as the magnitude of the displacement profile for each coordinate direction for the 0-degree orientation, as defined on Figure 2-8, are presented on Figure 2-10.

In general, the input force will be complex-valued and the response of the structure will be complex-valued. The frequency domain representation of the signal can be presented at real and imaginary parts or magnitude and phase, with the latter as the more common representation. The real and imaginary will depend on the properties of the input and the transfer function of the

structure but will also depend on the relationship of the signal with regards the origin of the time history and the numerical implementation of the Fast Fourier Transform (the FFT). Due to the difficulty associated with distinctly identifying the real and imaginary parts of the signal from the artifacts introduced by numerical analysis, the response is analyzed in terms of the magnitude of the displacements rather than separate real and imaginary parts. The magnitude of the displacements is computed by

$$Magnitude = \sqrt{\mathrm{Re}^2 + \mathrm{Im}^2} \qquad (2\text{-}43)$$

where Re is the real part of the displacement and Im is the imaginary part of the displacement.

The figures in the left-hand column, i.e., 2-8a, 2-8c, 2-8e, 2-9a, 2-9c, and 2-9e, represent the real and imaginary parts of the signal. Because the measured signal is the composite wave and its real and imaginary parts cannot be isolated, the displacements are analyzed in terms of the magnitude. The figures in the right-hand column, i.e., 2-8b, 2-8d, 2-9f, 2-9b, 2-9d, and 2-9f,represent the magnitudes of the displacements in the left-hand column At the nondimensional frequency selected, modes are expected on the F(1,1), F(1,2), and F(1,3) branches but not the F(1,4) branch or any higher branches.

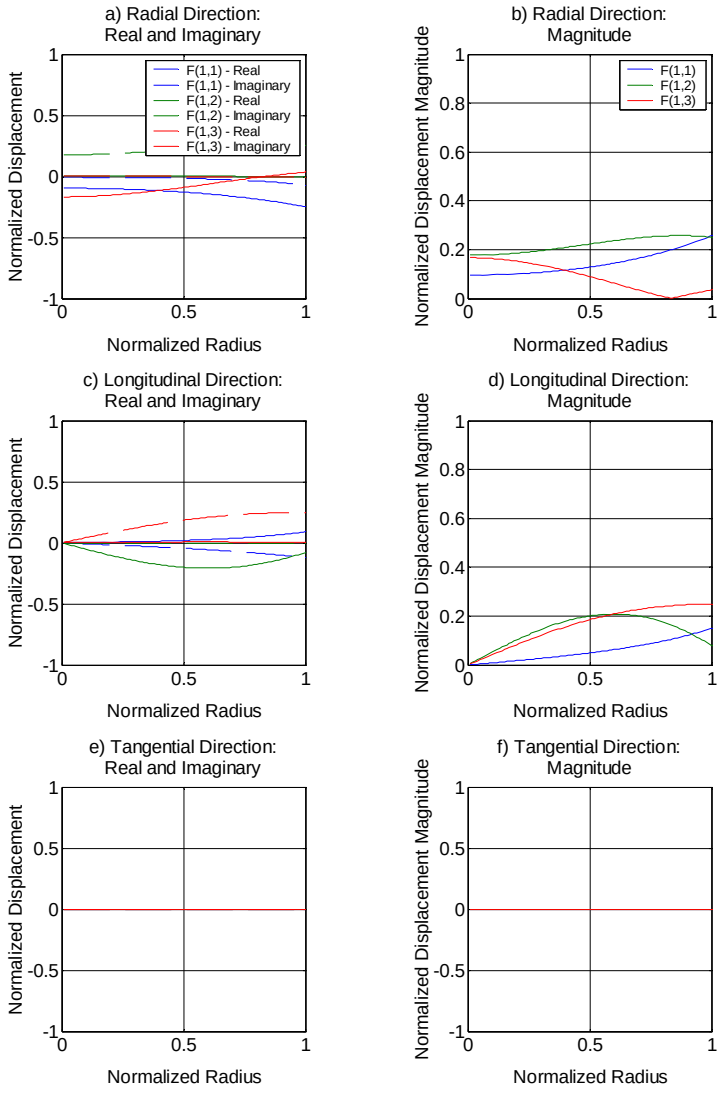

Figure 2-8: Normalized displacement profiles for first three flexural branches for concrete with Poisson's ratio of 0.20, soil with Poisson's ratio of 0.30 shear modulus ratio of 3250, and density ratio of 13.3 with nondimensional frequency of 3.527 at 0-degree orientations

To illustrate responses at a 90-degree orientation, the displacement profile for a nondimensional frequency of 3.527 is presented on Figure 2-9.

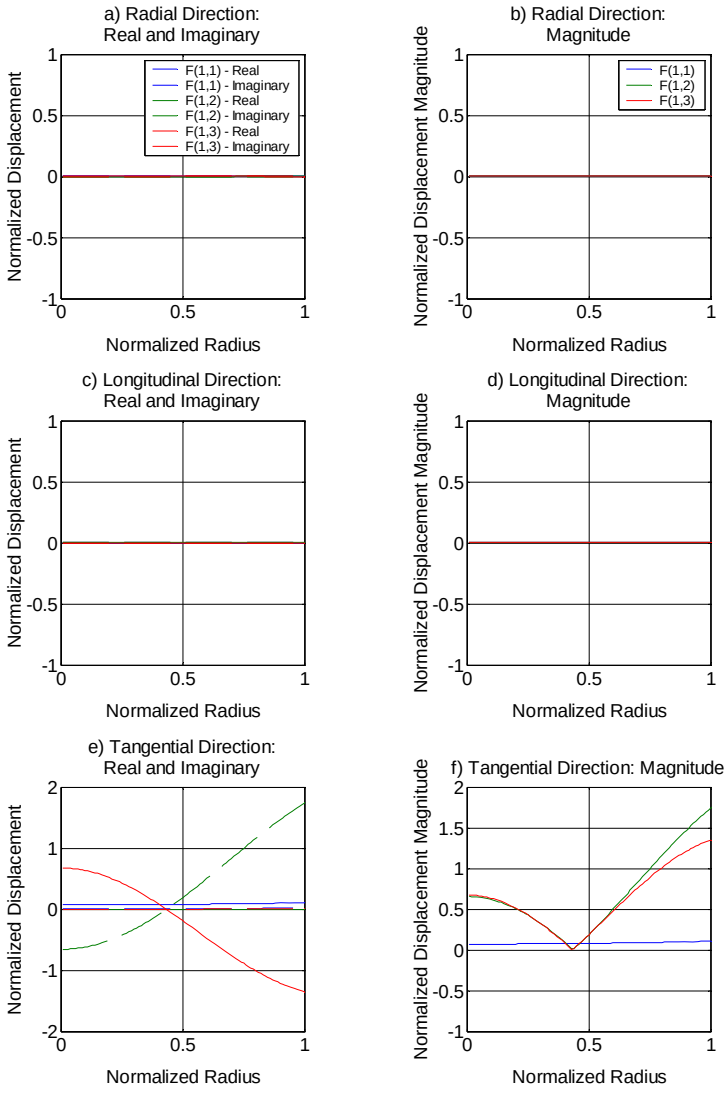

Figure 2-9: Normalized displacement profile for first three flexural branches for concrete with Poisson's ratio of 0.20, soil with Poisson's ratio of 0.30 shear modulus ratio of 3250, and density ratio of 13.3 with nondimensional frequency of 3.527 at 90-degree orientations

As predicted based on the trigonometric function that defines the displacement profiles, the displacement profiles in the radial and longitudinal directions are uniformly zero and the displacement profiles in the tangential direction are generally nonzero.

As implied on Figures 2-8 and 2-9, the displacement profiles in the radial and longitudinal directions depend on the cosine of the angle between the input and the measured response, and the displacement profile in the tangential direction depends on the sine of the angle between the input and the measured response. For the 0-degree orientation, the radial and longitudinal displacements will be maximum and the tangential displacement will be zero. For the 90-degree orientation, the radial and longitudinal displacements will be zero and the tangential displacement will be maximum.

2.4 Summary

The sonic echo (SE) and impulse-response (IR) Methods are commonly-used procedures for nondestructive evaluation of deep foundations. An intervening structure on top of the deep foundation element limits the amount of energy transmitted into the deep foundation element, thereby, limiting the effectiveness of the SE and IR methods to identify reflections. When the top of the deep foundation element is not accessible, but a portion of the side is, the lateral impacts can be used to induce flexural waves into such a pile.

The wavelengths of a stress wave generated by a hammer impact will be relatively long compared to the size of the defects to be identified. The long wavelengths compared to the defect size limits the size of the defects that can be identified in an impact method and the resolution with which defects can be identified.

Methods in which the input frequency is higher than the input frequency that can be generated in an impact method could generate stress waves with shorter wavelengths than those generated in an impact method. As the wavelength decreases, smaller defects could potentially be identified and defect locations could theoretically be identified more accurately. Analysis of the results of controlled frequency test as well as lateral impact tests, is based on the three-dimensional guided wave theory, as the waves are dispersive.

The solution of the three-dimensional wave equation is presented in terms of dispersion curves that relate nondimensional frequency to the complex-valued nondimensional wavenumber. The real part of the nondimensional wavenumber is related to the wavelength and the imaginary part of the nondimensional wavenumber is related to attenuation. The phase velocities and group velocities as functions of nondimensional frequency are computed from the relationship between the nondimensional frequency and the real part of the nondimensional wavenumber.

Attenuation coefficients and displacement profiles were computed at a selected nondimensional frequency. The frequency equation is solved for the selected value of

nondimensional frequency, providing the complex-valued nondimensional wavenumber. The attenuation is calculated directly from the imaginary part of the nondimensional wavenumber. The mode shapes are computed numerically with nondimensional frequency and nondimensional wavenumber as input values.

Chapter 3: Experimental Procedures, Equipment and Data Reduction

The guided wave theory presented in Chapter 2 is verified experimentally herein by the lateral impact and controlled frequency methods. The experimental verification consists of comparing the experimental and theoretical values of an ordered pair of frequency and group velocity or the ordered pair of frequency and phase velocity of individual phases within a wave group.

The lateral impact method uses a hammer to generate a broadband, low frequency stress wave. The controlled frequency method uses a piezoelectric shaker to generate a stress wave of known frequency content, duration, and amplitude. For both the lateral impact and controlled frequency methods, the dynamic force induces a propagating flexural wave, the responses of which is measured with accelerometers mounted on the side of the pile. The accelerometers can be mounted at different orientations to the input and at different positions along the pile length.

The results analyzed are the average of several individual impacts for the impact test or dynamic forces for the controlled frequency test, and those results are typically filtered to remove noise that falls outside the desired frequency range of the test. A set of

impact test data typically consists of 5 impacts and a set of controlled frequency test data typically consists of 10 applications of the dynamic force. Each set of test results are analyzed to

determine group velocity or phase velocity, using combinations of time domain and frequency domain analysis.

The test result data contain the pile response and noise. A portion of the noise will have a frequency content that falls within the frequency content of the pile response and a portion that falls outside the frequency content of the pile response. Random noise, including that noise for which the frequency content falls within the frequency range of the test, can be reduced by averaging several test results. The signal is filtered to remove the portion of the signal that falls outside the frequency range of the pile response.

The group velocity is determined by identifying successive returns of the stress wave and dividing the travel distance by the return time. The frequency content of the stress wave is determined by computing the Fourier Transform of the signal. In the lateral impact, the return time is identified in the time history. In the controlled frequency test, the frequency content of the signal can vary as a function of time, so directly identifying the return in the time history may not be possible. The mode identification procedure was developed by Chao (2002) to isolate the return of a specific component of the stress wave when the composite wave contains a time-varying frequency content, such as when modes may be excited on more than one branch in a controlled frequency test. The mode identification method is based on joint time frequency analysis (JTFA).

The velocity values are experimentally-determined from which one expects uncertainty or variability in the test results. Different analytical methods applied to the one set of test data can produce different output values. To evaluate the uncertainty or variability in the test method and analytical methods, each set of tests was performed more than one time. The test equipment was dismounted from the prototype pile between sets of tests. The variation in output values can be evaluated statistically to establish the expected uncertainty in a test.

3.1 Experimental Procedures for Flexural Guided Waves

Propagating flexural waves are generated by applying a dynamic force to the side of the pile and the responses are measured with one or more accelerometers mounted on the side of the pile. For the flexural branches, the angle between the input location and accelerometer location must be considered because the responses are not axisymmetric. The orientation convention is shown on Figure 3-1. Figure 3-1 shows the orientation for the lateral impact test, but the same definition of orientation applies to the controlled frequency test with the shaker replacing the impact hammer.

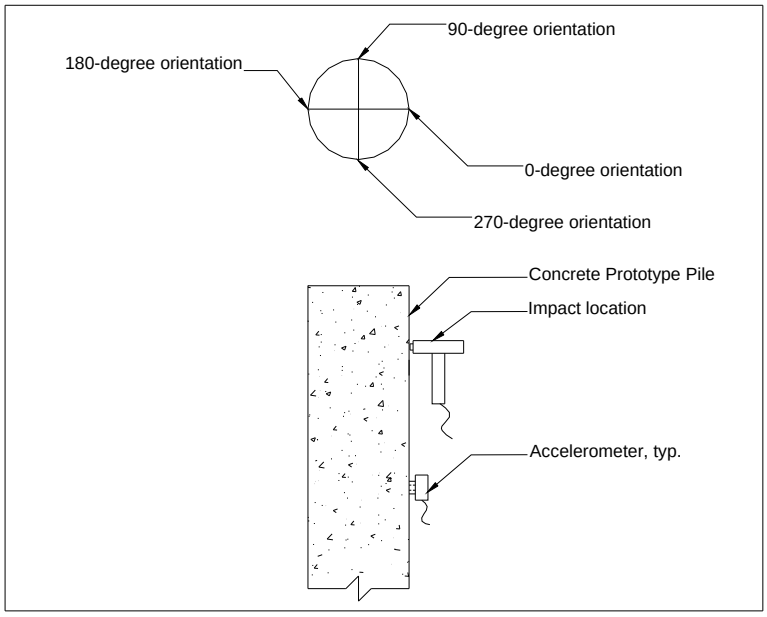

Figure 3-1: Orientation convention for input and response for flexural modes

The propagating flexural wave induced by the hammer impact shown on Figure 3-1 starts as a small disturbance that at the impact location and the disturbance spreads as it propagates from the location of the source, as shown on Figure 3-2.

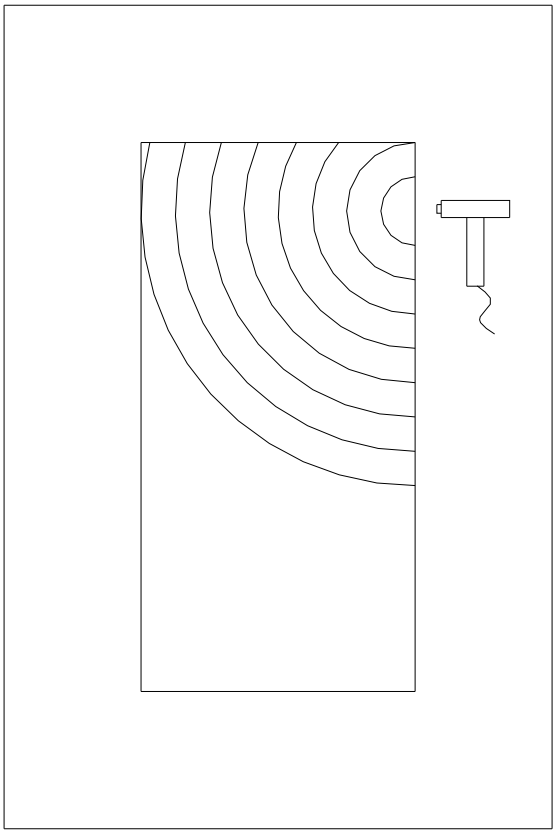

Figure 3-2: Typical propagating flexural stress wave

As the wavefront propagates further from the source, the radius of curvature increases. Eventually, the radius of curvature becomes so large that the wave becomes a plane wave.

3.1.1 Lateral Impact Experiments

Lateral impact tests are performed by hitting the side of the pile with a modal hammer and measuring the responses with accelerometers mounted on the pile at different locations and at different orientations. In this work, the stress waves are generated with either of two hammers and the responses measured with two different types of accelerometers. Of the two impulse

hammers, one is lighter with a stiffer tip, and the other is heavier with a softer head. The lighter hammer with the stiffer tip generates a higher maximum frequency than the heavier hammer with the softer head. The response is measured with either uniaxial or triaxial accelerometers. The experimental setup for performing the lateral impact test on a prototype pile is shown on Figure 3-3.

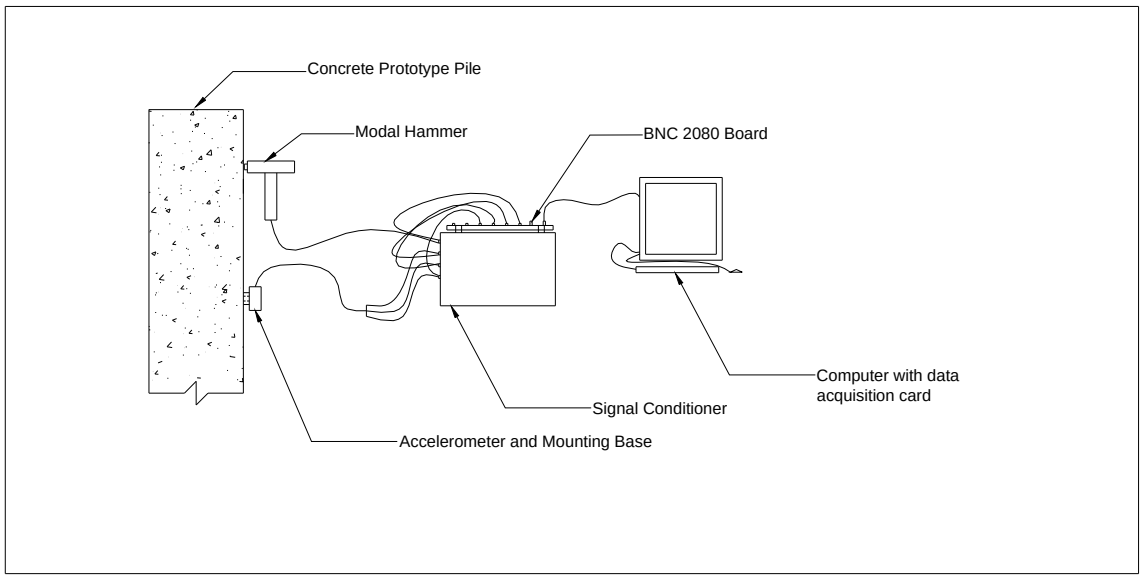

Figure 3-3: Test schematic and data acquisition equipment for lateral impact test

The computer contains the data acquisition card and all software required to operate the data acquisition card. It is used to record and process the data. The signal conditioner is required to power the piezoelectric sensors in the modal hammer and accelerometers. The BNC 2080 board is required to collect the analog signals from the signal conditioner into one shielded cable that connects to the data acquisition card. The pile is shown with one triaxial accelerometer mounted to the side of the pile, but more than one accelerometer can be used. The accelerometer shown is

one unit that houses three separate accelerometer crystals and one output cable. The cable that is attached to the accelerometer casing terminates in a four-pin female connector. A splitter with a four-pin male connector attaches to the single cable and terminates in three BNC connectors.

The procedure for the lateral impact test is

1. Prepare the concrete surface for testing
2. Attach the mounting base to the prepared concrete surface with epoxy. The test can be performed with one or more accelerometers and each accelerometer requires a separate mounting base.
3. Once the epoxy has cured, attach the accelerometer(s) to the mounting base(s).
4. Connect the coaxial cables from the hammer and accelerometers to the inputs on the signal conditioner.
5. Connect the outputs of the signal conditioner to the analog inputs (AI) on the BNC 2080 Board via coaxial cable.
6. Connect the BNC 2080 Board to the Data Acquisition Card via a shielded cable.
7. Plug in and turn on the computer and signal conditioner.
8. Verify communication in each channel using “Measurement & Automation” program by National Instrument, Inc.
9. Launch the data acquisition program and set the parameters (see Section 3.2.2).
10. Perform the required number of repetitions of the test.
11. If the results are acceptable, save the data.

Surface preparation can include cleaning the concrete with a wire brush, grinding the concrete with an electric grinder, or both. A BNC connector is the standard termination for the coaxial cables from the modal hammer and accelerometers. The coaxial cable that connects the signal conditioner to the BNC board comes standard with BNC connectors at both ends. The shielded cable that connects the BNC 2080 Board to the data acquisition board is model number SH6850 manufactured by National Instruments, Inc.

The “Measurement & Automation” program is part of the software suite from National Instruments, Inc. and is designed to manage plug-and-play devices such as data acquisition cards. When the data acquisition card is first installed, the input and output (I/O) parameters of the device are defined through the “Measurement & Automation” program and the I/O channels are created. The “Measurement & Automation” program has a “Test Panel” routine that allows one to monitor the input voltage to each channel from the device connected to that channel. If the channel, data acquisition card, and BNC 2080 board are configured properly, the voltage from the device to the computer will be zero when no load is applied to the transducers. The sensors in the accelerometer and the force transducer in the modal hammer have warm-up times. If the Test Panel is run before the sensor has warmed up, the measured voltage will not be zero. If the Test Panel is run to monitor the response of a channel that does not have a sensor providing input to the channel, the measured voltage may not be zero.

Once all devices are warmed up, the tests can be performed. The data are recorded by a virtual instrument that displays the results on a virtual oscilloscope and writes the data to a spreadsheet file. Details of the virtual instrument will be provided in Section 3.2.2. The stress wave is generated by striking the side of the pile with a modal hammer, and the response of the pile is measured with one or more accelerometers. The details of the modal hammer and accelerometers are provided in Section 3.3. The test is repeated to obtain the average response. Each test will contain noise, but if the noise is random with zero mean, averaging the results of multiple tests will tend to cancel out the noise.

3.1.2 Controlled Frequency Experiments

The purpose of a controlled frequency experiment is to generate a propagating flexural wave with a higher frequency and, consequently, a shorter wavelength than can be generated in an impact test. The propagating flexural wave is generated with a computer-controlled, piezoelectric shaker. The magnitude, duration, and frequency of the force applied with the piezoelectric shaker are user-defined for each test and are set through the software that controls the shaker. As with the lateral impact method, the response of the pile is measured with accelerometers. The experimental setup for a controlled frequency test is shown on Figure 3-4.

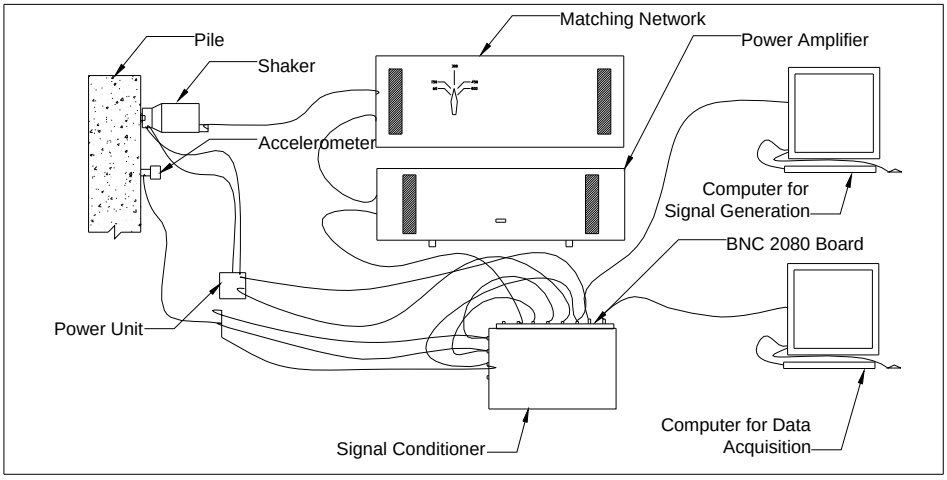

Figure 3-4: Equipment configuration for controlled frequency test

The propagating flexural wave is generated with an F7 piezoelectric shaker manufactured by Wilcoxon, Inc. The shaker has an embedded force transducer and an embedded accelerometer to allow measurement of the input and response at the shaker. The power amplifier, matching

network, and computer for signal generation are required to control the F7 piezoelectric shaker. The accelerometer, signal conditioner, BNC board, and computer for data acquisition are the same as in the lateral impact test described in Section 3.3.1.

The procedure for the controlled frequency test is

1. Drill a hole into the concrete surface for the threaded rod for the shaker.
2. Epoxy the threaded rod into the hole drilled in Step 1.
3. Prepare the surface of the concrete for the accelerometer base(s).
4. Attach the mounting base(s) to the prepared concrete surface with epoxy. The test can be performed with one or more accelerometers and each accelerometer requires a separate mounting base.
5. Once the epoxy has cured, attach the accelerometer(s) to the mounting base(s).
6. Connect the coaxial cables from the accelerometer(s) to the inputs on the signal conditioner.
7. Connect the outputs from the signal conditioner to the AI on the BNC 2080 Board via coaxial cables.
8. Connect the BNC 2080 Board to the Data Acquisition Cards in the computers via two shielded cables. Two computers are required: one for signal generation and one for data acquisition.
9. Connect the analog output (AO) on the BNC 2080 Board to the BNC input on the power amplifier.
10. Connect the output cable from power amplifier to the input port on the matching network.
11. Connect the shaker to the threaded rod.
12. Connect the output from matching network to the input on shaker.
13. Connect the outputs from the force gauge and accelerometer mounted in impedance head of shaker to the inputs on power unit.
14. Connect outputs from power unit to the (AI) of BNC 2080 Board.
15. Plug in and turn on the power amplifier, computers, and signal conditioner.
16. Verify communication in each channel using “Measurement & Automation” program by National Instrument, Inc.
17. Launch the virtual pulse generator program and set parameters (see Section 3.2.3).
18. Launch the data acquisition program and set parameters (see Section 3.2.2).
19. Perform required number of repetitions of test.
20. If the results are acceptable, save the data.

3.2 Data Acquisition and Control

The data acquisition system consists of a computer that houses the data acquisition card and contains the software to control the data acquisition card, acquire the data, and process the data. The same set of equipment is also used for generating the signal in the controlled frequency tests.

The hardware consists of a field-ready computer and a PXI data acquisition card with the capability of acquiring 16 single-ended or 8 differential inputs and generating 2 outputs. The PXI card is controlled by software loaded in the computer. The data acquisition for impact tests and controlled frequency tests and the signal generation for controlled frequency tests are performed by virtual instrument programs loaded on the computer. With a virtual instrument, the operator can control the number of channels of data collected, the sampling rate, and the number of data points collected for data acquisition; as well as the frequency, amplitude, and duration of the output signal for a controlled frequency test.

3.2.1 Computer and Data Acquisition Card

The computer used for data acquisition and processing has a Pentium III processor with a 768 MHz clock speed, 768 MB of ram and 30 GB of hard drive storage. The computer is field ready but comparable in size to a desktop computer, which allows the data acquisition card to be installed inside the computer. The data acquisition card is an NI-PCI-MIO-16E-1 PXI card

manufactured by National Instruments, Inc. The card uses the PXI Bus and fits into an expansion slot on the computer. The data acquisition card is a Plug-and-Play device and the driver is included with the Measurement and Automation program published by National Instruments, Inc. The data acquisition system is controlled by a virtual instrument written in the LabVIEW programming language, published by National Instrument, Inc. The details of the data acquisition card are provided on Table 3-1.

Table 3-1: Key specifications of NI-PCI-MIO-16E-1 DAQ board
(After Chao, 2002)

Number of AI[a] channels	16 single-ended or 8 differential
Resolution	12 bits
Maximum sampling rate	1.25 MS/s
Polarity	Unipolar or bipolar
Board Range	Unipolar: 0V to +10V Bipolar: -5V to +5V
Number of AO[b] Channels	2
Trigger	AI Channel <0..15>, external PFI[c] <0..9>

Notes: a. AI = Analog Input
b. AO = Analog Output
c. PFI = Programmable Function Input

Sampling the signal at discrete time intervals and resolving the signal to discrete voltage intervals can produce noise in the recorded signal.

A large variety of data acquisition systems are available and each system has its advantages and disadvantages. The system to be used for this investigation was designed by Chao (2002).

3.2.2 Virtual Oscilloscope

The virtual oscilloscope is a LabVIEW program written to record the digitized data sent to the data acquisition card and to display the results. The results are presented as a time history of current record for all channels, a time history of all responses, a time history of average response, and a frequency spectrum of average response. If the results are deemed acceptable, they can be saved to a spreadsheet file. The virtual oscilloscope records six channels of data. The virtual oscilloscope is programmable to accommodate different triggering criteria and different resolution in the time and frequency domains.

The following input values are required for the virtual instrument that controls the data acquisition

1. Number of channels to record
2. Trigger channel
3. Triggering criteria
4. Sampling rate
5. Buffer size (number of samples to store in the buffer)
6. Total number of samples to record
7. Number of pretrigger scans to record

The number of channels to record depends on the type of data required for the particular test. The triggering channel is typically the input, and is attached to the lowest number channel (zero for products by National Instruments, Inc., or one for the PCB482A20 signal conditioner). The sampling rate depends on the highest expected frequency for the input and response. The minimum sampling frequency required to prevent aliasing, called the Nyquist frequency (Bishop, 2001), is twice the highest frequency measured during the test. The sampling rate required for

accuracy of measurement is much higher than the Nyquist frequency. The buffer size is typically 2048 samples. The minimum for the total number of samples required is enough for the stress wave to make one complete pass; however, a larger number of samples are typically acquired for better resolution in the frequency domain. The typical values for tests performed on prototype piles are

- Sampling rate: 100 kHz or 160 kHz
- Total number of samples: 4096 or 8192

The highest frequency generated in an impact test is about 8 kHz and the highest frequency generated in a controlled frequency test is 14 kHz. The sampling rate is about 11 to 20 times the highest frequency excited in the tests. The travel time for the stress waves will be on the order of 1 to 3 ms, which would require 100 to 300 samples to capture one complete pass of the wave. The larger number of samples is required to compute the FFT with adequate frequency resolution.

The triggering criterion is a voltage of 0.15 V with a rising slope, i.e., the voltage is increaseing. The number of pretrigger scans is 100 for tests performed with a sampling rate of 100 kHz and 160 samples for tests performed with a sampling rate of 160 kHz.

The virtual instrument was coded with the Intermediate Analog Input Functions that are preprogrammed with LabVIEW ™. The following functions are required to acquire the data

1. Initialize the virtual instrument
2. Start collecting data
3. Store the data in a buffer
4. Set up a conditional retrieve based on the triggering criteria
5. Clear the instrument

The virtual instrument required for collecting the data is a virtual oscilloscope designed to acquire six channels of data. Six channels of data are recorded regardless of the number of sensors providing input. If fewer than six channels are recorded, the remaining columns of data are filled with duplicates of another channel or random noise.

3.2.3 Virtual Pulse Generator

The signal for the controlled frequency test is generated by a Virtual Pulse Generator that sends a digital signal to a PXI Card mounted in the computer on which the virtual pulse generator is loaded. The output voltage from the PXI card is transmitted to the power amplifier described in Section 3.3.2. The PXI Card that converts the digital signal to an analog signal is the same model card that is used in the data acquisition system in both controlled frequency and impact tests.

The required input parameters for the virtual pulse generator are

1. Update rate (updates / sec)
2. Number of updates per cycle
3. Total number of updates
4. Maximum voltage
5. Minimum voltage

The update rate is defined in terms of updates per second. The frequency of the wave is

$$f = \frac{Updates/\sec}{Updates/cycle} \tag{3-1}$$

where f is the frequency in Hz. The duration of the input is

$$Signal\ Duration = \frac{Number\ of\ Updates}{Updates/\sec} \tag{3-2}$$

3.3 Signal Generation and Observation

The equipment required for signal generation are the modal hammers and shaker, and the equipment required for signal observation are accelerometers. The equipment for signal generation and observation was shown schematically on Figures 3-3 and 3-4 and was described briefly in Sections 3.1.1 and 3.1.2. The properties and operation of these devices are presented in this section.

3.3.1 Impact Hammers

The two hammers used to generate the stress waves in the lateral impact were manufactured by PCB Piezotronics, Inc. Both hammers have embedded force transducers which allow measurement of the force – time history generated during the impact. The key parameters of a hammer and tip/head combination are the frequency range, maximum force, and transducer

sensitivity. Table 3-2 provides the key parameters for the two types of hammers used in this investigation.

Table 3-2: Properties of Modal Hammers

Hammer Model	Frequency Range (Hz)	Maximum Force (N)	Sensitivity (mV/N)
PCB 086C04	0 to 8000	4450	1.12
PCB 086M54	0 to 2000	22240	0.20

The PCB 086M54 hammer has several tips of different materials, which correspond to different stiffness constants. By using a head with a different stiffness constant, a different maximum frequency can be generated. The hammer is available with an aluminum head, which is the stiffest head, and four rubber heads, each of which has a different stiffness. According to the manufacturer's data, the maximum value of the frequency range presented in Table 3-2 was generated by striking a steel mass.

3.3.2 Piezoelectric Shaker, Power Amplifier and Matching Network

The controlled frequency stress wave is generated with an F7 piezoelectric shaker manufactured by Wilcoxon, Inc. The shaker includes a vibration generator and an impedance head. The impedance head, which is the portion of the shaker that butts up to the structure, contains an embedded force transducer and an embedded accelerometer to allow measurement of the input and response at the shaker. The important properties of the F7 piezoelectric shaker and its embedded transducers are presented on Table 3-3.

Table 3-3: Details of F7 Piezoelectric Vibration Generator

Vibration Generator	
Usable frequency range	500 to >20,000 Hz
Maximum input	800 V rms
Maximum acceleration	1000 g
Maximum output force	444 N
Accelerometer Nominal Values	
Charge sensitivity	0.92 pC/m/s2
Voltage sensitivity	13 mV/g
Frequency range ±3 dB	10 to 20000 Hz
Force Gage Nominal Values	
Charge sensitivity	40 pC/N

The manufacturer's data on the F7 piezoelectric shaker state that it can generate signals with frequencies greater than 20,000 Hz and does not list an upper limit. The maximum force that can be generated by the F7 piezoelectric shaker decreases at frequencies greater than 20,000 Hz and the transducers embedded in the impedance head are not calibrated above 20,000 Hz. The maximum input of 800 V rms is provided by a PA8 power amplifier, also manufactured by Wilcoxon, Inc. An N8L Matching Network, which serves as a step up transformer and provides impedance matching, links the power amplifier and shaker. The step up transformer portion is designed to increase the voltage at the impedance head, thereby generating a greater force. The matching network has five selectable output voltage settings from 60 Volts to 800 Volts. The impedance matching function depends on the frequency range of the test. The shaker is modeled as an RC Circuit, in which the impedance of the resistor is constant with frequency and the impedance of the capacitor decreases with increasing frequency. The power amplifier is designed to operate at a 4-Ohm impedance, which is the reason that the impedance matching is required. The matching network is a set of inductors for which the impedance increases as the

frequency increases. The increasing impedance of the inductor counters the decreasing impedance of the capacitor, i.e., the impedance value is matched.

3.3.3 Accelerometers

The response of a pile to a propagating flexural wave is measured with piezoelectric accelerometers mounted on its side. Both types of accelerometers used in this study were manufactured by PCB Piezotronics, Inc. The key parameter for the accelerometers is the voltage sensitivity, which defines the resolution to which the acceleration can be measured. The voltage sensitivity and other parameters for the different types of accelerometers are listed on Table 3-4.

Table 3-4: Accelerometer details

Model	Voltage sensitivity (mV/g)	Measurement range (±g pk)	Frequency range (Hz)
629A11	100	50	0 to 5000
W352A78	100	50	5 to 15000

Accelerometer Model W352A78 is a uniaxial accelerometer and accelerometer 629A11 is a triaxial accelerometer. The uniaxial accelerometers have one coaxial cable that terminates in a BNC connection and the triaxial accelerometers have one output cable that splits into three cables, each of which terminates in a BNC connection.

The accelerometers manufactured by PCB Piezotronics, Inc. are calibrated by the back-to-back method, in which the accelerometer is mounted to a reference standard, which is, in turn,

mounted to a vibration exciter. The vibration exciter is operated over a range of frequencies by a function generator and the output voltages of both the accelerometer and reference standard are measured. The ratio of the accelerometer voltage to the reference voltage is computed at each frequency to determine the accuracy of the accelerometer. The results are presented as calibration curves and are available from the manufacturer. Recalibration by the manufacturer is recommended on an as-needed basis. One of the triaxial accelerometers was recalibrated during the course of this research. The performance of the recalibrated accelerometer fell within the permissible limits as defined by the manufacturer.

The properties of the accelerometer, their components, and the manufacturing process can induce unwanted signals or noise in the recorded data.

The piezoelectric crystal in an accelerometer has an axis that is oriented such that it responds to acceleration in the desired direction, but it also responds to acceleration in other directions. For example, a uniaxial accelerometer placed atop a structure is designed to measure the vertical component of a stress wave, but the accelerometer will also respond to the radial and tangential components of the stress wave. The manufacturer's literature indicates that the response of an accelerometer to acceleration components other than its intended axis, called cross-sensitivity, is on the order of 1 to 2 % of the sensitivity of the accelerometer in its intended axis.

Any current traveling through a wire produces a magnetic field that can induce a current in a near-by wire. If each wire transmits a current that contains a signal, the other near-by wires induce a current that contains part of its signal, thus contaminating the signals in the other wires. The triaxial accelerometer listed on Table 3-4 consists of three transducers enclosed in a single casing, and the signals are transmitted to and from the three transducers by a single cable containing three wires. The electrical field generated in one wire will induce an electrical field in the other wires, resulting in cross contamination of signals.

The effects of cross-contamination and energy leakage depend on the strength of the individual signals.

3.3.4 Signal Conditioning

The sensors in the F7 shaker, impulse hammers, and accelerometers are all piezoelectric devices that require a constant current to operate and generate a small voltage when loaded. The current that drives the F7 shaker also powers the transducers embedded in the impedance head of the F7, and, as such, no additional signal conditioning is required. The transducers in the accelerometers and modal hammers require a separate power supply. The PCB482A20 signal conditioner provides the current required to operate the accelerometers and hammer and also collects the voltages associated with the measured response.

The accelerometers require a constant current of 2 to 20 mA at 24 to 28 VDC; the PCB086C04 modal hammer requires a constant current of 2 to 20 mA at 18 to 30 VDC; and the PCB086C04 modal hammer requires a constant current less than 20 mA at a Voltage less than 30 VDC. The PCB482A20 signal conditioner is adjustable to provide a constant current with a range of 2 to 20 mA at a voltage of 24 ±1 VDC. The received signal has three programmable gain settings of 1x, 10x, and 100x magnification. The signals are transferred by 8 input BNC jacks and 8 output BNC jacks. The signal conditioner is designed for single-ended transducer cables. The output signals are collected on a BNC 2080 board and transmitted to the data acquisition card in the computer. The BNC 2080 board has 16 single-ended analog inputs and 2 single-ended analog outputs.

3.4 Theoretical Considerations

The experimental procedure for NDE of deep foundations based on guided wave theory is to generate a stress wave of known frequency content and to measure the response of the structure. Depending on the frequency content of the stress wave, it may contain modes on different branches of the dispersion solutions. Each mode on each branch has a displacement profile and propagation velocity. Ideally, transducers can be mounted such that the displacement is large for the mode on the branch of interest and small for all other modes. When more than one mode has a large displacement, the modes can be distinctly identified by considering the

propagation velocity. For the embedded condition, energy loss into the surrounding soil will attenuate some of the modes and, thus, should allow easier identification of reflections.

The cutoff frequency is the frequency at which the real part of the wavenumber becomes zero, i.e., the mode is evanescent, or the imaginary part becomes infinite, i.e., the amplitude decays to zero instantaneously. Theoretically, modes will propagate on a specific branch if the input frequency is above cutoff frequency for the branch. From a practical consideration, the propagation of a mode also will be limited by the wavelength of the stress wave and the length of the pile. If the wavelength of the stress wave exceeds the pile length, the mode will not propagate.

Once the expected branches on which modes could propagate have been identified, the propagation velocity is determined for each mode. Each mode on each branch will propagate at a unique phase velocity and the composite of all modes will create a wave group. The group will travel at a group velocity that is a function of frequency and branch. The frequency of each phase and the group are identified by converting the measured time history to frequency domain. The velocity of the phase and group may be determined from the time domain or frequency domain representation of the signal, depending on the type of test.

3.4.1 Cutoff Frequency

The first consideration for the design of an experimental procedure is to identify the branches that may be active. The active branches are identified by comparing the expected frequency content of the input to the cutoff frequencies for the various branches. As an example, consider the first five flexural branches for concrete with a Poisson's ratio of 0.20. The nondimensional cutoff frequencies were determined numerically for both traction-free and embedded conditions. The embedded conditions were calculated for soil with Poisson's ratio of 0.30, a density ratio of 1.33 and the shear modulus ratio of 325, and the results are presented on Table 3-5.

Table 3-5: Nondimensional cutoff frequencies for both traction-free & embedded piles with $\nu_c = 0.20$

Mode	Traction-free piles	Embedded Piles[4]
F(1,1)	0	0
F(1,2)	1.87[1]	1.8
F(1,3)	2.65[2]	2.7
F(1,4)	5.19[2]	5.1
F(1,5)	5.53[3]	5.4

Notes:
1. Lowest value for which solution converged
2. Imaginary part exceeds 0.5
3. Real part less that 0.01
4. After Wang, 2004

The nondimensional cutoff frequencies were determined numerically. The algorithm used to solve the frequency equation for an embedded pile does not apply to a traction-free pile. The "Traction-free" case is solved approximately by setting the shear modulus ratio and density ratio two orders of magnitude larger than the shear modulus ratio and density ratio for soft/loose soil.

For the branches and conditions for which the real part is less than 0.01, one can assume that the real part would reach zero at the cutoff frequency. In some cases, the cutoff frequency was defined such that it was the lowest value for which the algorithm could find a solution. For the embedded case, the results were read from the nondimensional frequency – nondimensional wavenumber graphs. As with the "Traction-free" case, the real part of the wavenumber for the numerically-solved is less than 0.01 for some, but not all branches. For the branches in which the real part of the wavenumber is less than 0.01, the cutoff frequency can be easily identified. For some branches, the imaginary part becomes very large and the cutoff frequency must be extrapolated, especially if the solution algorithm becomes unstable. The "Traction-free" and embedded results presented herein are similar to each other and to the results presented by Zemanek (1971), as one would expect.

3.4.2 Frequency Range

3.4.2.1 Impact Tests

In a lateral impact test, the stress wave is generated with a hammer, the frequency of which ranges from DC to a maximum frequency that is proportional to the reciprocal of the contact time (Sansalone & Carino, 1986). The maximum frequency for the PCB 086M54 Hammer is 2000 Hz and the maximum frequency for the PCB 086C54 Hammer is 8000 Hz, according to the manufacturer's data.

To identify the modes that may be excited in a lateral impact, one must compute the nondimensional frequency values for a range of prototype pile diameters, and compare the nondimensional frequency to the cutoff frequencies for different branches. Curves for the nondimensional frequency and real part of the nondimensional wavenumber are presented on Figure 3-5 for the first five flexural branches of concrete with a Poisson's ratio of 0.20 and embedded in soft soil with a shear modulus ratio of 325 and a density ratio of 1.33.

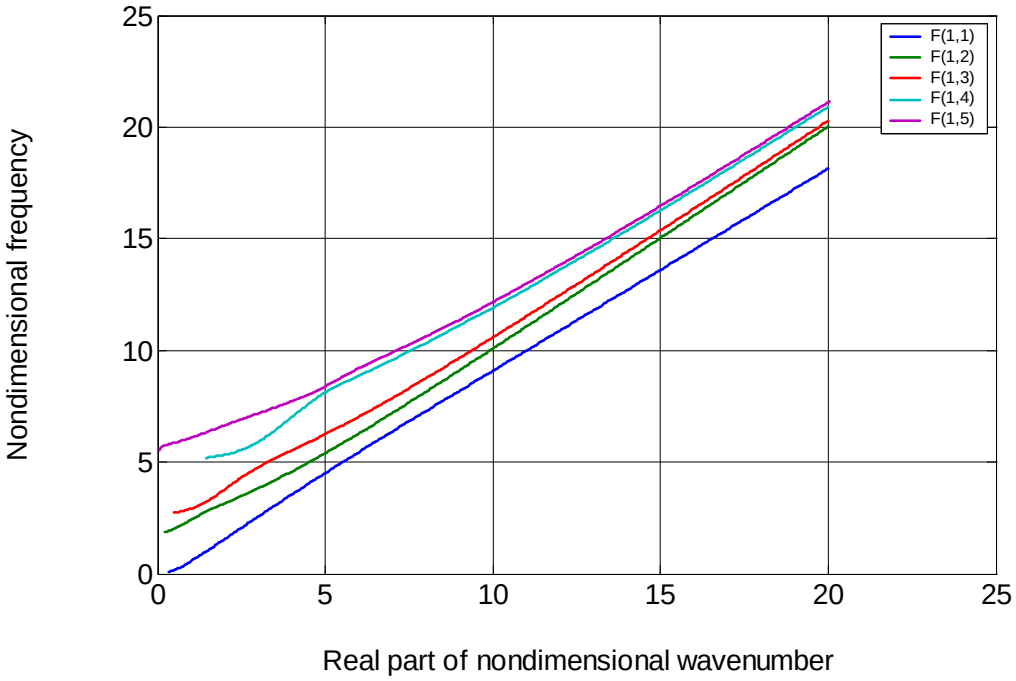

Figure 3-5: Nondimensional frequency – real part of nondimensional wavenumber for first five flexural branches, soft soil, $\nu_c = 0.20$

Sample calculations for nondimensional frequency are provided for the two hammers to be used in this investigation for a range of different pile sizes. The piles to be analyzed have diameters of 254 to 508 mm and shear wave velocities of 2300 to 2800 m/s. The

nondimensional frequencies, Ω, are calculated from the maximum frequency of the hammer and the assumed values of pile diameter and shear wave velocity by

$$\Omega = \frac{2\pi f a}{c_{T_c}} \qquad (3\text{-}3)$$

where *f* is the frequency in Hz, *a* is the pile radius in m, and c_{Tc} is the concrete shear wave velocity in m/s.

The pile properties, frequency, nondimensional frequency and the expected branches are shown on Table 3-6. The branches are identified based on the curves shown on Figure 3-5.

Table 3-6: Frequency, nondimensional frequency and expected flexural branches for prototype piles with $\nu_c = 0.20$

Pile Diameter (mm)	Frequency (Hz)	Shear Wave Velocity (m/s)	Nondimensional Frequency	Branches Expected
254	8000	2300	2.77	F(1,1) through F(1,3)
		2800	2.28	F(1,1) and F(1,2)
	2000	2300	0.69	F(1,1)
		2800	0.57	F(1,1)
508	8000	2300	5.55	F(1,1) through F(1,4)
		2800	4.55	F(1,1) through F(1,3)
	2000	2300	1.38	F(1,1)
		2800	1.13	F(1,1)

The results presented on Table 3-6 indicate that a lateral impact test will always generate modes on the F(1,1) branch and may, in theory, generate modes on branches as high as the fourth. Practical considerations such as the actual maximum frequency generated during an impact, pile

length, and mode shape may prevent modes on the F(1,2) branch and higher branches from propagating.

The maximum frequency values presented on Table 3-6 are the highest frequencies that can be generated by that hammer, but the actual frequency is likely to be lower based on the condition of the hammer tip/head at the time of the impact, the stiffness of the surface being struck and the condition of the surface. As an example, the force spectrum for an impact by the PCB086C54 is shown on Figure 3-6.

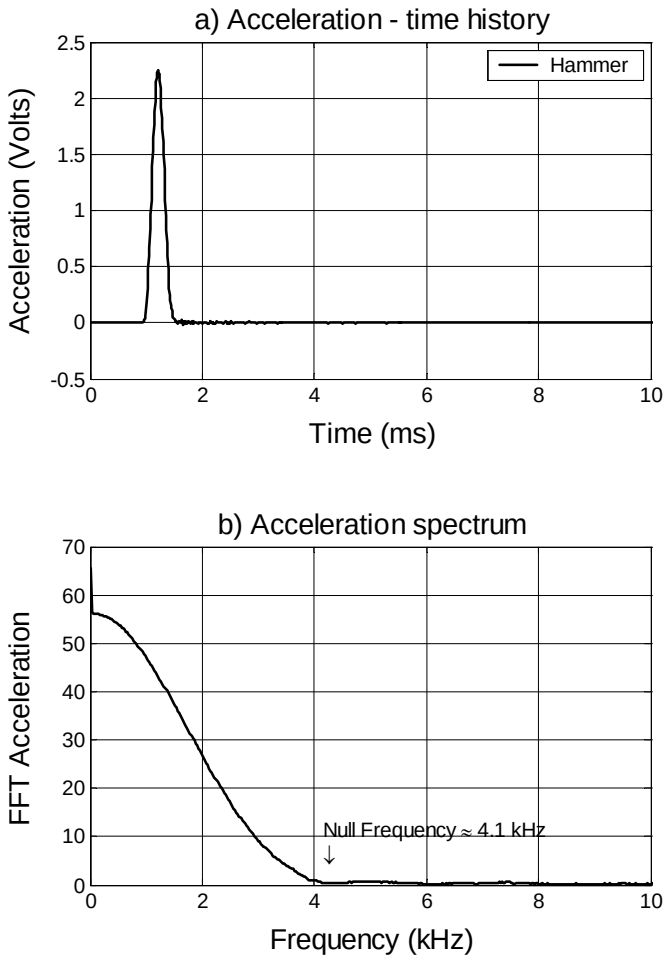

Figure 3-6: Typical response for hammer impact

Two key points shown on Figure 3-6b are that the magnitude of the force decreases as the frequency increases and that the maximum frequency is less than the 8 kHz manufacturer's limit based on an impact on a steel mass. The results presented on Figure 3-6 are from an impact on concrete, which is not as stiff as steel. Due to the lower stiffness of the concrete compared to steel, one would expect a longer contact time and, consequently, a lower maximum frequency

compared to steel. The effects of the decreasing force are illustrated by considering the response of a pile to the hammer impact shown on Figure 3-6.

The data on Table 3-6 was developed assuming all modes within the frequency range of the pile can be generated. Modes on the F(1,1) branch and F(1,2) branch will be considered, which have nondimensional cutoff frequencies, Ω_c, of 0 and 1.88, respectively. The nondimensional cutoff frequencies, Ω_c, are converted to cutoff frequency, f_c, by

$$f_c = \frac{\Omega_c c_{T_c}}{2\pi a} \qquad (3\text{-}4)$$

The nondimensional cutoff frequencies for 254 mm and 508 mm diameter piles with shear wave velocities, c_{Tc}, of 2300 m/s to 2800 m/s are presented on Table 3-7.

Table 3-7: Cutoff frequencies of F(1,2) branch for prototype piles with $\nu_c = 0.20$

Pile Diameter (mm)	Shear Wave Velocity (m/s)	Cutoff Frequency for F(1,2) branch (Hz)
254	2300	5400
	2800	6600
508	2300	2700
	2800	3300

The maximum frequency for the impact on Figure 3-6 is 4100 Hz. For the 254 mm diameter pile, all modes excited by the impact should lie on the F(1,1) branch. For the 508 mm diameter pile, modes could be excited on either the F(1,1) or F(1,2) branches.

Guided wave theory was derived for an infinitely long pile, suggesting that modes will propagate on all branches excited by the input force. Actual structures are of finite length placing a lower bound on modes that can propagate. If the wavelength for a given mode exceeds the pile length, the stress wave will not propagate at that mode. The lower bound of the nondimensional wavenumber can be computed by relating nondimensional wavenumber to wavelength. The wavenumber, ξ, is related to wavelength, λ, by:

$$\mathrm{Re}(\xi) = \frac{2\pi}{\lambda} \tag{3-5}$$

The frequency equation was solved in terms of nondimensional frequency, Ω, and nondimensional wavenumber, ξ_a, rather than frequency and wavenumber. The conversion from nondimensional wavenumber to wavenumber is

$$\xi = \frac{\xi_a}{a} \tag{3-6}$$

where a is the pile diameter. Substituting Equation 3-6 into Equation 3-5 and rearranging terms, the wavelength in terms of nondimensional wavenumber and pile diameter is

$$\lambda = \frac{2\pi a}{\mathrm{Re}(\xi_a)} \tag{3-7}$$

Equation 3-7 indicates that as the real part of the nondimensional wavenumber approaches zero, the wavelength becomes infinite. For a finite length pile, an infinite wavelength wave cannot propagate, nor will modes for which the wavelength exceeds the pile length. By considering the pile dimensions, one can compute the minimum wavenumber, $\xi_{a(\min)}$, for which modes will propagate

$$\mathrm{Re}(\xi_{a(\min)}) = \frac{2\pi a}{L} \qquad (3\text{-}8)$$

where L is the pile length. To consider the practical lower bound of a wave that can propagate in a pile, consider a pile that is 254 mm in diameter by 2 meters long. For a mode to propagate in this pile, the real part of the nondimensional wavenumber must be greater than 0.4, based on Equation 3-8. The nondimensional frequency corresponding to the 0.40 real part of the nondimensional wavenumber is identified from the nondimensional dispersion curve for the Poisson's ratio of the concrete. The nondimensional frequency is converted to frequency in Hz by

$$f = \frac{\Omega c_{T_c}}{2\pi a} \qquad (3\text{-}9)$$

The selected nondimensional frequency and the computed frequency are presented on Table 3-8. The assumed pile geometry is 254 mm in diameter by 2 m long, and the assumed concrete properties are the shear wave velocity, c_{Tc}, is 2500 m/s and the Poisson's ratio, ν_c, is 0.20.

Table 3-8: Nondimensional frequency and frequency for longest wavelength that can propagate in a 254-mm diameter, 2-m long pile with c_{Tc} = 2500 m/s and ν_c = 0.20

Branch	Nondimensional Frequency	Frequency (Hz)
F(1,1)	0.12	190
F(1,2)	1.96	3070
F(1,3)	2.73	4280
F(1,4)	N/C	N/A
F(1,5)	5.84	9150

Notes: N/C – Algorithm did not converge for this branch
N/A – Not applicable

The mode shapes become more complicated as the branch number increases. A more complicated mode shape would require a greater travel distance to develop than a less complicated mode shape (Chao, 2002). Depending on the travel distance, modes on the F(1,2) branch or higher may not develop.

3.4.2.2 Controlled Frequency Test

The F7 Shaker used in the controlled frequency test is rated to operate over a frequency range of 500 Hz to greater than 20000 Hz, as such, it can generate modes on a wide range of branches. The response of the shaker is nominally defined by the central frequency of the input. As an example, the measured response at the impedance head of the F7 shaker is presented for a central frequency of 14 kHz on Figure 3-7.

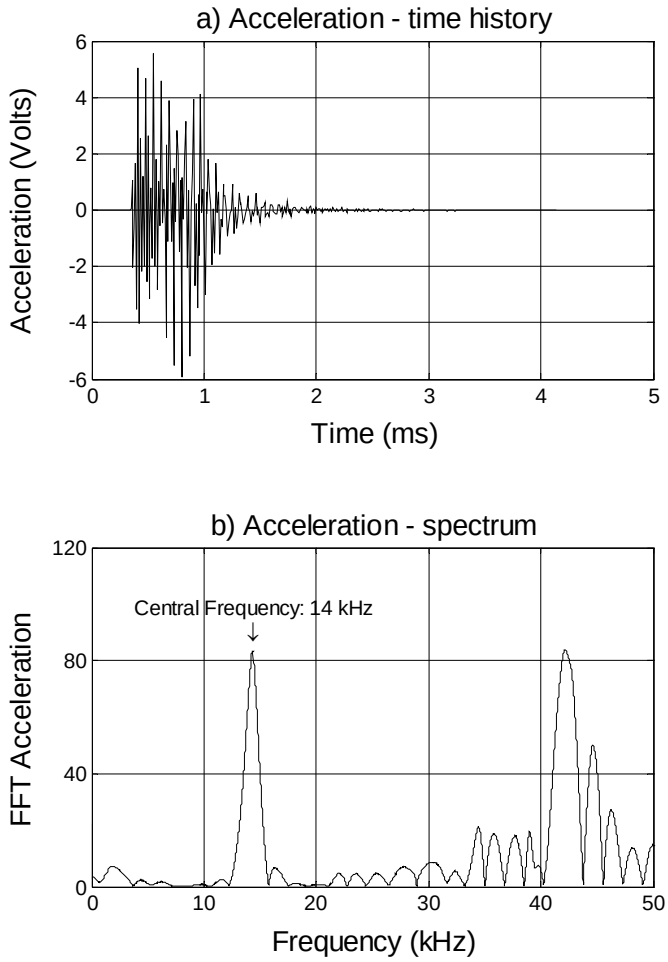

Figure 3-7: F7 piezoelectric shaker, response at 14 kHz

The acceleration spectrum shown on Figure 3-7b shows a large peak at about 14 kHz, which is the central frequency of the input. Another large peak is centered at about 42 kHz with other peaks on the sides of the two large peaks. The peak at 42 kHz is caused by harmonic distortion, which is equipment nonlinearity that manifests itself as odd-numbered harmonics (help files included with LabVIEW program). The frequencies outside the input central frequency are removed by filtering.

Chao (2002) reported that the F7 Shaker does not perform equally at all frequencies. At an input of 14 kHz, the largest peak occurs at the central frequency. A central frequency of 8 kHz is a frequency at which the shaker does not perform as well as 14 kHz, and the 8 kHz response is shown on Figure 3-8.

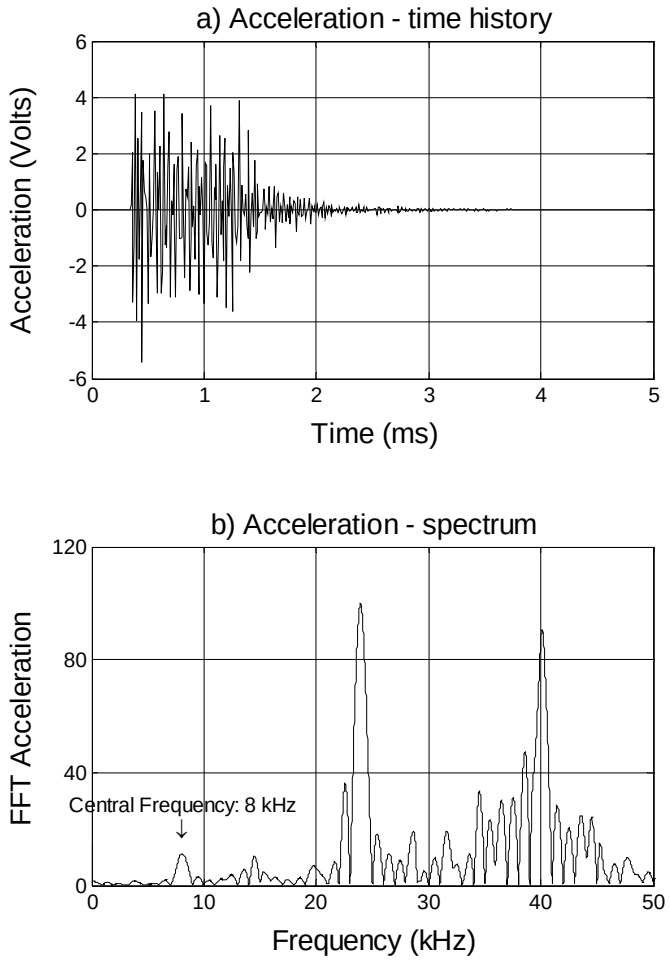

Figure 3-8: F7 piezoelectric shaker, response at 8 kHz

For an input frequency of 8 kHz, the generated wave form contains an 8-kHz component but the components at 24 kHz and 40 kHz have larger Fourier transform coefficients than the desired

frequency of 8 kHz. The peaks at 24 kHz and 40 kHz are the third and fifth harmonic of the input frequency, again corresponding to the effects of harmonic distortion. The peaks at 24 kHz and 40 kHz are removed by digital filtering.

For the input central frequency of 14 kHz, the magnitude of the acceleration spectrum coefficients at 14 kHz and 42 kHz are on the same order. For the input central frequency of 8 kHz, the magnitude of the acceleration spectrum coefficients at 24 kHz and 40 kHz are larger than the magnitude of the acceleration spectrum coefficient at 8 kHz, which reduces the energy at the desired frequency.

The actual performance of the F7 Shaker compared to performance listed in the manufacturer's literature may limit the frequencies at which controlled frequency tests are performed. Tests must be performed over a range of frequencies to determine the best values of central frequency for the pile to be tested.

The pile properties, frequency, nondimensional frequency and the expected branches to be excited in a controlled frequency, as described in Section 3.1.2, are shown on Table 3-9. The branches are identified based on the curves shown on Figure 3-5.

Table 3-9: Frequency, nondimensional frequency and expected flexural branches for prototype piles with $\nu_c = 0.20$

Pile Diameter (mm)	Frequency (Hz)	Shear Wave Velocity (m/s)	Nondimensional Frequency	Branches Expected
254	8000	2300	2.77	F(1,1) through F(1,3)
		2800	2.28	F(1,1) and F(1,2)
	14000	2300	4.86	F(1,1) through F(1,3)
		2800	3.99	F(1,1) through F(1,3)
508	8000	2300	5.55	F(1,1) through F(1,4)
		2800	4.55	F(1,1) through F(1,3)
	14000	2300	9.71	F(1,1) through F(1,6)
		2800	7.98	F(1,1) through F(1,7)

The results presented on Table 3-9 indicate that the controlled frequency test will always generate modes on the F(1,1) branch and may, in theory, generate modes on higher branches. The modes that will propagate depend on the travel distance required for the mode to develop compared to the pile length, as well as the wavelength of the phase corresponding to the mode compared to the pile length. The travel distance required for the mode to develop becomes increasingly important as the branch number increases and the mode shapes become more complicated. The wavelength compared to pile length is important when the central frequency of the input is close to the cutoff frequency for a branch. For modes that do propagate within a pile, identification of the reflected wave may be limited by attenuation.

3.4.3 Phase and Group Velocity

In a typical impact or controlled frequency test, the time history includes a first pass of the wave and one or more returns of a reflected wave. Each mode on each branch will propagate at a given phase velocity and the composite wave will propagate at a group velocity. Tests can be performed with an accelerometer mounted atop the pile or along its side, or they can be performed with multiple accelerometers along the side of the pile.

The phase velocity, c_p, can be calculated from the following relationship

$$c_p = \frac{2Lf_n}{n} \qquad (3\text{-}10)$$

where L is the pile length, n is the harmonic number and f_n is the frequency at harmonic n. Equation 3-10 requires that all harmonics are excited, from the fundamental frequency and the test-specific maximum frequency. The maximum frequency depends on the frequency content of the input and the natural frequencies of the pile. The pile length is used in equation 3-10 because the individual phases correspond to resonant conditions within the pile. The individual phases due to resonance of the pile would not occur in an infinitely long pile, which is the assumed geometry for the theory presented in Section 2.3, but do occur in finite length pile, such as those evaluated as part of this work.

The group velocity, c_g, can be calculated from the following relationship

$$c_g = \frac{2L}{\Delta t} \qquad (3\text{-}11)$$

where L is the distance from the transducer location to the reflection source, so that $2L$ is the travel length, and Δt is the time lag between returns of the wave. Two possible configurations are shown on Figure 3-9

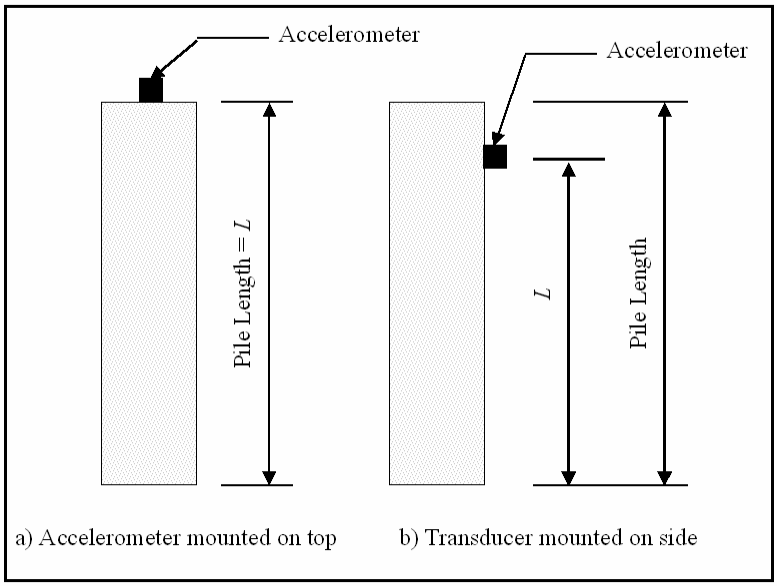

Figure 3-9: Travel distances for waves in a pile with one accelerometer

In Figure 3-9a, the distance from the transducer to the reflection source, L, is the pile length because the transducer is mounted atop the pile. In Figure 3-9b, the distance from the transducer to the reflection source, L, is less than the pile length because the transducer is mounted on the side of the pile, below its top.

The frequency content of the group is determined from the frequency domain representation of the signal. When interpreting the SE Method based on one-dimensional theory, it is assumed that the group travels at the fundamental frequency of the structure. As such, one

need consider only the time domain or the frequency domain, not both. When the group travels at the fundamental frequency, i.e., when the harmonic number is 1, the frequency of the group is determined from the time history as

$$f = \frac{1}{\Delta t} \qquad (3\text{-}12)$$

or the velocity of the group is determined from the frequency domain representation of the signal as

$$c_g = 2Lf \qquad (3\text{-}13)$$

If the group and phase velocities are different from each other, the wave will be dispersive, i.e., energy will be spread about the center of the group, and its velocities will depend on frequency. If the wave propagation is dispersive, the group velocity can still be computed from equation 3-11, but the relationships presented in equations 3-12 and 3-13 do not hold true.

If multiple transducers are mounted along the pile lengths, it may be possible to compute the group velocity based on the first arrival at each transducer using

$$c_g = \frac{\Delta L}{\Delta t} \qquad (3\text{-}14)$$

where ΔL is the transducer spacing, as shown on Figure 3-10, and Δt is the time lag between the first arrival at the two transducers.

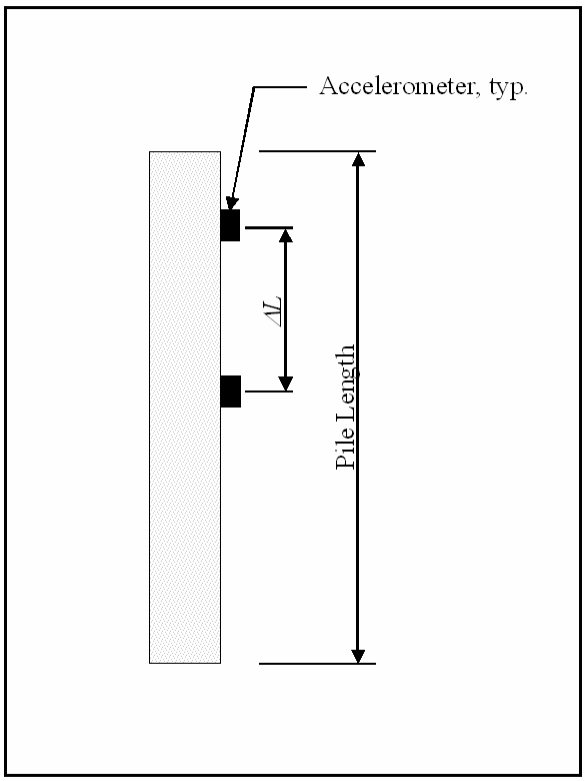

Figure 3-10: Travel distances for waves in a pile with
2 accelerometers mounted on the side of the pile

The transducer spacing is measured when the test equipment is set up, and the first arrival is determined from the acceleration – time histories at each accelerometer.

3.4.4 Attenuation

The three-dimensional wave propagation theory in Chapter 2 assumes that geometric attenuation occurs as energy leaks into the surrounding soil. This attenuation is a function of the

imaginary part of the wavenumber, ξ, and an expression for attenuation was derived in section 2.3.7. The amplitude ratio of the propagating stress wave as a function of pile radius, *a*, travel distance, ΔL, and nondimensional wavenumber, ξ_a can be expressed as

$$\frac{u_2}{u_1} = 10^{-\left(\frac{\mathrm{Im}(\xi_a)\Delta L}{2.3062a}\right)} \qquad (3\text{-}15)$$

Equation 3-15 applies to test configurations in which the same wave is measured at two different positions or cases in which the incident and reflected stress wave are measured at the same position. When the same stress wave is measured at two different positions, u_1 is the amplitude of the stress wave at the transducer closer to the source, u_2 is the amplitude of the stress wave further from the source, and ΔL is the transducer spacing. When an incident and reflected stress wave are measured at the same position, u_1 is the amplitude of the incident stress wave, u_2 is the amplitude of the reflected stress wave, and ΔL is twice the distance from the transducer position to the sources of reflections.

The amplitude ratios defined by equation 3-15 have been calculated for hypothetical piles of various lengths. The travel distance for the analysis is twice the pile length. The sample values were computed for concrete with a Poisson's ratio of 0.20 embedded in soft/loose soil with a Poisson's ratio of 0.30. The normalized properties for soft/loose soil are

- Shear modulus ratio: 325
- Density ratio: 1.33

The frequency equation was solved by the procedure outlined in Section 2.3.4, to determine the nondimensional wavenumber, which provides one of the required input values for equation 3-15. The frequency equation was solved for all active branches at nondimensional frequencies of 0.5, 3, and 6. The nondimensional frequency of 0.5 represents an impact test and the nondimensional frequencies of 3 and 6 represent controlled frequency tests. The nondimensional frequency – nondimensional wavenumber results are presented on Table 3-10.

Table 3-10: Nondimensional frequency – nondimensional wavenumber results for Concrete pile with $\nu_c = 0.20$ and embedded in soft/loose soil

Nondimensional Frequency	Branch	Wavenumber	
		Real Part	Imaginary Part
0.5	F(1,1)	0.917393064	0.07983299
3	F(1,1)	3.432594461	0.123899444
	F(1,2)	1.769018195	0.05672334
	F(1,3)	1.125942742	0.130311163
6	F(1,1)	6.583977897	0.177681652
	F(1,2)	5.684451891	0.052720392
	F(1,3)	4.647352279	0.099304299
	F(1,4)	3.096782745	0.093913477
	F(1,5)	0.804597847	0.124567987

The amplitude ratio is computed by equation 3-15 using the imaginary part of the wavenumber on Table 3-10 for a 254-mm diameter example pile. The amplitude ratios for pile lengths are presented on Table 3-11. The travel distance, ΔL, in equation 3-15 is twice the pile length.

Table 3-11: Amplitude ratio of stress waves as a function of travel distance

Nondimensional Frequency	Branch	Amplitude ratio (%) computed from equation 3-13 as a function of travel distance (m)				
		2	4	6	8	10
0.5 (Impact)	F(1,1)	28.5	8.1	2.3	0.7	0.2
3	F(1,1)	14.3	2.0	0.2	0.04	0.006
	F(1,2)	41.0	16.8	6.9	2.8	1.2
	F(1,3)	12.9	1.7	2.1	0.03	0.004
6	F(1,1)	6.1	0.4	0.02	0.001	8.5 E-5
	F(1,2)	43.7	19.1	8.3	3.6	1.6
	F(1,3)	21.0	4.4	0.9	0.2	0.04
	F(1,4)	22.8	5.2	1.2	0.3	0.06
	F(1,5)	14.1	2.0	0.3	0.04	0.006

For the values shown on Table 3-11, the attenuation of the F(1,1) branch increased, as noted by the smaller amplitude ratio in the table, as the nondimensional frequency increased. The attenuation was smallest on the F(1,2) branch at both the nondimensional frequency of 3 and 6. In the evaluation of experimental data, one must consider the mode shape in addition to the attenuation. Reflections would be identified in modes with large normalized displacements and low attenuation values. As the travel distance increases, the amplitude of the reflected stress wave decreases. The decrease in signal amplitude limits the ability of the reflection to be identified. All sensors have a lower limit below which the signal will not excite the sensor. All signals contain noise in addition to the stress wave. When the amplitude of the reflected wave is on the same order as the amplitude of the noise, the signal cannot be identified. The quality of a signal is usually expressed in terms of the signal to noise ratio (SNR), which is the ratio of the signal power to the noise power (Porat, 1997). The SNR can be expressed as a ratio or in dB. The SNR can be estimated by

1. Assume a function that describes the noise (typically Gaussian).
2. Compute the noise power based on the assumed distribution.
3. Compute the signal power from the measured response.
4. Compute the SNR as the ratio of the signal power to the noise power.

A simplified method of computing the SNR, as applied to test results from NDE of deep foundations, is

1. Compute the mean amplitude of the recorded response during a pass of the stress wave (assume this is the signal).
2. Compute the mean amplitude of the recorded response between passes of the stress wave (assume this is the noise).
3. Compute the SNR as the amplitude of the signal from step 1 to the amplitude of the noise in step 2.

As an example, consider a stress wave propagating in the pile for which the data on Table 3-11 were developed. If the nondimensional frequency is 0.5, which corresponds to an impact test, and the measured response at the first pass is 1 V. If the pile is 2 m long (travel distance = 4 m), the amplitude of the reflected wave is 0.08 V. If the average noise amplitude is 0.02 V, the first reflection can be identified because its amplitude is greater than the noise amplitude. A second reflection has a travel distance is 8 m., which is equivalent to the wave propagating in a 4 m pile. The amplitude ratio for a 4 m pile from the data shown on Table 3-10 is 0.07%. The amplitude of the second reflection is 0.0007 V based on the response of the first pass as 1V. If the noise level is 0.02V, the second reflection could not be identified because its amplitude is less than the noise amplitude.

3.5 Data Reduction

3.5.1 Filtering of Data

All acquired signals contain noise and unwanted signals. Some sources of noise are errors in the Analog to Digital Conversion process, electronic noise in the hardware, and ambient vibrations of the structure being evaluated. Unwanted signals can consist of harmonics of the frequency of the test, vibrations caused by the natural frequency of the shaker (in the case of a controlled frequency test), and the natural frequency of the transducers. If the frequency content of the noise falls outside the frequency range of interest for the test, some or all of it can be removed by digital filtering. Digital filters are classified by their impulse response and their magnitude response. Within each impulse response class, there are many filter types, each with different performance characteristics. Each filter is governed by a different equation and they are typically named for the person who first proposed the filter. The basic procedure for digital filtering of data is

1. Convert the unfiltered data to the frequency domain.
2. Compute the frequency response of the digital filter.
3. Multiply the results of Step 2 by the results from Step 1.
4. Convert the results from Step 3 to the time domain.

Digital filters are classified as either finite impulse response (FIR) or infinite impulse response (IIR), based on their impulse response performance (Ifeachor and Jervis, 2002). The FIR Filters have a linear phase relationship, are stable, and are easier to design than IIR Filters. The difficulty with FIR Filters is that they require the calculation of a large number of

coefficients. IIR Filters are conditionally stable, but the parameters can be adjusted to ensure stability. IIR filters are more difficult to design than FIR Filters, but all filtering will be done with preprogrammed functions rather than a new type of filter. The main drawback of IIR filters is that the phase response is nonlinear. The digital filters to be used in this investigation are IIR Filters.

Each filter requires a cutoff frequency or a vector of low cutoff frequency and high cutoff frequency and is then classified by its magnitude response. The four types of magnitude response are lowpass filter, highpass filter, bandpass filter, and bandstop filter, as presented on Table 3-12.

Table 3-12: Types of filter based on magnitude response

Magnitude Response Type	Low Cutoff Frequency (f_L)	High Cutoff Frequency (f_H)	Response Characteristics
Lowpass	Yes	No	Passband: frequency (f) < f_L Stopband: f > f_L
Highpass	No	Yes	Passband: f > f_H Stopband: f < f_H
Bandpass	Yes	Yes	Passband: f_L > f < f_H Stopband: f < f_L and f > f_H
Bandstop	Yes	Yes	Passband: f_L < f > f_H Stopband: f > f_L and f < f_H

An ideal filter would have a magnitude response of one within the passband and a magnitude response of zero in the stopband and the transition from passband to stopband occurs at the cutoff frequency. IIR filters may have a magnitude response that matches the magnitude response of an ideal filter over part of the frequency range but not all of the frequency range. All

IIR filters will have a transition band between the passband and stopband. The three most common types of IIR Filters are the Butterworth, Chebychev, and Inverse Chebychev (also called the Chebychev II). The key features of the three filter types are presented on Table 3-13.

Table 3-13: Key features of IIR digital filters

Properties	Filter Type		
	Butterworth	Chebychev	Inverse Chebychev
Magnitude response in passband	Monotonic	Equiripple	Monotonic
Magnitude response in stopband	Monotonic	Monotonic	Equiripple
Rolloff in transition band	Long	Short	Short

The properties listed on Table 3-13 are presented graphically on Figure 3-11. Filter coefficients were created for lowpass filters of order 6 with a Nyquist frequency of 50 kHz and a cutoff frequency of 10 kHz.

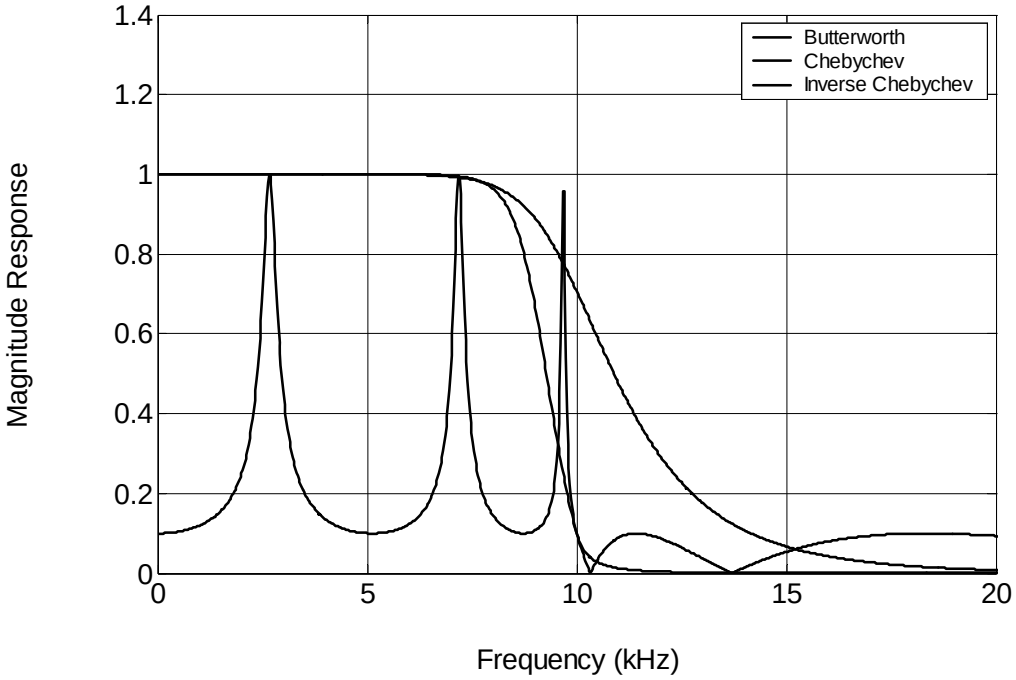

Figure 3-11: Typical magnitude response for different IIR filters

For the Butterworth Filter, the response is flat (monotonic) in both the passband and the stopband. In the example on Figure 3-11, the transition band starts at about 7 kHz and ends at about 19 kHz, for a transition band width of 12 kHz. For the Chebychev Filter, the magnitude response ranges from about 0.1 to 1.0 in the passband and is uniformly zero in the stopband. The transition band starts at a frequency of about 9.5 kHz and ends at a frequency of about 12 kHz, for a transition band width of 2.5 kHz. For the Inverse Chebychev Filter, the magnidtude response is 1 in the passband and ranges from 0 to 0.1 in the passband. The transition band starts at about 7.5 kHz and ends at about 10.5 kHz for a bandwidth of 3 kHz.

The Chebychev filter is used when narrow transition bandwidth is the primary concern. The Butterworth filter and Inverse Chebychev filter are used when monotonic response is required in the passband.

Each filter has a phase response in addition to the magnitude response. The phase response of the filter causes frequency dependent distortion of the signal, which manifests itself as time delays in the filtered signal compared to the unfiltered signal (Porat, 1997). The group and phase delay are calculated by the following procedure (Ifeachor and Jervis, 2002)

1. Consider a filter function that has the following frequency response, H(ω)

$$H(\omega) = H(e^{i\omega}) \tag{3-16}$$

2. Compute the phase angle, Θ(ω), of the frequency response

$$\Theta(\omega) = \arctan\left(\frac{\mathrm{Im}(H(\omega))}{\mathrm{Re}(H(\omega))}\right) \tag{3-17}$$

3. Compute the group delay, gd(ω)

$$gd(\omega) = -\frac{\partial\Theta(\omega)}{\partial\omega} \tag{3-18}$$

4. Compute the phase delay, pd(ω)

$$pd(\omega) = -\frac{\Theta(\omega)}{\omega} \tag{3-19}$$

The frequencies, ω, are defined in radians per second but can be converted to Hz by dividing ω by 2π. The phase angle must be unwrapped in computing the phase delay. An example of the group and phase delay for each filter type is presented on Figure 3-12.

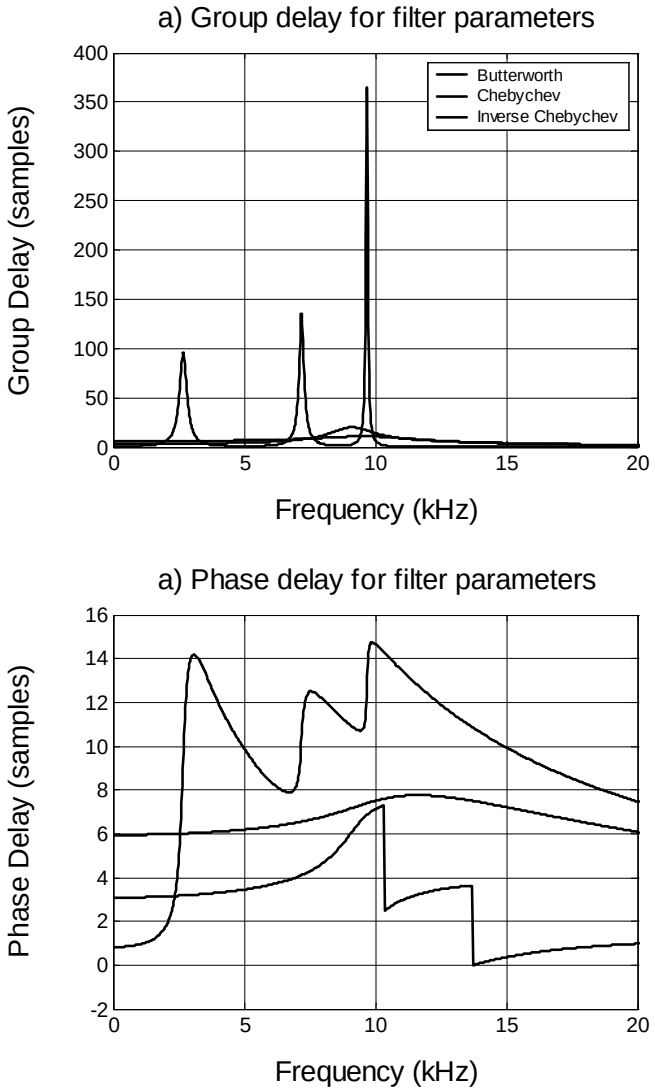

Figure 3-12: Filter behavior of Butterworth, Chebychev, and Inverse Chebychev filters for sampling frequency of 100 kHz, cutoff frequency of 10 kHz, and filter order of 6 ripple coefficient of 20 dB for Chebychev and Inverse Chebychev filters

The results presented on Figures 3-10 and 3-11 are examples of one combination of filter parameters and the effects of those parameters on a signal. For the analysis of test results, the cutoff frequencies and filter order will be different for different test types, as they have different frequency contents. Recommended filter types and parameters are presented in Chapter 5 for the lateral impact test and in Chapters 6 and 7 for the controlled frequency test.

3.5.2 Mode Identification Method

The stress waves generated during NDE of deep foundations will generally contain multiple frequencies. In the case of the impact tests, the input force has a broad bandwidth and the stress wave will contain all natural frequencies of the pile that fall within the bandwidth of the input force. In the controlled frequency test, the input contains a bandwidth centered about the input value of central frequency, but the shaker may generate other frequencies and each frequency may generate modes on more than one branch.

In conventional analysis of the data from NDE of deep foundations, the return of the stress wave is identified from peaks in the time history and the frequency content is identified from the FFT of the time history. For dispersive waves, i.e., one in which the frequency content of the stress wave changes with time, the return of a stress wave with a specific frequency content may not be identifiable by conventional time and frequency analysis. To identify the return of the stress wave, one must use an analytical method that accounts for the time-varying frequency content of the stress wave. The mode identification method (Chao, 2002) was proposed as a method to identify the reflection of a mode of the stress wave on a specific branch and is part of the analysis of controlled frequency results.

The mode identification method is implemented by

1. determininge the time-varying frequency content of the recorded time history,
2. converting from time to velocity, and
3. comparing the experimental values of velocity to theoretical values to identify the modes.

The details of the mode identification are presented herein. The time-varying frequency content is determined by numerical implementation of the Gabor transform through the Short Time Fourier Transform (STFT). The time is converted to velocity from a predefined travel distance and initial time. The experimental values are compared to the theoretical values by generating a contour plot of frequency as a function of velocity and superimposing numerically-determined group velocity – frequency curves on the contour plot.

One set of artificial data is analyzed by the STFT to illustrate the parameters required to compute the transform. The contour plot of frequency as a function of velocity is applied to the same set of data based to illustrate that procedure. The controlled frequency results presented in Chapters 6 and 7 are analyzed by the mode identification method described herein.

3.5.2.1 Calculation of Short Time Fourier Transform

The Short Time Fourier Transform (STFT) algorithm was proposed in by Gabor (1946) as a method to analyze signals in which the frequency content changes as a function of time. The procedure for analyzing a signal by the STFT is

1. Isolate a portion of the signal with a window function.
2. Perform a Fourier Transform on the windowed portion of the signal.
3. Offset the window function by specified time (or number of samples)
4. Repeat Steps 1 and 2 with the new window position
5. Repeat Steps 3 and 4 until the entire signal has been analyzed.

The output is an m by n matrix of complex-valued amplitude coefficients in Fourier Space. The array will have n-rows with each row corresponding to a position on the frequency axis and m-columns with each column corresponding to position on the time axis. The Gabor Transform is too computationally intensive to perform by hand and, until recently, was too computationally intensive to regularly perform by computer.

The STFT is now available as a standard function in LabVIEW ™ and the Matlab ® Signal Processing toolbox. Matlab ® will be the software used to analyze test results presented herein.

The Matlab ® command is “specgram” and has a variable number of input arguments and output arguments. The required output argument is the complex-valued matrix of FFT coefficients and the required input argument is the input signal which, in the case of data collected from NDE of deep foundations, will be real-valued. Optional input arguments are the number of points to be considered in the Fourier Transform (which is also the window length), the sampling frequency, the window type, and the number of samples by which the next window will overlap the current window. When the window length and sampling frequency are provided, the additional output arguments of the frequency array and time array can be obtained. The offset between adjacent windows is the window length minus the number of points by which the windows overlap.

The frequency array, if computed, ranges from DC to the Nyquist Frequency. The frequency spacing is the sampling frequency divided by the number of points in the discrete Fourier transform as implemented by the Fast Fourier Transform (FFT) algorithm. The time array, if computed, ranges from 0 to the start of the final window, and the time spacing is the start of the final window divided by the number of times the window is shifted. The start of the last window is the duration of the signal minus the number of points in the Fourier Transform. It should be emphasized that the FFT is performed with the number of points in the window, not the number of points in the total signal; consequently, the resolution of the STFT will be less than the resolution of an FFT performed on the entire signal. The tradeoff in performing the joint time frequency analysis with the STFT is in obtaining enough accuracy in the time domain while still obtaining the required resolution in the frequency domain.

3.5.2.2 Signal Analysis by Joint Time Frequency Analysis

Examples of joint time frequency analysis of artificial signals are presented to illustrate the relationship among the time domain, frequency domain, and Spectrogram I, as well as the numerical implementation of the STFT in Matlab ®. The sampling frequency is assumed to be 100 kHz, which is the same as the sampling frequency to be used in some of the controlled frequency tests presented in Chapters 6 and 7. All calculations were performed with the default Hanning window.

The application of the STFT is illustrated by analyzing an artificial signal, called *S*, that is 1024 points long and was created with a time increment of 0.01 ms. The array contains a 5 kHz tapered sine wave, *s*, for which the maximum value of one occurs at 4 ms, and is zero at the ends, which are at 2.42 and 5.42 ms. The time history and frequency domain representation are presented on Figure 3-13. The maximum Fourier Transform Coefficient occurs at 5 kHz. The ripples on the side lobes of the peak occur because the time history is not centered at zero.

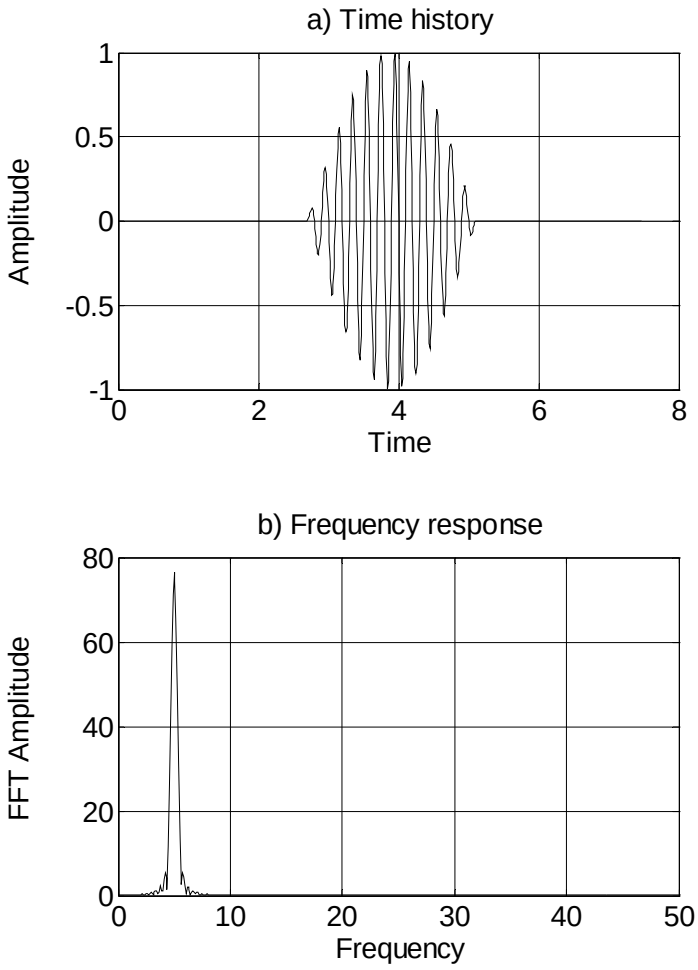

Figure 3-13: Modulated 5 kHz sine wave, time and frequency representation

The signal shown on Figure 3-13 was analyzed by the STFT with the following parameters

- Window Length: 128 samples
- Offset between adjacent windows: 64 samples
- Window Type: Hanning

The Hanning window, w, is defined numerically as

$$w[k+1] = 0.5\left(1-\cos\left(\frac{2\pi k}{n-1}\right)\right) \qquad (3\text{-}20)$$

where k is the point on the array $k = 0, 1, \ldots n$, and n is the window length in samples. The signal to be analyzed by the STFT is an array of N samples, and n must be less than or equal to N. The window function defined by equation 3-20 is incorporated into an array, W, which is the window function to be applied to the array that defines the signal. The array, W, is initially defined as

$$W[K] = \begin{cases} w[k], & 0 \le K \le n-1 \\ 0, & n-1 \le K \le N \end{cases} \qquad (3\text{-}21)$$

where K is the point in the array W. The array, W, is multiplied S, and FFT of the product is computed. The window is offset a prescribed number of samples, m, and W is recomputed as

$$W[K] = \begin{cases} 0, & 0 \le K \le m \\ w[k], & m \le K \le m+n \\ 0, & m+n \le K \end{cases} \qquad (3\text{-}22)$$

The array, W, is multiplied by the signal by the time history of the signal and the FFT of the window is computed. The process of shifting m, computing W, multiplying it by S, and computing the FFT is repeated until S is completely analyzed. The results of the STFT calculations are illustrated by considering the following combinations of S and W

1. When *m* = 0, *W* is nonzero between 1 and 128 samples, but *S* is zero over the entire interval. The product of *W* and *S* is therefore zero.
2. When *m* = 300 samples, *W* is nonzero between 301 and 428 samples, and *S* is nonzero over the entire interval. The output array from the product of W and *S* is therefore nonzero.
3. When *m* = 300 samples, *W* is nonzero from 301 to 428 samples, and *S* is zero over the entire interval. The output array from the product of W and *S* is therefore zero.
4. When m = 200 samples, *W* is nonzero from 201 to 328 samples. The nonzero part of *S* begins at 242 samples. The output array from the product of *W* and *S* is nonzero though not as large as in case 2.
5. When m = 500 samples, *W* is nonzero from 501 to 628 samples. The nonzero part of *S* ends at 542 samples. The output array from the product of *W* and *S* is nonzero though not as large as in case 2.

The time history and joint time frequency representation are presented on Figure 3-14.

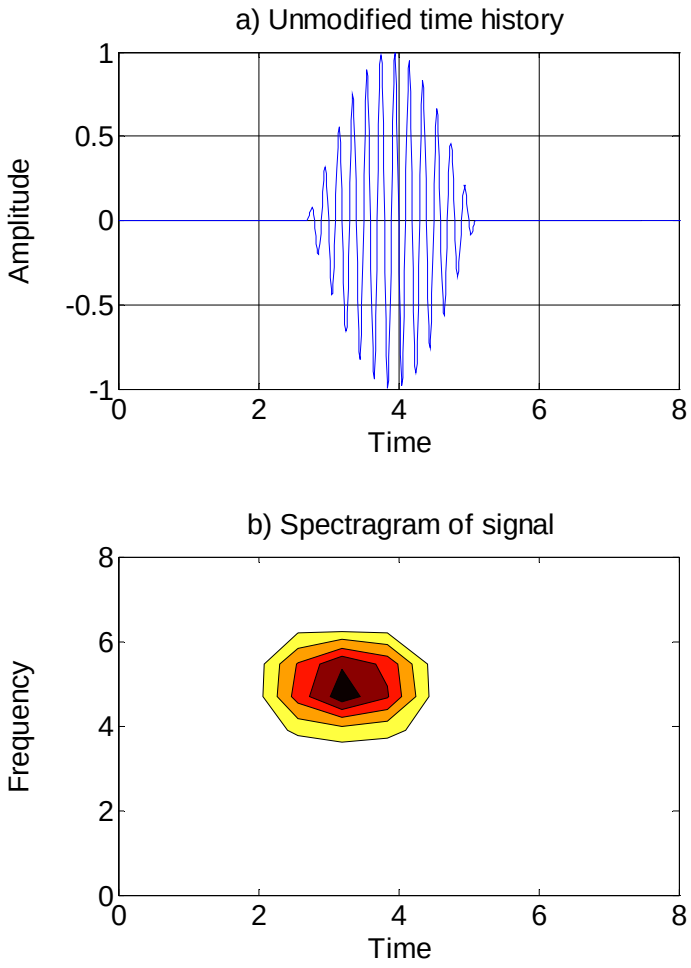

Figure 3-14: Modulated 5 kHz sine wave, time history and Spectrogram I

The contour plot shows the magnitude of the complex-valued FFT coefficients. The maximum value in the time domain occurs at 4 ms, but the largest value of the FFT coefficient occurs at a time value of approximately 2 ms. The discrepancy occurs because the time array output from the spectrogram algorithm defines the start of the window, not the center of the window.

To have the time values on the time history and contour plot match, either the time history or the time array for the JTFA must be adjusted. The former is selected. The adjusted time history and joint time frequency domain representation are presented on Figure 3-15.

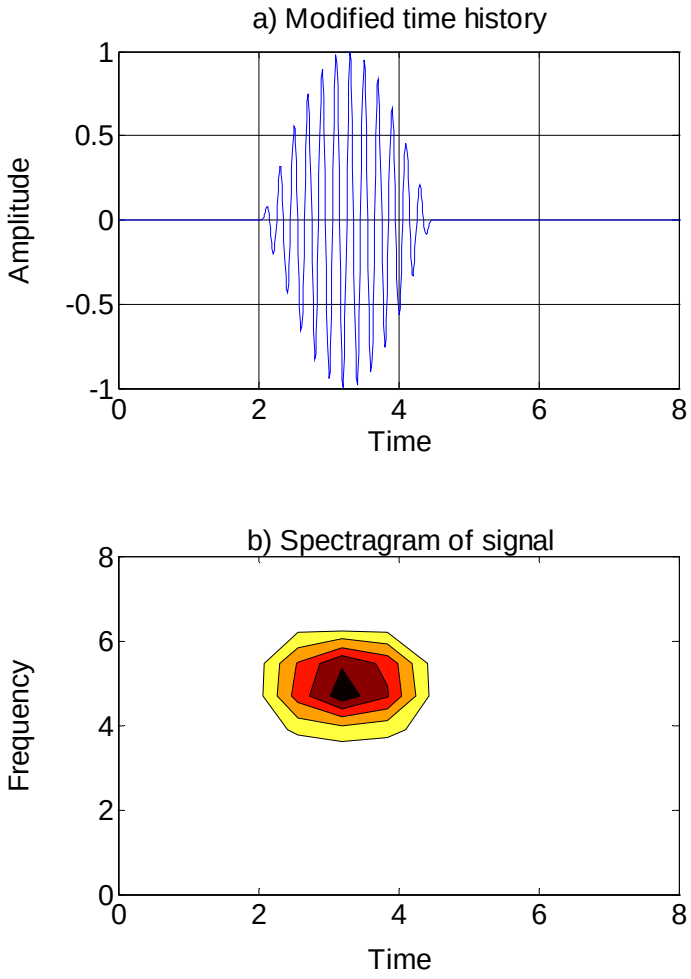

Figure 3-15: Modulated 5 kHz sine wave, time history and Spectrogram I

The time array has been recalculated such that half of the window length has been subtracted from the signal. The maximum value of the modified time history now matches the center of the largest FFT coefficient of the joint time frequency domain representation of the signal. All remaining analysis of the artificial signals and real data are performed on modified time histories.

An example of JTFA applied to a signal with a “First Pass” and two “Returns” of a stress wave will now be presented. Each “Pass” of the stress wave is the same modulated sine wave presented on Figure 3-13. The starting position for the first pass is centered at 3.27 ms, and the two returns are centered at 6.27 ms and 9.27 ms for the first and second returns, respectively. The duration of the entire signal is 2.048 ms. The time history and frequency domain representation of that signal are presented on Figure 3-16.

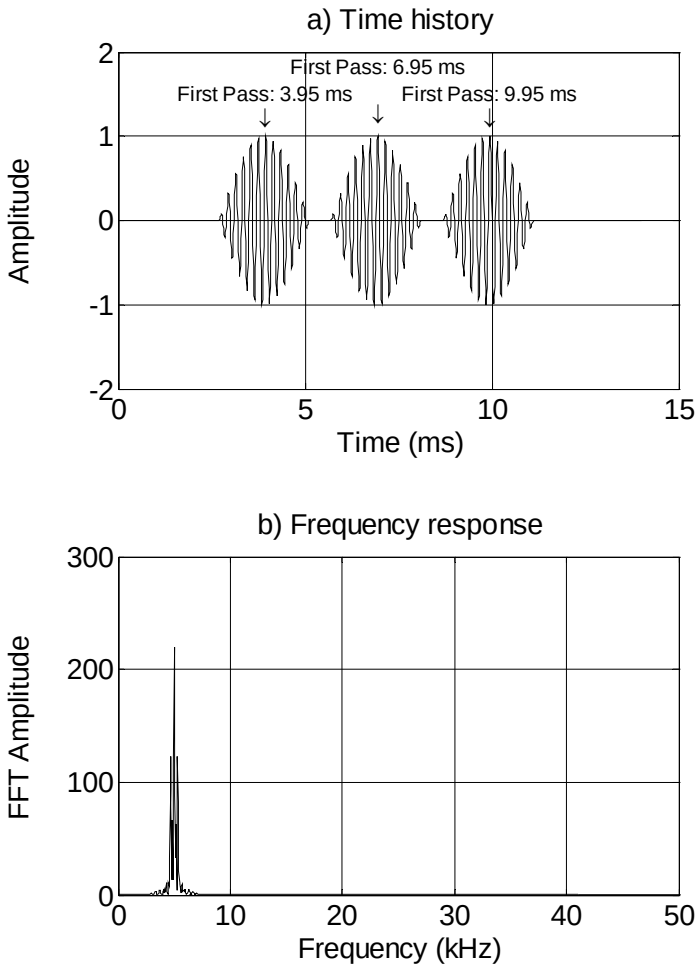

Figure 3-16: Multiple modulated 5 kHz sine waves, time and frequency representation

The frequency domain representation of the signal is centered at 5 kHz, but the ripples in the side lobes are larger than those shown in Figure 3-13. The larger ripples are caused by the multiple returns of the signal.

Figure 3-17 shows the modified time history and Spectrogram I of the time history.

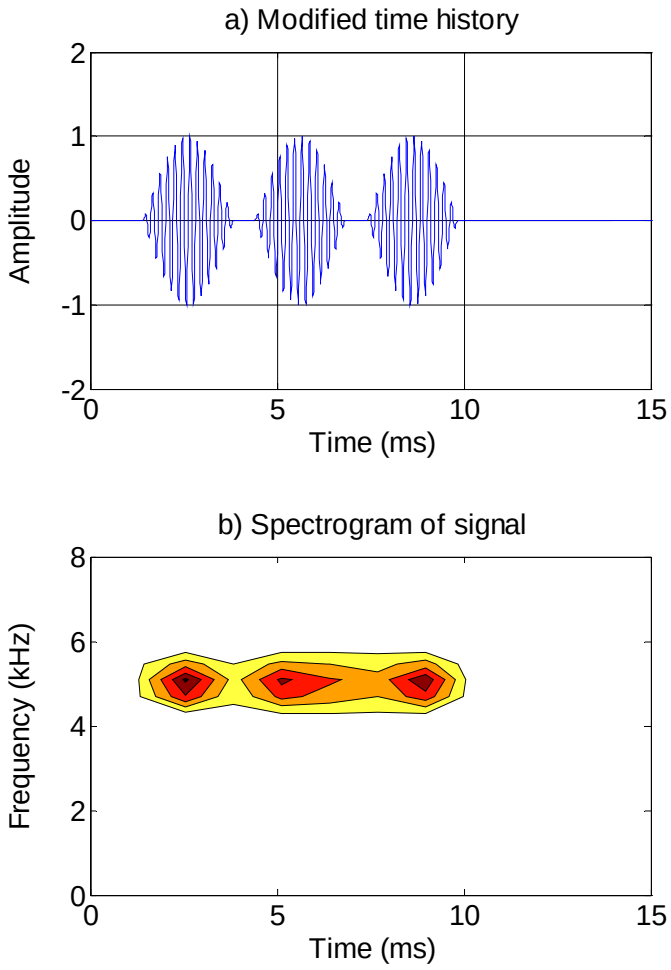

Figure 3-17: Multiple modulated 5 kHz sine waves, time history and Spectrogram I

The contour plot generated by the STFT shows three distinct peaks, each corresponding to the modulated sine waves on the time history.

The STFT parameters were selected to illustrate the applicability of the STFT to identify reflections in a signal that has a time-varying frequency content. To analyze the test results from

NDE of deep foundations, the window length and offset time must be selected to provide the desired resolution in both the time domain and frequency domain, based on the expected time lag between successive returns of the stress wave and the frequency content of the stress wave.

3.5.2.3 Reflection identification by Joint Velocity Frequency Analysis

In NDE of deep foundations, the goal of the data processing is to identify the return of the stress wave and either to compute the propagation velocity or the depth to a reflection source. The results to be presented in this thesis are from tests performed on prototype piles of known length, in which case the goal of the data interpretation is to determine the propagation velocity and to compare that experimentally-determined propagation velocity to a theoretical value. The method to identify reflections will be to convert the time ordinate of the joint time frequency spectrum of the signal to a velocity array.

1. Obtain the time history of the input and response.
2. Transform the measured response to the spectrogram in the joint time-frequency domain by applying the STFT algorithm. This spectrogram is represented as Spectrogram I.
3. Convert the time ordinate, t, of Spectrogram I to the velocity ordinate by

$$c_k = \frac{L}{t_k - t_0} \qquad (3\text{-}23)$$

   where L is the predetermined travel distance, c_k is the computed velocity and t_k is the time at column k of the STFT array, and t_0 is the initial time corresponding to the start of the wave. The output from this step is a contour plot of frequency as a function of velocity.
4. Superimpose the numerically-determined group velocity –frequency curves for the branches that are excited by the input on the contour plot generated in Step 3. This plot is called Spectrogram II.

5. Identify the branches on which modes may be active from the intersection of the numerically-determined group velocity – frequency curves and the contours with large FFT coefficients on Spectrogram II.
6. Identify a range of propagation velocity values , c_{max} and $c_{min}$from Spectrogram II.
7. Compute a range of time values from

$$t_{\min} = \frac{L}{c_{\max}} + t_0 \qquad (3\text{-}24)$$

$$t_{\max} = \frac{L}{c_{\min}} + t_0 \qquad (3\text{-}25)$$

where t_{min} is the earliest time at which the wave group is expected to pass the accelerometer and t_{max} is the latest time at which the wave group is expected to pass the accelerometer.
8. Identify the time values computed by equations 3-24 and 3-25 on the acceleration – time history of the pile response.
9. Identify the wave group that falls within the time range from Step 7.
10. Identify the center of the wave group from Step 9. The center of the wave group is designated as the return time, t_r.
11. Compute the group velocity, c_g by

$$c_g = \frac{L}{t_r - t_0} \qquad (3\text{-}26)$$

For tests in which the shaker is mounted on top of the pile, the travel distance is twice the depth to the reflection source below the top of the pile. For tests in which the shaker is mounted on the side of the pile, the travel distance is the distance from the shaker to the reflection source plus the distance from the reflection source to the transducer location. The initial time defined in Step 3 can be the input at the shaker or the first pass of the stress wave, with the former as the selected option. The input at the shaker was selected because identification of the first pass may be difficult. The numerical values were calculated for a pile of infinite length, in which case the signal develops as soon as the load is applied. The actual piles are of finite length, in which case a finite time is required for the stress wave to develop.

The mode identification procedure indicates whether modes are excited on a particular branch but the resolution of the STFT is not adequate to compute the velocity. To compute the actual velocity, one must identify the wave packet that corresponded to the identified reflection and compute the actual velocity.

To illustrate the procedure, the mode identification procedure is applied to the artificial signal presented on Figure 3-16. The time domain was created with a time lag of 3 ms between successive returns of the signal. The JVFA Spectrogram was created with a travel distance of 6 meters, which corresponds to a propagation velocity of 2000 m/s.

The results of the Mode Identification Method are presented on Figure 3-18.

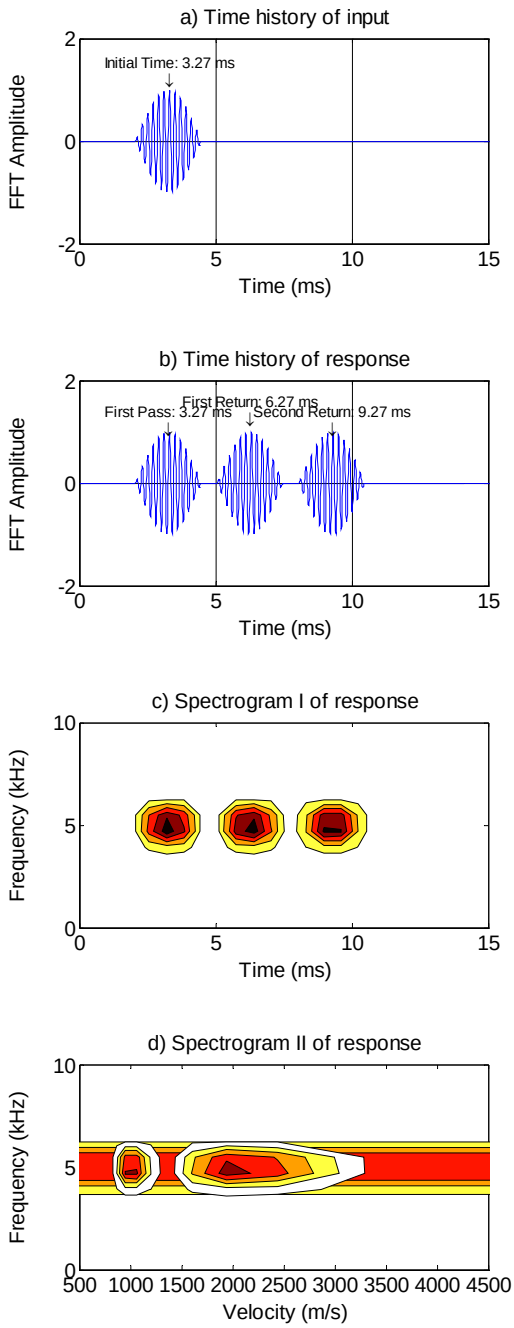

Figure 3-18: Mode identification method applied to artificial data

The center of the input occurs at 3.27 ms and the center of the first pass of the wave occurs at 3.27 ms. The time history contains two returns of the stress wave, one centered at 6.27 ms and the other at 9.27 ms.

In the JTFA Spectrogram, the three peaks were centered at 3.24 ms, 6.32 ms, and 9.27 ms, compared to 3.27, 6.27, and 9.27 ms for the time history. The frequency ordinate was centered at 4.96 kHz, 4.94 kHz, and 4.76 kHz, compared to 5 kHz for the actual signal. The frequency resolution in the STFT is 781.25 Hz, which places all average frequency values for the JTFA within one point on the STFT frequency axis of the actual frequency value.

One set of reflections was identified with a velocity of 2000 m/s and a second set of reflections was identified with a velocity of 1000 m/s. The reflection identified with a velocity of 2000 m/s corresponds to the actual return of the wave. The reflection identified with a velocity of 1000 m/s corresponds to the second reflection of the wave. It still has a velocity of 2000 m/s but its travel distance is twice the travel distance of the first reflection. The second reflection should be excluded from a spectrogram based on a 6-meter travel distance. Either the graph limits should be adjusted to exclude the second reflection or the time history should be windowed to remove the second reflection from the signal.

3.5.3 Uncertainty Analysis

When one repeatedly measures a property, the measured value will vary due to, among other things, operator error, equipment performance and limitations, and environmental effects. If the measured properties are input parameters in the calculation of another property, the variability in the measured properties (inputs) results in variability of the calculated property (output). The development of an experimental procedure requires one to quantify the variability in the input parameters and output properties and, ultimately, confidence in the results.

The most direct method of evaluating test results is to perform a large number of tests and plot a histogram of the results. If enough tests are performed, the variability in the results typically follows the normal distribution (Holman, 2001). The limitation of this method is that a minimum of 30 tests are required to establish an acceptable mean and standard deviation (Montgomery & Runger, 2003).

The uncertainty in experimental results can be evaluated by calculating the output property with the combination of input parameters that produce the largest and smallest possible values of the output property. Depending on the number of measurements taken and the range of measured values, the calculated range of output values may be unrealistically large or unrealistically small. Consider two possibilities.

1. The largest or smallest measured input value falls on a portion of the normal distribution curve for which the probability of a larger or smaller value is very low, i.e., it is an outlier, or
2. The largest or smallest measured value falls on a portion of the normal distribution curve for which the probability of a larger or smaller value is high.

For Case 1, calculating the range of the output value with these input parameters would produce an unrealistically large range in output values. For Case 2, calculating the range of the output value with these input parameters could produce an unrealistically small range in output values. Furthermore, the probability is low that a single test will contain every input parameter required to produce the extreme values of the output property (Kline & McClintock, 1953).

Kline & McClintock (1953) proposed a method of quantifying the uncertainty in experimental data based on the uncertainty of the input parameters and the sensitivity of the output value to the input parameters. The output property is a function *F*, which is a function of several input parameters such that

$$F = f(x_1 x_2 x_3 ... x_n) \tag{3-27}$$

where x_1 through x_n are the input parameters, and any arbitrary input parameter is x_i. The uncertainty in *F*, w_F, is computed as

$$w_F = \left[\left(\frac{\partial F}{\partial x_1} w_1 \right)^2 + \left(\frac{\partial F}{\partial x_2} w_2 \right)^2 + \left(\frac{\partial F}{\partial x_3} w_3 \right)^2 + ... + \left(\frac{\partial F}{\partial x_n} w_n \right)^2 \right]^{0.5} \tag{3-28}$$

where w_i is the uncertainty in the i^{th} input parameter and the partial derivatives represent the sensitivity of *F* to each input parameter.

The uncertainty of the input parameters can be determined by measuring each input parameter several times and applying a statistical method of evaluating the uncertainty of the input parameters through a tolerance interval (Montgomery & Runger, 2003). The tolerance interval is

$$m - ks, \quad m + ks \tag{3-29}$$

where m is the mean value, k is a constant which is a function of the tolerance interval, and s is the standard deviation. The tolerance interval is the probability of a single measurement falling within that range.

The uncertainty analysis method proposed by Kline & McClintock (1953) will be applied to the results of a sonic echo test performed on a concrete prototype pile of known length. The bar wave velocity, c_B, is computed as

$$c_B = \frac{2L}{\Delta t} \tag{3-30}$$

where L is the prototype pile length and Δt is the travel time. If the prototype pile were 2000 mm long and the travel time were 1 ms, the bar wave velocity would be 4000 m/s. The actual length of the prototype pile can vary depending on the measurement location and environmental conditions. The measured length of the prototype pile can vary based on the measuring equipment and environmental conditions. The actual travel time can vary as the prototype pile length changes. The measured travel time can vary depending on the hardware and software used to measure the response. Furthermore, identification of travel time can be obscured by noise in the electronic data acquisition system.

The length of a prototype pile that is nominally 2000 mm long is typically measured with a steel tape, assuming it is under traction-free conditions. The conditions of the concrete surfaces, temperature of the concrete, resolution of the steel tape, and temperature of the steel tape can all contribute to the length measured as part of any individual test.

The top and bottom surfaces of the finished prototype pile would be plane and level within a certain tolerance, but they would not be perfectly plane and level. The deviations from plane and level conditions of the top and bottom surfaces mean that the prototype pile length will be different when measured at different locations around the surface of the pile. Furthermore, the finished surface may contain imperfections that cause an even larger deviation in prototype pile length than the deviations from plane and level conditions. The concrete would be cast at a certain temperature. If the concrete temperature at the time of the test differed from the temperature at the time the prototype pile was cast, its length would be different.

The steel tape used to measure that prototype pile length would read to 1 or 2 mm, and would have been fabricated at a certain temperature. If the ambient temperature varied from test to test, and the ambient temperature at the time of the individual tests differed from the temperature at the time the tape was fabricated, the distance between divisions would be different from the distance between division when the steel tape was fabricated.

The travel time is determined by identifying peaks in the velocity – time history or acceleration – time history, as described in Section 2.1.

Suppose the pile length is measured multiple times and the SE test is performed multiple times. Hypothetical values of length measurement and travel time are presented on Table 3-14.

Table 3-14: Hypothetical measurements for SE tests performed on prototype pile

Property	Mean Value	Standard Deviation	Range of Values	
			Maximum	Minimum
Length (mm)	2000	2.7	2004	1996
Travel Time (ms)	1.00	0.01	1.02	0.99

One could compute the bar wave velocity from the mean values of length and travel time, from which the bar wave velocity would be 4000 m/s. One could compute the possible range of bar wave velocity values from the maximum and minimum values of length and travel time. The largest value of length and shortest value of travel time will produce the largest value of bar wave velocity, and it is 4050 m/s. The smallest value of length and the longest value of travel time will produce the smallest value of bar wave velocity, and it is 3910 m/s. The analysis of the variability of test results based on the mean values, and the combination of measured values that produce the largest and smallest values of the output may not realistically capture the range of output values.

The range of length values is ±4 mm, which are ±1.48 standard deviations from the mean. Assuming the measurements are normally distributed, the probability of a single measurement falling below 1996 mm is 6.94% and the probability of a single measurement falling above 2004

mm is 6.94%, i.e., the probability of any single measurement falling outside the range presented on Table 3.14 is 13.88%.

The range of travel time values is –0.01 ms to +0.02 ms, which is –1 to +2 standard deviations from the mean. Assuming the measurements are normally distributed, the probability of a single measurement falling below 0.99 ms is 15.87% and the probability of a single measurement falling above 1.02 ms is 2.28%, i.e., the probability of any single measurement falling outside the range presented on Table 3-14 is 18.16%.

The prototype pile length measurement and travel time measurement are analyzed to determine the 95% tolerance interval, for which *k* is 1.96. The mean and standard deviation of the prototype pile length measurements are 2000 mm and 2.7 mm, respectively. The mean and standard deviation of the travel time measurements are 1.00 ms and 0.01 ms, respectively. The 95% tolerance interval of the length is 1995 mm to 2005 mm, and the 95% tolerance interval of the travel time is 0.98 ms to 1.02 ms.

The uncertainty in the group velocity is computed by applying the method of equation 3-27 to the bar wave velocity equation presented in equation 3-30.

$$\begin{aligned} w_{c_b} &= \left[\left(\frac{\partial c_b}{\partial L} w_L \right)^2 + \left(\frac{\partial c_b}{\partial \Delta t} w_{\Delta t} \right)^2 \right]^{0.5} \\ &= \left[\left(\frac{2}{\Delta t} w_L \right)^2 + \left(-\frac{2L}{\Delta t^2} w_{\Delta t} \right)^2 \right]^{0.5} \end{aligned} \qquad (3\text{-}31)$$

where w_L is the uncertainty in the length and $w_{\Delta t}$ is the uncertainty in the travel time. The values of L and Δt used in equation 3-31 are the mean values, i.e., 2000 mm and 1.00 ms, and the uncertainties in the values of L and Δt used in equation 3-31 are 5 mm and 0.02 ms, from which the uncertainty in the bar wave velocity is 80 m/s. The expected range of bar wave velocity values is 3920 m/s to 4080 m/s.

The lowest bar wave velocity value computed from the extreme values of the input parameters is 3910 m/s, which is lower than the lowest expected bar wave velocity value based on the Kline & McClintock (1953) method. The highest bar wave velocity value computed from the extreme values of the input parameters is 4080 m/s, which is the same as the expected bar wave velocity value based on the Kline & McClintock (1953) method. Calculation of the expected range of bar wave velocity values based on the extreme values of the input produced a larger range of bar wave velocity values than the expected range based on the Kline & McClintock (1953) method, suggesting the extreme values are unlikely to occur.

3.6 Summary

The lateral impact and controlled frequency methods described in Sections 3.1 represent two experimental procedures by which deep foundations can be evaluated nondestructively. Both methods require a dynamic force to generate a transient stress wave in the pile, and the

response of the pile is measured with one or more accelerometers mounted on the side of the pile, as described in Section 3.3.

The data processing consists of removing unwanted portions of the signal or isolating desired portions of the signal and determining the frequency and velocity of the desired portions of the signal. Digital filtering is used to remove unwanted portions of the signal. The acceleration – time history and acceleration spectrum are used to determine frequency content and velocity for results of the FWI Method and the mode identification method is used to determine the frequency content and velocity for the results of the controlled frequency method.

Data analyses are performed with programs written in Matlab ®, with the signal processing toolbox as an add-on. Matlab ® and the signal processing toolbox have preprogrammed functions for Fourier Transforms, windowing, digital filtering, and STFT. Those preprogrammed functions along with file I/O for reading and writing data, matrix manipulation for generating arrays, and graphing functions for generating x-y plots and contour plots have been incorporated into script files for data processing. The Matlab® programs along with the procedures in Section 3.5 are used to analyze the results of FWI and controlled frequency tests.

The uncertainty in test results can be evaluated by considering the uncertainty of the input parameters and the sensitivity of the output parameter to the uncertainty in the input parameters.

Chapter 4: Characterization of Prototype Pile

A new prototype pile, herein called C355-2430, was cast as part of this research and evaluated to theoretically verify results obtained by the lateral impact method, and to develop and verify a controlled frequency method to induce flexural waves. The pile length was selected based on overhead clearance in the laboratory and the diameter is representative of concrete piles. The new prototype pile for nondestructive evaluation is 355 mm in diameter by 2.43 meters long, and was designed for a 28-day compressive strength of 27.5 MPa.

The concrete mix was designed in accordance with ACI 211.1-91: Standard Practice for Selecting Proportions for Normal, Heavyweight and Mass Concrete, and mixed in accordance with ASTM C192-02: Standard Practice for Making and Curing Concrete Test Specimens in the Laboratory. The prototype pile was cast in four lifts in a cardboard mold. Each lift was consolidated by internal vibration in accordance with the recommendation of ACI 309R-96: Guide for Consolidation of Concrete.

The prototype pile has been tested with the sonic echo method and the data analyzed to determine the bar wave velocity, shear wave velocity, and Poisson's ratio. Where applicable, the uncertainties in the values have been determined.

4.1 Concrete Mix Proportions, Casting and Curing of Prototype Pile

The concrete mix consisted of fine aggregate (FA), coarse aggregate (CA), Type I Portland Cement (cement), and tap water. The aggregates were supplied by a commercial ready mix concrete supplier; their properties are shown on Table 4-1.

Table 4-1: Properties of aggregates for prototype piles

Aggregate	Specific Gravity	Absorption (%)
Coarse	2.62	1.3
Fine	2.70	2.3

The moisture content of the FA was 4.6% at the time of casting. The CA was air-dry and the moisture content was assumed to be negligible. The amount of water added to the mix was adjusted to account for the excess water on the FA and deficiency of water on the CA.

The mix proportions for the concrete are shown on Table 4-2.

Table 4-2: Mix proportions to produce 1 m^3 of fresh concrete

Ingredient	Mass per m^3
Portland Cement	340
Water [a]	200
Coarse Aggregate [b]	1125
Fine Aggregate [b]	700

Notes a. Water is the total mixing water including water adsorbed onto the aggregate.
b. Aggregate masses are oven-dry masses

The cardboard mold was left on the prototype pile for seven days. After removal of the cardboard mold, the prototype pile was cured in air for seven days before the first tests were conducted. The concrete was cured in accordance with ACI 308R-01: Guide to Curing Concrete.

Three standard cylinders were cast from the final batch for compressive strength testing. The cylinders were cast in accordance with ASTM C31-03: Standard Practice for Making and Curing Concrete Test Specimens in the Field. The concrete cylinders were molded in plastic cylinders and allowed to cure in the plastic molds for one day. The plastic molds were removed the day after casting and the cylinders were placed in the cure room at Northwestern Univeristy for the duration of curing

After curing, the length of the prototype pile was determined at four locations. The average length is 2.43 m, with a variation of 0.01 m. The diameter was not measured and was assumed to be the same as the mold, i.e., 355 mm.

4.2 Dynamic Properties

The physical properties of concern for the concrete prototype pile are its dynamic Young's modulus, E, Poisson's ratio, ν, and shear modulus, G, as well as its density. The 28-day compressive strength of standard test cylinders is commonly used for correlation with other

properties, including E, and for comparison between batches. Consequently, the compressive strength of concrete cylinders cast from the same concrete as the prototype pile was determined. The values of E and G were not directly determined; rather, the bar wave velocity and shear wave velocity were determined, which are related to the Young's modulus and shear modulus, respectively.

4.2.1 Evaluation of Test Cylinders

The test cylinders cast at the time of the prototype pile casting were evaluated nondestructively and destructively to determine the density of the concrete and the compressive strength, as well as to estimate the Poisson's ratio. The test cylinder dimensions were standard 150-mm diameter by 300-mm length.

The compressive strength was determined at 28-days for two cylinders, in accordance with ASTM C39-01: Standard Test Method for Compressive Strength of Cylindrical Concrete Specimens. The compressive strengths of the two cylinders were 28.0 MPa and 28.2 MPa.

Prior to testing, the cylinders were capped with sulfur capping compound in accordance with ASTM C617-98 Standard Practice for Capping Cylindrical Concrete Specimens. The density of the hardened concrete was calculated from the measured length, diameter, and mass of each cylinder.

The Poisson's ratio of the concrete was estimated from the results of impact tests performed on the test cylinders. The elastic properties were determined using Equations 4-1 through 4-10 (Subramanian et al., 2001).

$$\upsilon = A_1\left(\frac{f_1}{f_0}\right)^2 + B_1\left(\frac{f_1}{f_0}\right) + C_1 \tag{4-1}$$

$$E = 2(1+\nu)\rho\left(\frac{\pi f_0 d}{\alpha}\right)^2 \tag{4-2}$$

$$G = \frac{E}{2(1+\upsilon)} \tag{4-3}$$

The constants A_1, B_1, and C_1 are functions of the length to diameter (L/D) ratio, and are given by

$$A_1 = -8.6457\left(\frac{L}{D}\right)^2 + 24.4431\left(\frac{L}{D}\right) - 12.4778 \tag{4-4}$$

$$B_1 = 34.5986\left(\frac{L}{D}\right)^2 - 101.7207\left(\frac{L}{D}\right) + 56.1720 \tag{4-5}$$

$$C_1 - 34.6807\left(\frac{L}{D}\right)^2 + 105.9790\left(\frac{L}{D}\right) - 62.7310 \qquad (4\text{-}6)$$

The parameter α is a function of the Poisson's ratio and is given by

$$\alpha = A_2\nu^2 + B_2\nu + C_2 \qquad (4\text{-}7)$$

The constants A_2, B_2, and C_2 are functions of the length to diameter (L/D) ratio, and are given by

$$A_2 = -0.2792\left(\frac{L}{D}\right)^2 + 0.4585\left(\frac{L}{D}\right) - 2.1093 \qquad (4\text{-}8)$$

$$B_2 = 0.0846\left(\frac{L}{D}\right)^2 - 0.5868\left(\frac{L}{D}\right) + 1.3791 \qquad (4\text{-}9)$$

$$C_2 = 0.2850\left(\frac{L}{D}\right)^2 - 1.7026\left(\frac{L}{D}\right) - 3.3769 \qquad (4\text{-}10)$$

Each of the three cylinders cast was evaluated by the SE Method and the data from each evaluation were analyzed by the Subramanian et al. method. The results of the analyses are shown on Table 4-3.

Table 4-3: Sonic echo results for concrete cylinders and elastic constants determined from Subramanian et al. approach (2001)

Specimen	f_0 (Hz)	f_1 (Hz)	f_1/f_0	L/D	ν	E (Gpa)	G (Gpa)
S1	6350	11990	1.89	1.99	0.25	43.8	17.5
S2	6270	11890	1.90	1.99	0.23	41.4	16.8
S3	6350	11990	1.89	1.99	0.25	43.7	17.5
Average Values					0.24	43.0	17.3

The average values of elastic constants presented in Table 4-3 are within the expected range for concrete.

4.2.2 Sonic Echo Results

The prototype pile was evaluated by the sonic echo method to determine the bar wave velocity, phase velocities, and universal mode frequency (UMF). The sonic echo tests were performed 28 days after casting. The Poisson's ratio can be estimated from the phase velocities by the Point Matching Method (Chao, 2002). The shear wave velocity can be calculated from the UMF (Chao, 2002), and the Poisson's ratio can be calculated from the elastic relationship among bar wave velocity, shear wave velocity, and Poisson's ratio.

4.2.2.1 Bar Wave Velocity Determination by Time and Frequency Analysis

The bar wave velocity can be computed from the time lag between returns of the wave group as identified in the time domain, or from the lowest natural frequency in the frequency domain of the acceleration – time history, assuming the pile length is known.

The bar wave velocity, c_B, is calculated from the time history by

$$c_B = \frac{2L}{\Delta t} \qquad (4\text{-}11)$$

where L is the pile length and Δt is the travel time.

An example of the calculation of propagation velocity from the time domain data is shown on Figure 4-1.

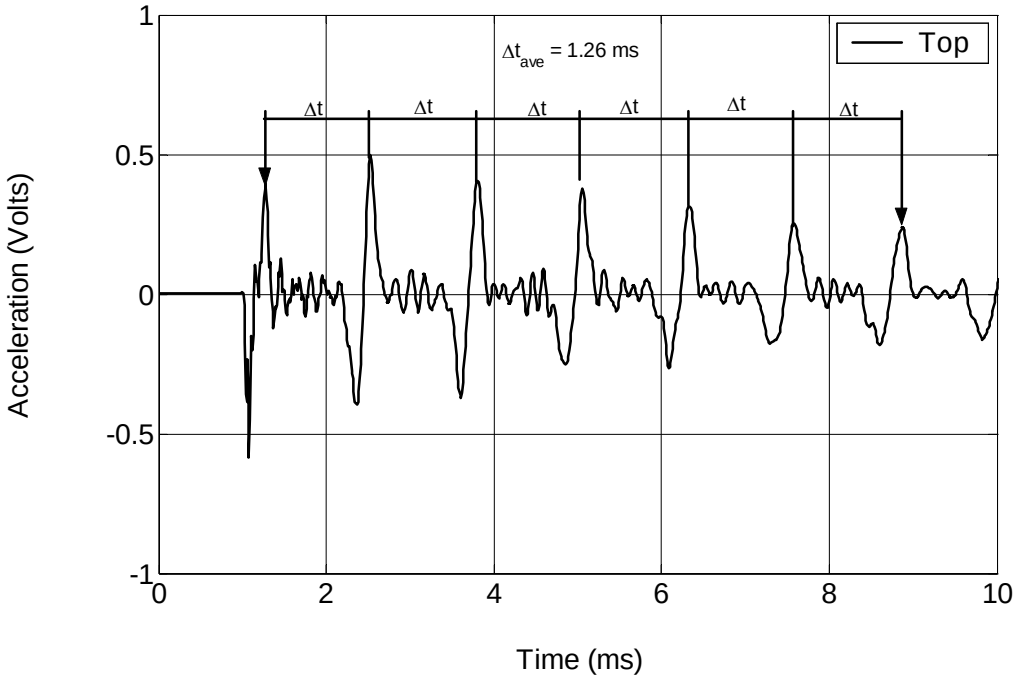

Figure 4-1: Bar wave velocity calculated from acceleration – time history of sonic echo test

The nominal pile length is 2.43 meters and the average return period is 1.26 ms. The bar wave velocity, as calculated from equation 4-11, is 3900 m/s, which is within the typical range of 3500 m/s to 4500 m/s for good quality concrete (Davis and Robertson, 1975). The uncertainty in the bar wave velocity was determined by the procedure presented in Section 3.5.3.

The uncertainty in the bar wave velocity, w_c, is computed from

$$w_c = \left[\left(\frac{2}{\Delta t} w_L \right)^2 + \left(\frac{-2L}{(\Delta t)^2} w_{\Delta t} \right)^2 \right]^{0.5} \qquad (4\text{-}12)$$

where w_L is the uncertainty in the length and $w_{\Delta t}$ is the uncertainty in the travel time. The uncertainty in the input parameters is determined from the analysis of test results to determine the 95 % tolerance interval.

The nominal pile length is 2.43 m ± 0.10 m, as discussed in Section 4.1. For the data presented on Figure 4-1, the average travel time is 1.26 ms, and the standard deviation is 0.021 ms. The expected range of the travel time, $r_{\Delta t}$, is computed from

$$r_{\Delta t} = k\sigma_{\Delta t} \qquad (4\text{-}13)$$

where k is a constant that is a function of the desired tolerance interval and $\sigma_{\Delta t}$ is the standard deviation of the travel time. For a 95 % tolerance interval, k is 1.96, in which case, $r_{\Delta t}$ is 0.041 ms for the data presented on Figure 4-1.

Substituting L of 2.43 m ± 0.10 m, and Δt of 1.26 ms ± 0.041 ms into equation 4-12, the uncertainty in the bar wave velocity is 130 m/s, or 3.3 % of the average value. Several more sonic echo tests were performed on Prototype pile C355-2430, although their results are not presented herein. The tests were performed to evaluate the variability of the bar wave velocity. For the entire data set, including the results presented on Figure 4-1, the average bar wave velocity was 1.26 ms with a standard deviation of 0.033 ms. For a data set with a standard deviation of 0.033 ms, the 95 % tolerance interval is 0.065 ms. Substituting L of 2.43 m ± 0.10 m, and Δt of 1.26 ms ± 0.065 ms into equation 4-12, the uncertainty in the bar wave velocity is 200 m/s, or 5.1 % of the average value.

To calculate the bar wave velocity from the frequency data, the first peak in the acceleration spectrum, which is the Fourier Transform of the acceleration – time history is identified. The bar wave velocity, c_B, is then calculated by

$$c_B = 2Lf \tag{4-14}$$

where L is the pile length and f is the fundamental frequency.

An example of the calculation of the propagation velocity is shown on Figure 4-2.

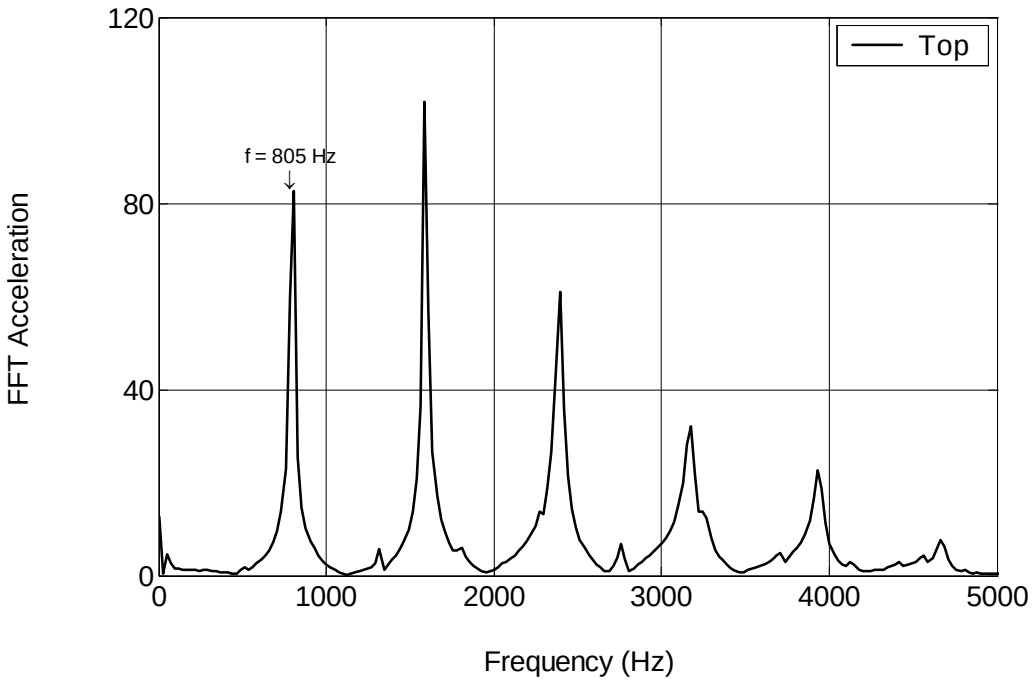

Figure 4-2: Bar wave velocity calculated from acceleration spectrum of sonic echo test

The frequency of the lowest peak is 805 Hz. The bar wave velocity, as calculated from equation 4-14, is 3910 m/s, which is within the typical range of 3500 m/s to 4500 m/s for good quality concrete (Davis and Robertson, 1975).

The uncertainty in the bar wave velocity, w_c, was determined by the procedure presented in Section 3.5.3. The procedure presented in Section 3.5.3 applied to equation 4-14 produces

$$w_c = \left[(2fw_L)^2 + (2Lw_f)^2 \right]^{0.5} \qquad (4\text{-}15)$$

where w_L is the uncertainty in the length and w_f is the uncertainty in the fundamental frequency. The uncertainty in the input parameters is determined from the analysis of test results. The fundamental frequency of the pile, as determined from the data presented on Figure 4-2, is 805 Hz. Several more sonic echo tests were performed on the test over a period of time, and the fundamental frequency was 805 Hz for all tests. As such, the uncertainty in fundamental frequency is 12 Hz, or half the frequency spacing in the FFT array. Substituting a pile length of 2.43 m ± 0.01 m and a fundamental frequency of 805 Hz ± 12 Hz into equation 4-15, the uncertainty in the bar wave velocity is 60 m/s.

The bar wave velocity calculated from the time history was 3900 m/s, and the bar wave velocity calculated from the frequency domain was 3910 m/s. Given that the values are reported to the nearest 10 m/s, the sampling frequency is 0.01 ms, and the frequency spacing is 25 Hz, the values of bar wave velocity determined by the two methods are essentially the same.

4.2.2.2 Shear Wave Velocity and Poisson' Ratio Determination by Universal Mode Frequency Analysis and Point Matching Method

The shear wave velocity can be determined from the universal mode frequency (UMF) identification method (Chao, 2002). The UMF is the point on the family of dispersion curves for a given branch that has the same ordered pair of frequency and wavenumber for all values of Poisson's ratio, and the UMF manifests itself as a spurious resonance on the acceleration spectrum. The Poisson's ratio can be computed from based on Hooke's law using the bar wave velocity, and shear wave velocity, or by the point matching method (Chao, 2002). The sonic echo results presented on Figures 4-1 and 4-2 are analyzed to determine the shear wave velocity and Poisson's ratio by the UMF and point matching methods.

The concept of the universal mode was identified by Hudson (1943), and can be calculated by solving

$$J'(\xi a_n) = 0 \qquad (4\text{-}16)$$

Equation 4-16 has an infinite number of solutions in terms of the nondimensional wavenumber, with each solution corresponding to the universal mode on one longitudinal branch, e.g., the first root of Equation 4-16 corresponds to the universal mode on the L(0,1) branch. The nondimensional frequency corresponding to the values of nondimensional wavenumber satisfying Equation 4-16 can be calculated by

$$\Omega_n = \sqrt{2}\xi a_n \qquad (4\text{-}17)$$

For the L(0,1) branch, the nondimensional frequency corresponding to the UMF is 2.6. The nondimensional frequency, Ω, in terms of angular frequency, ω, pile radius, *a*, and concrete shear wave velocity, c_{Tc} is

$$\Omega = \frac{\omega a}{c_{T_c}} \qquad (4\text{-}18)$$

Substituting ω=2πf, and Ω = 2.6 into Equation 4-18, the UMF, f_{UMF}, in Hz is

$$f_{UMF} = \frac{2.6 c_T}{2\pi a} \qquad (4\text{-}19)$$

The shear wave velocity can be determined from the UMF provided the frequency can be identified in test results by the following procedure (Chao, 2002)

1. Determine the bar wave velocity from the results of the sonic echo test.
2. Determine the range of expected shear wave velocity values from

$$c_T = \frac{c_B}{\sqrt{2(1+\nu)}} \qquad (4\text{-}20)$$

   using a range of Poisson's ratio values of 0.15 to 0.30.
3. Determine the range of expected UMF values from estimated shear wave velocity calculated in Step 2 and equation 4-19.
4. Identify peak(s) in acceleration spectrum that falls within the expected range of UMF values.
5. Verify that the peak identified in Step 4 is the UMF, not a natural frequency of the pile if only one peak is identified, or determine which peak corresponds to the UMF if more than one peak is identified.
6. Compute the shear wave velocity by rearranging equation 4-19.

The procedure only works if the UMF falls within the range of frequencies excited by the input force. In a sonic echo test that excites the structure in the range of the UMF, a spurious peak will appear in the frequency domain response of the structure (Chao, 2002). The spurious peak attributed to the UMF can be separated from the peaks corresponding to the natural frequency of the system by calculating the phase velocity values with and without the alleged UMF. Both sets of phase velocity – frequency values are analyzed by the point matching method (Chao, 2002). If the peak does correspond to the UMF, the experimentally-determined phase velocity – frequency relationship will not follow the numerically-determined phase velocity – frequency relationship when the alleged UMF is included in the calculations (Chao, 2002). In contrast, when the alleged UMF is excluded from the phase velocity calculations, the experimentally-determined values will again follow the numerically-determined values.

The point matching method allows the Poisson's ratio of concrete in the prototype pile to be estimated by superimposing experimentally-determined phase velocity values on a set of numerically-determined phase velocity – frequency curves (Chao, 2002). The experimental values are obtained from conventional impact tests, and the numerical curves are determined from guided wave theory for a range of values of Poisson's ratio.

The relationship between nondimensional frequency and nondimensional wavenumber depends, in part, on the shear wave velocity and the Poisson's ratio of the concrete. The

procedure for estimating Poisson's ratio based on point matching with an assumed shear wave velocity is

1. Perform a sonic echo test and analyze the data to determine
   a. The bar wave velocity using the procedures presented in Section 4.2.2.1 and the shear wave velocity from the UMF procedure (Chao, 2002).
   b. The natural frequencies of the pile excited by the impact
2. Compute the phase velocity corresponding to each natural frequency excited in the test by

$$c_p = \frac{2Lf_n}{n} \qquad (4\text{-}21)$$

   where L is the length of the pile, f_n is the frequency identified from the test results, and n is the harmonic number.
3. Solve the frequency equation for the L(0,1) branch for different values of Poisson's ratio.
4. Compute the nondimensional phase velocity – nondimensional frequency relationships from the results of Step 3 by

$$c_{p(ND)} = \frac{\Omega}{\mathrm{Re}(\xi_a)} \qquad (4\text{-}22)$$

   where $c_{p(ND)}$ is the nondimensional phase velocity, Ω is the nondimensional frequency, and $\mathrm{Re}(\xi_a)$ is the real part of the nondimensional wavenumber.
5. Convert the results of Step 4 from nondimensional form to dimensional form by

$$f = \frac{\Omega c_{T_c}}{2\pi a} \qquad (4\text{-}23)$$

$$c_p = c_{p(ND)} c_{T_c} \qquad (4\text{-}24)$$

   where f is the frequency in Hz, Ω is the nondimensional frequency, c_{Tc} is the shear wave velocity, a is the pile radius, and c_p is the phase velocity.
6. Overlay the experimentally determined phase velocity values on the family of phase velocity – frequency curves.

The Poisson's ratio for the concrete is the value for the numerical curve that most closely fits the experimental value.

The bar wave velocity of the prototype pile is 3900 m/s, as presented in Section 4.2.2.1, and Poisson's ratio for concrete typically ranges from 0.15 to 0.30. Substituting the bar wave velocity and Poisson's ratio values into equation 4-20, the shear wave velocity should range from 2400 m/s to 2600 m/s. Substituting the expected values of shear wave velocity into equation 4-19, the UMF should occur between 5600 Hz and 6050 Hz. The frequency domain results of a sonic echo test is shown on Figure 4-3.

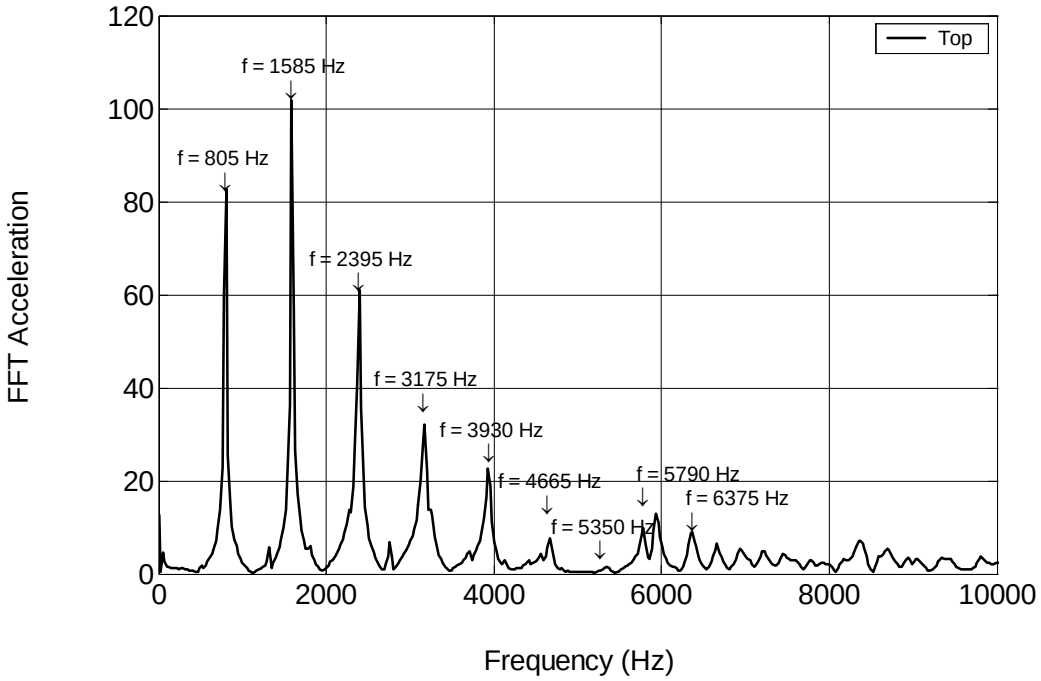

Figure 4-3: Acceleration spectrum with first nine natural frequencies identified from sonic echo test

Two frequencies were identified between 5600 Hz and 6050 Hz, one at 5790 Hz and one at 5930 Hz. Assuming the UMF is 5930 Hz, the shear wave velocity is calculated to be 2530 m/s

by substituting the frequency of 5930 Hz into Equation 4-17. The Poisson's ratio, ν, is computed by the relationship among Poisson's ratio, bar wave velocity, c_B, and shear wave velocity, c_{Tc} by

$$\nu = \frac{1}{2}\left(\frac{c_B}{c_{T_c}}\right)^2 - 1 \qquad (4\text{-}25)$$

Substituting c_B = 3900 m/s and c_{Tc} = 2530 m/s into equation 4-25, the Poisson's ratio is 0.20.

The assumption of 5930 Hz as the UMF is verified by the point matching method applied to the results presented on Figure 4-3. The first nine natural frequencies and the calculated phase velocity values are shown on Table 4-4, assuming the peak at 5930 Hz is the UMF and not a natural frequency of the pile. The uncertainty in the phase velocity was computed using a pile length of 2.43 m ± 0.01 m and an assumed uncertainty of ± 12 Hz in the frequency.

Table 4-4: Prototype Pile C355-2430-ND, results of sonic echo test phase velocity values for first nine natural frequencies

Harmonic Number	Frequency (Hz)	Phase Velocity (m/s)	Uncertainty in Phase Velocity (m/s)
1	805	3910	60
2	1585	3850	35
3	2395	3880	25
4	3175	3860	20
5	3930	3820	20
6	4665	3780	20
7	5350	3710	15
8	5790	3520	15
9	6375	3440	15

The experimentally determined values of phase velocity as a function of frequency are superimposed on the numerically determined phase velocity – frequency curves for various values of Poisson's ratio, as shown on Figure 4-4.

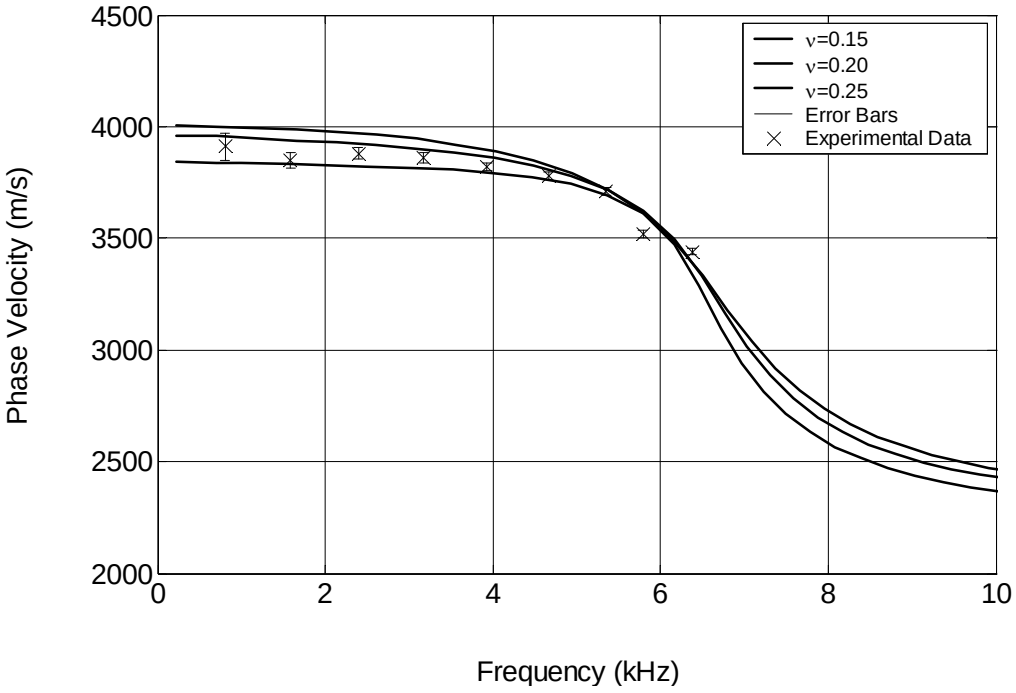

Figure 4-4: Poisson's ratio of prototype pile from point matching method

The experimental data falls between the curves for values of Poisson's ratio of 0.15 and 0.20, and more closely matches the curve for the Poisson's ratio value of 0.20.

The frequency identified at 5930 Hz was attributed to the UMF, not a resonance corresponding to a phase. The frequency – phase velocity relationship presented on Figure 4-3 has been recalculated assuming the UMF is a phase. The results of the frequency – phase velocity relationship with and without the UMF are shown on Figure 4-5.

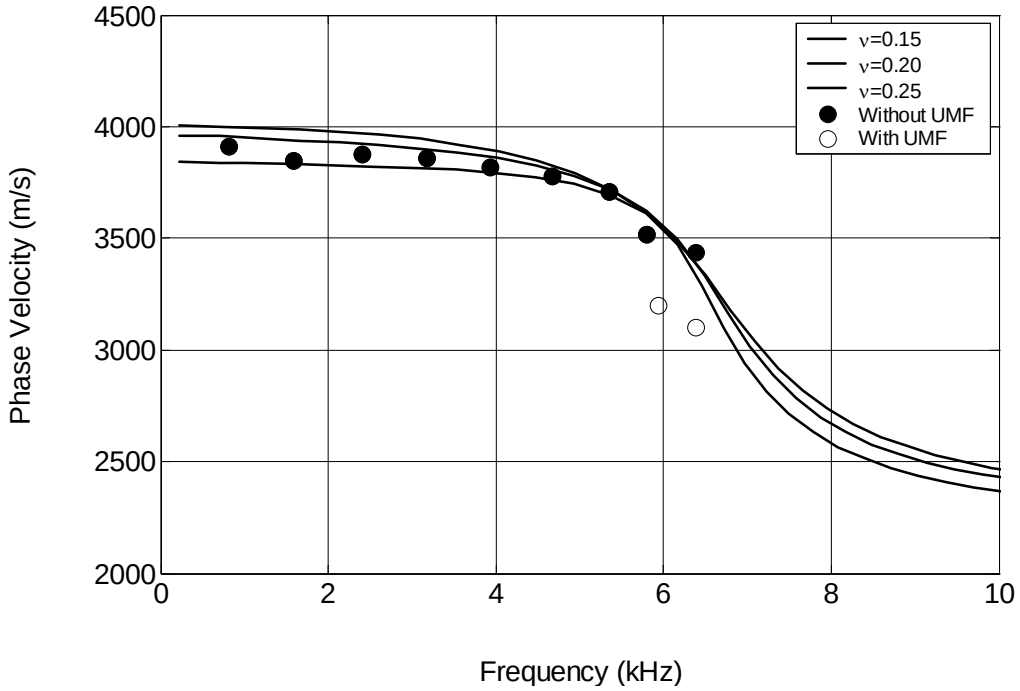

Figure 4-5: Point matching method with UMF included in resonant frequency array and UMF excluded from resonant frequency array

The open circles correspond to the data presented on Figure 4-4, and the closed circles correspond to the phase velocities calculated assuming the frequency at 5930 Hz is a resonance. The closed circles do not follow the trend of the numerically-determined frequency – phase velocity relationship, indicating that the frequency at 5930 Hz is the UMF and not a resonance.

4.2.3 Summary of Elastic Parameters

The prototype pile has been evaluated by the sonic echo method and the results of the sonic echo test have been analyzed by conventional one-dimensional methods, as well as provided by three-dimensional guided wave theory. Test cylinders cast from one batch of concrete for the fabrication the prototype pile have also been evaluated. Results of the sonic echo analyses are summarized and comparisons are made between cylinder and prototype pile results, where appropriate. The bar wave velocity values for the prototype pile presented on Table 4-5 fall within the expected range for good quality concrete (Davis and Robertson, 1975).

Table 4-5: Prototype Pile C355-2430-ND; Summary of bar wave velocity values determined from sonic echo tests

Method of Determination	Bar Wave Velocity (m/s)	Density (kg/m3)	Young's Modulus (GPa)
Time Domain	3900	2350	35.7
Frequency Domain	3900	2350	35.7
Average	**3900**	**2350**	**35.7**

The shear wave velocity value was calculated to be 2530 m/s for Prototype Pile C355-2430-ND. Shear wave velocity is not reported as part of the typical NDE of deep foundations but the expected range can be calculated based on the typical range of values for bar wave velocity and Poisson's ratio, as stated in Section 4.2.2.2.

The Poisson's ratio can be estimated from the point matching method of phase velocities (Chao, 2002), the UMF Method, or calculated from the elastic relationships among bar wave velocity, c_B, shear wave velocity, c_{Tc}, and Poisson's ratio given as

$$\nu = \frac{1}{2}\left(\frac{c_B}{c_{T_c}}\right)^2 - 1 \qquad (4\text{-}26)$$

The values of Poisson's ratio are presented on Table 4-6. The Poisson's ratio determined from tests performed on concrete cylinders (Subramanian et al., 2001) is provided for comparison.

Table 4-6: Summary of Poisson's ratio values determined from sonic echo test results on prototype pile and test cylinders

Method of Analysis	Poisson's ratio
Bar wave velocity (time history) and UMF	0.19
Bar wave velocity (frequency domain) and UMF	0.19
Bar wave velocity (average) and UMF	**0.19**
Point matching	0.20
Subramanian et al. (2001)	0.24
Average value of Poisson's ratio	**0.20**

The average value of 0.20 will be used in all subsequent analyses, and falls within the typical range of values for concrete.

4.3 Dimensional form of dispersion curves

Experimental verification of flexural guided wave theory is performed by comparing the experimental results of lateral impact tests and controlled frequency tests to theoretical values obtained by solving the frequency equation. The test results are analyzed to determine group velocity – frequency values and phase velocity – frequency values, which are superimposed on the theoretical curves. The theoretical curves are developed by

1. Determine the bar wave velocity, shear wave velocity, and Poisson's ratio of the concrete by the procedures in Sections 4.2.2.1 and 4.2.2.2. Determine the density of the concrete.
2. Determine the shear wave velocity, Poisson's ratio, and density of the soil.
3. Solve the frequency equation for the concrete and soil properties from Steps 1 and 2, using the procedures presented in Section 2.3.4.
4. Convert the values of nondimensional frequency – nondimensional wavenumber to nondimensional group velocity – nondimensional frequency and nondimensional phase velocity – nondimensional frequency by the procedures presented in Section 2.3.6.
5. Convert from nondimensional form to dimensional form.

The experimental results are then superimposed on the dimensional velocity – frequency curves determined in Step 5.

The nondimensional frequency – nondimensional wavenumber curves have been generated for the first five flexural branches using the Poisson's ratio value of 0.20 and "traction-free" conditions. The curves for the real part of the nondimensional wavenumber and nondimensional frequency are presented on Figure 4-6.

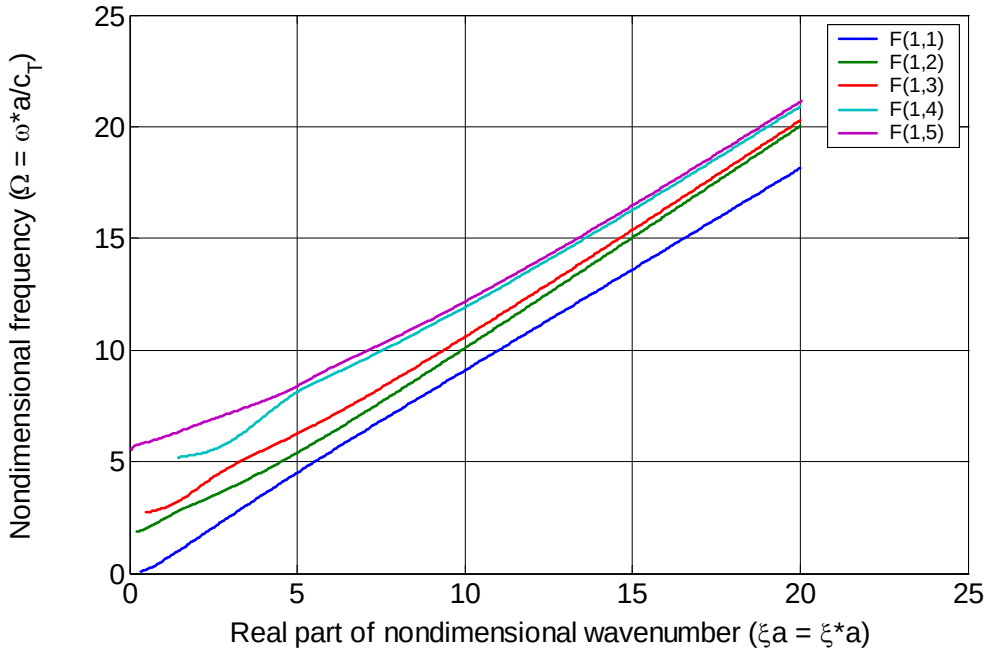

Figure 4-6: Nondimensional frequency – real part of nondimensional wavenumber for first five flexural branches, for concrete with $\nu_c = 0.20$ under traction-free conditions

The nondimensional frequencies, Ω, for the branches presented on Figure 4-6 are converted to frequencies, *f*, in Hz by

$$f = \frac{\Omega c_{T_c}}{2\pi a} \qquad (4\text{-}27)$$

The nondimensional cutoff frequencies and cutoff frequencies in Hz are presented on Table 4-7 using a pile radius, *a*, of 355 mm and a concrete shear wave velocity, c_{Tc}, of 2530 m/s.

Table 4-7: Nondimensional cutoff frequencies and cutoff frequencies for 355 mm diameter pile with c_T = 2530 m/s and ν_c = 0.20

Mode	Nondimensional Frequency	Frequency (Hz)
F(1,1)	0	0
F(1,2)	1.871[1]	4240
F(1,3)	2.630[2]	5970
F(1,4)	5.190[3]	11770
F(1,5)	5.553[3]	12600

Notes:
1. Lowest value for which solution converged
2. Real part less than 0.1
3. Imaginary part exceeds 0.5

The values of nondimensional frequency, Ω, and nondimensional wavenumber, ξ, shown graphically on Figure 4-6, are converted to nondimensional phase velocity, $c_{p(ND)}$ by

$$c_{p(ND)} = \frac{\Omega}{R(\xi_a)} \qquad (4\text{-}28)$$

and the y-axis of nondimensional frequency on Figure 4-6 becomes the x-axis for the nondimensional phase velocity – nondimensional frequency curves shown on Figure 4-7.

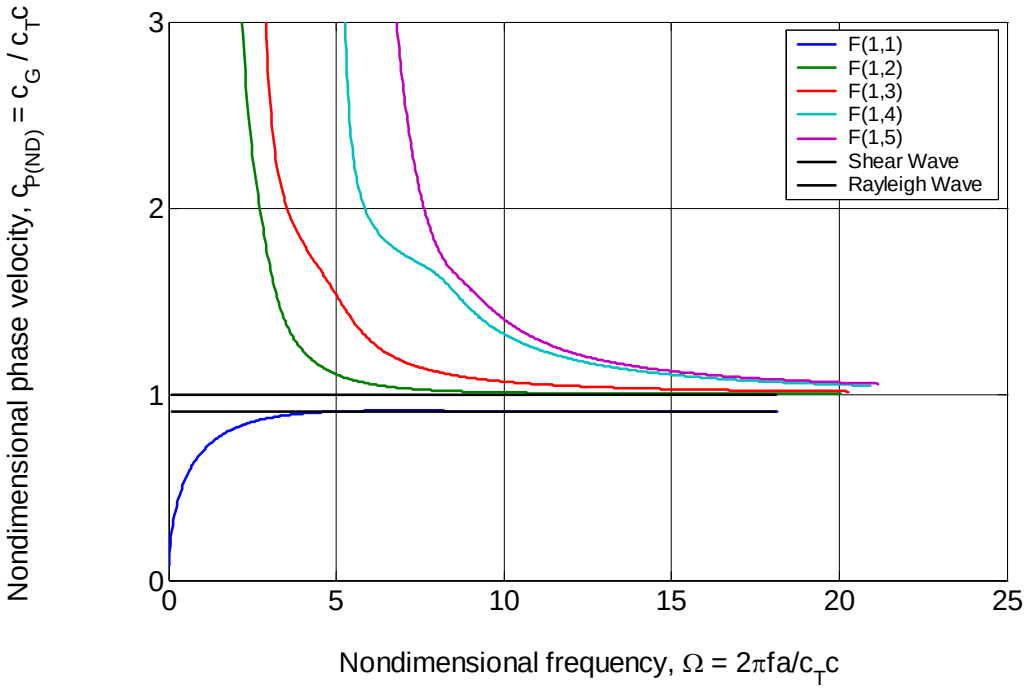

Figure 4-7: Nondimensional phase velocity – nondimensional frequency curves for first five flexural branches for concrete with $\nu_c = 0.20$

The nondimensional phase velocity, $c_{p(ND),}$ is converted to phase velocity, c_p, by

$$c_p = c_{p(ND)} c_{T_c} \qquad (4\text{-}29)$$

and the nondimensional frequency is converted to frequency in Hz by equation 4-27.

The curves shown on Figure 4-7 were converted to dimensional form by substituting a shear wave velocity, c_{Tc}, of 2530 m/s and radius, *a*, of 177.5 mm into equations 4-27 and 4-29. The phase velocity – frequency curves for the first five flexural branches are shown on Figure 4-8.

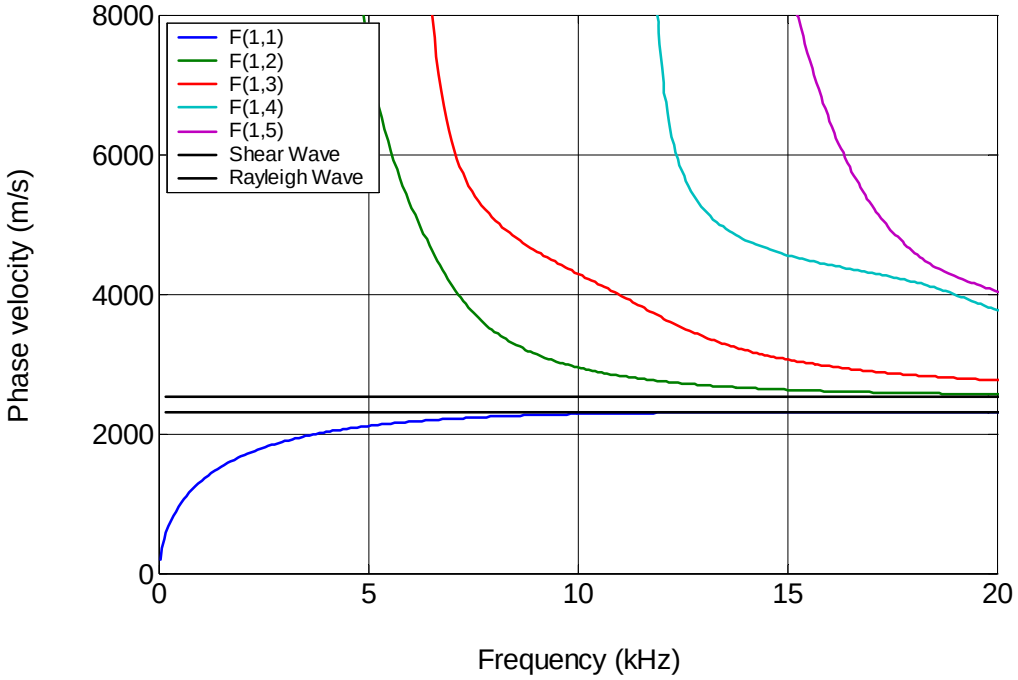

Figure 4-8: First five numerically-determined flexural phase velocity - frequency curves for 355 mm diameter pile with c_T = 2530 m/s and ν_c = 0.20

The phase velocity for the F(1,1) branch is zero at a nondimensional frequency of zero and becomes asymptotic to the Rayleigh wave velocity at a frequency of 11 kHz. For the F(1,2) branch and F(1,3) branch, the phase velocities become very large near the cutoff frequency and decrease with increasing frequency to become asymptotic to the shear wave velocity at large frequencies. The phase velocity for the F(1,2) branch becomes asymptotic to the shear wave velocity at a frequency of 19 kHz, and the phase velocity for the F(1,3) branch becomes asymptotic to the shear wave velocity at a frequency greater than the maximum frequency shown on Figure 4-5.

The values of nondimensional group velocity, $c_{g(ND)}$, are calculated by

$$c_{g(ND)} = \frac{\partial \Omega}{\partial R(\xi_a)} \tag{4-30}$$

using the nondimensional frequency – nondimensional wavenumber data from which Figure 4-6 was generated. The nondimensional group velocity – nondimensional frequency curves for the first five flexural branches are shown on Figure 4-9.

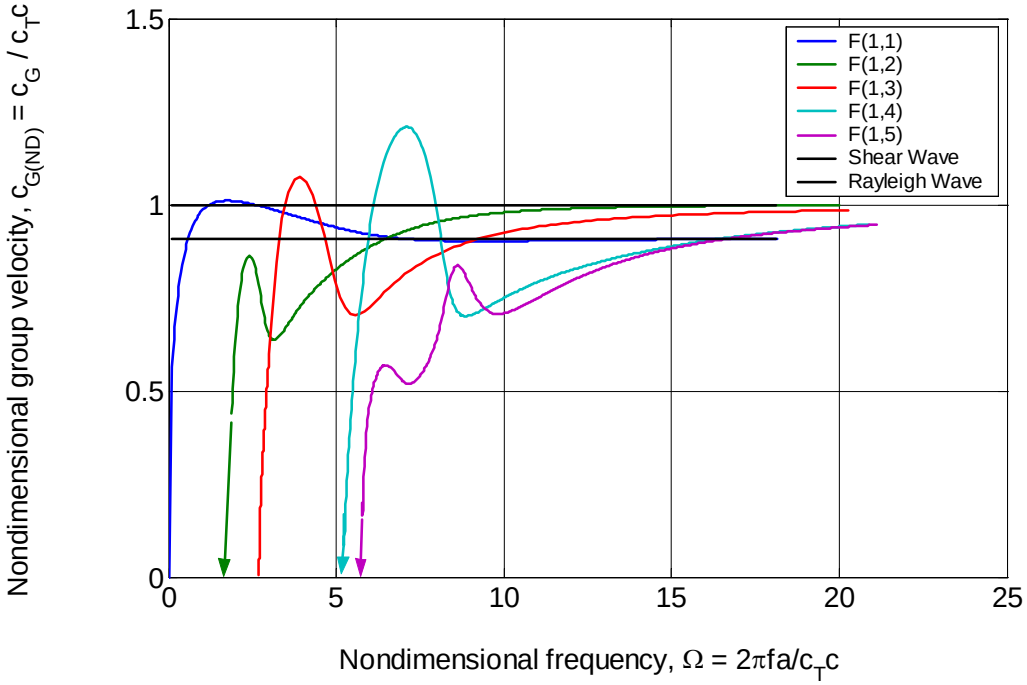

Figure 4-9: Nondimensional group velocity – nondimensional frequency curves for first five flexural branches for concrete with $\nu_c = 0.20$

The nondimensional group velocity is converted to group velocity by

$$c_g = c_{g(ND)} c_{T_c} \tag{4-31}$$

and the nondimensional frequency is converted to frequency by equation 4-24. The group velocity – frequency curves for the first three flexural branches are shown on Figure 4-10.

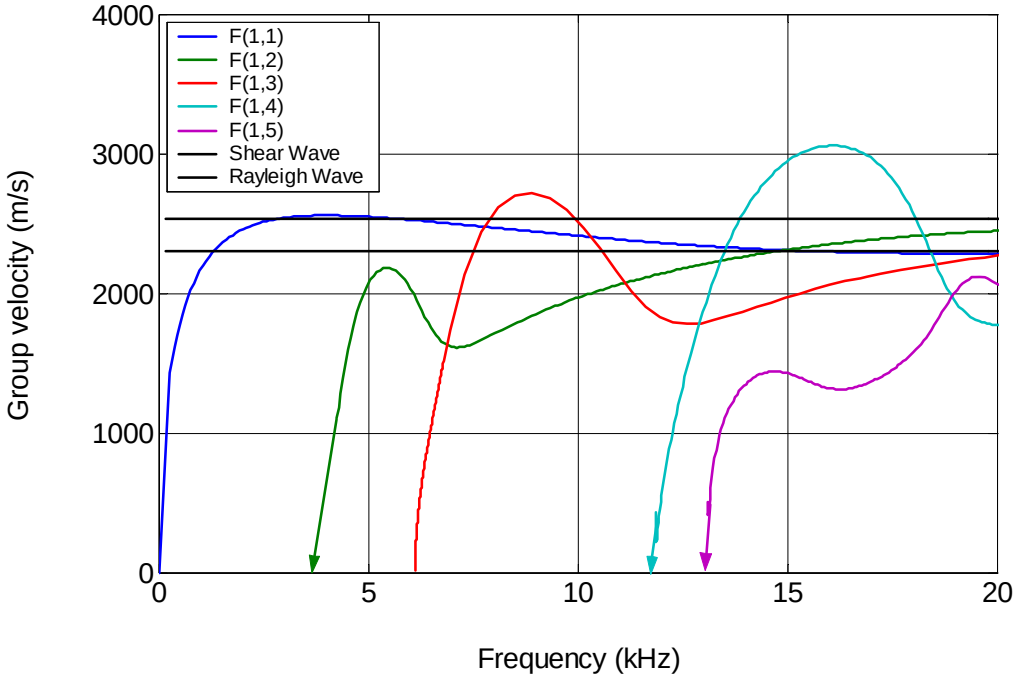

Figure 4-10: First five numerically-determined flexural group velocity – frequency curves for 355 mm diameter pile with c_T = 2530 m/s and ν_c = 0.20

The approximate cutoff frequencies for the F(1,n), branches for n ranging from 1 to 5, are 0, 4.5, 6, 12, and 13 kHz, respectively. For the F(1,1) branch, the maximum group velocity occurs between 3 and 5 kHz, and becomes asymptotic to the Rayleigh Wave Velocity at about 15 kHz. The maximum group velocity for the F(1,2) branch occurs at a frequency of about 5.5 kHz, the maximum group velocity for the F(1,3) branch occurs at a frequency of about 9.5 kHz and the maximum group velocity for the F(1,4) branch occurs at a frequency of about 17 kHz. The group velocities for the F(1,2), F(1,3) and F(1,4) branches becomes asymptotic to the shear wave

velocity, but the frequencies at which the group velocities approach the shear wave velocity are greater than the maximum frequency shown on Figure 4-10. The group velocity for the F(1,5) branch has a local maximum of about 1400 m/s that occurs at a frequency of about 14 kHz, followed by a decrease in group velocity to a local minimum of 1300 m/s, occurring at about 17 kHz. After the local minimum, the group velocity increases to a local maximum of 2100 m/s, occurring at about 19 kHz. The remaining curve is not shown on Figure 4-10, but it has another local minimum followed by an increase until it becomes asymptotic with the shear wave velocity.

Results of lateral impact tests are used to determine the phase velocity at different frequencies and the group velocity at the frequency of the group. These values are superimposed on Figures 4-9 and 4-11 in Chapter 5. Controlled frequency results are analyzed to determine the group velocity and frequency of the group and superimposed on Figure 4-10 in Chapters 6 and 7.

4.4 Summary

A new prototype pile has been cast for the purpose of verifying the antisymmetric guide wave theory for NDE of deep foundations. The new prototype pile has a bar wave velocity, c_B, of 3900 m/s, a shear wave velocity, c_{Tc}, of 2530 m/s, and a Poisson's ratio, ν_c, of 0.20, and a concrete density of 2350 kg/m^3. The velocities and Poisson's ratio are based on tests conducted 28 days after the concrete was cast and represent the average values based on the results of several sets of tests and a variety of analytical techniques applied to each data set. The Poisson's ratio, shear wave velocity and density are used in the numerical analysis to develop dispersion curves and to compute mode shapes.

Curves of the frequency – group velocity and frequency – phase velocity have been developed for the first three flexural branches using the Poisson's ratio, shear wave velocity, and density for the new prototype pile, and those curves have been presented in Section 4.3. The prototype pile was tested using the lateral impact and controlled frequency methods. The experimental values of frequency and phase velocity or frequency and group velocity presented in Chapters 5, 6, and 7 will be superimposed on the numerically-determined curves presented in Section 4.3.

Chapter 5: Flexural Wave Identification in Lateral Impacts Test Results

Prototype pile C355-2430, described in Chapter 4, and the Group B prototype piles, described in Section 2.2, have been evaluated nondestructively by lateral impact tests to verify the flexural guided wave theory presented in Section 2.3 and to evaluate the applicability of the lateral impact method for nondestructive evaluation of deep foundations. Prototype pile C355-2430 was tested under traction-free conditions and all piles were evaluated embedded in the sand fill at the NGES described in Section 2.2. A flexural wave was induced by an impact to the side of the pile from a modal hammer described in Section 3.3.1, and the response was measured with a triaxial accelerometer described in Section 3.3.3. The lateral impact test results were analyzed to determine the phase velocity – frequency relationship for the phases within the frequency range of the impact, and the group velocity – frequency relationship. The experimental results were compared to theoretical results to verify the guided wave theory. In particular, experimental results are compared with the numerically-derived group velocity – frequency and phase velocity – frequency relationships. Part of the data analysis includes lowpass filtering of the data to remove high frequency noise and unwanted portions of the signal that fall outside the test range.

5.1 Analysis of Lateral Impact Results

The piles were tested by the lateral impact method described in section 3.1.1. The response was measured with one triaxial accelerometer mounted on the side of the pile at the position shown on Figure 5-1 and impacts were performed at four different orientations with the convention shown on Figure 5-1.

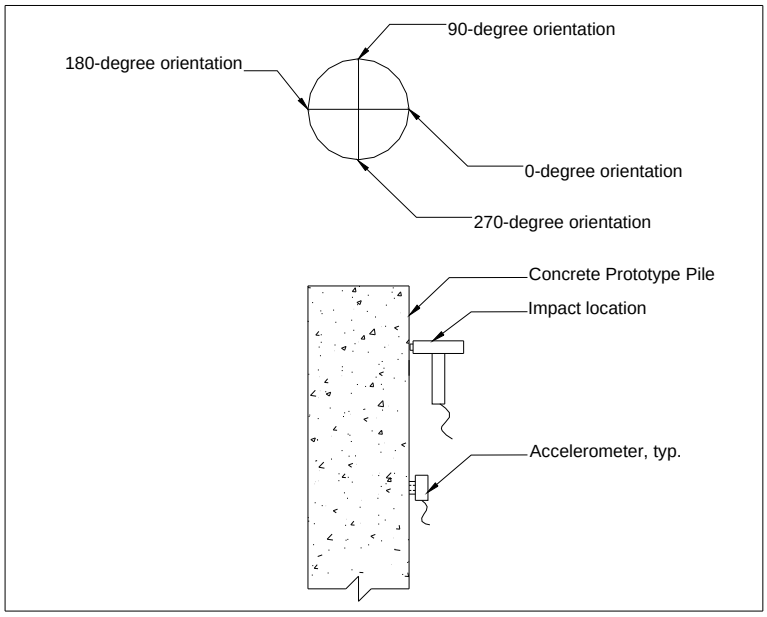

Figure 5-1: Orientation convention for input and response for flexural modes

In general, a propagating stress wave induced by a lateral impact results in radial, longitudinal and tangential displacements in a pile. The equations for the displacement components presented in Section 2.3.8 indicate that the radial and longitudinal displacements

depend on the cosine of the angle between the impact and measurement locations, and the tangential displacement depends on the sine of the angle between the impact and measurement locations. The maximum magnitude of the cosine occurs at 0-degrees and 180-degrees, which are the angles at which the sine is zero; conversely, the maximum magnitude of the sine occurs at 90-degrees and 270-degrees, at which the magnitude of the cosine is zero. Based on the displacement equations, the results are analyzed in the longitudinal and radial directions in for the 0-degree and 180-degree orientations and the tangential direction in the 90-degree and 270-degree orientations.

The filtered lateral impact results are analyzed as part of the verification of the guided wave theory presented in Section 2.3. The criteria for experimental verification of the flexural guided wave (Wang, 2004) theory are

- Determine the frequency range to be included in the analysis,
- Identify the branches on which modes may propagate,
- Evaluate relative magnitudes of displacement.
    - For the 0-degree and 180-degree orientations, the radial and longitudinal responses should be nonzero and the tangential response should be negligible.
    - For the 90-degree and 270-degree orientations, the radial and longitudinal responses should be negligible and the tangential response should be nonzero.
    - The pile response to impacts on opposite faces should be 180-degrees out of phase.
- Determine the phase velocity – frequency relationship and compare the experimental results to numerical results,
- Determine the group velocity – frequency values and compare the experimental results to the numerical results,

5.2 Evaluation of Prototype Pile C355-2430 under Traction-free Conditions

The prototype pile was tested with one triaxial accelerometer mounted on the side of the pile at the position shown on Figure 5-2. The experimental phase and group velocities were computed by the procedures presented in Section 3.4.3, and the pile geometry shown on Figure 5-2.

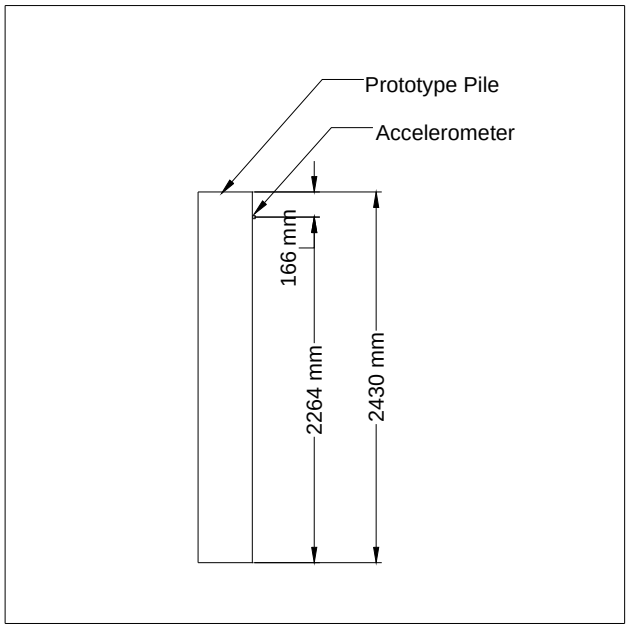

Figure 5-2: Prototype pile C355-2430, accelerometer position for lateral impact test under traction-free conditions

The pile is 2430 mm long and the phase velocity is calculated with that length. The distance from the accelerometer to the tip of the pile is 2264 mm, and the group velocity is calculated with that length.

5.2.1 Identification of Frequency Range and Expected Branches

The time history and frequency response of the hammer impact and pile response are analyzed to determine the frequency range to be included in the analysis. Based on the frequency range to be included in the analysis, one determines the cutoff frequency for the filter and identifies the possible branches on which modes are expected.

The frequencies of the individual phases induced by a lateral impact depend on the maximum frequency of the input, called the null frequency as described in Section 3.4.2.1. The null frequency is less than or equal to the maximum frequency that the hammer can induce according to the manufacturer's data. The recorded response may be contaminated by noise from the sampling process, as described in Section 3.2.1, and by other modes of vibration and the cross-sensitivity of the accelerometer, as described in Section 3.3.3. If the noise and unwanted components of response mask the flexural wave in the acceleration – time history and the frequency of the noise and unwanted components fall outside the frequency range of the flexural wave, they can be removed by digital filtering. The frequency content of the flexural wave, possible noise, and possible other modes of vibration are identified by the acceleration spectrum of the measured response.

The unfiltered test results for the impacts on the 0-degree and 180-degree orientations are presented on Figure 5-3.

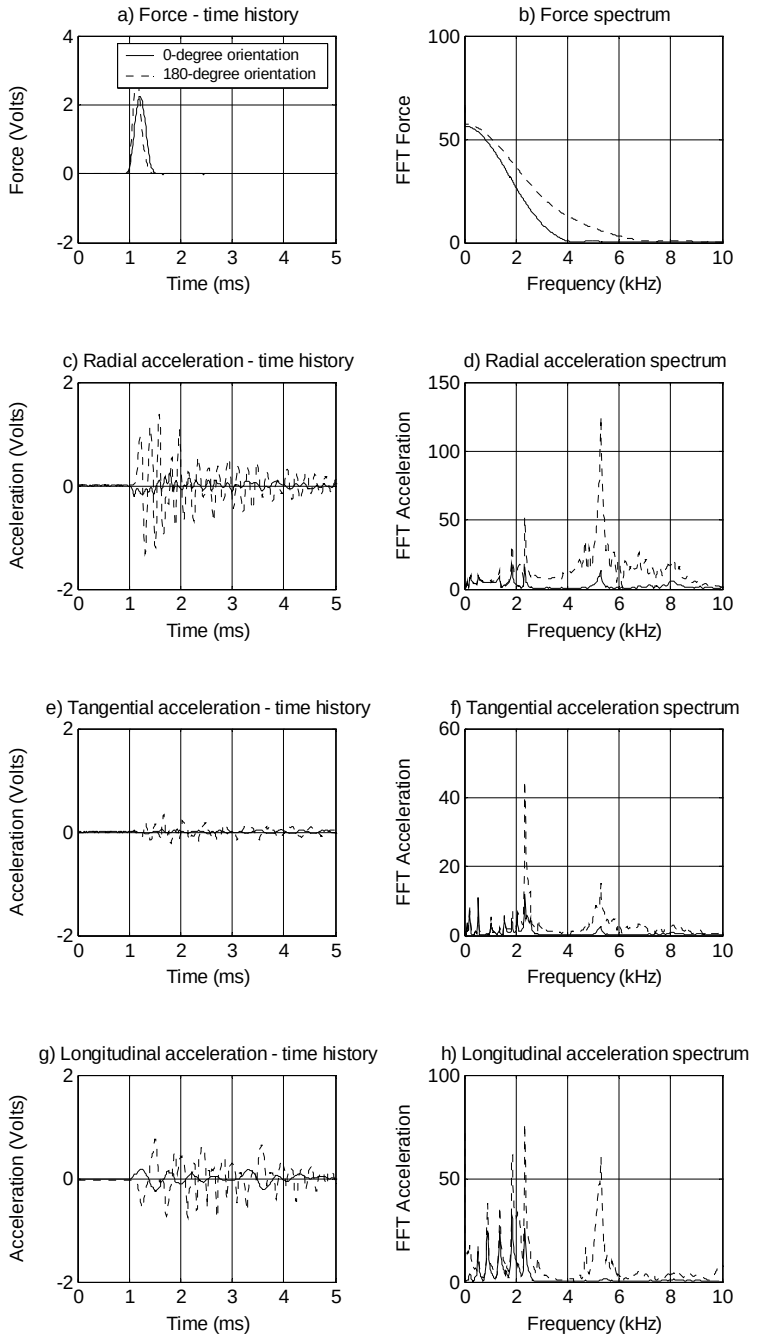

Figure 5-3: Prototype pile C355-2430, unfiltered lateral impact results for 0-degree orientation and 180-degree orientation

The null frequencies for the hammer impacts on Figure 5-3b are at approximately 4.5 kHz and 7 kHz for the impacts on the 0-degree and 180-degree faces, respectively. The pile response, shown on Figures 5-3d, 5-3f and 5-3h, contains a set of peaks between DC and 2500 Hz, which are assumed to be the modes of the flexural wave, and another peak at 5300 Hz. For purposes of analysis of lateral impact results, the peak at 5300 Hz is to be removed by filtering because it masks identification of reflections of the flexural wave. The peak at 5300 Hz is smaller in the longitudinal direction than in the radial direction, which implies that the cutoff frequency of the filter could be set higher for the analysis of the response measured in the longitudinal direction than in the radial direction, but that is not recommended if direct comparison of the longitudinal and radial responses is desired. The group delay and phase delay values presented in Section 3.5.1 are functions of the filter type, cutoff frequency and filter order. All data were filtered with a lowpass Butterworth filter of order 6, leaving cutoff frequency as the parameter to be adjusted. Filtering the results of different tests, or of the same test measured in a different direction, with different cutoff frequencies results in different phase delay and group delay values for different tests or directions of measurement.

The unfiltered test results for the impacts on the 90-degree and 270-degree orientations are presented on Figure 5-4.

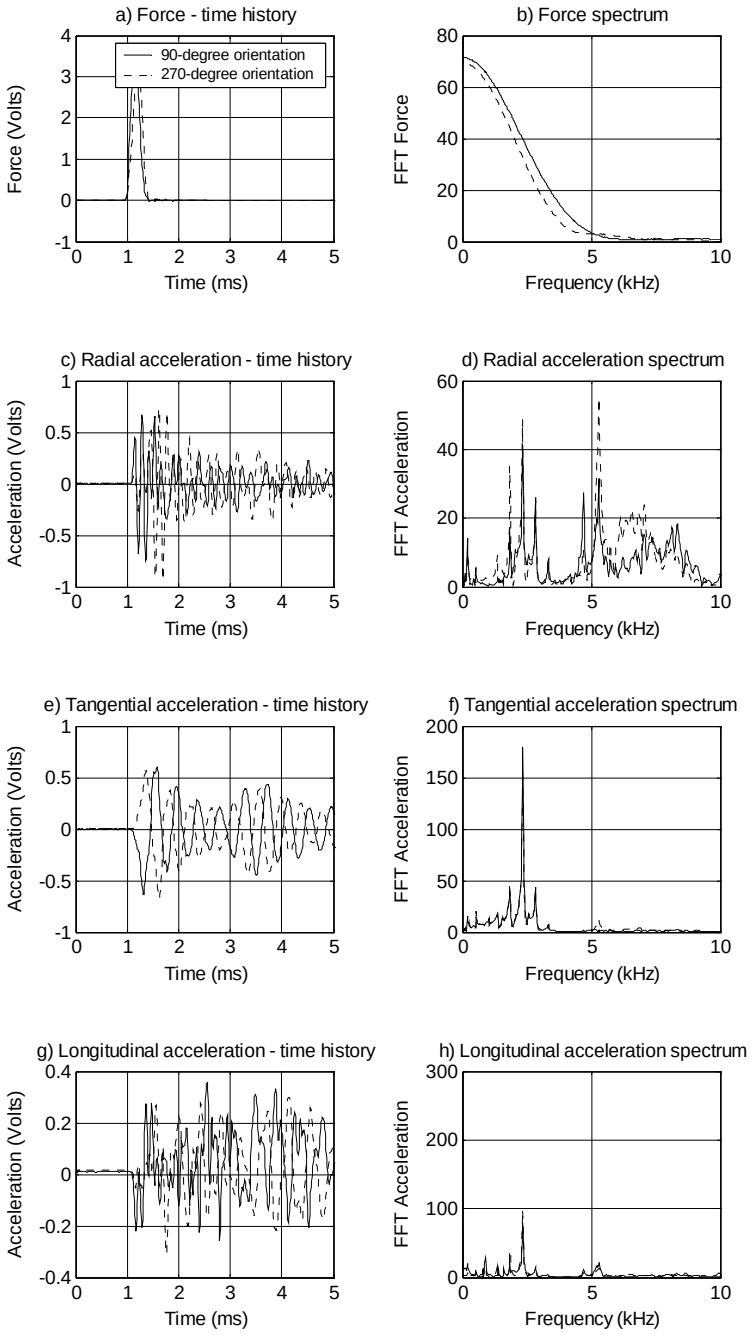

Figure 5-4: Prototype pile C355-2430, unfiltered lateral impact results for 90-degree orientation and 270-degree orientation

The null frequencies for the hammer impacts on Figure 5-4b are at approximately 6 kHz for both sets of impacts. The pile response, shown on Figures 5-4d, 5-4f and 5-4h, contains a set of peaks between DC and 2500 Hz, which are assumed to be the modes of the flexural wave, and another peak at 5300 Hz. For the 90-degree and 270-degree orientation tests, only the tangential component of the response is analyzed. The first pass and return of the stress wave can be identified in the tangential acceleration – time history because the peak at 5300 Hz is smaller than the peaks between DC and 2500 Hz, and is smaller than the peak at 5300 Hz in the radial direction of the tests performed with impacts at the 0-degree and 180-degree orientations. The data for the tests performed at the 90-degree and 270-degree orientations were filtered with the same cutoff frequency as the tests performed at the 0-degree and 180-degree orientations so that the phase delays and group delay were the same for all sets of tests.

The unfiltered test results presented on Figures 5-3 and 5-4 have been filtered with a lowpass Butterworth filter of order 6 and a cutoff frequency of 3000 Hz. The cutoff frequency was selected to remove the portion of the wave at 5300 Hz because it masks the reflections of the expected flexural wave.

The filtered acceleration – time histories and acceleration spectra of the impacts at the 0-degree and 180-degree orientations are presented on Figure 5-5.

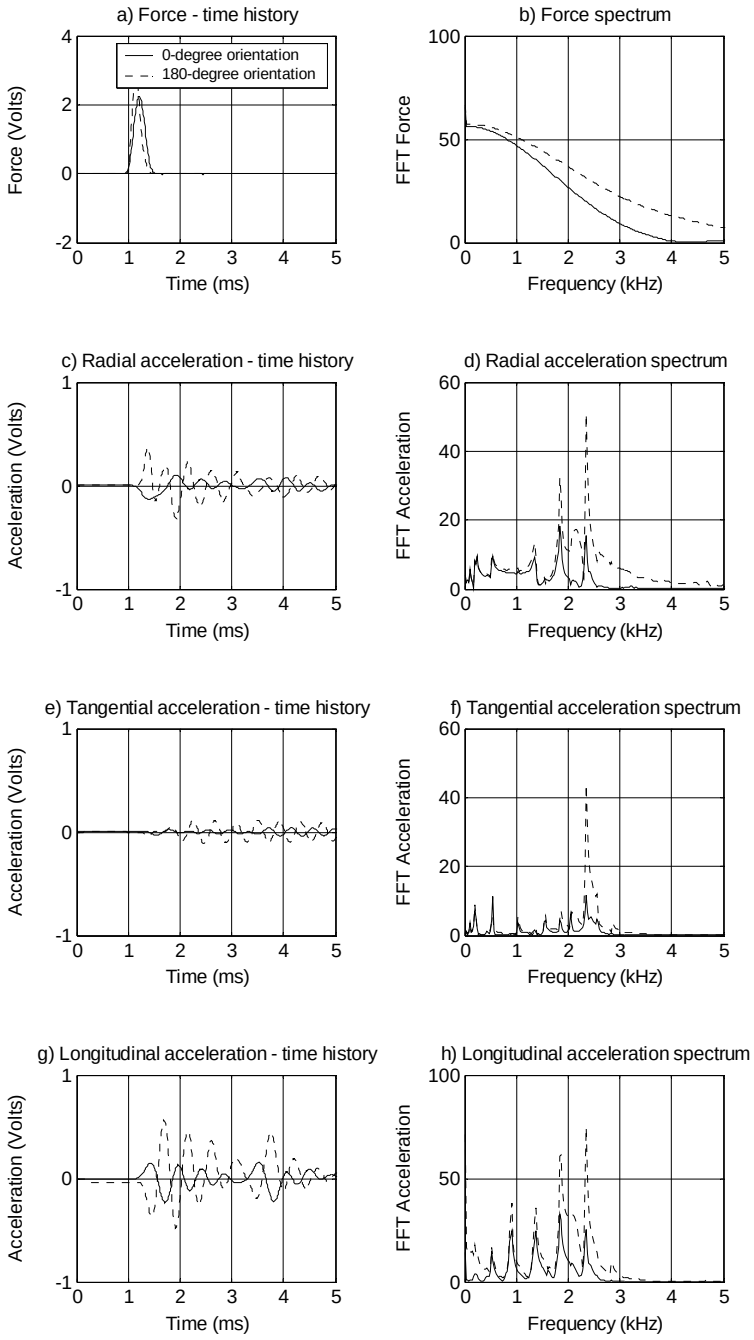

Figure 5-5: Prototype pile C355-2430, lateral impact results for 0-degree and 180-degree orientations

The selected digital filter and its parameters completely removed the peak at 5300 Hz but did not remove all frequency components at or above 3000 Hz, which is the cutoff frequency. The frequency components above the cutoff frequency were not completely removed because the data were filtered with a Butterworth filter, which has a long transition band, as described in Section 3.5.1.

The filtered acceleration – time histories and acceleration spectra for the impacts at the 90-degree and 270-degree orientations are presented on Figure 5-6. The acceleration – time histories were filtered with a cutoff frequency of 3000 Hz, which is the same cutoff frequency used to analyze the results of the impacts on the 0-degree face and 180-degree face.

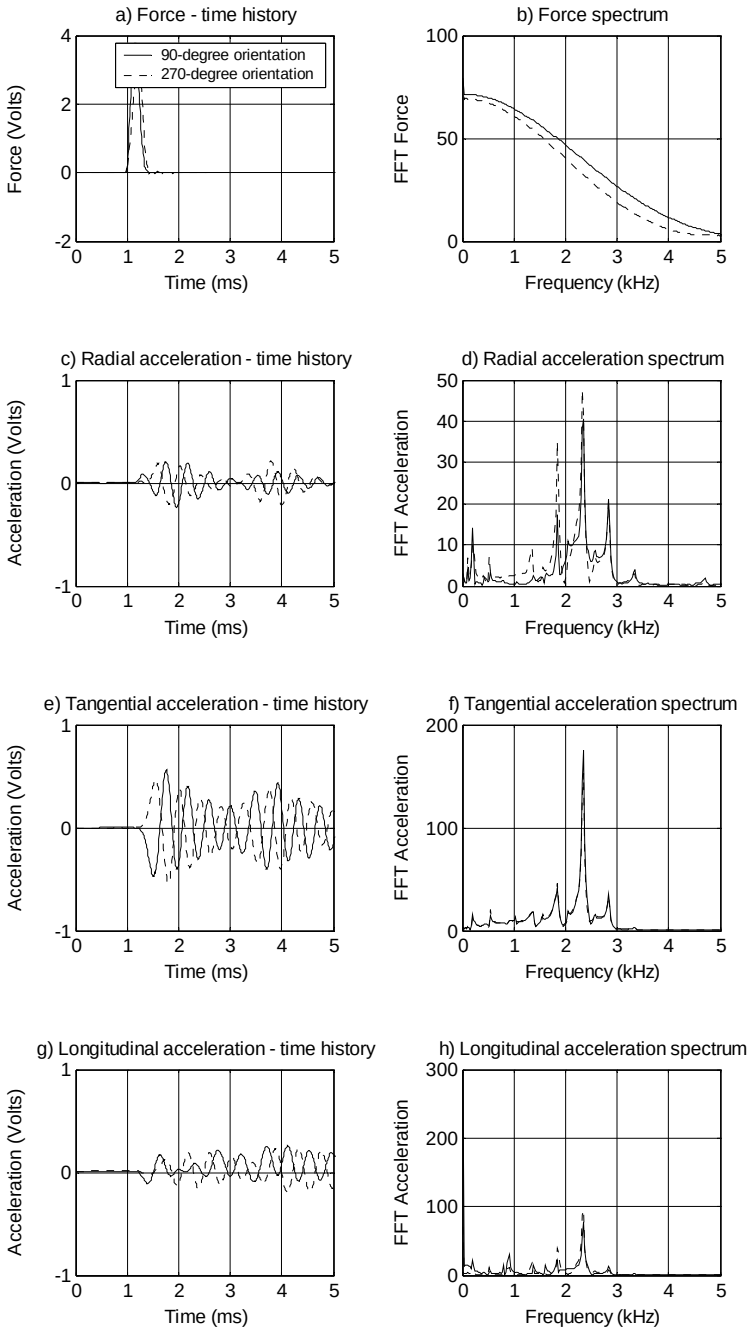

Figure 5-6: Prototype pile C355-2430, lateral impact results for 90-degree and 270-degree orientations

As with the data from the tests performed at the 0-degree and 180-degree orientations, the selected digital filter and its parameters completely removed the peak at 5300 Hz but did not remove all frequency components at or above 3000 Hz, which is the cutoff frequency.

The frequencies identified in the filtered data are compared to the cutoff frequencies for the various branches to identify the branch or branches on which modes are expected to propagate. The nondimensional cutoff frequencies of the first five flexural branches were computed for concrete with a Poisson's ratio of 0.20, which is the Poisson's ratio of prototype pile C355-2430, traction-free conditions. The nondimensional cutoff frequencies were converted to cutoff frequency for prototype pile C355-2430 in Section 4.3.

The cutoff frequencies of the first five branches, as presented in Section 4.3, are summarized on Table 5-1.

Table 5-1: Prototype pile C355-2430 under traction-free conditions, cutoff frequencies of first five flexural branches

Mode	Frequency (Hz)
F(1,1)	0
F(1,2)	4240
F(1,3)	5970
F(1,4)	11770
F(1,5)	12600

The highest frequency identified in the filtered data on Figure 5-4d, 5-4h, and 5-5f are about 2500 Hz, which is below the cutoff frequency for the F(1,2) branch. Comparison of the

maximum frequency included in the analysis and the cutoff frequencies for the various branches indicates that modes can be excited on the F(1,1) branch but not the F(1,2) branch or any higher flexural branch.

5.2.2 Responses as Functions of Orientation

The filtered responses for the impacts at the 0-degree and 180-degree faces were presented on Figure 5-4. The tangential component of the acceleration was not zero but it was much smaller than the radial and longitudinal components. The responses for the impacts at the 90-degree and 270-degree faces were presented on Figure 5-5. The longitudinal and radial components of the response were not zero but they were much smaller than the tangential component.

The tangential component of the acceleration for the 0-degree and 180-degree orientations should be zero, as should the radial and longitudinal components of the acceleration for the impacts at the 90-degree and 270-degree orientations, but they were not. Cross-sensitivity of the accelerometer and portions of the signal leaking across wires, as discussed in Section 3.3.3, could cause the nonzero response for directions that are theoretically zero.

The radial and longitudinal components of the acceleration depend on the cosine of the angle which, for 0 degrees and 180 degrees have the same magnitude but opposite signs. The

tangential component of the acceleration depends on the sine of the angle, which, for 90 degrees and 270 degrees have the same magnitude but different signs, suggesting that the response of the pile due to hits on opposite faces should have opposite signs, i.e., they should be 180-degrees out of phase. The concept of waves being 180-degrees out of phase is illustrated by considering the response of the pile to impacts on opposite faces.

The longitudinal component of the acceleration – time history due to impacts at the 0-degree and 180-degree orientations is shown on Figure 5-7 as an example.

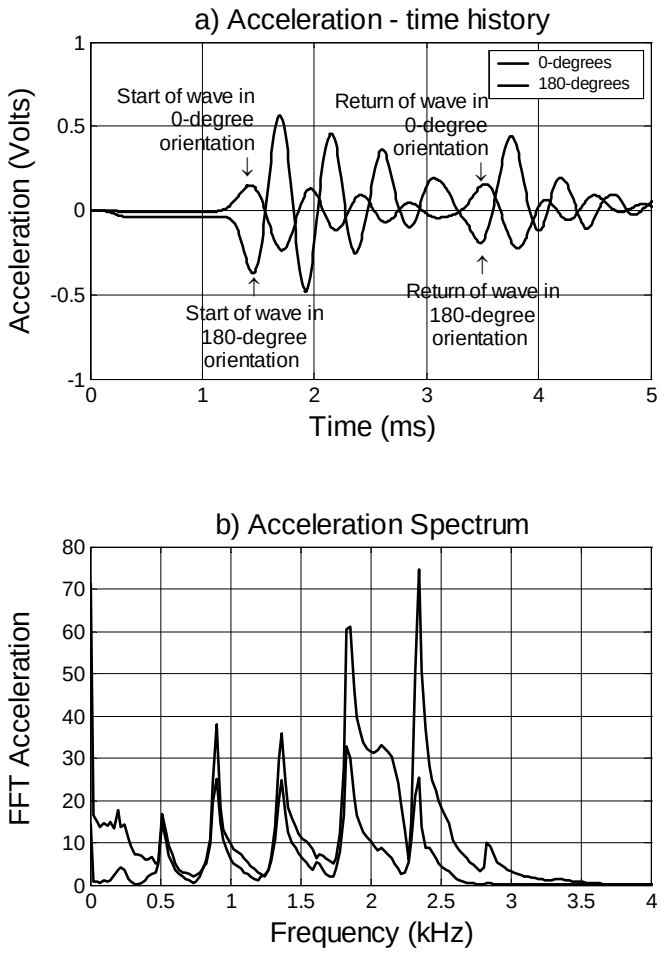

Figure 5-7: Prototype pile C355-2430, lateral impact results for 0-degree and 180-degree orientations

The peaks in the acceleration spectrum shown on Figure 5-7b occur at the same frequencies, but the magnitudes are different. The time histories, shown on Figure 5-7a, indicate that the first pass and return of the stress wave have the opposite signs. At the 0-degree orientation, the voltage of the first peak is positive and the acceleration of the largest peak of the first pass is

negative; at the 180-degree orientation, the acceleration of the first peak is negative and the acceleration of the largest peak of the first pass is positive. For both tests, the voltage is zero at 1.56 ms. The return of the stress wave starts at about 3.3 ms, as indicated by an increase in response. The acceleration of the first peak of the return is positive for the impact at the 0-degree orientation and negative for the first peak at the 180-degree orientation. For the largest peak of the return, which is centered at 3.76 ms, the voltage is negative for the impact at the 0-degree orientation and positive for the 180-degree orientation. Between the first pass and return, the response of the pile to the two impacts is not necessarily 180-degrees out of phase because it contains the transient response and is influenced by noise in the signal. The two responses are 180-degrees out of phase at the return of the reflected wave.

5.2.3 Phase Velocity Measurement and Verification

The phase velocity is determined from impact test results by the procedure outlined in Section 3.4.3. The phase velocity, c_p, is computed from the frequency domain representation of the signal by

$$c_p = \frac{2Lf_n}{n} \qquad (5\text{-}1)$$

where L is the pile length and f_n is the frequency of harmonic n. For pile C355-2430, the pile length is 2.43 m. The experimental results are superimposed on the numerically-determined phase velocity – frequency curve for the F(1,1) branch to determine if a lateral impact induces waves that lie along the F(1,1) branch.

The longitudinal and radial responses for the 0-degree and 180-degree orientations, and the tangential response for the 90-degree and 270-degree orientations were analyzed. Complete results for the longitudinal response of the 0-degree orientation are provided as an example, complete analysis of all tests can be found in Appendix B, and the summary of all results is presented in this section.

The results of the impact on the 0-degree face with the response measured in the longitudinal direction are presented on Figure 5-8.

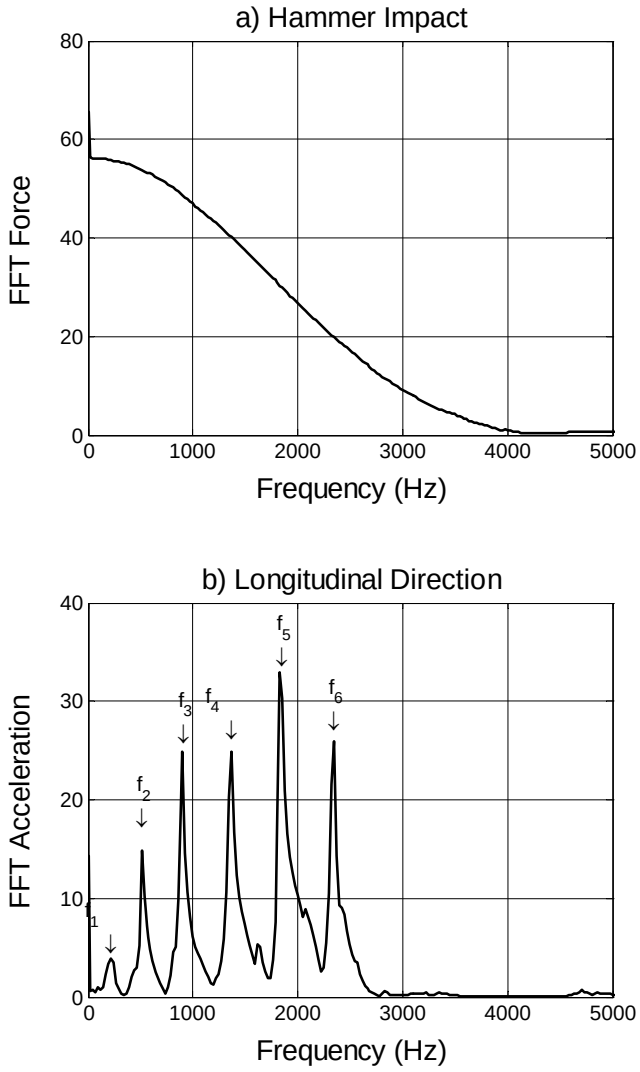

Figure 5-8: Prototype pile C355-2430, lateral impact results for 0-degree orientation with response measured in longitudinal direction

The frequencies identified on Figure 5-8b, along with the phase velocities computed by equation 5-1, are presented on Table 5-2.

Table 5-2: Prototype pile C355-2430, lateral impact results for 0-degree orientation natural frequencies of pile excited by impact and corresponding phase velocities

Harmonic	Frequency (Hz)	Phase Velocity (m/s)
1	220	1070
2	515	1250
3	905	1470
4	1365	1660
5	1830	1780
6	2345	1900

The phase velocity – frequency data presented on Table 5-2 are superimposed on the numerically-determined phase velocity - frequency curve for the F(1,1) branch (Section 4.3) on Figure 5-9.

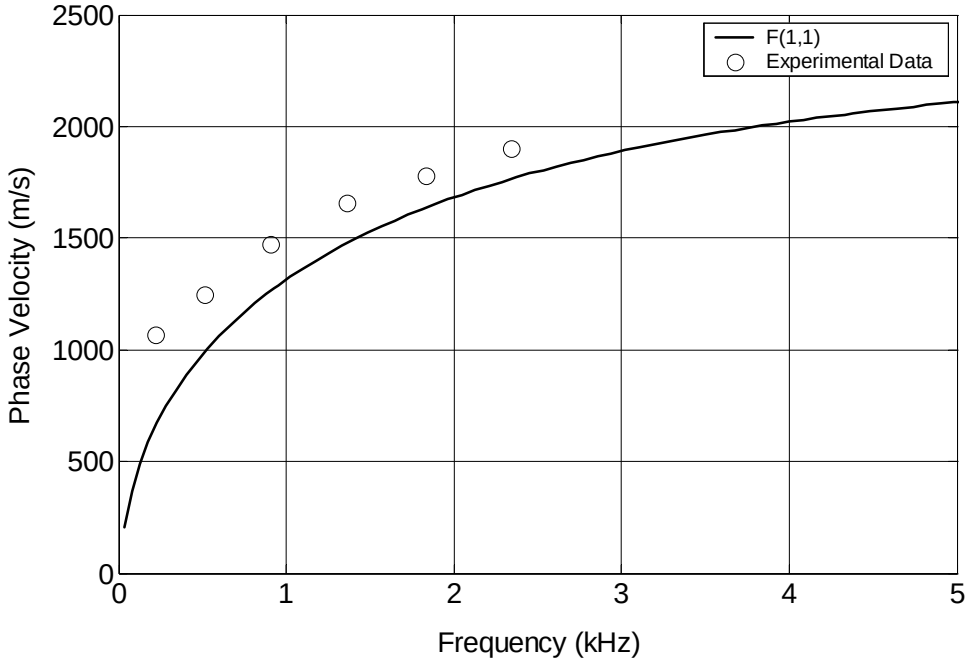

Figure 5-9: Prototype pile C355-2430, lateral impact results for 0-degree orientation, longitudinal phase velocity – frequency data superimposed on numerically-determined phase velocity – frequency curve for concrete with $\nu_c = 0.20$

Guided wave theory suggests that modes on the F(1,1) branch are dispersive at low frequencies as shown by the solid line. The open circles corresponding to the experimental data follow the shape of the numerical curve, indicating that the lateral impact does induce flexural modes on the F(1,1) branch, and that those modes are dispersive.

The frequencies of the individual phases were identified for each test and measurement direction listed in Section 5.1. The individual graphs of the force spectrum and acceleration

spectrum for each test are provided in the Appendix B. The phase velocity – frequency data computed from the graphs in Appendix B, are presented on Table 5-3.

Table 5-3: Prototype Pile C355-2430, frequencies and phase velocities determined from lateral impact tests

Longitudinal direction				Radial direction				Tangential direction			
0-degree face		180-degree face		0-degree face		180-degree face		90-degree face		270-degree face	
f (Hz)	c_p (m/s)	f (Hz)	c_p (m/s)	f (Hz)	c_p (m/s)	f (Hz)	c_p (m/s)	f (Hz)	c_p (m/s)	f (Hz)	c_p (m/s)
220	1070	195	950	245	1190	245	1190	195	950	195	950
515	1250	515	1250	535	1300	535	1300	535	1300	535	1300
905	1470	905	1470	1025	1660	N/I	N/I	1025	1660	1025	1660
1365	1660	1365	1660	1345	1630	1345	1630	1365	1660	1345	1630
1830	1780	1855	1800	1830	1780	1830	1780	1830	1780	1830	1780
2345	1900	2345	1900	2345	1900	2345	1900	2345	1900	2345	1900
N/I	N/I	N/I	N/I	N/I	N/I	N/I	N/I	2830	1960	2830	1960

Note: N/I indicates that the harmonic was not identified in the specified test and measurement direction.

The frequency spacing of the FFT array is approximately 24, which indicates that most of the frequencies identified in the tests are within one point of each other. For the first harmonic, the variation was 3 points, and for the fourth harmonic, the variation was 4 points. The ordered pairs of frequency and phase velocity presented on Table 5-3 are superimposed on the numerically-determined phase velocity – frequency curve for the L(0,1) and F(1,1) branches, on Figure 5-10.

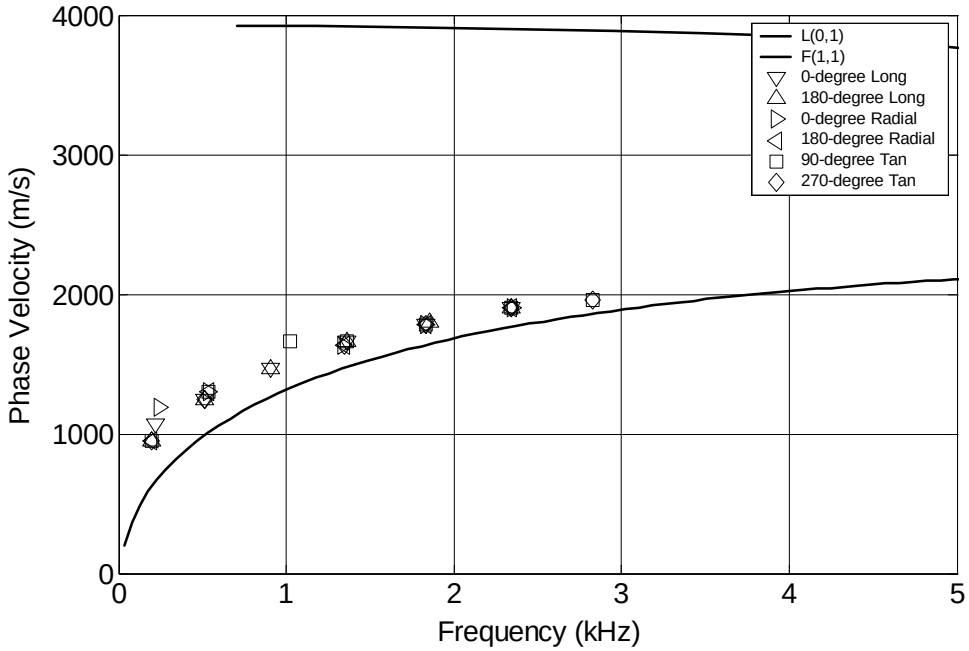

Figure 5-10: Prototype pile C355-2430, lateral impact results
phase velocity – frequency data superimposed on numerically-determined
phase velocity – frequency curves for concrete with $\nu_c = 0.20$

The experimental results presented on Figure 5-10 include the values presented on Figure 5-9, which are the results from the impact at the 0-degree orientation with the response measured in the longitudinal direction. The experimental results presented on Figure 5-10 indicate that all of the lateral impacts considered herein produce dispersive waves for which the phases lie along the F(1,1) branch. The phase velocity – frequency curve for the L(0,1) branch was included for comparison to indicate that the lateral impacts do not excite any modes on the L(0,1) branch.

5.2.4 Group Velocity Measurement and Verification

Guided wave theory suggests that flexural waves are dispersive, which requires the group velocity and frequency to be determined separately from each other, which is different from the interpretation of the one dimensional tests such as the sonic echo and impulse response tests described in Section 2.1. The displacement equations presented in Section 2.3.8 indicate that the first pass of the wave for hits on opposite faces are 180 degrees out of phase with each other, as are the reflections. The free vibration and noise in between the first pass and return may or may not be 180-degrees out of phase for hits on opposite faces. The relationship between acceleration – time histories of hits on opposite faces was illustrated on Figure 5-6.

To identify the first pass and return of the stress wave, one plots the response from hits on opposite faces and identifies paired peaks, as presented in Section 5.2.2. The group velocity is computed by the procedure outlined in Section 3.4.3, using equation 5-2.

$$c_g = \frac{2L}{\Delta t} \qquad (5\text{-}2)$$

For prototype pile C355-2430 under traction-free conditions, the accelerometer is mounted on the side of the pile, 166 mm below its top. The first pass of the stress wave and return of the reflected stress wave are identified on the acceleration – time history. Because the travel time for the group is identified from the first pass and return at an accelerometer mounted on the side of the pile, below it top, L in equation 5-2 is the distance from the accelerometer to the pile tip, and the travel distance is $2L$. From the dimensions on Figure 5-2, L is 2264 mm.

The frequency of the wave group cannot be computed as the reciprocal of the travel time because flexural waves are dispersive; rather, the frequency of the wave group is computed from the period of the wave that comprises the first pass of the wave group.

The longitudinal response of lateral impact test results for the impacts at the 0-degree and 180-degree orientations are presented on Figure 5-11.

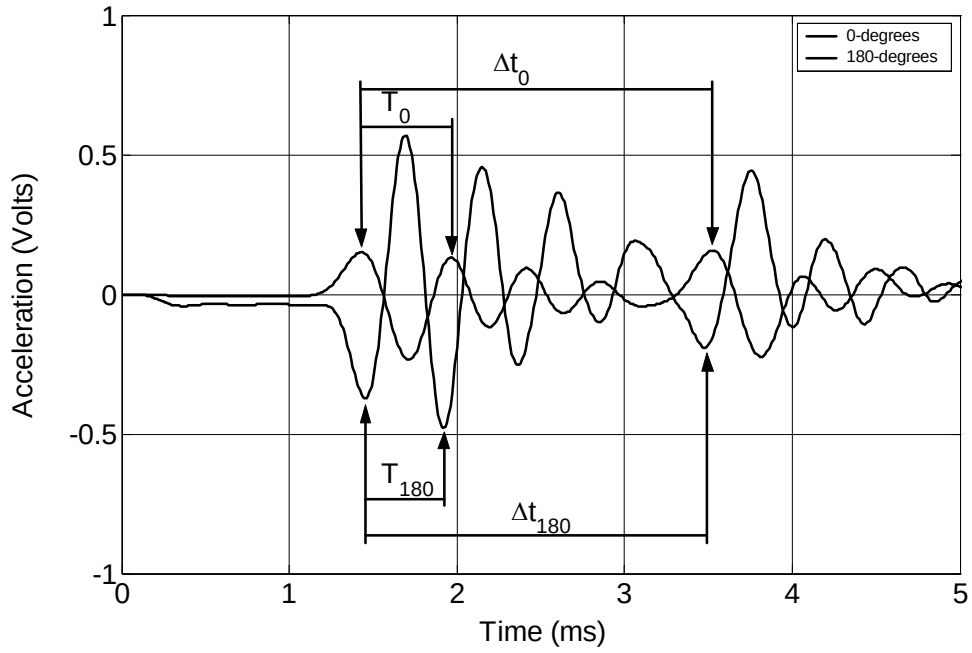

Figure 5-11: Prototype Pile C355-2430, lateral impact results for 0-degree and 180-degree orientations, longitudinal direction

The first pass and returns of the stress wave shown on Figure 5-11 are 180-degrees out of phase, as discussed in Section 5.2.2. For the 0-degree orientation, the period of the propagating stress wave, T_0, is 0.43 ms, for a frequency of 2325 Hz, and the travel time for the first pass and reflection of the stress wave, Δt_0, is 2.09 ms. The group velocity is 2170 m/s, as computed by equation 5-2 with L = 2264 mm and Δt = 2.09 ms. For the 180-degree orientation, the period of the propagating stress wave, T_{180}, is 0.47 ms, for a frequency of 2130 Hz, and the travel time for the first pass and reflection of the stress wave, Δt_{180}, is 2.01 ms. The group velocity is 2250 m/s, as computed by equation 5-2 with L = 2264 mm and Δt = 2.01 ms.

The radial responses of the impacts at the 0-degree and 180-degree orientations are presented on Figure 5-12.

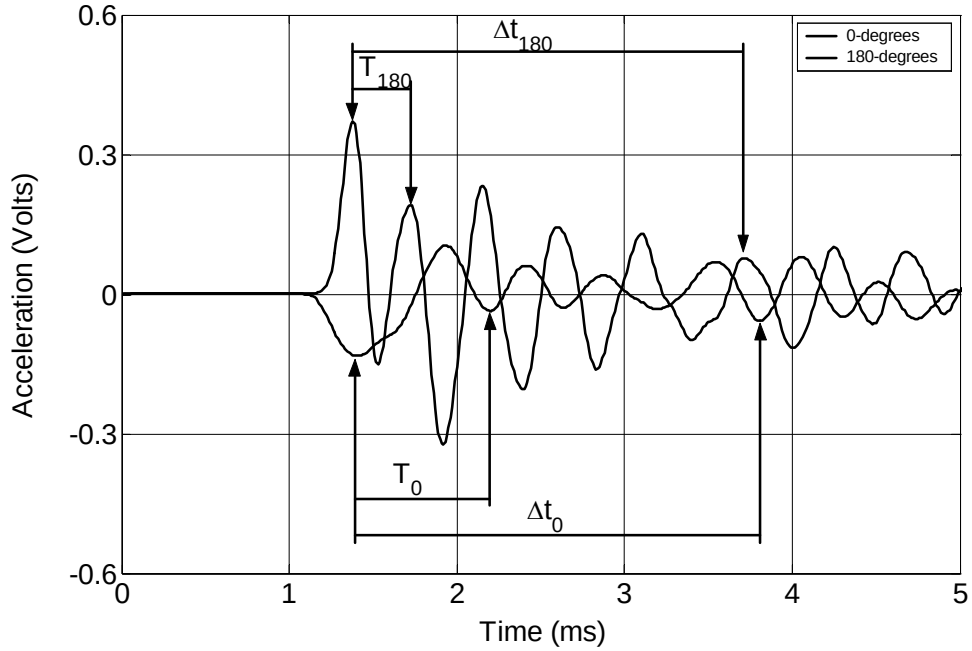

Figure 5-12: Prototype Pile C355-2430, lateral impact results for 0-degree and 180-degree orientations, radial direction

The first pass and returns of the stress wave shown on Figure 5-12 are 180-degrees out of phase, as discussed in Section 5.2.2. For the 0-degree orientation, the period of the propagating stress wave, T_0, is 0.80 ms, for a frequency of 1250 Hz, and the travel time for the first pass and reflection of the stress wave, Δt_0, is 2.39 ms. The group velocity is 1900 m/s, as computed by equation 5-2 with L = 2264 mm and Δt = 2.39 ms. For the 180-degree orientation, the period of the propagating stress wave, T_{180}, is 0.34 ms, for a frequency of 2940 Hz, and the travel time for the first pass and reflection of the stress wave, Δt_{180}, is 2.33 ms. The group velocity is 1940 m/s, as computed by equation 5-2 with L = 2264 mm and Δt = 2.33 ms.

The results of the analysis of the tangential results of the lateral impact tests performed on the 90-degree and 270-degree face are presented on Figure 5-13.

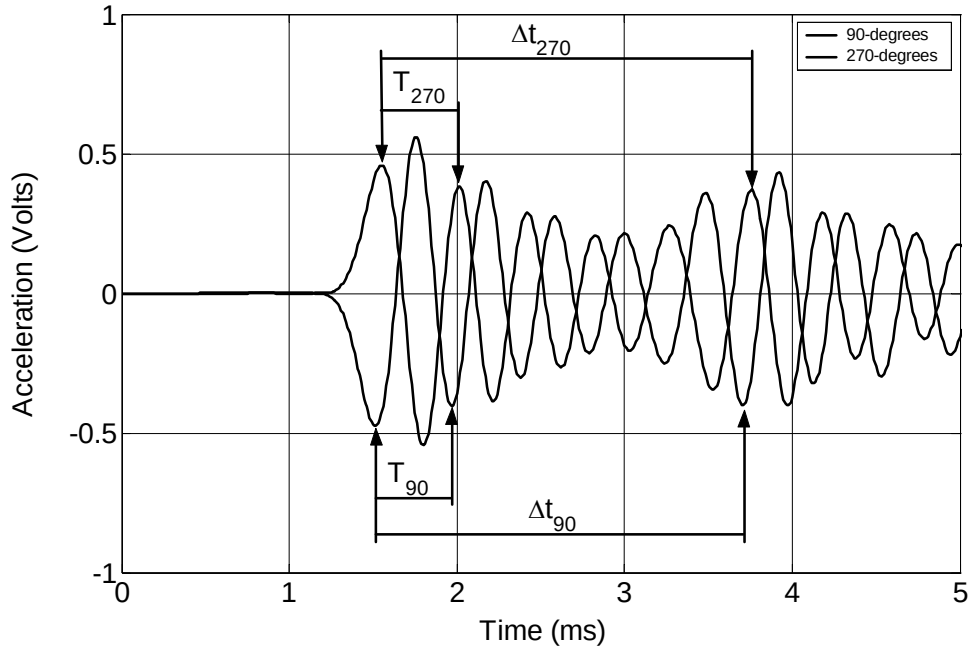

Figure 5-13: Prototype Pile C355-2430, lateral impact results for 90-degree and 270-degree orientations, tangential direction

The first pass and returns of the stress wave shown on Figure 5-13 are 180-degrees out of phase, as discussed in Section 5.2.2. For the 90-degree orientation, the period of the propagating stress wave, T_{90}, is 0.45 ms, for a frequency of 2220 Hz, and the travel time for the first pass and reflection of the stress wave, Δt_{90}, is 2.21 ms. The group velocity is 2050 m/s, as computed by equation 5-2 with L = 2264 mm and Δt = 2.21 ms. For the 270-degree orientation, the period of the propagating stress wave, T_{270}, is 0.48 ms, for a frequency of 2080 Hz, and the travel time for

the first pass and reflection of the stress wave, Δt_{270}, is 2.21 ms. The group velocity is 2050 m/s, as computed by equation 5-2 with L = 2264 mm and Δt = 2.21 ms.

The group velocities and corresponding frequencies for the lateral impact tests performed on prototype pile C355-2430 under traction-free conditions are presented on Table 5-4.

Table 5-4: Prototype pile C355-2430, summary of group velocity and frequency values from lateral impact results

Measurement Direction	Test Orientation	Group Velocity (m/s)	Group Frequency (Hz)
Longitudinal	0-degree	2170	2325
	180-degree	2250	2130
Radial	0-degree	1900	1250
	180-degree	1940	2940
Tangential	90-degree	2050	2220
	270-degree	2050	2220

The ordered pairs of group velocity and frequency are superimposed on the numerically-determined group velocity – frequency curve for the L(0,1) and F(1,1) branches on Figure 5-14.

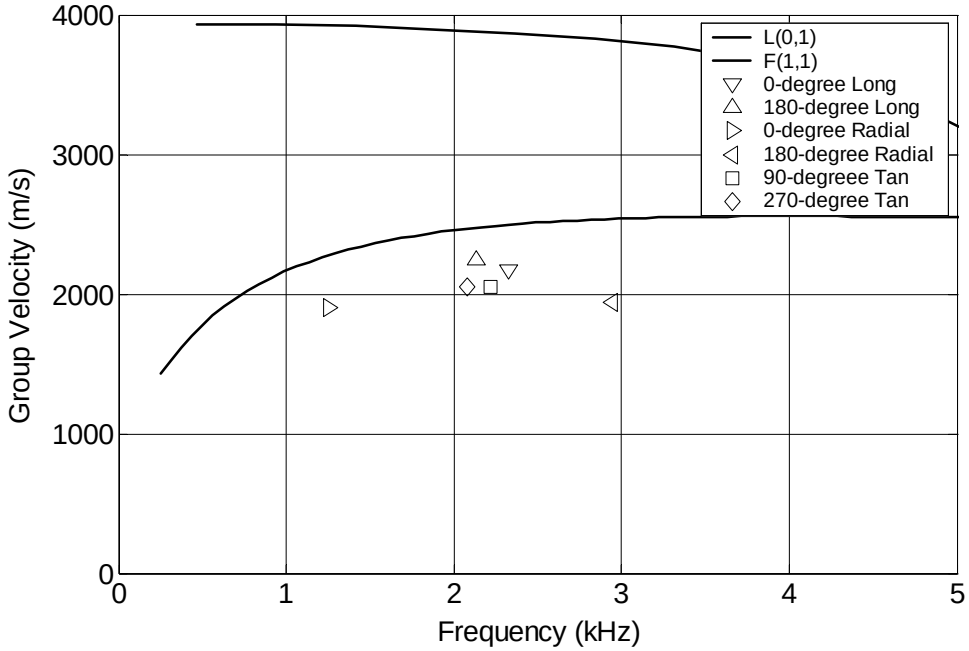

Figure 5-14: Prototype pile C355-2430, lateral impact results
group velocity – frequency results superimposed on numerically-determined
group velocity – frequency curves for concrete with $\nu_c = 0.20$

The experimental values of frequency and group velocity follow the trend of the F(1,1) branch and are much closer to the group velocity – frequency curve for the F(1,1) branch than to the group velocity – frequency curve for the L(0,1) branch, indicating that a lateral impact induces flexural waves. The ordered pairs of frequency and group velocity for the longitudinal direction of the impacts at the 0-degree and 180-degree orientations and the tangential direction of the impacts at the 90-degree and 270-degree orientations had the smallest scatter; whereas, the ordered pairs of frequency and group velocity for the radial direction of the impacts at the 0-degree and 180-degree orientations had the largest scatter.

5.2.5 Conclusions

Lateral impact results were performed on Prototype pile C355-2430 under traction-free conditions. The analysis of the filtered test results and comparison with theoretical phase and group velocity values indicate that the lateral impact method does induce a propagating stress wave that falls along the F(1,1) branch, and, consequently, verifies the flexural guided wave theory.

5.3 Evaluation of Prototype Piles under Embedded Conditions

Three prototype piles were evaluated with lateral impact tests under embedded conditions to determine the phase and group velocity – frequency relationships. In addition to prototype pile C355-2430, the other two prototype piles described in Section 2.2 were evaluated by the lateral impact method. The two existing prototype piles were cast and embedded prior to the start of the current investigation and, consequently, they were not evaluated under traction-free conditions by lateral impact tests. The embedment conditions and mounting base locations are shown on Figure 5-15.

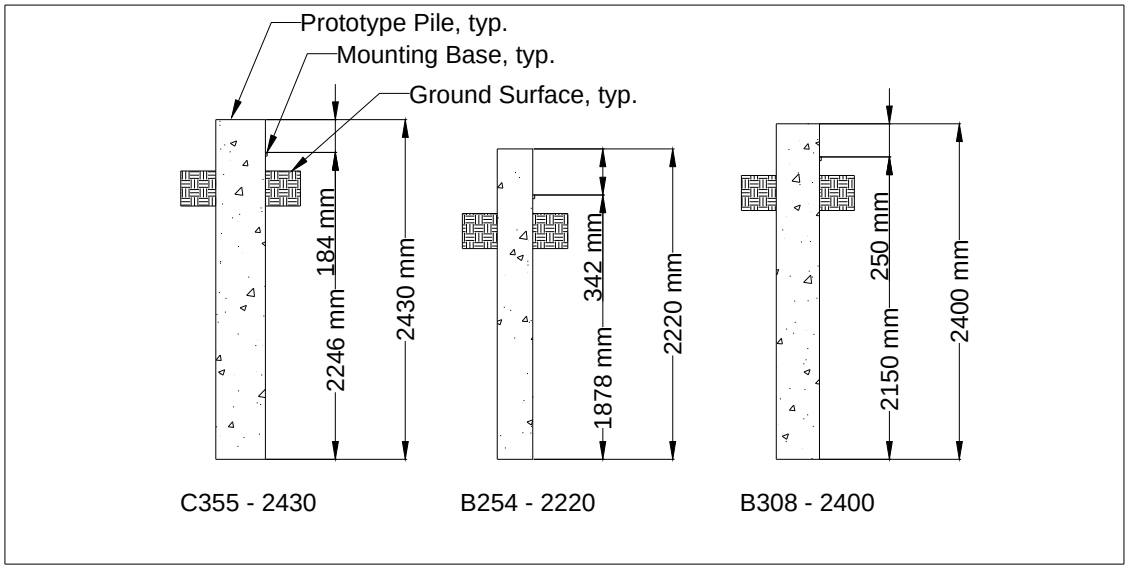

Figure 5-15: Prototype piles, accelerometer mounting base positions for lateral impact tests under embedded conditions

The piles were cast and cured prior to installation into the soil. They were installed by digging an excavation, placing the pile into the excavation, and backfilling the excavation. The depth of excavation was selected so that the top of the pile would be flush with the ground surface, except for prototype pile B254-2220 which stuck up about 100 mm above the ground surface after installation. To perform the lateral impact tests, the soil around each prototype pile was excavated to depths of about 300 mm to 450 mm below the top of the pile, to allow the accelerometer mounting bases to be installed on the pile, leaving 115 mm ± 5 mm to attach the accelerometer to the mounting base.

Lateral impact tests were performed at 0-degrees, 90-degrees, 180-degrees, and 270-degrees, just as in the traction-free conditions presented in Section 5.1. For impacts in the 0-

degree and 180-degree orientations, the longitudinal and radial responses were analyzed; for the impacts in the 90-degree and 270-degree orientations, the tangential responses were analyzed. The experimental results are compared to the numerically-determined values for the respective piles.

5.3.1 Generation of Dispersion Curves

The dispersion curves for the embedded case are developed by the same procedure by which the traction-free curves were developed, except that the actual density ratio and shear modulus ratio must be used. The concrete properties from which the density ratio and shear modulus ratio are computed are presented on Table 5-5.

Table 5-5: Summary of dynamic properties for prototype piles

Pile	Bar Wave Velocity c_{Lc} (m/s)	Shear Wave Velocity c_{Tc} (m/s)	Poisson's ratio ν_c	Density ρ_c (kg/m^3)
C355-2430	3900	2530	0.20	2350
B254-2220	4510	2730	0.18	2400
B308-2400	4150	2780	0.28	2365

The Poisson's ratio of the concrete, ν_c, is computed from the bar wave velocity, c_{Lc}, and the shear wave velocity, c_{Tc} by

$$\nu_c = \frac{1}{2}\left(\frac{c_{Lc}}{c_{Tc}}\right)^2 - 1 \qquad (5\text{-}3)$$

and is an input required to develop the nondimensional dispersion curves for both traction-free and embedded conditions. The soil properties required to develop the dispersion curves are ν_s, which is assumed to be 0.30, c_{Ts}, which is 105 m/s, and ρ_s, which is 1600 kg/m^3 (Finno & Gassman, 1998). The input properties used to develop the nondimensional dispersion curves for embedded conditions are presented on Table 5-6.

Table 5-6: Summary of input properties for generation of nondimensional dispersion curves

Pile	ν_c	ν_s	Density ratio	Shear modulus ratio
C355-2430	0.20	0.30	1.5	825
B254-2220	0.18	0.30	1.5	1125
B308-2400	0.28	0.30	1.5	1025

The values presented on Table 5-6 were used as inputs in the "Flexural_Dispersion.mws" program, found in appendix A, to compute the nondimensional frequency – nondimensional wavenumber relationship for the F(1,n) branches for n of 1 through 5, inclusive.

The nondimensional cutoff frequencies, Ω, for each pile under embedded conditions are shown on Table 5-7.

Table 5-7: Nondimensional cutoff frequencies for prototype piles embedded in very loose sand

Pile	Nondimensional cutoff frequencies for various branches				
	F(1,1)	F(1,2)	F(1,3)	F(1,4)	F(1,5)
C355-2430	0	1.8[3]	2.7[1]	5.1[2]	5.4[2]
B254-2220	0	1.60[3]	2.95[1]	5.17[2]	5.44[2]
B308-2220	0	1.60[3]	2.74[3]	5.31[3]	6.24[3]

Notes
1. Lowest value for which solution converged
2. Real part of nondimensional wavenumber less than 0.01
3. Values interpolated from graph

The nondimensional cutoff frequencies, Ω, on Table 5-7 are converted to cutoff frequencies by

$$f = \frac{\Omega c_{Tc}}{2\pi a} \qquad (5\text{-}4)$$

where c_{Tc} is the shear wave velocity of the concrete, and a is the pile radius. The cutoff frequencies are presented on Table 5-8.

Table 5-8: Cutoff frequencies for prototype piles embedded in very loose sand

Pile	Cutoff frequencies for various branches (Hz)				
	F(1,1)	F(1,2)	F(1,3)	F(1,4)	F(1,5)
C355-2430	0	4085	6125	11570	12250
B254-2220	0	5470	10090	17650	18610
B308-2220	0	4660	7980	15450	18160

Possible modes to be excited in a test are identified by comparing the frequency response of the impact to the cutoff frequencies listed on Table 5-9. The PCB 086C04 hammer can generate stress waves up to 8000 Hz, which indicates that modes are expected on the F(1,1) branch and F(1,2) branch, and possibly on the F(1,3) branch. The PCB 086M54 hammer can generate stress waves up to 2000 Hz. The recorded test results were filtered with a lowpass Butterworth filter of

order 6 and a cutoff frequency of 3000 Hz, as described in Sections 3.5.1 and 5.2.1. The combination of hammer performance and digital filtering parameters limit possible modes to the F(1,1) branch.

5.3.2 Prototype pile C355-2430

Lateral impact tests were performed on prototype pile C355-2430 under embedded conditions with the configuration shown on Figure 5-15. Tests were performed at the 0-degree, 90-degree, 180-degree, and 270-degree orientations, as defined on Figure 5-1. The results analyzed were the longitudinal and radial directions for the 0-degree and 180-degree orientations, and the tangential direction for the 90-degree and 270-degree orientations.

5.3.2.1 Phase Velocity Determination and Verification

The frequencies of the individual phases were identified from the acceleration spectrum, by the procedure presented in Section 5.2.3, and the phase velocities were computed by the procedure presented in Section 5.2.3, and complete results can be found in Appendix B. The phase velocity – frequency data for lateral impact tests performed on prototype Pile C355-2430 under embedded conditions are presented on Table 5-9.

Table 5-9: Prototype Pile C355-2430, frequencies and phase velocities determined from lateral impact tests

Longitudinal direction				Radial direction				Tangential direction			
0-degree face		180-degree face		0-degree face		180-degree face		90-degree face		270-degree face	
f (Hz)	c_p (m/s)	f (Hz)	c_p (m/s)	f (Hz)	c_p (m/s)	f (Hz)	c_p (m/s)	f (Hz)	c_p (m/s)	f (Hz)	c_p (m/s)
220	1070	210	1020	220	1070	230	1120	230	1120	230	1120
515	1250	530	1290	525	1280	535	1300	515	1250	550	1340
915	1480	915	1480	915	1480	925	1500	990	1600	N/I	N/I
1365	1660	1380	1680	1365	1660	1405	1710	1380	1680	1365	1660
1870	1820	2015	1960	1845	1790	2065	2010	1845	1790	1845	1790
N/I	N/I	N/I	N/I	N/I	N/I	N/I	N/I	2830	1960	2830	1960

Note: N/I indicates that the harmonic was not identified in the specified test and measurement direction.

The frequency spacing of the FFT array was approximately 12, which indicates that the frequencies identified in the tests are within six points of each other, except for the highest harmonic, for which the variation is 18 points. The ordered pairs of frequency and phase velocity presented on Table 5-9 are superimposed on the numerically-determined phase velocity – frequency curve for the L(0,1) and F(1,1) branches, on Figure 5-16.

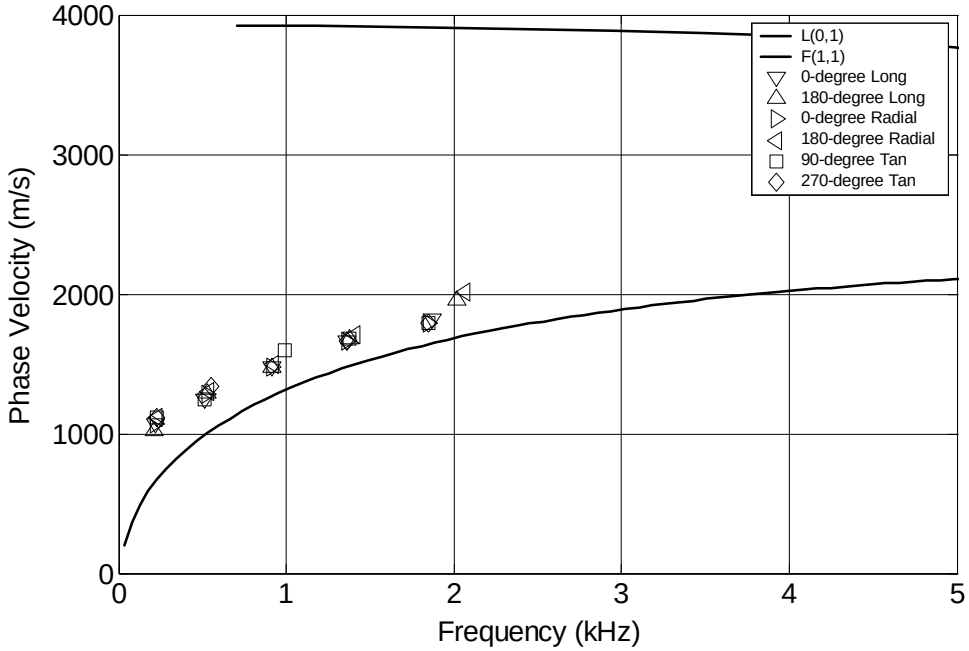

Figure 5-16: Prototype pile C355-2430, lateral impact results
phase velocity – frequency data superimposed on numerically-determined
phase velocity – frequency curves for concrete with $\nu_c = 0.20$

Guided wave theory suggests that modes on the F(1,1) branch are dispersive at low frequencies as shown by the dashed line. The individual points corresponding to the experimental data follow the shape of the numerical curve of the F(1,1) branch, indicating that the lateral impact does induce flexural modes on the F(1,1) branch, and that those modes are dispersive. The phase velocity – frequency curve for the L(0,1) branch is included to illustrate that a lateral impact does not induce modes that lie along the L(0,1) branch.

5.3.2.2 Group Velocity Determination and Verification

The group velocity and frequency of the group velocity were determined by the procedures presented in Section 5.2.4. Complete analysis of lateral impact tests performed on Prototype pile C355-2430 under embedded conditions can be found in Appendix C. The ordered pairs of group velocity and frequency obtained from the analysis of the lateral impact tests are summarized on Table 5-10.

Table 5-10: Prototype pile C355-2430, summary of group velocity and frequency values from lateral impact results

Measurement Direction	Test Orientation	Group Velocity (m/s)	Group Frequency (Hz)
Longitudinal	0-degree	2430	1410
	180-degree	2520	1370
Radial	0-degree	2290	3330
	180-degree	2430	2330
Tangential	90-degree	2050	1820
	270-degree	1960	1560

The ordered pairs of group velocity and frequency on Table 5-10 are superimposed on the numerically-determined group velocity – frequency curve for the L(0,1) and F(1,1) branches on Figure 5-17.

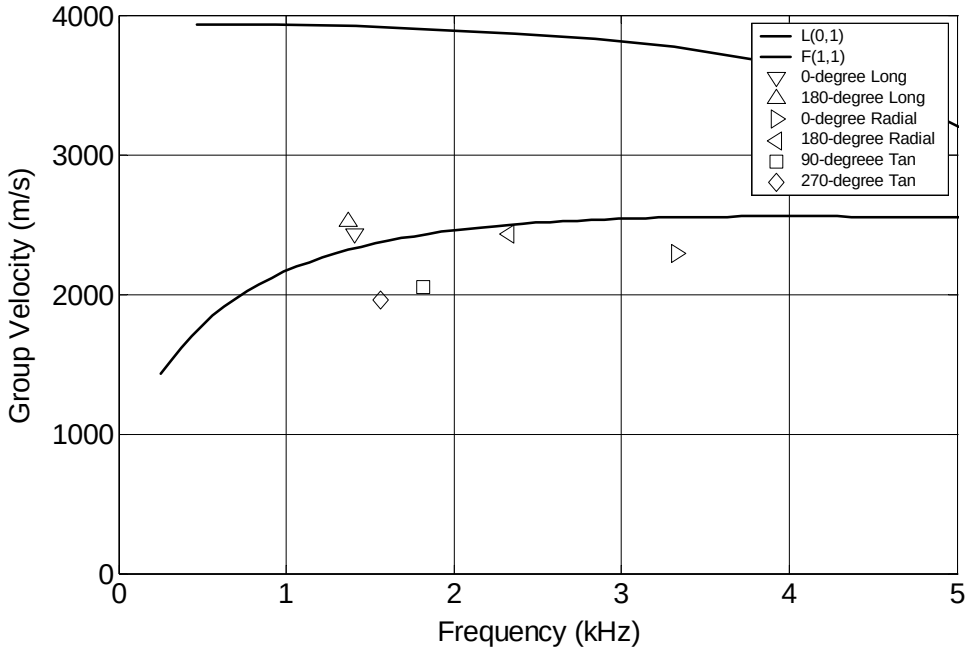

Figure 5-17: Prototype pile C355-2430, lateral impact results
group velocity – frequency data superimposed on numerically-determined
group velocity – frequency curves for concrete with $\nu_c = 0.20$

The ordered pairs of group velocity and frequency follow the shape of the numerically-determined group velocity – frequency curve for the F(1,1) branch, indicating that a lateral impact induces flexural waves. The numerically-determined group velocity – frequency curve for the L(0,1) branch is presented to show that the lateral impact does not induce longitudinal waves.

5.3.3 Prototype Pile B254-2220

Lateral impact tests were performed on prototype pile B254-2220 under embedded conditions with the configuration shown on Figure 5-15. Tests were performed at the 0-degree, 90-degree, 180-degree, and 270-degree orientations, as defined on Figure 5-1. The results analyzed were the longitudinal and radial directions for the 0-degree and 180-degree orientations, and the tangential direction for the 90-degree and 270-degree orientations.

5.3.3.1 Phase Velocity Determination and Verification

The lateral impact test results listed in Section 5.3.3 were analyzed to determine the ordered pairs of phase velocity and frequency for verification of the flexural guided wave theory. The phase velocity values were computed by the procedure outlined in Section 5.2.3. Complete results can be found in Appendix B. The phase velocity – frequency data for all tests are presented on Table 5-11.

Table 5-11: Prototype Pile B254-2220, frequencies and phase velocities determined from lateral impact tests

Longitudinal direction				Radial direction				Tangential direction			
0-degree face		180-degree face		0-degree face		180-degree face		90-degree face		270-degree face	
f (Hz)	c_p (m/s)	f (Hz)	c_p (m/s)	f (Hz)	c_p (m/s)	f (Hz)	c_p (m/s)	f (Hz)	c_p (m/s)	f (Hz)	c_p (m/s)
220	980	245	1090	220	980	220	980	N/I	N/I	220	980
535	1190	535	1190	560	1240	560	1240	585	1300	585	1300
925	1370	950	1410	950	1410	975	1440	1025	1520	1025	1520
1440	1600	1465	1630	1465	1630	1490	1650	1540	1710	1540	1710
2000	1780	2000	1780	2125	1890	2050	1820	N/I	N/I	N/I	N/I
220	980	245	1090	220	980	220	980	N/I	N/I	220	980
2565	1900	2590	1920	2660	1970	2660	1970	N/I	N/I	N/I	N/I

Note: N/I indicates that the harmonic was not identified in the specified test and measurement direction.

The frequency spacing of the FFT array was approximately 24 Hz. The variation in identified frequencies is 25 to 250 Hz. The ordered pairs of frequency and phase velocity presented on Table 5-11 are superimposed on the numerically-determined phase velocity – frequency curve for the L(0,1) and F(1,1) branches, on Figure 5-18.

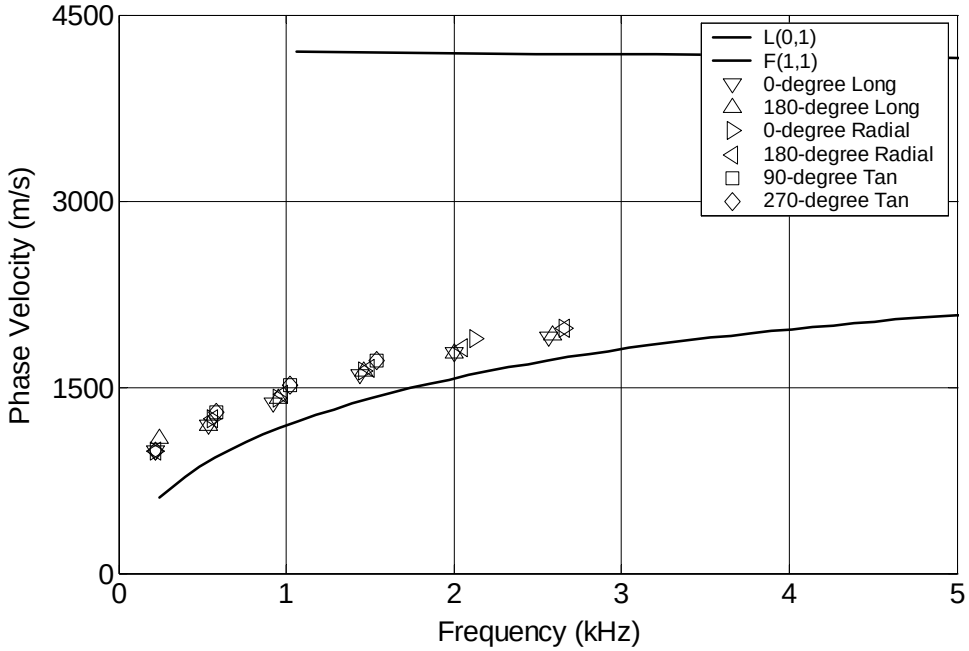

Figure 5-18: Prototype pile B254-2220, lateral impact results
phase velocity – frequency data superimposed on numerically-determined
phase velocity – frequency curves for concrete with $\nu_c = 0.18$

Guided wave theory suggests that modes on the F(1,1) branch are dispersive at low frequencies as shown by the dashed line. The individual points corresponding to experimental data follow the shape of the numerical curve for the F(1,1) branch, indicating that the lateral impact does induce flexural modes on the F(1,1) branch, and that those modes are dispersive. The phase velocity – frequency curve for the L(0,1) branch is included to illustrate that a lateral impact does not induce modes that lie along the L(0,1) branch.

5.3.3.2 Group Velocity Determination and Verification

The group velocity and frequency of the group velocity were determined by the procedures presented in Section 5.2.4. Complete analysis of lateral impact tests performed on Prototype pile B254-2220 under embedded conditions can be found in Appendix C. The ordered pairs of group velocity and frequency obtained from the analysis of the lateral impact tests are summarized on Table 5-12.

Table 5-12: Prototype pile B254-2220, summary of group velocity and frequency values from lateral impact results

Measurement Direction	Test Orientation	Group Velocity (m/s)	Group Frequency (Hz)
Longitudinal	0-degree	1890	1820
	180-degree	1910	1890
Radial	0-degree	2060	2780
	180-degree	2080	2860
Tangential	90-degree	1950	1560
	270-degree	1920	1610

The ordered pairs of group velocity and frequency are superimposed on the numerically-determined group velocity – frequency curve for the L(0,1) and F(1,1) branches on Figure 5-19.

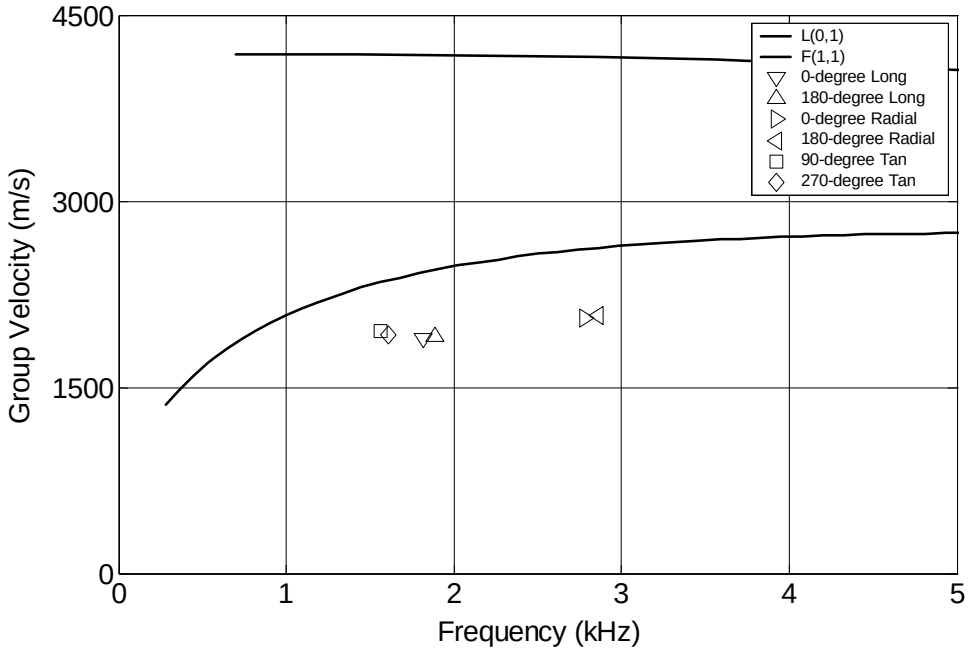

Figure 5-19: Prototype pile B254-2220, lateral impact results
group velocity – frequency data superimposed on numerically-determined
group velocity – frequency curves for concrete with $\nu_c = 0.18$

The ordered pairs of group velocity and frequency follow the shape of the numerically-determined group velocity – frequency curve for the F(1,1) branch, indicating that a lateral impact induces flexural waves. The numerically-determined group velocity – frequency curve for the L(0,1) branch is presented to show that the lateral impact does not induce longitudinal waves.

5.3.4 Prototype Pile B308-2400

Lateral impact tests were performed on prototype pile B308-2400 under embedded conditions with the configuration shown on Figure 5-15. Tests were performed at the 0-degree, 90-degree, 180-degree, and 270-degree orientations, as defined on Figure 5-1. The results analyzed were the longitudinal and radial directions for the 0-degree and 180-degree orientations, and the tangential direction for the 90-degree and 270-degree orientations.

5.3.4.1 Phase Velocity Determination and Verification

The lateral impact test results listed in Section 5.3.3 were analyzed to determine the ordered pairs of phase velocity and frequency for verification of the flexural guided wave theory. The phase velocity values were computed by the procedure outlined in Section 5.2.3. Complete results can be found in Appendix B. The phase velocity – frequency data for all tests are presented on Table 5-13.

Table 5-13: Prototype Pile B308-2400, frequencies and phase velocities determined from lateral impact tests

Longitudinal direction				Radial direction				Tangential direction			
0-degree face		180-degree face		0-degree face		180-degree face		90-degree face		270-degree face	
f (Hz)	c_p (m/s)	f (Hz)	c_p (m/s)	f (Hz)	c_p (m/s)	f (Hz)	c_p (m/s)	f (Hz)	c_p (m/s)	f (Hz)	c_p (m/s)
220	1060	220	1060	195	940	245	1180	220	1060	220	1060
525	1260	535	1280	550	1320	560	1340	560	1340	605	1450
940	1500	950	1520	940	1500	890	1420	880	1410	890	1420
1450	1740	1530	1840	1450	1740	1380	1660	1405	1690	1380	1660
2090	2010	2085	2000	1950	1870	1095	1050	N/I	N/I	1940	1860

Note: N/I indicates that the harmonic was not identified in the specified test and measurement direction.

The frequency spacing of the FFT array was approximately 12 Hz. The variation in frequency ranges from 3 to 18 samples. The ordered pairs of frequency and phase velocity presented on Table 5-13 are superimposed on the numerically-determined phase velocity – frequency curve for the L(0,1) and F(1,1) branches, on Figure 5-20.

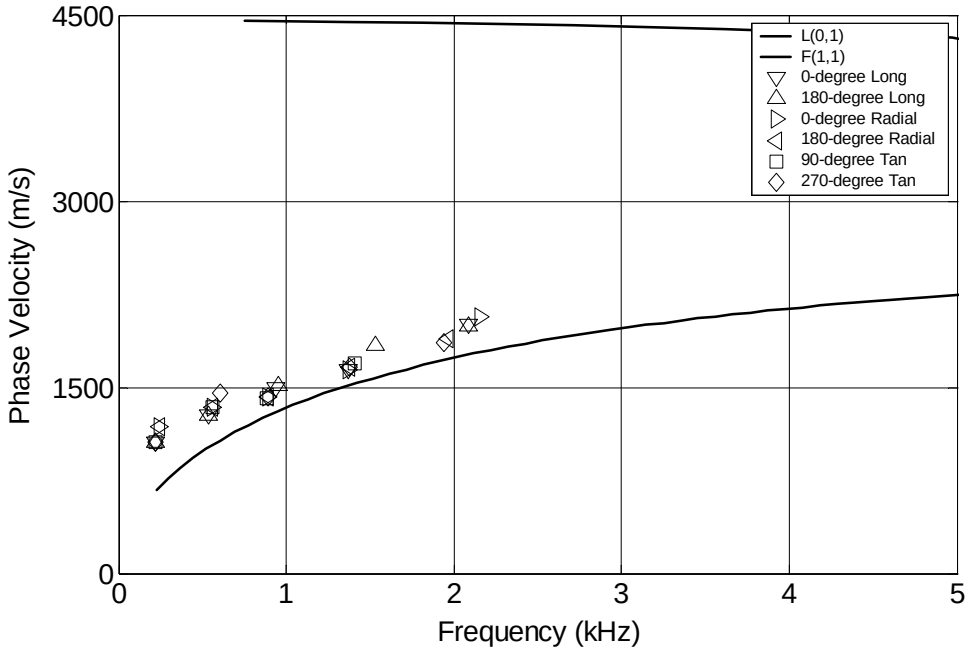

Figure 5-20: Prototype pile B308-2400, lateral impact results
phase velocity – frequency data superimposed on numerically-determined
phase velocity – frequency curves for concrete with $\nu_c = 0.28$

Guided wave theory suggests that modes on the F(1,1) branch are dispersive at low frequencies as shown by the dashed line. The individual points corresponding to experimental data follow the shape of the numerical curve for the F(1,1) branch, indicating that the lateral impact does induce flexural modes on the F(1,1) branch, and that those modes are dispersive. The phase velocity – frequency curve for the L(0,1) branch is included to illustrate that a lateral impact does not induce modes that lie along the L(0,1) branch.

5.3.4.2 Group Velocity Determination and Verification

The group velocity and frequency of the group velocity were determined by the procedures presented in Section 5.2.4. Complete analysis of lateral impact tests performed on Prototype pile B254-2220 under embedded conditions can be found in Appendix C. The ordered pairs of group velocity and frequency obtained from the analysis of the lateral impact tests are summarized on Table 5-14.

Table 5-14: Prototype pile C355-2430, summary of group velocity and frequency values from lateral impact results

Measurement Direction	Test Orientation	Group Velocity (m/s)	Group Frequency (Hz)
Longitudinal	0-degree	2250	1750
	180-degree	2240	1720
Radial	0-degree	2500	1300
	180-degree	2650	1350
Tangential	90-degree	2020	1590
	270-degree	2040	1560

The ordered pairs of group velocity and frequency are superimposed on the numerically-determined group velocity – frequency curve for the L(0,1) and F(1,1) branches on Figure 5-21.

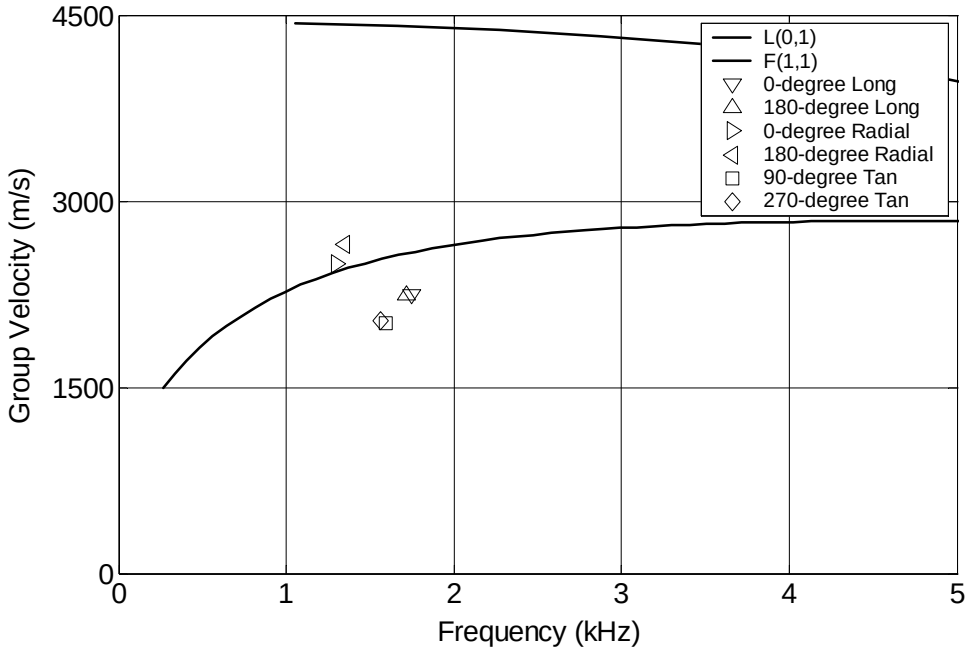

Figure 5-21: Prototype pile B308-2400, group velocity – frequency results for lateral impact tests

The ordered pairs of group velocity and frequency follow the shape of the numerically-determined group velocity – frequency curve for the F(1,1) branch, indicating that a lateral impact induces flexural waves. The numerically-determined group velocity – frequency curve for the L(0,1) branch is presented to show that the lateral impact does not induce longitudinal waves.

5.4 Recommended Test Configuration

For the evaluation of prototype pile C355-2430 under both traction-free and embedded conditions, as well as prototype piles B254-2220 and B308-2400 under embedded conditions, lateral impact tests were performed at the 0-degree, 90-degree, 180-degree, and 270-degree orientations, as shown on Figure 5-22.

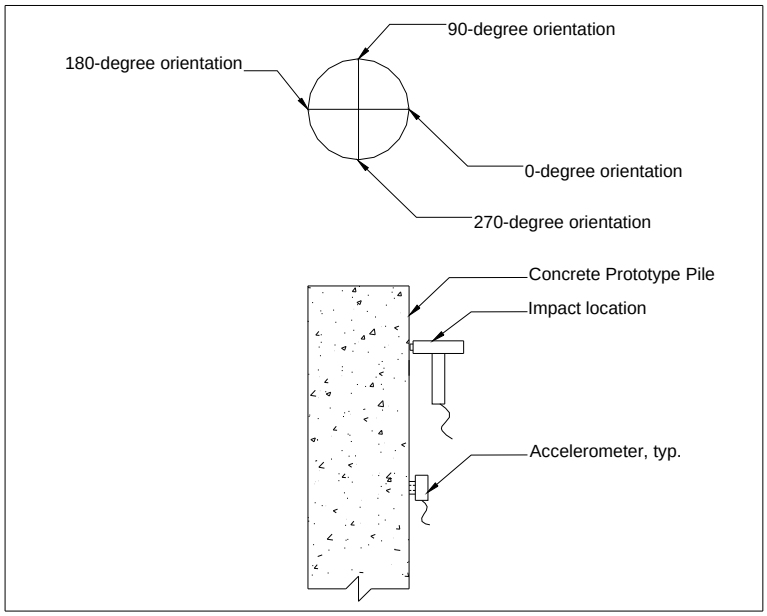

Figure 5-22: Orientation convention for input and response for flexural modes

The results were analyzed to determine the phase velocity – frequency relationship and the group velocity – frequency relationship, and the experimental results were compared to theoretical values. The tangential response of the impacts at the 90-degree and 270-degree orientations

provided the most consistent results, i.e., for both tests, the group frequency was the same. For the other tests, the group frequency was not the same for hits on opposite faces.

Based on the consistency of the results, impacts at the 90-degree and 270-degree orientations are recommended.

5.5 Summary and Conclusions

The stress waves induced in a lateral impact test fall on the F(1,1) branch but not any other branch for prototype piles 254 to 355 mm in diameter and constructed of concrete for which the density, shear wave velocity, and Poisson's ratio fall within the typical range for those properties. The maximum frequency induced by the impact falls below the cutoff frequency for the F(1,2) branch for some tests; consequently, modes will not be excited on the F(1,n) branch for n greater than or equal to 2. The impacts do not induce modes on the longitudinal branches. For some tests, the maximum frequency of the hammer impact did fall above the cutoff frequency for the F(1,2) branch but the data were filtered with a cutoff frequency that was below the cutoff frequency for the F(1,2) branch.

The acceleration – time histories for impacts measured in the same direction but on opposite faces are 180-degrees out of phase. For example, a longitudinal acceleration – time

history on the 180-degree face has the opposite sign as a longitudinal acceleration – time history of the 0-degree face. The acceleration spectra for the two impacts are the same within experimental error.

The phase velocity frequency relationship was determined from the acceleration spectrum for the longitudinal and radial directions in the 0-degree orientation and the 180-degree orientation, and from the acceleration spectrum for the tangential direction in the 90-degree orientation and 270-degree orientation. The natural frequencies are identified as the peaks in the acceleration spectrum between DC and the null frequency of the impact or the cutoff frequency of the filter, whichever is lower. The frequencies are converted to phase velocities and the phase velocity –frequency values are superimposed on the theoretical curve and correspond to modes on the F(1,1) Branch.

The group velocity and frequency are determined from the acceleration – time history. The group velocity frequency relationship was determined from the longitudinal and radial results in the 0-degree orientation and the 180-degree orientation, or from the tangential results in the 90-degree orientation and 270-degree orientation. The group velocity is computed from the travel distance and the time lag between the first pass of the wave and the return of the reflected wave. The frequency of the wave is computed from the period of the wave as identified on the acceleration – time history. The group velocity and frequency of the group determined

from the lateral impact tests are superimposed on the theoretical curves and correspond to modes on the F(1,1) Branch.

Comparison of the experimental and theoretical values of phase velocity and group velocity indicates that the lateral impact test does induce a flexural wave, which verifies the flexural guided wave theory and suggests that the lateral impact method could be used as a method for nondestructive evaluation of deep foundations.

The best results were obtained by analyzing the tangential component of the response for impacts at the 90-degree and 270-degree orientations.

Chapter 6 Controlled Frequency Results for Prototype Pile C355-2430 under Traction-free Conditions

Prototype pile C355-2430, described in Chapter 4, was evaluated nondestructively by the controlled frequency method under traction-free conditions to verify the flexural guided wave theory presented in Section 2.3. A flexural wave was induced with the shaker mounted to the side of the pile and the response was measured with two triaxial accelerometers mounted to the side of the pile, as described in Section 3.3.3. The controlled frequency test results were analyzed to determine the group velocity – frequency relationship. The experimental results were compared to theoretical results to verify the guided wave theory. In particular, experimental results are compared with the numerically-derived group velocity – frequency relationships.

For the controlled frequency tests, the test frequencies were high enough that modes may be excited on the F(1,1) branch and branches as high as the F(1,5) branch, contrasted with the impact test results presented in Chapter 5 for which the modes were limited to the F(1,1) branch. To identify the branch on which modes are excited, the analysis includes consideration of the relative magnitudes of the displacements corresponding to the branches that may be excited in addition to the group velocity – frequency relationship. Part of the data analysis includes bandpass filtering of the data to remove high frequency noise and unwanted portions of the signal that fall outside the test range. Because modes may be excited on multiple branches and

the frequency content of the signal can vary as a function of time, the mode identification method described in Section 3.5.2 has been applied to select test results to verify the branch on which modes are identified.

6.1 Analysis of Controlled Frequency Results

The pile was tested with the shaker mounted on the side of the pile and triaxial accelerometers mounted on the side of the pile, as shown on Figure 6-1. The position of the shaker was the same for all tests and the orientation of the test was changed by moving the accelerometers.

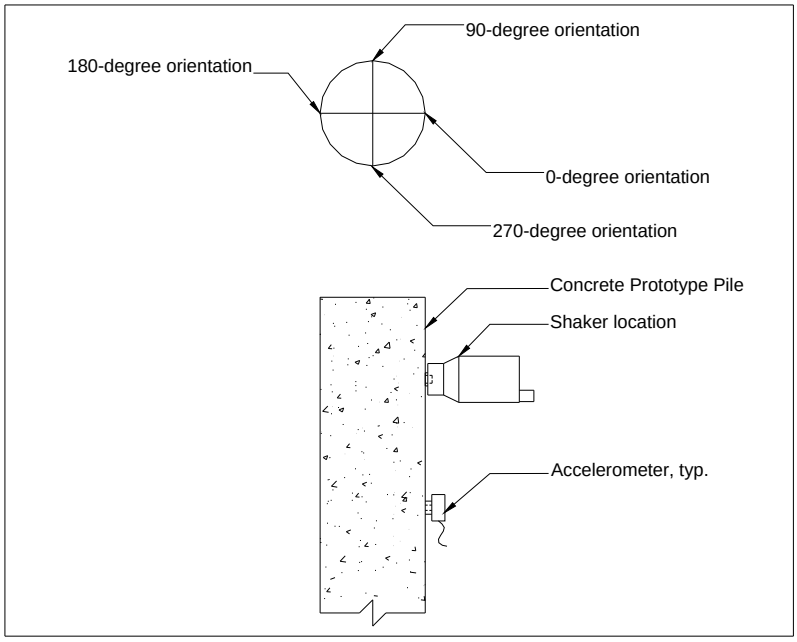

Figure 6-1: Prototype pile C355-2430, test configuration for controlled frequency tests under traction-free conditions

Figure 6-1 shows one triaxial accelerometer on the same face as the shaker, which is defined as the 0-degree orientation. The tests were performed at the 0-degree and 180-degree orientations and the results of those tests will be presented. Tests were also performed at the 90-degree and 270-degree orientations but the results of those tests did not provide results from which reflections could be identified.

The equations for displacement components presented in Section 2.3.8 indicate that the radial and longitudinal displacements depend on the cosine of the angle between the shaker and the measurement locations, and the tangential component of depends on the sine of the angle between the shaker and the measurement locations. The maximum magnitude of the cosine

occurs at the 0-degree and 180-degree orientations, which are the angles at which the sine is zero; conversely, the maximum magnitude of the sine occurs at 90-degrees and 270-degrees, at which the magnitude of the cosine is zero.

The filtered controlled frequency results are analyzed as part of the verification of the guided wave theory presented in Section 2.3. The criteria for experimental verification of the flexural guided wave theory (Wang, 2004) are

- Identify the branches on which modes are expected,
- Evaluate the relative magnitudes of displacements,
  - For the 0-degree and 180-degree orientations, the radial and longitudinal responses should be nonzero and the tangential response should be negligible.
  - For the 90-degree and 270-degree orientations, the radial and longitudinal responses should be negligible and the tangential response should be nonzero.
- Determine the group velocity or group velocities of the stress wave and compare the experimental results to the numerical results.

For the impact results presented in Chapter 5, the maximum frequency of the hammer impact was below the cutoff frequency for the F(1,2) branch, indicating that all modes were expected to lie along the F(1,1) branch. The controlled frequency tests were performed at higher frequencies than the impact tests, and those frequencies were above the cutoff frequency for the F(1,2) branch. The number of branches on which modes may be excited depends on the central frequency of the input compared to the cutoff frequencies for the various branches. When modes on more than one branch may be excited in a test, the branches are identified by considering

- The group velocity of each branch at the test frequency
- The normalized displacement of each mode on each branch at the test frequency.

The mode identification method described in Section 3.5.2 provides an additional method with which to analyze the test results.

Based on the equations for normalized displacement presented in Section 2.3.8, the longitudinal and radial responses will be analyzed for tests performed at the 0-degree and 180-degree orientations. Tests were initially performed at the 90-degree and 270-degree orientations as well, but those tests did not produce results that were consistent with the expected response of the pile to the controlled frequency tests. Possible explanations for the poor quality results in the 90-degree and 270-degree orientations are

- Limitations of the equipment as mounted to the prototype pile
- Limitations of the controlled frequency method
- The presence of waves other than a flexural wave

6.2 Selection of Test Frequencies

The manufacturer's data for the F7 shaker described in Section 3.3.2 suggests that it will produce a dynamic force with a single frequency equal to the input frequency from its control system. The preliminary analysis of the shaker behavior when mounted to a concrete prototype pile presented in Section 3.4.2.2 indicates that the dynamic force produced by the shaker contains the input frequency, but the force may contain other frequencies as well. The input frequency is the central frequency of the test and all frequencies higher and lower than the central frequency are considered to be undesirable frequencies. The pile, in turn, responds to all

of the frequencies contained within the dynamic force applied by the shaker. The difference between the actual response of the shaker mounted to the prototype pile and the ideal response published by the manufacturer contributes to the need for digital filtering of the data and may limit the suitability of any arbitrary frequency to be used in controlled frequency tests.

The controlled frequency tests were performed by the procedures presented in Section 3.1.2 using the hardware described in Section 3.3 and controlled by the virtual pulse generator described in Section 3.2.3. The voltage setting on the matching network, as well as the maximum and minimum voltages on the virtual pulse generator were selected such that the measured response fell between ±10 Volts.

The ideal response of the shaker is zero before the start of the input force, followed by a signal that increases to a maximum value and decreases to zero, and it consists of a sine wave of a single frequency, as shown in Figure 6-2.

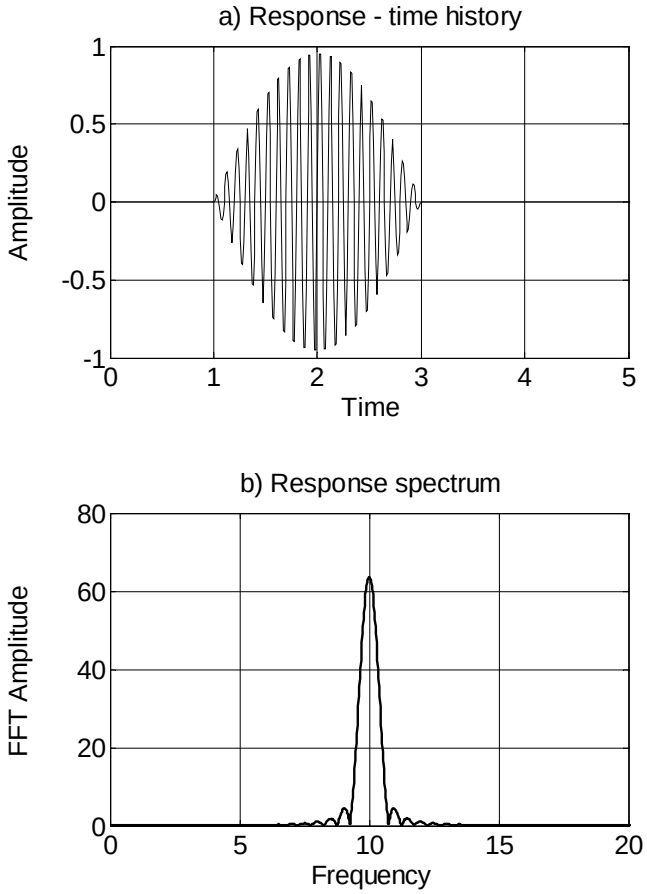

Figure 6-2: Ideal response of shaker

The response of the pile should consist of a first pass followed by one or more returns of the reflected wave, each of which should have the same shape and frequency content as the response measured at the shaker.

Controlled frequency tests were performed on prototype pile C355-2430 at input frequencies of 4000 Hz to 20000 Hz in 2000 Hz increments, and at a few other input frequencies. The results of all tests were evaluated to identify criteria required to select a suitable input frequency, and the results of tests performed at a suitable frequency were analyzed as verification of the flexural guided wave theory. Three different types of pile response quality were identified and some of their key characteristics are presented on Table 6-1.

Table 6-1: Typical responses for controlled frequency tests & key characteristics of the typical responses

Response type	Key characteristics
Type 1	The peak at the central frequency is large.
	Other large peaks can be removed by digital filtering.
	After filtering, the peak at the central frequency has essentially the same magnitude as prior to filtering.
	Of the peaks not removed by digital filtering, the peak at the central frequency is much larger than all other peaks.
Type 2	The peak at the central frequency is large, although not as large as for a Type 1 response.
	Other large peaks can be removed by digital filtering.
	After filtering, the peak at the central frequency has essentially the same magnitude as prior to filtering.
	Of the peaks not removed by digital filtering, the peak at the central frequency is larger than all other peaks, although not as pronounced as in the case of a Type 1 response.
Type 3	The peak at the central frequency is not large.
	Other large peaks cannot be removed by digital filtering.
	After filtering, the peak at the central frequency has essentially the same magnitude as prior to filtering.
	Of the peaks not removed by digital filtering, the peak at the central frequency may not be larger than all other peaks.

Examples of each type will be presented in Section 6.2.2.1

6.2.1 Filtering of Data

The sampled response of the shaker and pile contain the desired input frequency and may contain other modes of vibration, spurious frequencies from the shaker and accelerometers, and distortion introduced from the sampling process. Some of the unwanted portions of the signal can be removed through digital filtering. The controlled frequency test results were filtered with a bandpass filter described in Section 3.5.1 to remove all frequencies other than the central frequency of the input. The filtering of the controlled frequency results is contrasted with the filtering of the lateral impact results presented in Chapter 5, which were filtered with a lowpass filter to remove all frequencies above the test-specific maximum frequency.

A bandpass filter requires the selection of a filter type, filter order, low cutoff frequency, and high cutoff frequency, as discussed in Section 3.5.1. The test results were filtered with a bandpass Butterworth filter of Order 6, leaving the low and high cutoff frequencies as the parameters to be adjusted based on the central frequency of the test.

As an example of the filtering of controlled frequency results with a bandpass filter, consider the unfiltered input and response of a test performed at a central frequency of 14000 Hz. The acceleration – time histories and acceleration spectra of the shaker and upper triaxial accelerometer are presented on Figure 6-3.

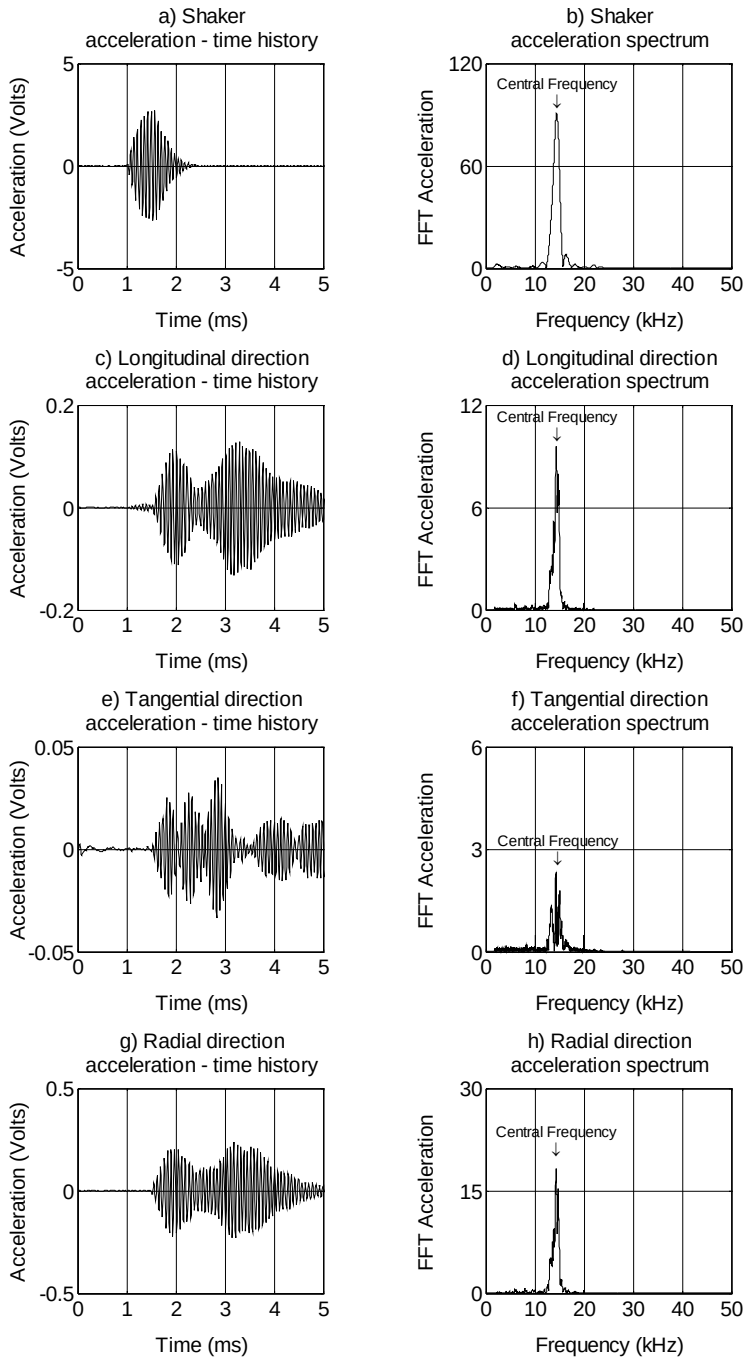

Figure 6-3: Prototype pile C355-2430, unfiltered controlled frequency results with CF = 14000 Hz and accelerometers at 0-degree and 180-degree orientations

The response measured at the shaker contains the central frequency of 14000 Hz but also contains other peaks, particularly above 25000 Hz. The peaks other than the one at 14000 Hz are a combination of other wave types, resonance of the shaker or accelerometers, and noise, and, as such, should be removed from the signal prior to analysis. Furthermore, the manufacturer's data presented in Section 3.3.2 indicates that the shaker can generate signals with a frequency above 20000 Hz, but that the results may not be reliable because the embedded sensors are not calibrated for such high frequencies.

For a Butterworth filter, which is the filter type used to filter the controlled frequency results, the magnitude of the frequency response is unity in the passband, zero in the stopband, and decreases monotonically from unity to zero in the transition band. The width of the passband and, consequently, the start of the transition band are controlled by adjusting the high and low cutoff frequencies.

If the high and low cutoff frequencies are selected to provide a wide passband, the magnitude response will be unity at the central frequency but the unwanted portions of the signal may not be adequately removed if the unwanted portions will fall within the transition band. On the other hand, if the passband is too narrow, the unwanted portions of the signal will be adequately removed but the magnitude response at the central frequency will not be unity.

The results presented on Figure 6-3 were filtered with a bandpass Butterworth filter of order 6, and the cutoff frequency values were adjusted to provide an acceptable frequency response of the filtered data. A low cutoff frequency of 2000 Hz and a high cutoff frequency of 20000 Hz adequately removed the unwanted frequency components without distorting the portion of the signal at the central frequency. The filtered results are presented on Figure 6-4.

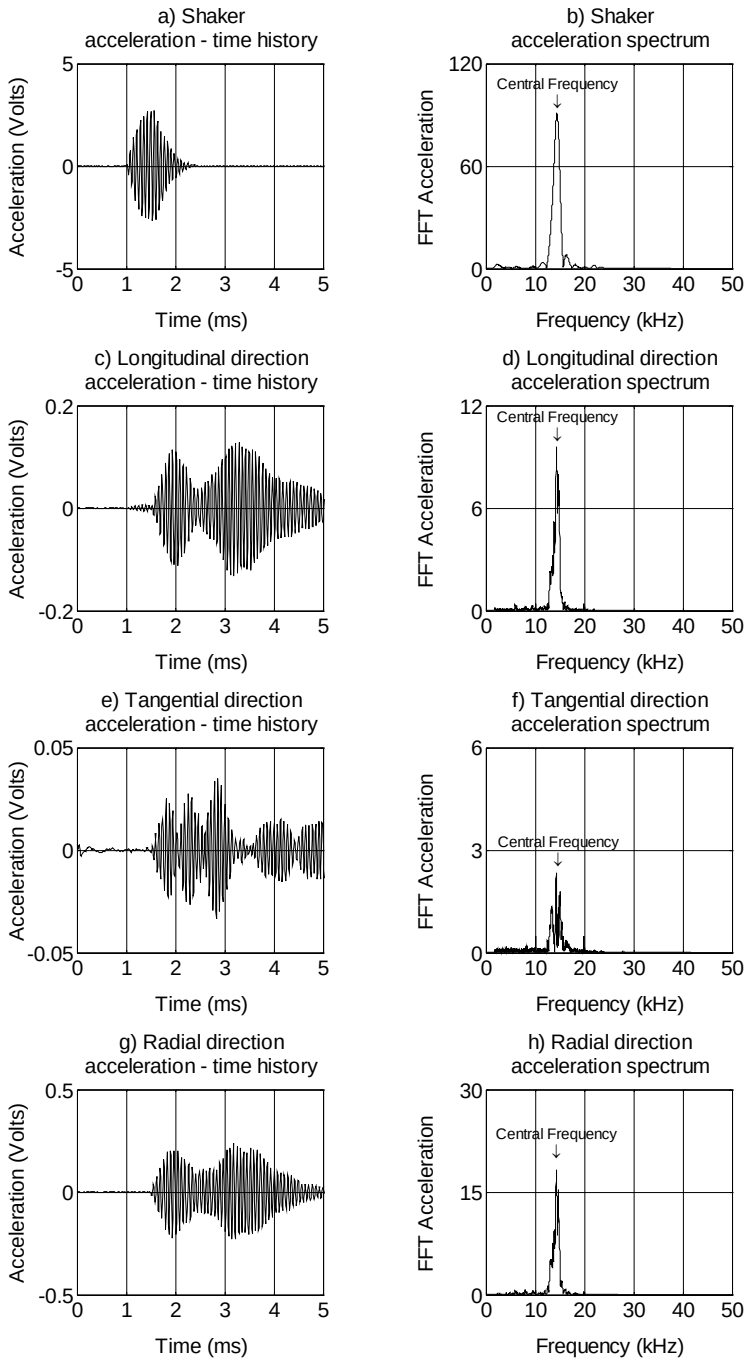

Figure 6-4: Prototype pile C355-2430, filtered controlled frequency results with CF = 14000 Hz and accelerometers at 0-degree and 180-degree orientations

The filtering completely removed the unwanted portions of the signal above 25000 Hz, and partially removed the low frequency peak at about 2000 Hz.

All test results to be presented in Section 6.2.2 and the results to be analyzed for verification of the flexural guided wave theory were filtered with a bandpass Butterworth filter of order 6, and the high and low cutoff frequencies were adjusted.

As discussed in Section 6.2, tests were initially performed at several frequencies between 4000 Hz and 20000 Hz, and those results were evaluated to identify suitable test frequencies. Three frequencies that correspond to the typical responses presented on Table 6-1 have been selected to illustrate the types of response. The filter parameters, including the low and high cutoff frequency values and the magnitude response at the central frequency, are presented on Table 6-2 for each of the tests to be presented as illustration of the types of response.

Table 6-2: Cutoff frequencies, magnitude response, group delay, and phase delay at CF values used in flexural controlled frequency test

Central frequency (Hz)	Cutoff frequencies (Hz)		Magnitude response at cutoff frequency
	Low	High	
5300	2000	10000	1
8000	2000	12000	0.99
14000	2000	20000	0.98

The magnitudes at the central frequency are close enough to 1 for all three values of central frequency that the passband is not too narrow.

6.2.2 Performance of Shaker at Different Frequencies

The filtered response of the pile has been analyzed to identify the key features of the response quality, and the filtered and unfiltered response of the shaker has been analyzed to determine if features can be identified in the input that would contribute to the quality of the pile response.

The tests were performed multiple times to establish consistency and repeatability. The tests were performed at all three frequencies during one set of experiments, thereby reducing the effects of environmental factors and equipment mounting on the test results.

6.2.2.1 Typical Input Characteristics and Pile Responses

One test corresponding to each of the three types of response listed in Section 6.2 has been analyzed to identify specific characteristics that comprise each type of response.

The filtered and unfiltered results of a controlled frequency test with a central frequency of 14000 Hz are presented on Figure 6-3, including the presented results are the acceleration – time history and acceleration spectrum of the input measured at the shaker. This is an example of a Type 1 response.

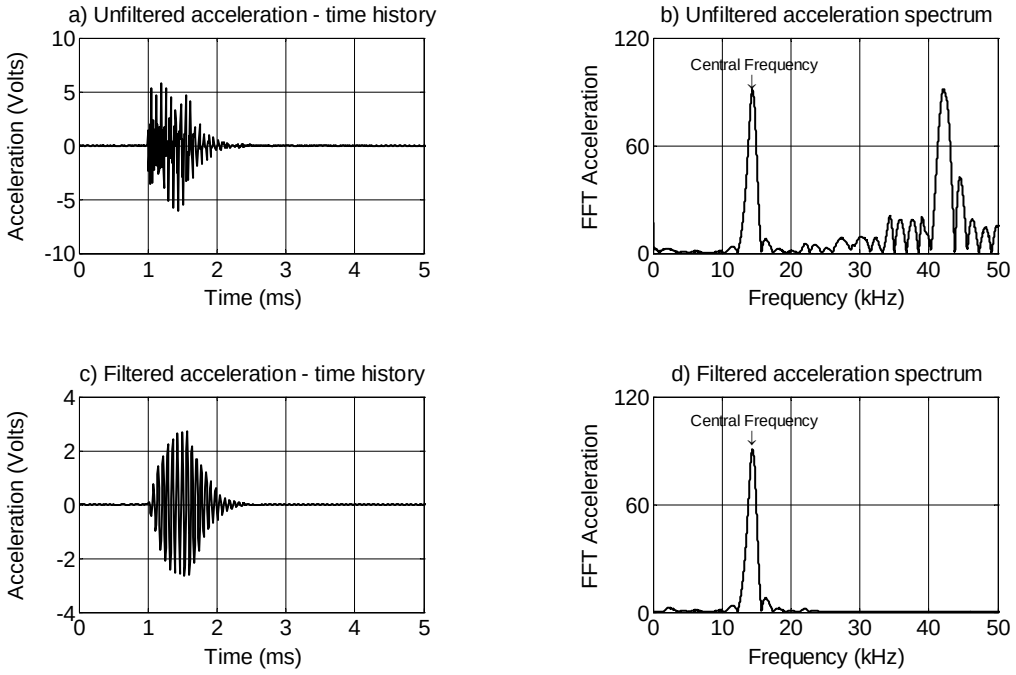

Figure 6-5: Type 1 response for prototype pile C355-2430, controlled frequency results with CF = 14000 Hz unfiltered and filtered response measured at shaker

The unfiltered response measured at the shaker, shown on Figure 6-5a, is approximately zero until about 1 ms and is zero again at about 2 ms. The largest peak on the unfiltered acceleration spectrum, shown on Figure 6-5b, occurs at 14000 Hz, and is labeled "Central Frequency." Another large peak occurs at 42000 Hz, and several smaller peaks are present at other frequencies. As discussed in Section 6.2.1, filter parameters are selected to isolate, to the extent possible, the frequency component corresponding to the central frequency of the test, which is 14000 Hz in this case. The filtered response at the shaker, shown on Figure 6-5c, is approximately zero until 1 ms, the maximum value occurs at about 1.5 ms, and it is again zero at

about 2 ms. The largest peak on the acceleration spectrum, shown on Figure 6-5b, occurs at 14000 Hz, which is the central frequency of the input.

The filtered response on Figure 6-5c and 6-5d, along with the acceleration – time histories and acceleration spectra of the pile responses measured in the radial, tangential, and longitudinal directions with a triaxial accelerometer oriented at 0-degrees to the shaker are presented on Figure 6-6.

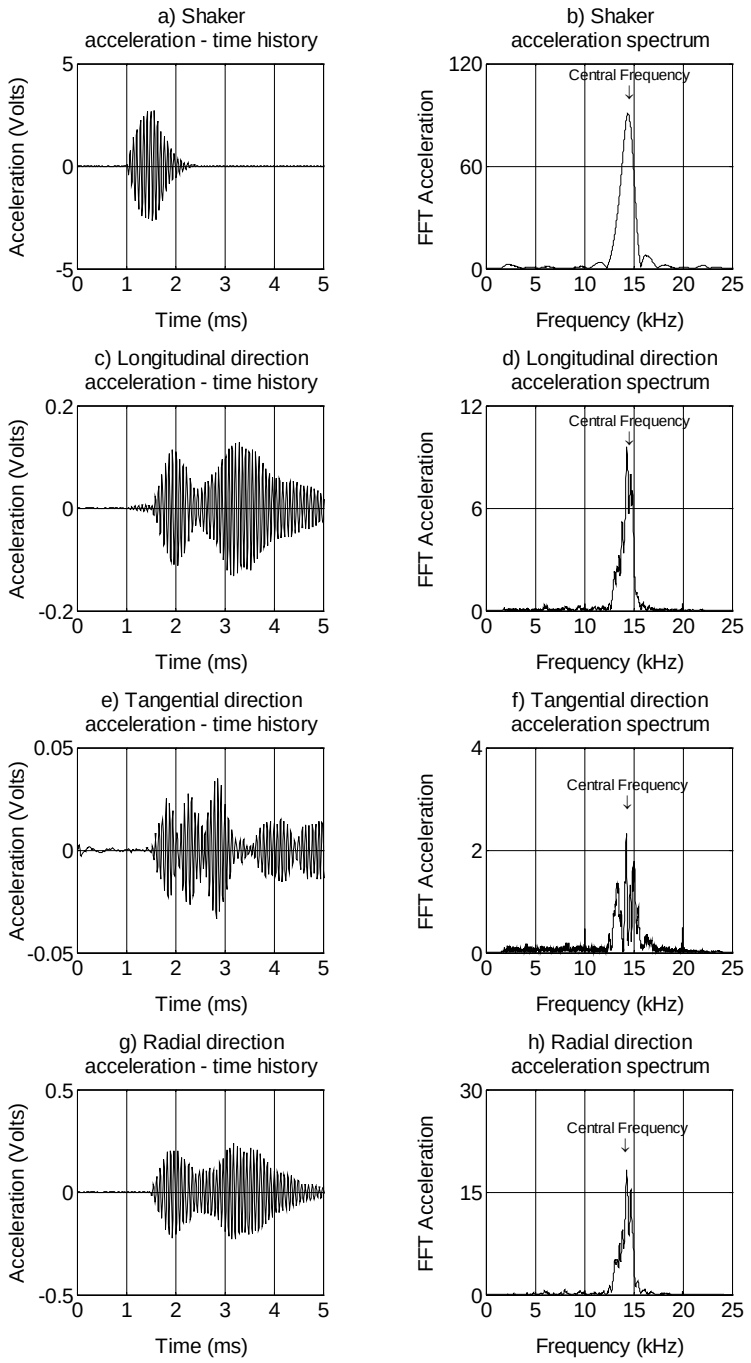

Figure 6-6: Prototype pile C355-2430, controlled frequency results with CF = 14000 Hz for an accelerometer oriented at 0-degrees to the shaker

The acceleration – time histories of the pile response consist several wave groups corresponding to the first pass and possible reflections. The wave group is dominated by the 14000 Hz-frequency, as shown on the acceleration spectrum. The wave groups of the pile response have the same general shape as the input measured at the shaker, and closely match the ideal response shown on Figure 6-2. The results presented on Figure 6-6 are representative of controlled frequency tests performed with a central frequency of 14000 Hz. The 14000 Hz-frequency meets the criteria of a good input.

The filtered and unfiltered results of a controlled frequency test with a central frequency of 8000 Hz are presented on Figure 6-7, including the presented results are the acceleration – time history and acceleration spectrum of the input measured at the shaker. This is an example of a Type 2 response.

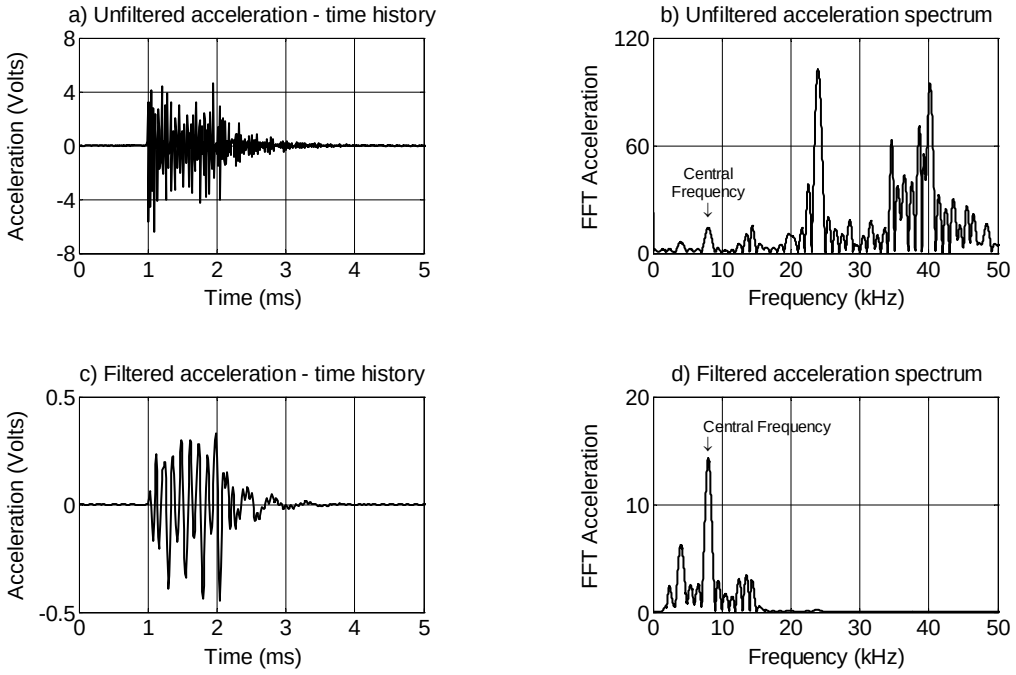

Figure 6-7: Type 2 response for prototype pile C355-2430, controlled frequency results with CF = 8000 Hz unfiltered and filtered response measured at shaker

The unfiltered response measured at the shaker, shown on Figure 6-7a, is approximately zero until about 1 ms and is zero again at about 2.5 ms. The largest peak on the unfiltered acceleration spectrum, shown on Figure 6-7b, does not occur at 8000 Hz, which is the central frequency of the input, rather the largest peaks occur at 24000 Hz and 40000 Hz. Several smaller peaks are present at frequencies other than 8000 Hz, 24000 Hz, and 40000 Hz. The filtered response at the shaker, shown on Figure 6-7a, is approximately zero until 1 ms, and is again zero at about 2.5 ms. The largest peak on the filtered acceleration spectrum, shown on Figure 6-7b, occurs at 8000 Hz, which is the central frequency of the input.

The filtered response on Figure 6-7c and 6-7d, along with the acceleration – time histories and acceleration spectra of the pile responses measured in the radial, tangential, and longitudinal directions with a triaxial accelerometer oriented at 0-degrees to the shaker are presented on Figure 6-8.

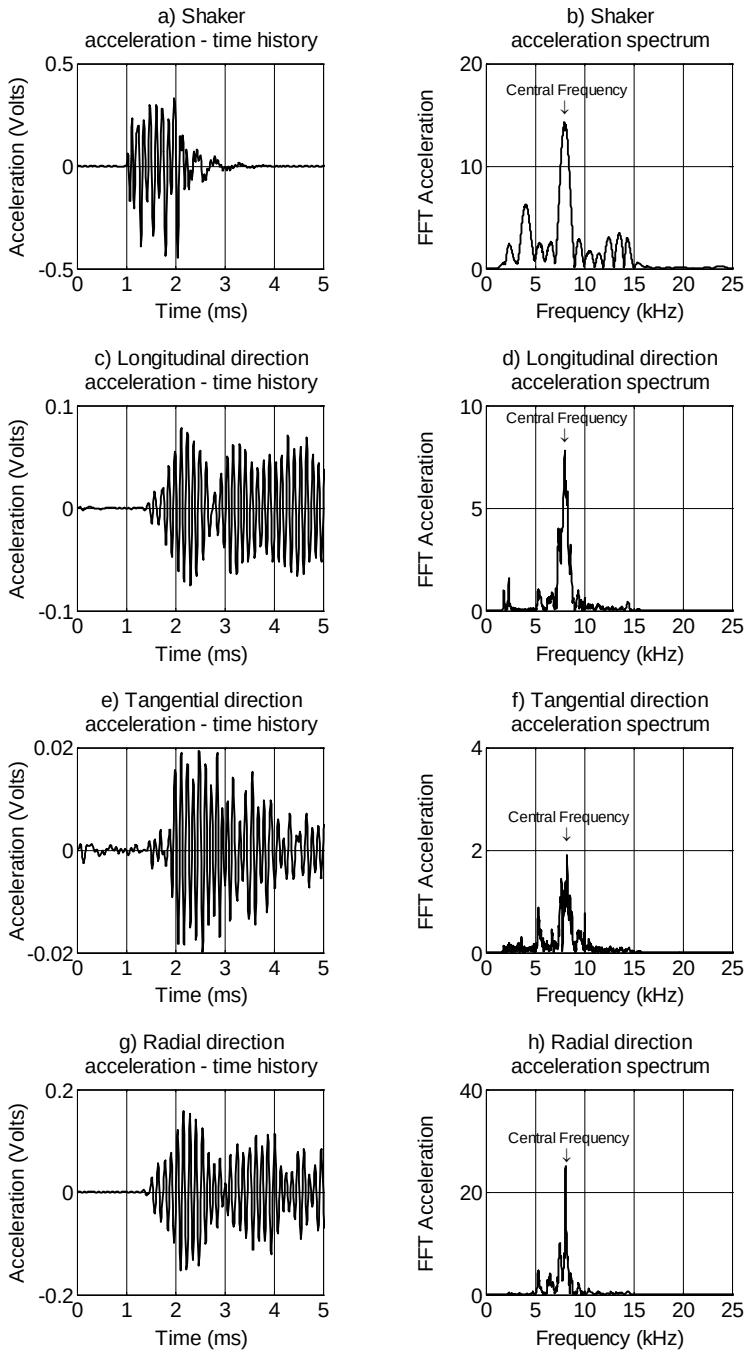

Figure 6-8: Prototype pile C355-2430, controlled frequency results with CF = 8000 Hz for an accelerometer oriented at 0-degrees to the shaker

The acceleration – time histories of the pile response consist several wave groups corresponding to the first pass and possible reflections. The wave group is dominated by the 8000 Hz-frequency, as shown on the acceleration spectrum. The wave group corresponding to the first pass of the wave group does not have the same general shape as the input measured at the shaker but does have the same general shape as the ideal response presented on Figure 6-2. The subsequent wave groups, corresponding to possible returns of the reflected wave, do not have the same general shape as the input measured at the shaker, and do not match the ideal response shown on Figure 6-2. The results presented on Figure 6-8 are representative of controlled frequency tests performed with a central frequency of 8000 Hz. The 8000 Hz-frequency does not meet the criteria of a good input.

The filtered and unfiltered results of a controlled frequency test with a central frequency of 5300 Hz are presented on Figure 6-9, including the presented results are the acceleration – time history and acceleration spectrum of the input measured at the shaker. This is an example of a Type 3 response.

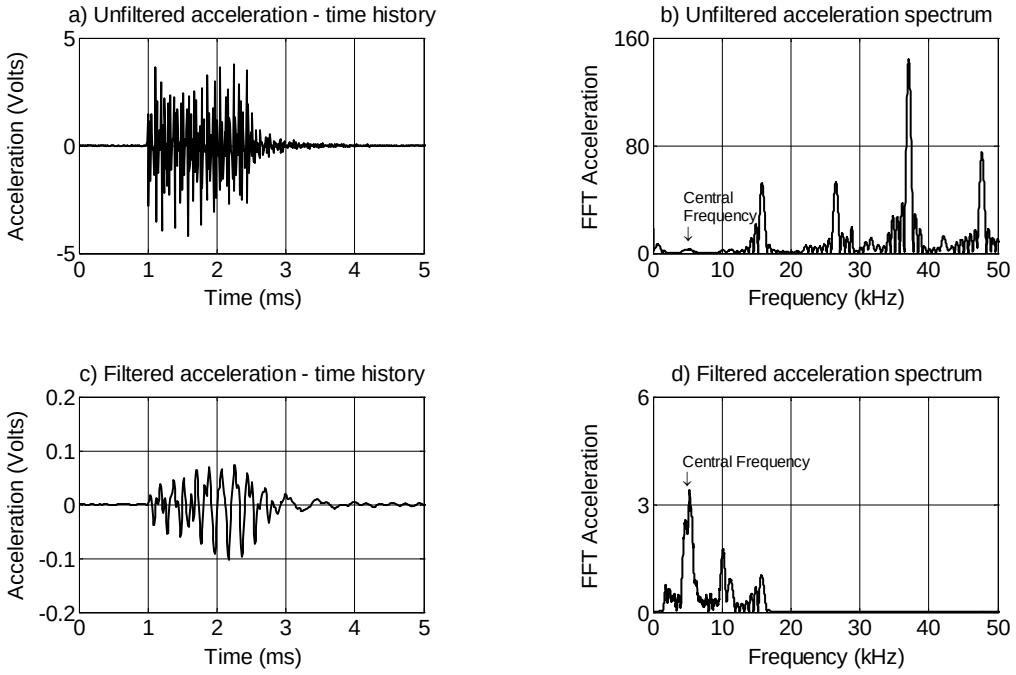

Figure 6-9: Type 3 response of prototype pile C355-2430, controlled frequency results with CF = 5300 Hz unfiltered and filtered response measured at shaker

The unfiltered response measured at the shaker, shown on Figure 6-9a, is approximately zero until about 1 ms and is zero again at about 2.5 ms. The largest peak on the unfiltered acceleration spectrum, shown on Figure 6-9b, does not occur at 5300 Hz, which is the central frequency of the input, rather the largest peak occurs at 37000 Hz and other large peaks occur at about 16000 Hz, 26000 Hz, and 48000 Hz. Several smaller peaks are present around each of the large peaks. The filtered response at the shaker, shown on Figure 6-9a, is approximately zero until 1 ms, and is again zero at about 2.5 ms. The largest peak on the filtered acceleration spectrum, shown on Figure 6-9b, occurs at 5300 Hz, which is the central frequency of the input. However, large peaks still remain after filtering of the data, particularly a large peak remains at

1000 Hz. The peak at 10000 Hz could potentially be removed by reducing the high cutoff frequency of 10000 Hz, but not without distorting the desired portion of the signal. The filtering of the data for the 8000 Hz and 14000 Hz tests removed the unwanted frequencies almost entirely without distorting the desired frequency, which is significantly different from the filtering of the data of the tests performed at 5300 Hz.

The filtered response on Figure 6-9c and 6-9d, along with the acceleration – time histories and acceleration spectra of the pile responses measured in the radial, tangential, and longitudinal directions with a triaxial accelerometer oriented at 0-degrees from the shaker are presented on Figure 6-10.

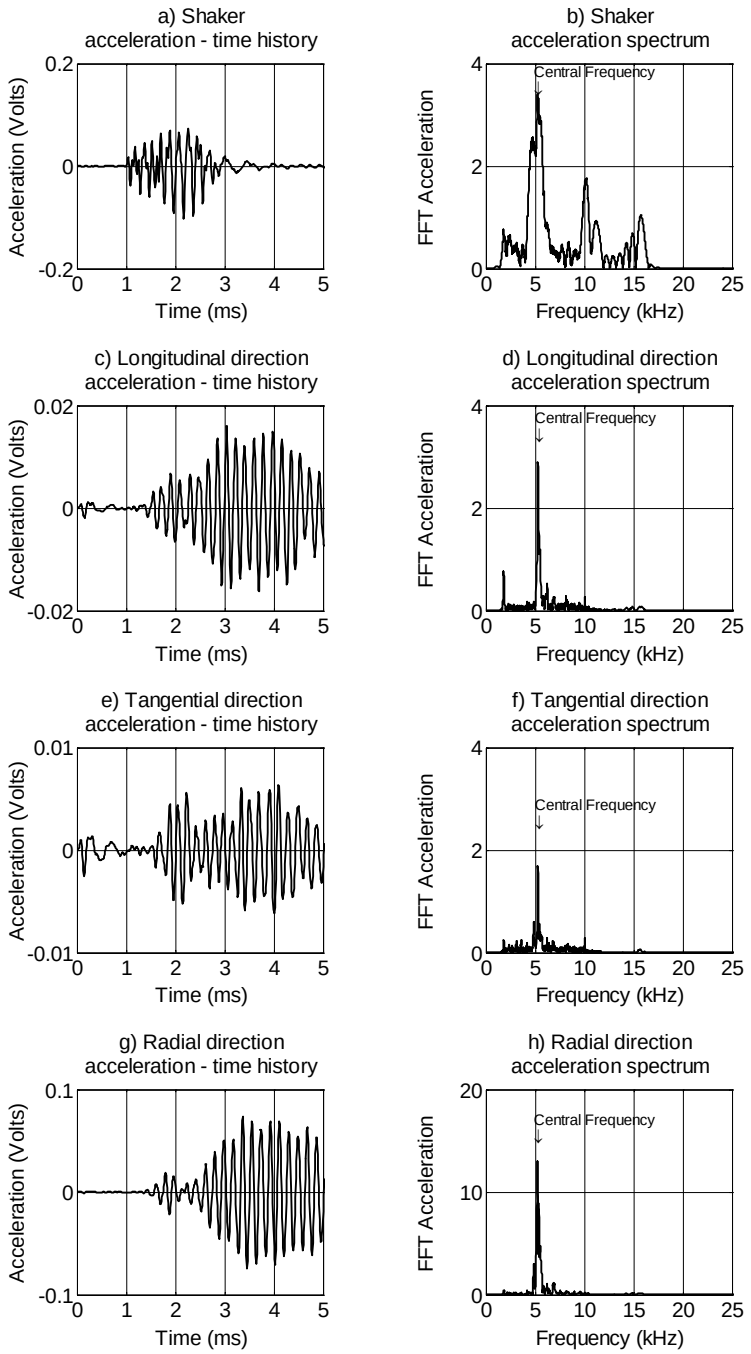

Figure 6-10: Prototype pile C355-2430, controlled frequency results with CF = 5300 Hz for an accelerometer oriented at 0-degrees from the shaker

The acceleration – time histories of the pile response, presented on Figures 6-10 c, e, and g, do not contain well-defined first passes and reflections and do not match the ideal response shown on Figure 6-2. The results presented on Figure 6-10 are representative of tests performed with a central frequency of 5300 Hz. The 5300 Hz-frequency does not meet the criteria of a good input.

6.2.2.2 Selection of Central Frequency Based on Properties of Input Signal

The filtered input and pile responses were presented for three different central frequencies in Section 6.2.2.1. A central frequency of 14000 Hz provided good results; a central frequency of 8000 Hz provided moderate results; and a central frequency of 5300 Hz did not provide good results. The filtered and unfiltered responses of the shaker at a particular frequency were evaluated to determine if the quality of the pile response could be predicted.

The filtered acceleration – time histories and acceleration spectra measured at the shaker for controlled frequency with central frequencies of 14000 Hz, 8000 Hz, and 5300 Hz are compared to each other and to the ideal response of a single-frequency sine wave on Figure 6-11.

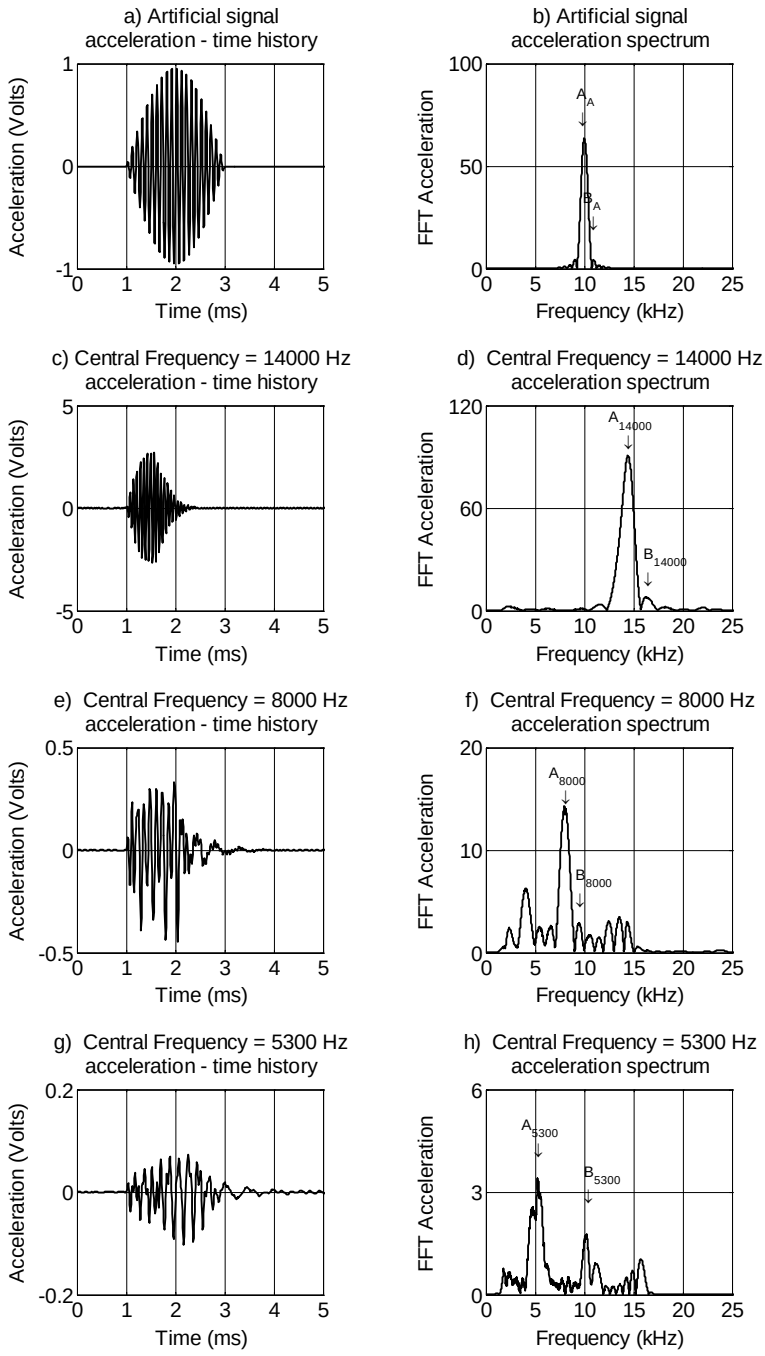

Figure 6-11: Comparison of filtered controlled frequency responses measured at shaker to ideal shaker response

For the artificial signal, the magnitude of the Fourier transform coefficient at the input frequency, labeled A_A on Figure 6-11b is 63.7 and the magnitude of the Fourier transform coefficient at the adjacent peak, labeled B_A on Figure 6-11b is 4.5. The ratio of A_A to B_A is 14.2. For the acceleration spectra of the tests presented on Figures 6-11d, f, and h, the magnitudes of the Fourier transform coefficients at the central frequency are labeled A_{14000}, A_{8000}, and A_{5300} for tests performed at central frequencies of 14000 Hz, 8000 Hz, an 5300 Hz, respectively. The magnitudes of the Fourier transform coefficients for the largest peak adjacent to the A peak is labeled B with a subscript corresponding to the central frequency of the test. The values of each A, B, and ratio A/B is presented on Table 6-3.

Table 6-3: Magnitudes of Fourier transform coefficients for ideal shaker response & filtered controlled frequency responses measured at shaker

Type of input	Frequency (Hz)	Analysis of peaks			Type of response
		A	B	Ratio A/B	
Artificial signal	10000	63.7	4.5	14.2	N/A
Controlled frequency test	14000	91.0	7.8	11.7	Type 1
	8000	14.3	2.9	4.9	Type 2
	5300	5.2	1.8	2.9	Type 3

Notes Type of response was defined in Section 6.2.
N/A indicates that Type of response is not applicable.

The A/B ratio for the test performed at a central frequency of 14000 Hz was the largest of the three test frequencies considered and provided the best pile response.

Based on the analysis of the input and pile response, one can determine whether a selected frequency will produce a good pile response, as defined by the three response types

defined in Section 6.2, by evaluating the acceleration – time history and acceleration spectrum of the response measured at the shaker. The criteria by which the response at the shaker will produce a good pile response are

1. The magnitude of the FFT coefficient of the central frequency must be at least a large as any other frequency component, prior to filtering.
2. The frequency spacing between the central frequency and any other significant frequency components must be large enough that they can be removed through digital filtering without distorting the component at the central frequency.
3. After filtering, the signal may contain frequency components other than the central frequency but the magnitude of their FFT coefficients must be much smaller than the magnitude of the FFT coefficient for the central frequency. The results presented on Figure 6-11 and Table 6-3 indicate that as the ratio of the magnitude of the FFT coefficient at the central frequency to the magnitude of the FFT coefficient of the adjacent peak increases (the A/B ratio), the quality of the response improves.

Based on the evaluation of the frequencies at which tests were performed, a central frequency of 14000 Hz produced a Type 1 response and the other central frequencies between 4000 Hz and 20000 Hz produced either a Type 2 or Type 3 response. The results of the tests performed at a central frequency of 14000 Hz are the only results to be presented as part of the verification of flexural guided wave theory (Wang, 2004) because it was the only frequency that provided a Type 1 response.

Possible explanations for the central frequency of 14000 Hz producing a Type 1 response and the other frequencies producing either a Type 2 or Type 3 response are effects of coupling of the shaker to the pile or the behavior of the piezoelectric crystal in the shaker.

6.3 Calculation of Group Velocity

The prototype pile was tested with one shaker and two triaxial accelerometers mounted on the side of the pile at the positions shown on Figure 6-12. The group velocities were computed by the procedures presented on Section 3.4.3, and the pile geometry shown on Figure 6-12.

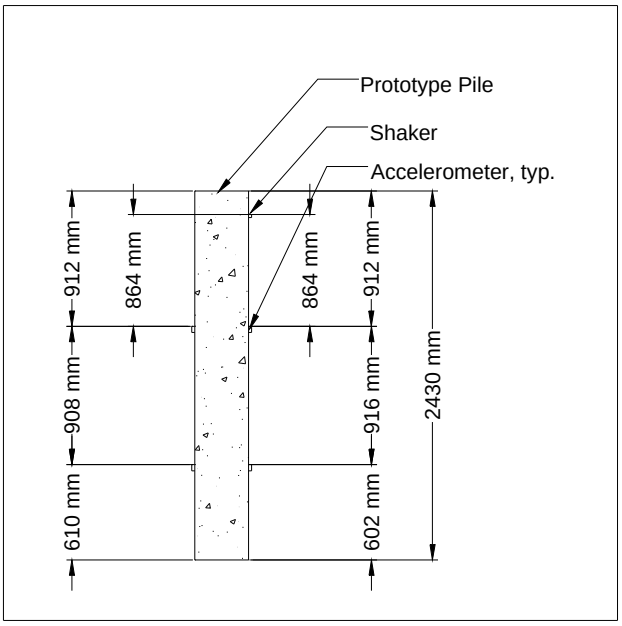

Figure 6-12: Prototype pile C355-2430, shaker and accelerometer positions for controlled frequency tests under traction-free conditions

The triaxial accelerometer closer to the top of the pile, and to the shaker, is called the upper triaxial accelerometer, and the triaxial accelerometer farther from the top of the pile, and from the shaker, is called the lower triaxial accelerometer.

Test results are presented for the 0-degree orientation and the 180-degree orientations, as defined on Figure 6-1, and the radial and longitudinal components of the pile response were analyzed. The group velocities are computed for various pairs of wave groups using the appropriate travel distance for each wave group.

A general procedure was outlined to determine the group velocity in Section 3.4.3. In general, the group velocity, c_g, is computed by

$$c_g = \frac{\Delta L}{\Delta t} \qquad (6\text{-}1)$$

where ΔL is the travel distance, and Δt is the travel time. The travel distance will be different depending on the pair of wave groups from which the group velocity is calculated and the orientation at which the test is performed.

The group velocity of the flexural wave has been computed by different methods

1. First pass of the wave
   a. Start of the wave at the shaker and first pass at the upper triaxial accelerometer,
   b. Start of the wave at the shaker and first pass at the lower triaxial accelerometer,
   c. First arrival at the upper and lower triaxial accelerometers.
2. Return of the reflected wave
   a. First pass and return of the reflected wave at the upper triaxial accelerometer,
   b. First pass and return of the reflected wave at the lower triaxial accelerometer.

Analysis of the same set of test data by different methods or with different combinations of peaks will likely produce different values of group velocity. For example, the group velocity calculated from the first arrival at the upper and lower triaxial accelerometers may not be the same as the group velocity calculated from the first pass and return of the reflected wave to the upper triaxial accelerometer. Furthermore, the analysis of the same set of peaks but from different tests may produce different values of group velocity. For example, the group velocity calculated from the 0-degree orientation may not be the same as the group velocity calculated from the 180-degree orientation. The variability in calculated group velocity can be caused by equipment performance factors, such as those discussed in Sections 3.3.3 and 3.4.2.2, or by limitations in the resolution of the data analysis. The different values computed from different sets of analysis and different data sets leads to uncertainty in the reported group velocity value.

The group velocity values will be reported in terms of their mean and standard deviation. The standard deviation will be used to compute the 95 % tolerance interval as discussed in Section 3.5.3. The experimentally-determined group velocity values will be presented with error bars showing the 95 % tolerance interval when the experimentally-determined values of group velocity are compared graphically to the theoretical values of group velocity for the various branches.

The assumed paths for the first arrival at the upper and lower accelerometers and return of the reflected wave to the triaxial accelerometers are shown on Figure 6-13 for the 0-degree orientation.

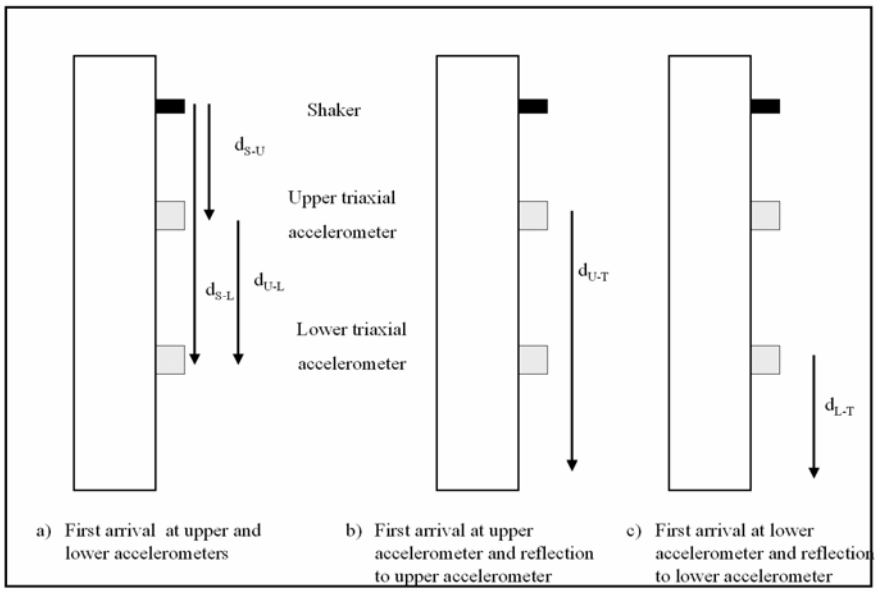

Figure 6-13: Possible travel paths for guided waves in a pile in 0-degree, orientation first pass and reflection

When the triaxial accelerometers are mounted in the 0-degree orientation, as defined on Figure 6-1, the component of the wave traveling down the pile passes the upper triaxial accelerometer, the lower triaxial accelerometer, and reflects off the pile tip. The reflected wave passes the lower triaxial accelerometer then passes the upper triaxial accelerometer. The travel distances for the first pass are the vertical distance from the shaker to the upper triaxial accelerometer, d_{S-U}, the vertical distance from the shaker to the lower triaxial accelerometer, d_{S-L}, and the vertical distance from the upper triaxial accelerometer to the lower triaxial accelerometer, d_{U-L}, as shown

on Figure 6-13a. The travel distance for the first pass at the upper triaxial accelerometer and return of the reflected wave to the upper triaxial accelerometer is twice the distance from the accelerometer position to the pile tip, d_{U-T}, as shown on Figure 6-13b. The travel distance for the first pass at the lower triaxial accelerometer and return of the reflected wave to the lower triaxial accelerometer is twice the distance from the accelerometer position to the pile tip, d_{L-T}, as shown on Figure 6-13c.

The assumed paths for the first arrival and return of the reflected wave are shown on Figure 6-14 for the 180-degree orientation.

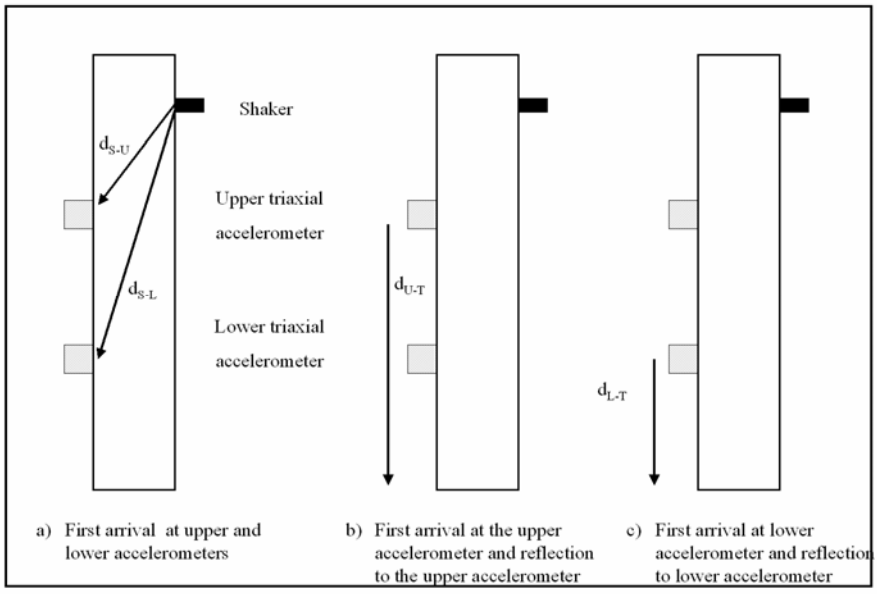

Figure 6-14: Possible travel paths for guided waves in a pile in 180-degree orientation, first pass and reflection

For the 0-degree orientation, the distance from the shaker to the upper triaxial accelerometer is 864 mm and the distance from the upper triaxial accelerometer to the lower

triaxial accelerometer is 916 mm. For the 180-degree face, the vertical distance from the shaker to the upper triaxial accelerometer is 864 mm and the vertical distance from the upper triaxial accelerometer to the lower triaxial accelerometer is 908 mm. The pile diameter is 355 mm. The travel distances have been computed for the first pass and reflection of the wave based on the travel paths and orientations shown on Figures 6-13 and 6-14, and are presented on Table 6-4.

Table 6-4: Prototype pile C355-2430, distances between shaker and accelerometers for controlled frequency tests performed under traction-free conditions

Orientation	Travel path	Distance (mm)
0-degree	Shaker – Upper	864
	Shaker – Lower	1780
	Upper – Lower	916
	Upper – Tip	1516
	Lower – Tip	602
180-degree	Shaker – Upper	934
	Shaker – Lower	1808
	Upper – Lower	874
	Upper – Tip	1516
	Lower – Tip	610

The group velocities are computed for different combinations of first pass and return. The travel distances used in the group velocity calculations, which are presented on Table 6-5, were computed using the geometries presented on Figures 6-13 and 6-14 and the values presented on Table 6-4.

Table 6-5: Prototype pile C355-2430, calculated travel distances for first pass and reflection for traction-free test configuration

Combination of peaks	Distances to be included	Accelerometer	Orientation	Distance (mm)
First pass at accelerometer and return of first reflection	Twice the distance from the accelerometer to the pile tip	Upper	0-degree	3032
			180-degree	3032
		Lower	0-degree	1204
			180-degree	1220
First pass at accelerometer and second pass of wave	Twice the distance from the accelerometer to the pile tip plus twice the distance from the accelerometer to the top of the pile (this is twice the pile length)	Upper	0-degree	4860
			180-degree	4860
		Lower	0-degree	4860
			180-degree	4860
First pass at accelerometer and return of second reflection	Twice the pile length plus twice the distance from the accelerometer to the pile tip	Upper	0-degree	7892
			180-degree	7892
		Lower	0-degree	6080
			180-degree	6064
Start of wave at shaker and return of first reflection to accelerometer	Distance from shaker to accelerometer and twice the distance from the accelerometer to the pile tip	Upper	0-degree	3896
			180-degree	3966
		Lower	0-degree	2984
			180-degree	3028
Start of wave at shaker and second pass of wave at accelerometer	Distance from shaker to accelerometer and twice the distance from the accelerometer to the pile tip plus twice the distance from the accelerometer to the top of the pile	Upper	0-degree	5724
			180-degree	5794
		Lower	0-degree	6640
			180-degree	6668
Start of wave at shaker and return of second reflection to accelerometer	Distance from shaker to accelerometer and twice the pile length plus twice the distance from the accelerometer to the pile tip	Upper	0-degree	8756
			180-degree	8826
		Lower	0-degree	7860
			180-degree	7872

6.4 Controlled Frequency Results for CF = 14000 Hz

A central frequency of 14000 Hz was the only frequency that consistently met the criteria of a good input, as defined in Section 6.2.2.1. Tests were performed at the 0-degree, 90-degree,

180-degree, and 270-degree orientation, as defined on Figure 6-1; however, only the tests performed at 0-degree and 180-degree orientations provided results from which reflections could be identified. The test results were analyzed with the combinations of peaks shown in Table 6-5 to determine the group velocity and those results were compared to the numerically-determined group velocity – frequency relationships to determine the most likely flexural branch on which modes may be excited. The mode identified based on group velocity is compared to the normalized displacement at the accelerometer location to determine if that mode is likely to be excited.

6.4.1 Identification of Expected Branches

The controlled frequency test performed on Prototype pile C355-2430 could potentially excite modes on the first five flexural branches based on the cutoff frequencies presented in Section 5.2.1. The actual branches on which modes were excited in a test are identified by considering the group velocities of the various branches at 14000 Hz and the normalized displacement of each mode.

The solution of the frequency equation in terms of nondimensional frequency and nondimensional wavenumber, conversion to the nondimensional group velocity – nondimensional frequency relationship, and conversion from nondimensional form to dimensional form was presented in Section 4.3. The group velocity – frequency relationship for the first five flexural branches is shown on Figure 6-15.

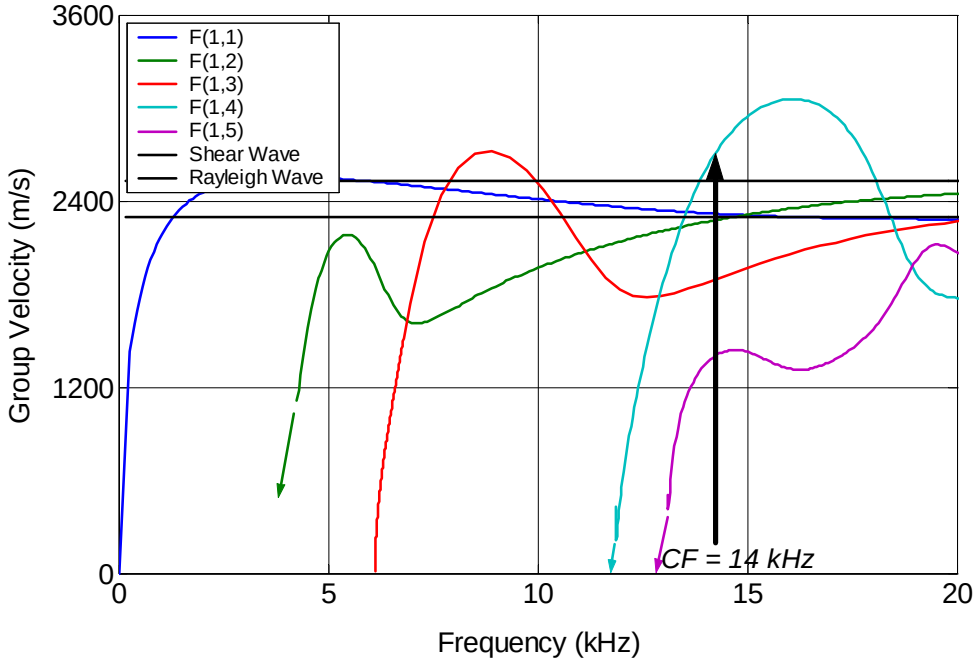

Figure 6-15: Prototype pile C355-2430, group velocity – frequency curve for first five flexural branches and test frequency identified

At a central frequency of 14000 Hz, modes may be excited on the F(1,1) branch through the F(1,5) branch.

In addition to the group velocity, the normalized displacement values can be used to evaluate whether a mode has been excited. The normalized displacement profiles have been calculated using the procedure presented in Section 2.3.8, as subsequently discussed.

The frequency equation was solved by the algorithm presented in Section 2.3.4 to determine the nondimensional wavenumber. The concrete and soil properties, expressed in terms of their ratios for "Traction-free" conditions are

- Shear modulus ratio: 32500
- Density ratio: 133

and the nondimensional frequency, Ω, is computed by

$$\Omega = \frac{2\pi f a}{c_{T_c}} \qquad (6\text{-}3)$$

Prototype pile C355-2430 has a radius, *a*, of 0.1775 m, and a shear wave velocity, c_{Tc}, of 2530 m/s, and the test was performed at a frequency, *f*, of 14000 Hz. Substituting the radius, shear wave velocity, and test frequency into equation 6-3, the nondimensional frequency is 6.171, rounded to 4 significant digits.

The nondimensional wavenumber that solves frequency equation was computed by the procedure presented in Section 2.3.4, using the properties of prototype pile under "Traction-free" conditions and the nondimensional frequency corresponding to a test frequency of 14000 Hz. The nondimensional wavenumber of each branch, rounded to 4 significant digits, is presented on Table 6-6.

Table 6-6: Prototype pile C355-2430 under traction-free conditions, nondimensional wavenumber for the flexural branches at nondimensional frequency of 6.127

Branch	Nondimensional wavenumber	
	Real part	Imaginary part
F(1,1)	6.784	0.001890
F(1,2)	5.879	0.0005546
F(1,3)	4.885	0.0009983
F(1,4)	3.271	0.0009076
F(1,5)	1.144	0.000659

The normalized displacements were computed at the outer edge of the pile (R = 1) for the first five flexural branches using the procedures outlined in Section 2.3.8.2, the properties of soil and concrete for Prototype pile C355-2430 under "Traction-free" conditions, a nondimensional frequency of 6.127, and the nondimensional wavenumber values presented on Table 6-6.

The group velocities of each branch along with the magnitudes of the longitudinal and tangential components of the normalized displacement at R = 1 are summarized on Table 6-7.

Table 6-7: Prototype pile C355-2430 (traction-free), group velocity and normalized displacement values at R = 1 for flexural branches at 14000 Hz

Branch	Group velocity (m/s)	Normalized displacement values at R = 1	
		Radial direction	Longitudinal direction
F(1,1)	2320	0.73	0.39
F(1,2)	2270	0.03	0.07
F(1,3)	1870	0.13	0.04
F(1,4)	2600	0.01	0.22
F(1,5)	1350	1.23	0.03

For the radial direction, the F(1,5) branch has the largest normalized displacement value and the F(1,1) branch has the second largest normalized displacement value. The group velocity of the mode on the F(1,1) branch is 1.7 times the group velocity of the mode on the F(1,5) branch. If modes are excited on both branches, the reflected waves could be distinctly identified in the time domain. In the longitudinal direction, the F(1,1) branch has the largest normalized displacement value.

The normalized displacement values presented on Table 6-7 were computed for the 0-degree orientation. The values are equally applicable to tests performed at the 180-degree orientation because the magnitude of the cosine is 1 for both angles.

6.4.2 Responses as Functions of Orientations

The flexural guided wave theory (Wang, 2004) implies that the relative magnitudes of the response are consistent with the displacement equations presented in Section 2.3.8. The controlled frequency tests were performed at the 0-degree and 180-degree orientations, as shown on Figure 6-1. One expects a large response in the radial and longitudinal directions, as they depend on the cosine of the angle between the shaker and the accelerometer, and a zero response in the tangential direction, as it depends on the sine of the angle between the shaker and the accelerometer.

The results of the controlled frequency tests performed at the 0-degree and 180-degree orientations with the responses measured at the upper triaxial accelerometer are presented on Figure 6-16.

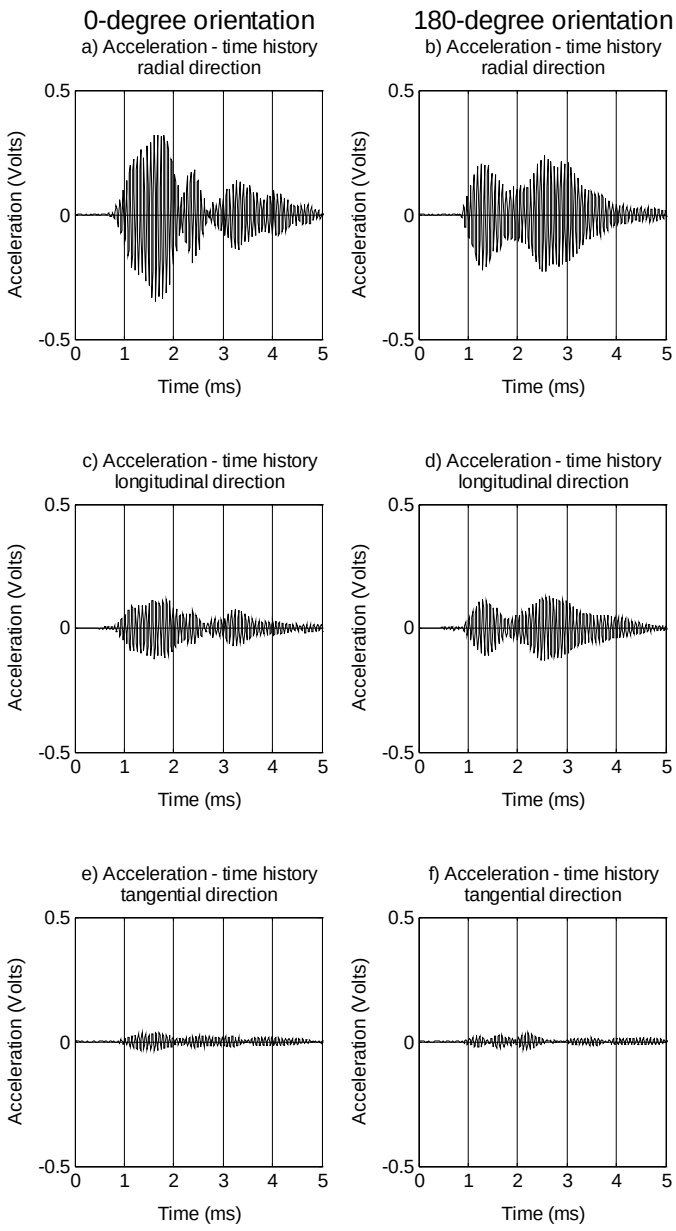

Figure 6-16: Prototype pile C355-2430 (traction-free), controlled frequency results with CF = 14000 Hz, response measured at upper triaxial accelerometer

The response in the radial direction was the largest of the three. The response measured in the longitudinal direction was smaller than the response measured in the radial direction, but the two responses were on the same order of magnitude. The response measured in the tangential direction was an order of magnitude smaller than the response measured in the radial or longitudinal direction. The results are in agreement with the theoretical results shown in Table 6-7.

The response in the tangential direction should be zero, but it is not. Factors that can contribute to the nonzero response in the tangential direction include human factors such as small deviations in the angle between the shaker and the accelerometer, misalignment of the accelerometer, and equipment performance factors such as cross-sensitivity described in Section 3.3.3, and electronic noise.

The results of the controlled frequency tests performed at the 0-degree and 180-degree orientations with the responses measured at the lower triaxial accelerometer are presented on Figure 6-17.

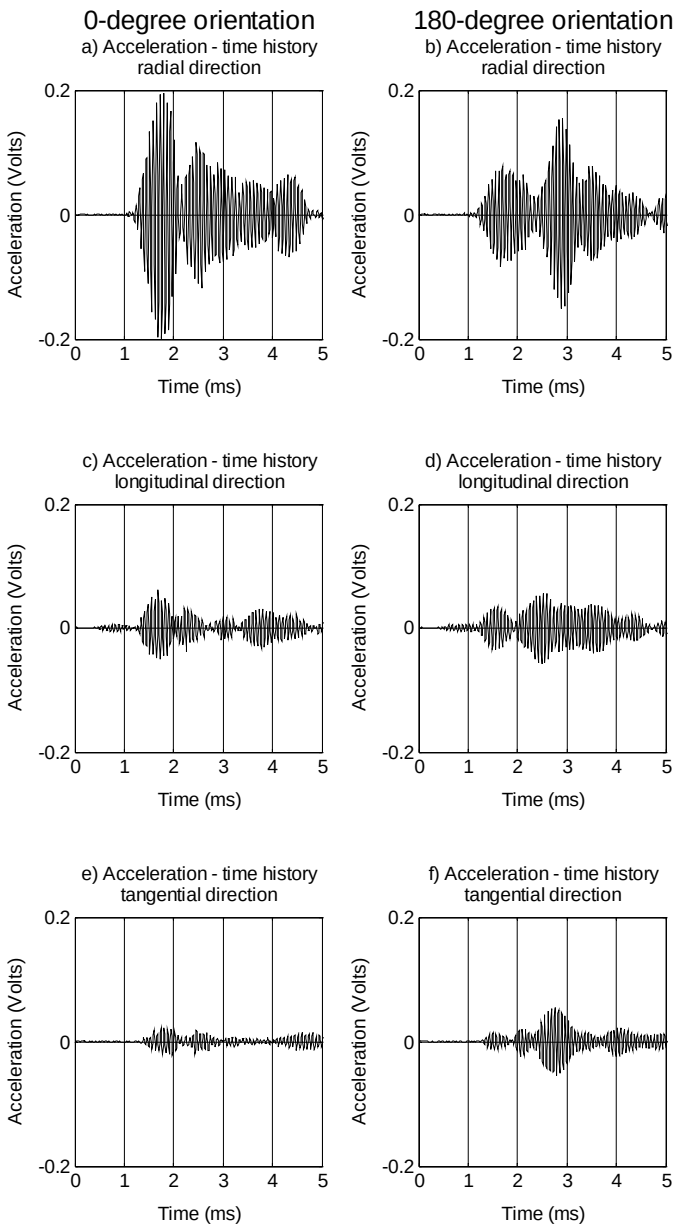

Figure 6-17: Prototype pile C355-2430 (traction-free), controlled frequency results with CF = 14000 Hz, response measured at lower triaxial accelerometer

The response in the radial direction was the largest of the three. The response measured in the longitudinal direction was smaller than the response measured in the radial direction, but the two responses were on the same order of magnitude. The response measured in the tangential direction was smaller than the response measured in the radial or longitudinal direction.

The large response in the radial and longitudinal direction compared to the response in the tangential direction for tests performed at the 0-degree and 180-degree orientations is consistent with the expected response based on the theoretical considerations presented in Section 2.3.8.

6.4.3 Analysis of Group Velocity

The theoretical considerations presented in Section 6.1 suggest that the radial and longitudinal components of the displacement should be analyzed for tests performed at the 0-degree and 180-degree orientations, which was confirmed by the results presented in Section 6.4.2. The flexural guided wave theory (Wang, 2004) can be further verified by attributing the identified wave groups to one of the flexural branches based on the group velocity and normalized displacements by comparing the experimental responses to the theoretical values presented on Figure 6-15 and Table 6-7.

The first pass is identified as the first wave group in the acceleration – time history and provides the easiest set of data from which to compute the group velocity. Once the group velocity has been computed based on first arrivals, its most likely branch is identified. The subsequent peaks are analyzed to determine if

1. They are a return of the initial wave, or
2. they are returns of a mode on a branch other than the one identified in the first pass.

6.4.3.1 Analysis of Radial Direction Results

The acceleration – time histories for the response measured at the shaker, upper triaxial accelerometer (radial direction), and lower triaxial accelerometer (radial direction) are shown on Figure 6-18.

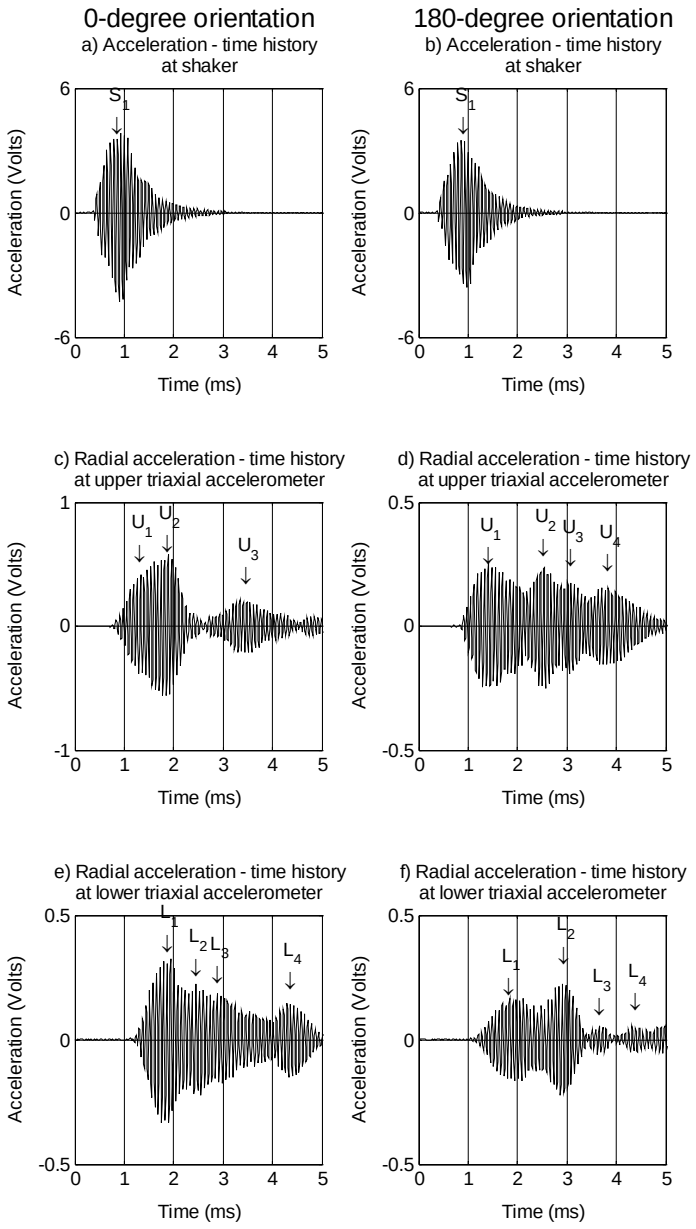

Figure 6-18: Prototype pile C355-2430 (traction-free), controlled frequency results with CF = 14000 Hz, upper and lower radial acceleration – time histories for 0-degree and 180-degree orientations

The peaks designated S_1, U_1, and L_1 represent the start of the wave at the shaker and the first arrival at the upper and lower triaxial accelerometers, respectively. The peaks designated U_2 through U_4 and L_2 through L_4 represent possible returns of the reflected wave. The times at which each peak occurred are presented on Table 6-8.

Table 6-8: Prototype Pile C355-2430 (traction-free), controlled frequency results with CF = 14000 Hz, peaks in measured responses (radial)

Peak designation	Time at which peak occurred (ms)	
	0-degree orientation	180-degree orientation
S_1	0.93	0.93
U_1	1.33	1.34
U_2	1.89	2.54
U_3	3.34	3.09
U_4	N/I	3.84
L_1	1.72	1.70
L_2	2.43	2.91
L_3	2.88	3.61
L_4	4.29	4.32

N/I Peak not identified

The time values presented on Table 6-8 were used to compute the group velocity values. The group velocity values were computed from various combinations of the start of the wave at the shaker, first arrival and return of the reflected wave at the upper and lower triaxial accelerometers. The assumed travel paths are defined on Figures 6-13 and 6-14, and the travel distances are presented on Tables 6-4 and 6-5. The time lag is the difference between the second and first peaks used in the analysis. For example, one of the group velocity calculations is the first arrival at the upper and lower triaxial accelerometers. From the values on Table 6-4, the

distance between the upper and lower triaxial accelerometers is 916 mm for the 0-degree orientation. The peaks to be analyzed are U_1 and L_1 shown on Figure 6-18, which occur at 1.33 ms and 1.72 ms, respectively. The time lag, Δt, is 0.39 ms. The group velocity is the travel distance divided by the time lag, or 2350 m/s.

The group velocity computed from the start of the wave at the shaker and the first arrival of the wave at each accelerometer is presented on Table 6-9. The distance between the two points is presented on Table 6-4.

Table 6-9: Prototype pile C355-2430 (traction-free), controlled frequency results with CF = 14000 Hz, group velocity values based on first arrival (radial)

Orientation	Combination of peaks	Travel distance, ΔL (mm)	Time lag, Δt (ms)	Group velocity, c_g (m/s)
0-degree	$S_1 - U_1$	864	0.40	2160
	$S_1 - L_1$	1780	0.79	2250
	$U_1 - L_1$	916	0.39	2350
180-degree	$S_1 - U_1$	934	0.41	2280
	$S_1 - L_1$	1808	0.77	2350
	$U_1 - L_1$	834	0.36	2320

The group velocity values range from 2160 to 2350 m/s with an average value of 2290 m/s and a standard deviation of 70 m/s or 3.1 % of the mean value. The branch on which the mode propagates is identified by comparing the experimental and theoretical group velocity and the normalized displacement.

The experimentally-determined group velocity most closely matches the theoretical group velocity value for the F(1,1) branch, which is 2320 m/s. Based on the normalized displacement values presented on Table 6-7, the mode on the F(1,5) branch has the largest normalized displacement. The mode on the F(1,1) branch has the second largest normalized displacement. The theoretical group velocity for the mode on the F(1,5) branch is 1350 m/s, compared to 2320 m/s for the mode on the F(1,1) branch. The mode identified for the experimental results is attributed to the F(1,1) branch based on group velocity and normalized displacement.

The incident wave is attributed to the F(1,1) branch, which means that the first return and subsequent passes of the wave should also fall along the F(1,1) branch. If all modes lie along the F(1,1) branch, the wave group after the first pass will be the return of the reflected wave, the wave group after the first return of the reflected wave will be the second pass, and the wave group after the second pass of the wave will be the return of the second reflection. The travel distances for successive passes of the wave was presented on Table 6-5. The group velocities have been calculated for various combinations of peaks shown on Figure 6-18 by substituting the appropriate travel distances from Table 6-5 and time lags from Table 6-8 into equation 6-1. The group velocity results are presented on Table 6-10.

Table 6-10: Prototype pile C355-2430 (traction-free), controlled frequency results for CF = 14000 Hz, group velocity values for reflected wave (radial)

Orientation	Combination of peaks	Expected travel path	Travel distance, ΔL (mm)	Travel time Δt (ms)	Group velocity, c_g (m/s)
0-degree	$U_3 - U_1$	Second pass	4860	2.01	2420
	$U_3 - S_1$		6640	2.41	2760
	$L_4 - L_1$	Second reflection	6080	2.57	2370
	$L_4 - S_1$		7860	3.36	2340
180-degree	$U_2 - U_1$	First reflection	3032	1.20	2530
	$U_2 - S_1$		3966	1.61	2460
	$U_3 - U_1$	Second pass	4860	1.74	2790
	$U_3 - S_1$		5794	2.16	2680
	$L_3 - L_1$	Second pass	4860	1.91	2540
	$L_3 - S_1$		6668	2.68	2490
	$L_4 - L_1$	Second reflection	6064	2.62	2310
	$L_4 - S_1$		7872	3.39	2320

The group velocity values range from 2310 to 2790 m/s with an average value of 2490 m/s and a standard deviation of 170 m/s or 6.8 % of the mean value. The experimentally-determined group velocity most closely matches the theoretical group velocity value for the F(1,1) branch, which is 2320 m/s.

Peaks U_2, L_2, and L_3 on the 0-degree orientation, could not be attributed to the F(1,1) branch, nor could peaks U_4 and L_2 on the 180-degree orientation. Three possible explanations for the peaks that do not lie along the F(1,1) branch are

1. They are modes on the F(1,5) branch.
2. They a wave type other than a flexural wave.
3. They are spurious responses.

The likelihood of the previously unidentified peaks falling on the F(1,5) branch or a wave type other than a flexural wave can be evaluated by considering the first pass. The group velocity computed from the start of the wave at the shaker and the first arrival of the wave at each accelerometer is presented on Table 6-11. The distance between the two points is presented on Table 6-4.

Table 6-11: Prototype pile C355-2430 (traction-free), controlled frequency results for CF = 14000 Hz, group velocity values based on first arrival (radial)

Orientation	Combination of peaks	Travel distance, ΔL (mm)	Time lag, Δt (ms)	Group velocity, c_g (m/s)
0-degree	$S_1 - U_2$	864	0.96	900
	$S_1 - L_2$	1780	1.50	1190
	$U_2 - L_2$	916	0.54	1700

The group velocity values range from 900 to 1900 m/s with an average value of 1260 m/s and a standard deviation of 410 m/s or 32.5 % of the mean value. The theoretical group velocity for a mode on the F(1,5) is 1350 m/s, which is only 7.1% greater than the average of the values presented on Table 6-11. However, peaks U_2 and L_2 are not modes on the F(1,5) branch because the scatter in the data of 32.5 % of the mean is very large compared to the scatter in the data computed from the analysis of peaks U_1, and L_1, of 3.1 % of the mean, and those peaks were attributed to modes on the F(1,1) branch. The conclusion that peaks U_2 and L_2 are spurious responses is further supported by the observation that they are present in the results of tests performed at the 0-degree orientation but not in the results of tests performed at the 180-degree orientation.

6.4.3.2 Analysis of Longitudinal Direction Results

The acceleration – time histories for the response measured at the shaker, upper triaxial accelerometer (longitudinal direction), and lower triaxial accelerometer (longitudinal direction) are shown on Figure 6-19.

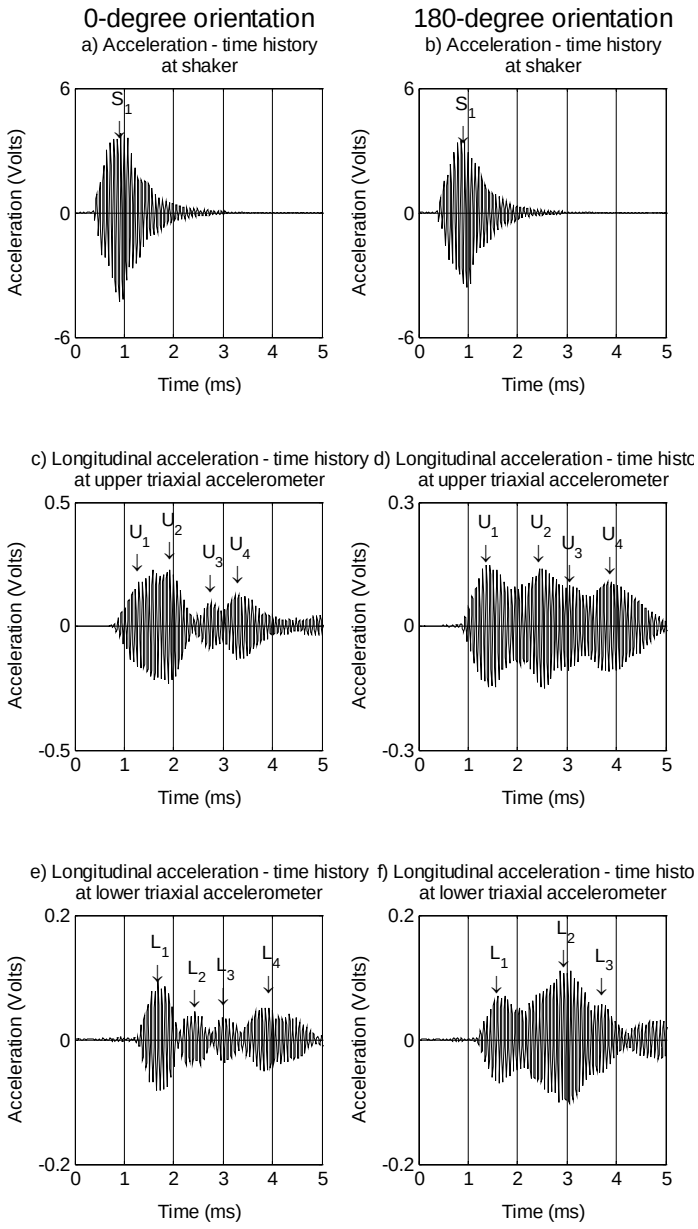

Figure 6-19: Prototype pile C355-2430 (traction-free), controlled frequency results with CF = 14000 Hz, upper and lower longitudinal acceleration – time histories for 0-degree and 180-degree orientations

The peaks designated S_1, U_1, and L_1 represent the start of the wave at the shaker and the first arrival at the upper and lower triaxial accelerometers, respectively. The peaks designated U_2 through U_4 and L_2 through L_4 represent possible returns of the reflected wave. The times at which each peak occurred are presented on Table 6-12.

Table 6-12: Prototype Pile C355-2430 (traction-free), controlled frequency results with CF = 14000 Hz, peaks in measured responses (longitudinal)

Peak designation	Time at which peak occurred (ms)	
	0-degree orientation	180-degree orientation
S_1	0.93	0.93
U_1	1.30	1.61
U_2	1.86	2.42
U_3	2.76	3.27
U_4	3.31	4.03
L_1	1.69	1.73
L_2	2.43	2.46
L_3	2.99	3.55
L_4	3.79	N/I

N/I No peak was identified

The time values presented on Table 6-12 were used to compute the group velocity values.

The group velocity computed from the start of the wave at the shaker and the first arrival of the wave at each accelerometer is presented on Table 6-13.

Table 6-13: Prototype pile C355-2430 (traction-free), controlled frequency results for CF = 14000 Hz, group velocity values based on first arrival (longitudinal)

Orientation	Combination of peaks	Travel distance, ΔL (mm)	Time lag, Δt (ms)	Group velocity, c_g (m/s)
0-degree	$S_1 - U_1$	864	0.37	2340
	$S_1 - L_1$	1780	0.76	2340
	$U_1 - L_1$	916	0.39	2330
180-degree	$S_1 - U_1$	934	0.44	2120
	$S_1 - L_1$	1808	0.74	2440
	$U_1 - L_1$	874	0.3	2910

The group velocity values range from 2120 to 2910 m/s with an average value of 2410 m/s and a standard deviation of 270 m/s or 11.2 % of the mean value. The experimentally-determined group velocity most closely matches the theoretical group velocity value for the F(1,1) branch, which is 2320 m/s. The mode on the F(1,1) branch also has the largest normalized displacement of the modes on any active branches at the test frequency. The mode identified for the experimental results is attributed to the F(1,1) branch based on group velocity and normalized displacement.

The incident wave is attributed to the F(1,1) branch, which means that the first return and subsequent passes of the wave should also fall along the F(1,1) branch. If all modes lie along the F(1,1) branch, the wave group after the first pass will be the return of the reflected wave, the wave group after the first return of the reflected wave will be the second pass, and the wave group after the second pass of the wave will be the return of the second reflection. The group velocities have been calculated for various combinations of peaks shown on Figure 6-19 by

substituting the appropriate travel distances from Table 6-5 and time lags from Table 6-12 into equation 6-1. The group velocity results for the reflected waves are presented on Table 6-14.

Table 6-14: Prototype pile C355-2430 (traction-free), controlled frequency results with CF = 14000 Hz, group velocity values for reflected wave (longitudinal)

Orientation	Combination of peaks	Expected travel path	Travel distance, ΔL (mm)	Travel time Δt (ms)	Group velocity, c_g (m/s)
0-degree	$U_3 - U_1$	First reflection	3032	1.46	2080
	$U_3 - S_1$		3896	1.83	2130
	$U_4 - U_1$	Second pass	4860	2.01	2420
	$U_4 - S_1$		5724	2.38	2410
	$L_4 - L_1$	Second pass	4860	2.10	2310
	$L_4 - S_1$		6640	2.86	2320
180-degree	$U_3 - U_1$	First reflection	3032	1.66	1830
	$U_3 - S_1$		3966	2.34	1700
	$U_4 - U_1$	Second reflection	6064	2.42	2510
	$U_4 - S_1$		8826	3.10	2850
	$L_3 - L_1$	Second pass	4860	1.82	2670
	$L_3 - S_1$		6668	2.62	2550

The group velocity values range from 1700 to 2850 m/s with an average value of 2320 m/s and a standard deviation of 330 m/s or 14.2 % of the mean value. The branch on which the mode propagates is identified by comparing the experimental and theoretical group velocity and the normalized displacement.

The experimentally-determined group velocity most closely matches the theoretical group velocity value for the F(1,1) branch, which is 2320 m/s, and the mode on the F(1,1) branch has the largest normalized displacement of the modes on any active branches at the test

frequency. The mode identified for the experimental results is attributed to the F(1,1) branch based on group velocity and normalized displacement.

Applying the analysis of peaks U_2 and L_2 in the 0-degree orientation of the radial response to peaks U_2 and L_2 in the 0-degree orientation of the longitudinal response, those peaks are also considered spurious responses.

6.4.3.3 Summary of Controlled Frequency Results

The analysis of the controlled frequency results indicate that a flexural wave is induced in the pile, and that that mode lies along the F(1,1) branch. The analysis of the test results, which were presented in the text of Sections 6.4.3.1 and 6.4.3.2, can be presented graphically by superimposing the group velocity – frequency data on the numerically-determined group velocity curves presented in Section 6.4.1, or by the mode identification method described in Section 3.5.2.

The group velocity data are summarized on Table 6-15.

Table 6-15: Prototype pile C355-2430 (traction-free), controlled frequency results for CF = 14000 Hz, summary of group velocity values

Direction	Branch	Group velocity (m/s)		
		Average	Standard deviation	Theoretical
Radial	F(1,1)	2410	170	2320
Longitudinal	F(1,1)	2360	280	2320

The scatter in the computed group velocity values for the longitudinal results is much larger than the scatter in the computed group velocity values for the radial results. The larger scatter for the longitudinal results can be explained by considering the normalized displacement magnitudes. The pile responses in the longitudinal direction were smaller than the pile responses in the radial direction, as shown on Figures 6-6 and 6-7, which means that the measured responses in the longitudinal direction would be affected by spurious responses, noise, and equipment limitations than the responses in the radial direction.

The smaller response in the longitudinal direction compared to the radial direction is consistent with the theoretical values based on the branch to which the modes are attributed. All peaks attributed to a flexural branch were attributed to the F(1,1) branch. From the results on Table 6-7, normalized displacement magnitude for the longitudinal direction is 0.39 compared to 0.79 for the radial direction.

The values presented on Table 6-15 are superimposed on the numerically-determined group velocity – frequency curve on Figure 6-20.

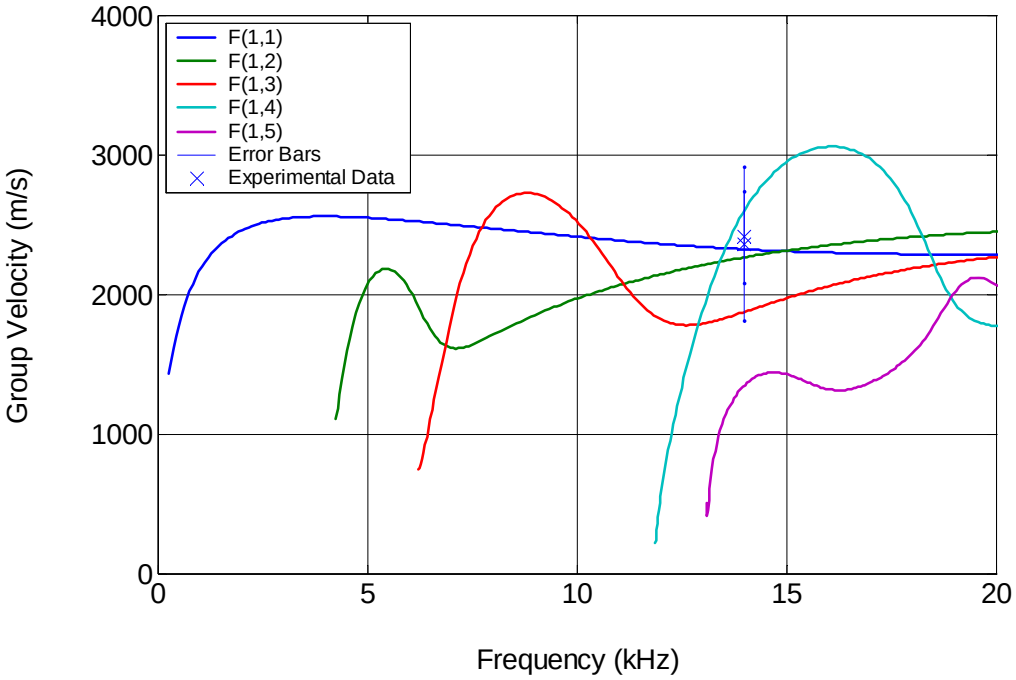

Figure 6-20: Prototype pile C355-2430 (traction-free) controlled frequency results with CF = 14000 Hz, superimposed on numerically-determined group velocity – frequency curves of first five flexural branches for concrete with $\nu_c = 0.20$

The two data points corresponding to modes attributed to the F(1,1) branch are near the theoretical group velocity for the F(1,1) branch; however, given the uncertainty in the data and the range of theoretical group velocity values for the first four flexural branches, the experimental data crosses all four group velocity – frequency curves. The modes on the F(1,2) and F(1,3) branch have small normalized displacement values for both the radial and longitudinal components, and the F(1,4) branch has a small normalized displacement value for the radial component. Based on the group velocity values and the normalized displacement values, the modes are attributed to the F(1,1) branch.

The results of the radial response for the 180-degree orientation analyzed by the mode identification method described in Section 3.5.2 are presented on Figure 6-21. The joint velocity frequency curve was generated using the start of the wave at the shaker and the return of the first reflection. The start of the wave at the shaker occurs at 0.93 ms, as presented on Table 6-8, and the travel length for the wave is 3966 mm, as presented on Table 6-5.

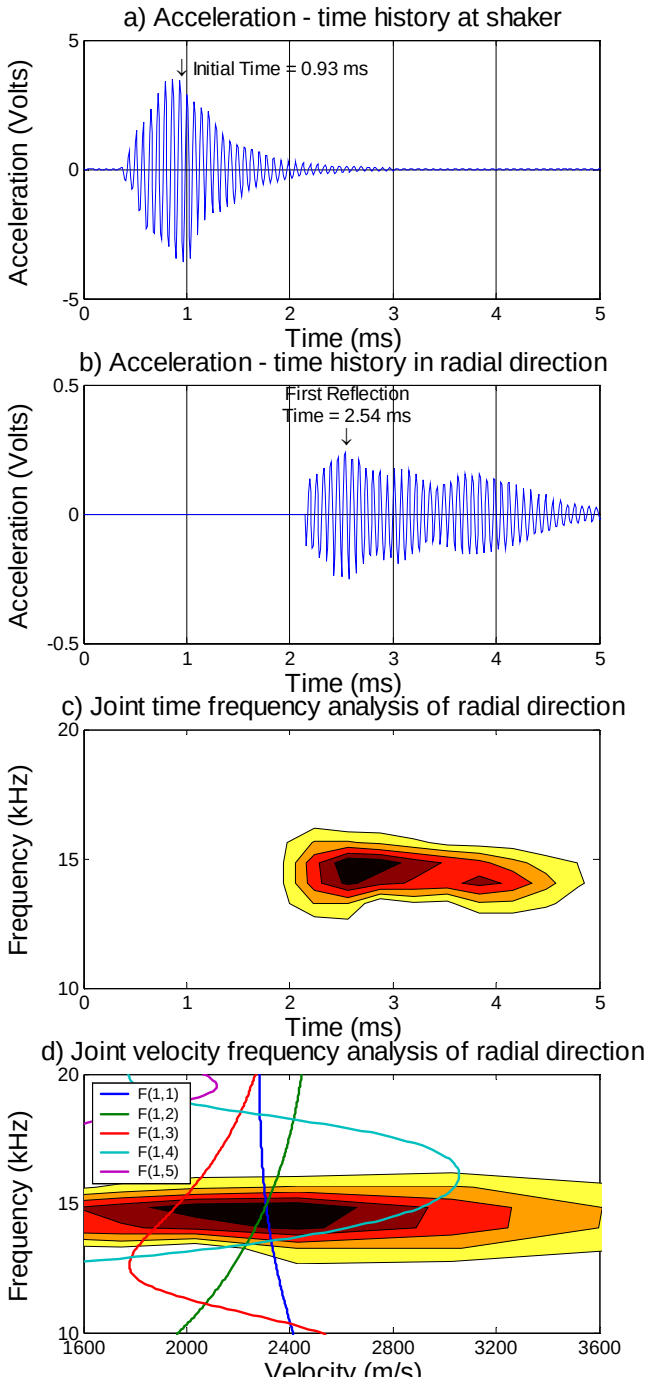

Figure 6-21: Prototype pile C355-2430 (traction-free) controlled frequency results with CF = 14000 Hz, 180-degree orientation, radial direction mode identification method

The largest contour on the joint velocity frequency analysis curve, shown on Figure 6-21d crosses the group velocity – frequency curve for the F(1,1), F(1,2), and F(1,3) branches. The theoretical group velocities for the F(1,1) and F(1,2) branches are so close to each other that the mode identification method cannot distinctly identify between the two branches; however, consideration of the normalized displacements indicate that the mode belongs to the F(1,1) branch and not the F(1,2) branch.

Analysis of the group velocity – frequency data by conventional time and frequency analysis or by the mode identification method, as well as the normalized displacements indicates that the controlled frequency tests performed on Prototype pile C355-2430 under traction-free conditions with a central frequency of 14000 Hz produces a flexural wave on the F(1,1) branch, which verifies the flexural guided wave theory (Wang, 2004).

Some limitations of the experimental verification of the flexural guided wave theory are

1. The presence of spurious response in the first pass of the wave in the 0-degree orientation,
2. Difficulty in identifying returns of the reflected wave, particularly in the response measured at the lower triaxial accelerometer, and
3. The poor results obtained from the tests performed at the 90-degree and 270-degree orientations.

Items 1 and 2 may be less pronounced for tests performed on a longer pile. The spurious response in the lower triaxial accelerometer was smaller than the spurious response in the upper triaxial accelerometer, suggesting greater distance between the shaker and upper triaxial

accelerometer would reduce this problem. Larger distance between the lower triaxial accelerometer and the pile tip would result in greater time between the wave group corresponding to the first pass and return of the reflected wave and may make the wave groups easier to identify.

6.6 Summary and Conclusions

Prototype pile C355-2430 was evaluated nondestructively under traction-free conditions, using the controlled frequency method. The results were evaluated to identify suitable test frequencies and the results of suitable test frequencies were analyzed to verify the flexural guided wave theory by comparing experimental and theoretical values of group velocity and by consideration of normalized displacement. The normalized displacement was considered to determine which response directions would be analyzed and to determine the branches on which modes are likely to be excited.

The controlled frequency tests were performed with a computer-controlled piezoelectric shaker to generate as stress wave and two triaxial accelerometers mounted on the side of the pile to measure the pile response. The input and response were measured with the embedded transducer in the shaker with which the force was applied and with the two triaxial accelerometers mounted on the side of the pile. Tests were performed at central frequencies of

4000 Hz to 20000 Hz in 2000 Hz increments, and at a central frequency of 5300 Hz. Three distinct types of responses were identified, one of which was suitable and the others were unsuitable. A central frequency of 14000 Hz was identified as a suitable frequency.

The tests were performed at the 0-degree and 180-degree orientations and the radial and longitudinal components of the response were analyzed. The radial and longitudinal responses were selected based on the normalized displacement magnitudes. The theoretical values of normalized displacement indicate that the radial and longitudinal components should be generally nonzero and that the tangential component should be uniformly zero for the 0-degree and 180-degree orientations, which was consistent with the experimental results.

Peaks corresponding to the possible first arrival and returns of the reflected wave were identified in responses measured at both the upper and lower triaxial accelerometers, and those peaks were analyzed to determine if they correspond to modes on one or more of the flexural branches based on group velocity and normalized displacement magnitude as part of the verification of the flexural guided wave theory (Wang, 2004). The group velocity was calculated for various combinations of peaks corresponding to the likely first pass and return of the reflected wave. The computed group velocity values were compared to theoretical values of group velocity by superimposing the experimental data on the numerically-determined group velocity – frequency curves and by the mode identification method (Chao, 2002) applied to a selected set of test data. The normalized displacements were considered to verify that the mode

identified based on group velocity should be excited based on its mode shape, i.e., it must have a large normalized displacement magnitude.

The group velocity was computed for the tests performed at a central frequency of 14000 Hz, and the group velocity was attributed to a mode on the F(1,1) branch, which verifies the flexural guided wave theory.

Chapter 7: Evaluation of Embedded Prototype Piles by Controlled Frequency Method

The evaluation of prototype pile C355-2430 under traction-free conditions indicated that flexural guided waves are induced by the controlled frequency method. To evaluate the applicability of the controlled frequency method to deep foundations, prototype pile C355-2430 and two group B prototype piles were evaluated nondestructively by the controlled frequency method under embedded conditions at the National Geotechnical Experimentation Site at Northwestern Univeristy. The force for the controlled frequency tests was induced with a piezoelectric shaker and the response of the pile was measured with one triaxial accelerometer.

The tests were performed at frequencies of 14000 Hz and the filtered test results were analyzed as part of the verification of the guided wave theory presented in Section 2.3. The criteria for experimental verification of the flexural guided wave theory (Wang, 2004) are

- Identify the branches on which modes are expected based on the cutoff frequencies of the various branches compared to the central frequency of the test,
- Evaluate the relative magnitudes of displacements,
  - For the 0-degree and 180-degree orientations, the radial and longitudinal responses should be nonzero and the tangential response should be negligible.
  - For the 90-degree and 270-degree orientations, the radial and longitudinal responses should be negligible and the tangential response should be nonzero.
- Determine the group velocity of the stress wave and compare the experimental results to the numerical results.
- Determine the attenuation coefficient per unit length based on the amplitudes of the incident and reflected wave.

When modes on more than one branch may be excited in a test, the branches are identified by considering

- The group velocity of each mode on each branch that may be excited at the test frequency,
- The normalized displacement of each mode on each branch that may be excited at the test frequency, and
- The attenuation of each mode on each branch that may be excited at the test frequency.

The mode identification method described in Section 3.5.2 provides an additional method with which to analyze the test results.

7.1 Analysis of Controlled Frequency Results

The piles were tested by the controlled frequency method described in Section 3.1.2. The shaker and one triaxial accelerometer were mounted on the side of a pile, as shown on Figure 7-1. The position of the shaker was the same for all tests and the orientation of the test was changed by moving the accelerometer.

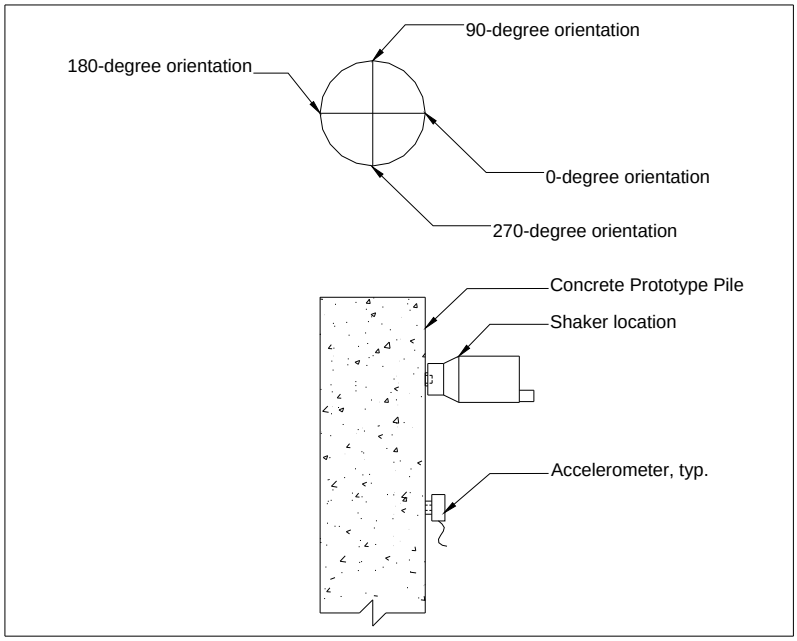

Figure 7-1: Test configuration for controlled frequency tests

Figure 7-1 shows one triaxial accelerometer in line with the shaker, which is defined as the 0-degree orientation. The tests were performed at the 0-degree and 180-degree orientations and the results of those tests will be presented. Tests were also performed at the 90-degree and 270-degree orientations but the results of those tests did not provide results from which reflections could be identified.

The distances used in the calculation of the group velocity and attenuation coefficients are based on assumed travel paths and the geometry of the embedded piles. The times used in the calculation of group velocity and the amplitudes used in the calculation of the attenuation coefficient are selected from wave groups identified on the acceleration – time histories.

7.1.1 Identification of Assumed Travel Paths

The assumed travel paths of a wave propagating within a pile are shown schematically on Figure 7-2.

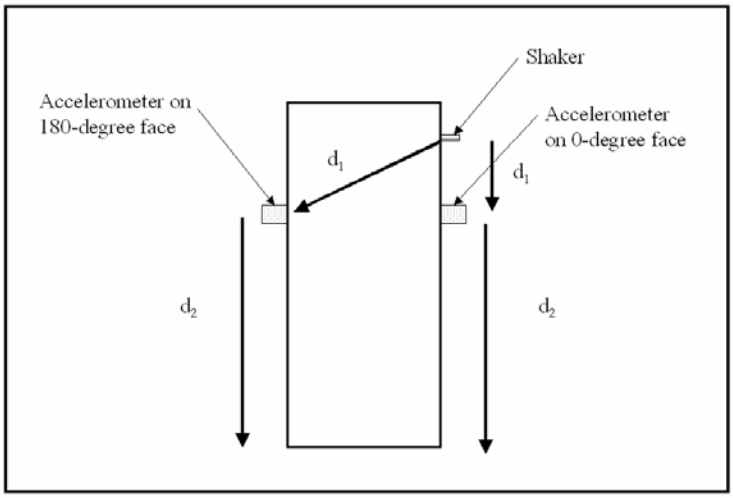

Figure 7-2: Typical travel paths of stress waves for
0-degree and 180-degree orientations

When the accelerometer is mounted in the 0-degree orientation, as defined on Figure 7-1, the component of the wave travels down the pile, passes the accelerometer, reflects off the tip, and travels back up the pile where it passes the accelerometer. The distance d_1 for the 0-degree orientation is vertical distance between the shaker and the accelerometer and the distance d_2 is the vertical distance between the accelerometer and the pile tip. When the accelerometer is mounted in the 180-degree orientation, the component of the wave travels through the pile,

passes the accelerometer, reflects off the tip, and travels back up the pile where it passes the accelerometer. The distance d_1 for the 180-degree orientation is

$$d_1 = \sqrt{(Pile\ diamter)^2 + (d_1\ \ for\ 0°\ \ face)^2} \qquad (7\text{-}1)$$

The distance d_2 is the vertical distance between the accelerometer and the pile tip.

7.1.2. Embedded Pile Geometry and Calculation of Travel Distances

The prototype piles evaluated nondestructively under embedded conditions are identified by their diameter and length in mm. The conditions under which the prototype piles were evaluated, including the location of the shaker and the location of the accelerometers, are presented on Figure 7-3.

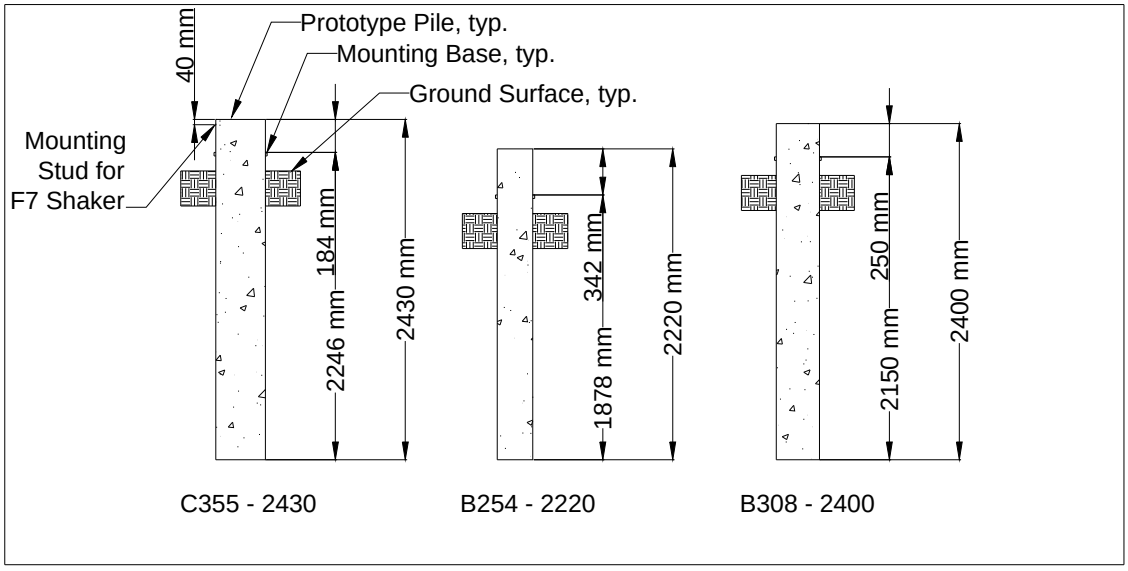

Figure 7-3: Prototype piles under embedded conditions

The piles were cast and cured prior to installation into the very loose fill sands at the NGES. They were installed by digging an excavation, placing the pile into the excavation, and backfilling the excavation. The depth of excavation was selected so that the top of the pile would be flush with the ground surface, except for prototype pile B254-2220 which stuck up about 100 mm above the ground surface after installation. To perform the tests, the sand around each prototype pile was excavated to depths of about 300 mm to 450 mm below the top of the pile, to allow the accelerometer mounting bases to be installed on the pile, leaving 115 mm ± 5 mm to attach the accelerometer to the mounting base.

The distances for each prototype pile corresponding to the assumed travel paths on Figure 7-2 and dimensions on Figure 7-3 are presented on Table 7-1.

Table 7-1: Distances between measurement points for embedded prototype piles

Combination of measurement points	Distance (mm)					
	C355-2430		B254-2220		B308-2400	
	0-degree	180-degree	0-degree	180-degree	0-degree	180-degree
Shaker – accelerometer	144	384	302	466	210	370
Accelerometer – pile tip	2246	2246	1878	1878	2150	2150

The travel distances have been calculated for the return of the first reflection, the second pass, and the return of the second reflection, and have been computed for the 0-degree and 180-degree orientations using the start of the wave at the shaker and the first pass of the wave at the accelerometer. The procedure used to compute the travel distances was presented in Section 6.3, and, as such, only the assumed travel paths and corresponding distances are presented on Table 7-2.

Table 7-2: Calculated travel distances for first pass and reflection for embedded prototype piles

Combination of peaks	Distance (mm)					
	C355-2430		B254-2220		B308-2400	
	0-degree	180-degree	0-degree	180-degree	0-degree	180-degree
First pass of accelerometer and return of reflected wave to accelerometer	4492	4492	3756	3756	4300	4300
First pass of accelerometer and second pass of accelerometer	4860	4860	4440	4440	4800	4800
First pass of accelerometer and return of second reflection to accelerometer	9352	9352	8196	8196	9100	9100
Start of wave at shaker and return of reflected wave to accelerometer	4636	4876	4058	4222	4510	4670
Start of wave at shaker and second pass of accelerometer	5004	5244	4742	4908	5010	5170
Start of wave at shaker and return of second reflection to accelerometer	9496	9736	8498	8662	9310	9470

7.1.3 Calculation of Group Velocity and Attenuation Coefficient

Each prototype pile was tested with one shaker and one triaxial accelerometer mounted on the side of the pile, as shown on Figure 7-1. The results are analyzed to determine the group velocity and attenuation coefficient.

The group velocities were computed with the general procedures presented in Section 3.4.3, for the combinations of first pass and return of the reflected wave listed on Table 7-2. In general, the group velocity, c_g, is calculated by

$$c_g = \frac{\Delta L}{\Delta t} \qquad (7\text{-}2)$$

where ΔL is the travel distance and Δt is the travel time. The travel distance will be different depending on the pair of wave groups from which the group velocity is calculated and the orientation at which the test is performed.

The attenuation coefficient, ϑ, is calculated from the ratio of the amplitude of the reflected wave to the amplitude of the incident wave as

$$\vartheta = \ln\left(\frac{u_2}{u_1}\right) \qquad (7\text{-}3)$$

where u_2 and u_1 are the amplitudes of the reflected and incident waves, respectively. The experimental value of attenuation coefficient per unit length, $\vartheta/\Delta L$ is

$$\vartheta / \Delta L = \ln\left(\frac{u_2}{u_1}\right) / \Delta L \qquad (7\text{-}4)$$

The theoretical background for the calculation of attenuation was presented in Section 2.3.7 and sample calculations were presented for hypothetical piles under embedded conditions in Section 3.4.4.

7.2 Theoretical Solutions

The experimental results, analyzed by the procedures presented in Section 7.1, are compared to the theoretical results which are developed by the procedures presented in Sections 2.3 and 4.3. The procedure followed herein is

1. Determine the soil properties
   a. Shear wave velocity, c_{Ts}
   b. Poisson's ratio, ν_s
   c. Density, ρ_s
2. Characterize the pile by the SE method to determine
   a. Bar wave velocity, c_B
   b. Shear wave velocity, c_{Tc}
   c. Poisson's ratio, ν_c
   d. Density, ρ_c
3. Compute the nondimensional ratios of concrete properties to soil properties
   a. Shear modulus ratio, *M*
   b. Density ratio, *r*
4. Develop the numerical solution to the frequency equation presented in Section 2.3.2.
   a. Determine the nondimensional frequency – nondimensional wavenumber relationship by the procedures presented in Section 2.3.4.

b. Compute the nondimensional group velocity – nondimensional frequency relationship by the procedures presented in section 2.3.6 and convert to dimensional form by the procedures presented in Section 4.3.

5. Select the test frequency, *f*.
6. Analyze the test frequency in nondimensional form.
   a. Compute the nondimensional frequency, Ω, by

$$\Omega = \frac{2\pi f a}{c_{T_c}} \qquad (7\text{-}6)$$

   where *a* is the pile radius
   b. Compute the nondimensional wavenumber at the nondimensional test frequency by the procedure presented in Section 2.3.4.
   c. Compute the attenuation coefficient per unit length, ϑ/ΔL, by

$$\vartheta / \Delta L = \frac{-\mathrm{Im}(\xi_a)}{a} \qquad (7\text{-}7)$$

   where Im(ξ_a) is the imaginary part of the nondimensional wavenumber, ΔL is the travel distance and *a* is the pile radius.
   d. Compute the normalized displacements by the procedures presented in Section 2.3.8.

The soil and concrete properties needed to solve the frequency equation are summarized on Table 7-3. A detailed discussion of the soil properties needed to solve the frequency equation was presented in Section 2.2, and a detailed discussion of the pile properties needed to solve the frequency equation was presented in Section 5.3.1.

Table 7-3: Summary of input properties for generation of nondimensional dispersion curves

Property	Prototype pile designation		
	C355-2430	B254-2220	B308-2400
ν_s	0.30	0.30	0.30
ν_c	0.20	0.18	0.28
M	825	1125	1025
r	1.5	1.5	1.5

The development of the theoretical nondimensional group velocity – nondimensional frequency curves and calculation of the normalized displacements were applied to prototype pile C355-2430 as part of the verification of the flexural guided wave theory by the controlled frequency method in Chapter 6, and, as such, details pertaining to the development of those relationships will not be repeated.

The concrete shear wave velocity, c_{Tc}, and the pile radius, *a*, which are required to convert the frequency, group velocity, and attenuation coefficient from nondimensional form to dimensional form are summarized on Table 7-4.

Table 7-4: Summary of input properties required to convert from nondimensional to dimensional form

Property	Prototype pile designation		
	C355-2430	B254-2220	B308-2400
c_{Tc} (m/s)	2530	2730	2780
a (mm)	177.5	118	154

7.3 Results for Prototype Pile C355-2430

Prototype pile C355-2430 has been embedded in the very loose fill sands at the NGES at Northwestern Univeristy, and evaluated nondestructively using the controlled frequency method. Tests were performed at several frequencies and those test results were evaluated by the criteria in Section 6.2 to identify useable test frequencies. As with the controlled frequency tests

performed on this prototype pile under traction-free conditions, a central frequency of 14000 Hz was the only frequency that produced consistently useable results. The test results were filtered with a bandpass Butterworth filter of order 6, with a low cutoff frequency of 2000 Hz and a high cutoff frequency of 20000 Hz.

The controlled frequency tests performed at a central frequency of 14000 Hz could potentially excite modes on the first five flexural branches based on the cutoff frequencies presented in Section 5.3.1. The actual branches on which modes were excited in a test are identified by considering the group velocities, attenuation, and normalized displacement of each mode on the various branches at 14000 Hz.

The theoretical group velocity – frequency relationship for the first five flexural branches, as well as the theoretical values of attenuation and normalized displacement value at the test frequency were computed by the procedure presented in Section 7.2, using the values on Tables 7-3 and 7-4. The nondimensional frequency is 6.171, rounded to 4 significant digits, and the corresponding nondimensional wavenumber values for each active flexural branch are presented on Table 7-5.

Table 7-5: Prototype pile C355-2430 embedded in very loose sand, nondimensional wavenumber for the flexural branches at nondimensional frequency of 6.171

Branch	Nondimensional wavenumber	
	Real part	Imaginary part
F(1,1)	6.778	0.1076
F(1,2)	5.878	0.03088
F(1,3)	4.883	0.05701
F(1,4)	3.271	0.05158
F(1,5)	1.143	0.05455

For the 0-degree and 180-degree orientations, the normalized displacements were computed at the outer edge of the pile (R = 1) for the first five flexural branches using the procedures outlined in Section 2.3.8.2. The attenuation coefficients per unit length were computed by equation 7-7. The results are summarized on Table 7-6.

Table 7-6: Prototype pile C355-2430 (embedded), group velocities, attenuation coefficients per unit length & normalized displacement values at R = 1 for flexural branches at 14000 Hz for 0-degree and 180-degree orientations

Branch	Group velocity (m/s)	Attenuation coefficient per unit length (nepers/meter)	Normalized displacement values at R = 1	
			Radial Direction	Longitudinal Direction
F(1,1)	2320	-0.6062	0.26	0.14
F(1,2)	2270	-0.1740	0.04	0.07
F(1,3)	1870	-0.3217	0.13	0.07
F(1,4)	2600	-0.2906	0.03	0.41
F(1,5)	1350	-0.3073	1.27	0.03

Based on the attenuation and the normalized displacements, modes are most likely to be identified on the F(1,1) and F(1,5) branches in the radial direction and on the F(1,1) and F(1,4) branches in the longitudinal direction, but not the F(1,2) or F(1,3) branches for either the radial or longitudinal direction. Furthermore, if modes are excited on more than one branch, the returns of the reflected wave on different branches could be distinctly identified based on the group velocity. The group velocity of the mode on the F(1,1) branch is 1.7 times greater than the group velocity of the mode on the F(1,5) branch, and the group velocity of the mode on the F(1,4) branch is 1.1 times greater than the group velocity of the mode on the F(1,1) branch.

7.3.1 Analysis of Radial Direction Results

The acceleration – time histories for the response measured at the shaker and the radial component of the pile response are shown on Figure 7-4.

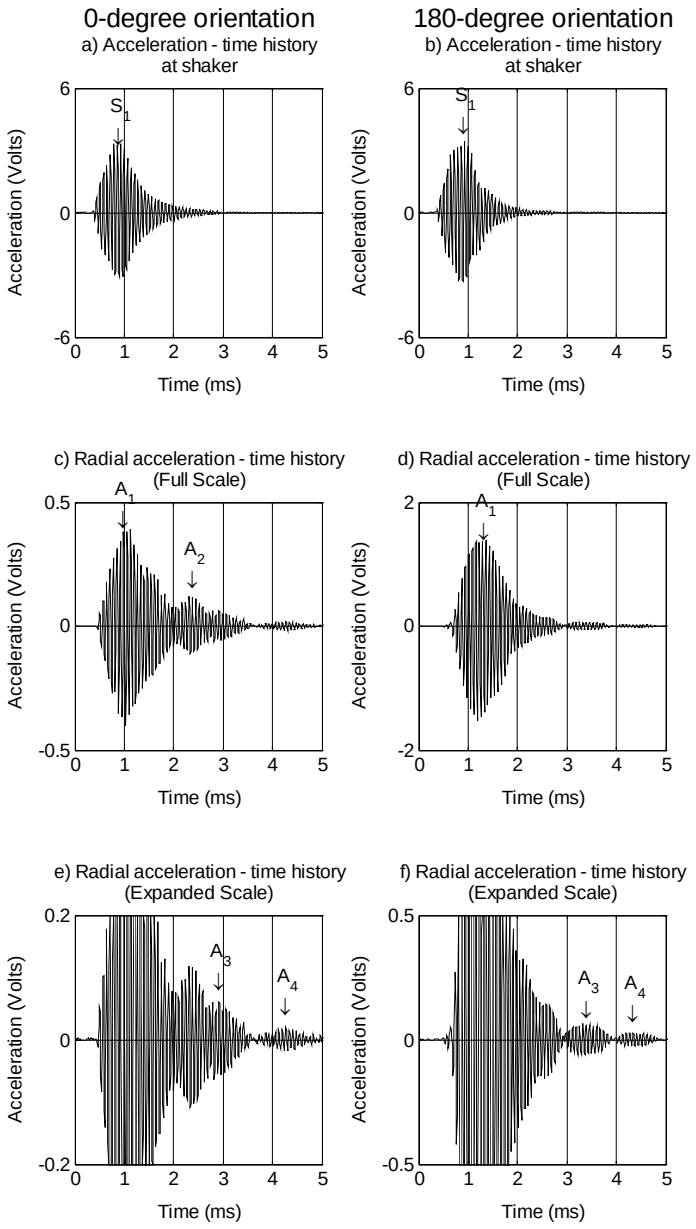

Figure 7-4: Prototype pile C355-2430 (embedded), controlled frequency test results with CF = 14000 Hz, radial acceleration – time histories for 0-degree and 180-degree orientations

The peaks designated S_1 and A_1 represent the start of the wave at the shaker and the first arrival at the triaxial accelerometer. The peaks designated A_2 through A_4 represent possible returns of the reflected wave. The times at which each peak occurred are presented on Table 7-7.

Table 7-7: Prototype Pile C355-2430 (embedded), controlled frequency results with CF = 14000 Hz, peaks in measured responses (radial)

Peak designation	Time at which peak occurred (ms)	
	0-degree orientation	180-degree orientation
S_1	0.93	0.93
A_1	1.06	1.23
A_2	2.31	N/I
A_3	2.92	3.32
A_4	4.27	4.34

N/I Peak not identified

The group velocity values were computed from various combinations of the start of the wave at the shaker, first arrival and return of the reflected wave at the triaxial accelerometer. The group velocity is computed from equation 7-2 using the assumed travel paths defined on Figure 7-2, the computed travel distances presented on Tables 7-3 and 7-4, and the recorded time values presented on Table 7-7. The calculated group velocities for selected peaks are presented on Table 7-8.

Table 7-8: Prototype pile C355-2430 (embedded), controlled frequency results with CF = 14000 Hz, group velocity values for reflected wave (radial)

Orientation	Combination of peaks	Expected travel path	Travel distance, ΔL (mm)	Travel time Δt (ms)	Group velocity (m/s)	Branch
0-degree	$A_3 - A_1$	First reflection	4492	1.86	2420	F(1,1)
	$A_3 - S_1$		4636	1.99	2330	
	$A_4 - A_1$	First reflection	4492	3.21	1400	F(1,5)
	$A_4 - S_1$		4636	3.34	1390	
180-degree	$A_3 - A_1$	First reflection	4492	2.09	2150	F(1,1)
	$A_3 - S_1$		4876	2.39	2040	
	$A_4 - A_1$	First reflection	4492	3.11	1440	F(1,5)
	$A_4 - S_1$		4876	3.41	1430	

Notes: F(1,1) theoretical group velocity is 2320 m/s
F(1,5) theoretical group velocity is 1350 m/s

Based on group velocity, modes were identified on the F(1,1) and F(1,5) branches, which are the branches with the largest normalized displacement values of the branches on which modes may be excited. For the mode on the F(1,1) branch, the group velocity values range from 2040 to 2420 m/s with an average value of 2240 m/s and a standard deviation of 170 m/s or 7.6 % of the average value. For the mode on the F(1,5) branch, the group velocity values range from 1390 to 1440 m/s with an average value of 1420 m/s and a standard deviation of 20 m/s or 1.4 % of the average value.

The attenuation coefficient per unit length presented on Table 7-6 cannot be evaluated directly because Peak A_1 contains modes attributed to both the F(1,1) and F(1,5) branches, but the return of the reflected wave on each branch occurs at different times. Conceptually, attenuation can be discussed in that the returns of the reflected wave have amplitudes that are much smaller than the amplitude of the incident wave.

Peak A_2 in the 0-degree orientation, could not be attributed to either the F(1,1) branch or the F(1,5) branch and a corresponding peak is not present in the 180-degree orientation, all of which suggest peak A_2 in the 0-degree orientation is a spurious response.

7.3.2 Analysis of Longitudinal Direction Results

The acceleration – time histories for the response measured at the shaker and the longitudinal component of the pile response are shown on Figure 7-5.

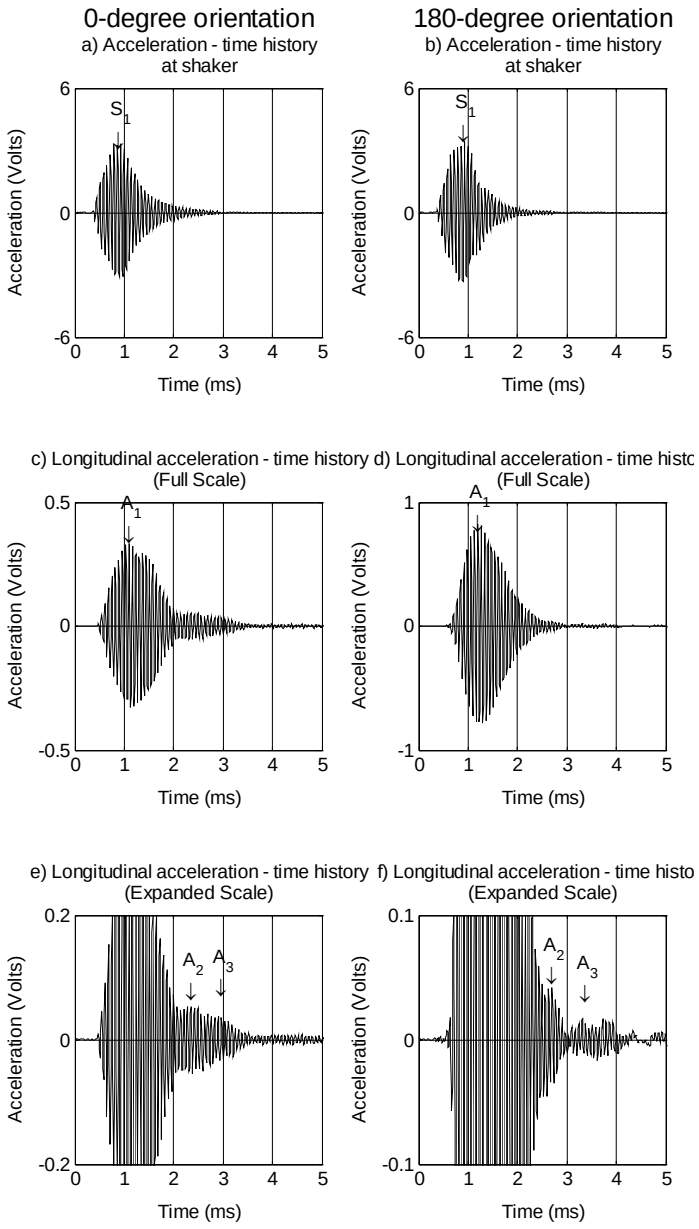

Figure 7-5: Prototype pile C355-2430 (embedded), controlled frequency test results with CF = 14000 Hz, longitudinal acceleration – time histories for 0-degree and 180-degree orientations

The peaks designated S_1 and A_1 represent the start of the wave at the shaker and the first arrival at the triaxial accelerometer, respectively. The peaks designated A_2 through A_4 represent possible returns of the reflected wave. The times at which each peak occurred are presented on Table 7-9.

Table 7-9: Prototype Pile C355-2430 (embedded), controlled frequency results with CF = 14000 Hz, peaks in measured responses (longitudinal)

Peak designation	Time at which peak occurred (ms)	
	0-degree orientation	180-degree orientation
S_1	0.93	0.93
A_1	1.10	1.20
A_2	2.49	2.70
A_3	2.90	3.30

N/I Peak not identified

The group velocity values were computed from various combinations of the start of the wave at the shaker, first arrival and return of the reflected wave at the triaxial accelerometer. The group velocity is computed from equation 7-2 using the assumed travel paths defined on Figure 7-2, the computed travel distances presented on Tables 7-3 and 7-4, and the recorded time values presented on Table 7-9. The calculated group velocities for selected peaks are presented on Table 7-10.

Table 7-10: Prototype pile C355-2430 (embedded), controlled frequency results with CF = 14000 Hz, group velocity values for reflected wave (radial)

Orientation	Combination of peaks	Expected travel path	Travel distance, ΔL (mm)	Travel time Δt (ms)	Group velocity (m/s)	Branch
0-degree	$A_3 - A_1$	First reflection	4492	1.80	2500	F(1,1)
	$A_3 - S_1$		4636	1.97	2350	
180-degree	$A_3 - A_1$	First reflection	4492	2.10	2140	F(1,1)
	$A_3 - S_1$		4636	2.37	1960	

Notes: F(1,1) theoretical group velocity is 2320 m/s

The group velocity values range from 1960 to 2500 m/s with an average value of 2240 m/s and a standard deviation of 240 m/s or 10.7 % of the average value. The mode on the F(1,4) branch has the largest normalized displacement, but the experimental group velocity more closely matches the theoretical group velocity for the F(1,1) branch of 2320 m/s than the theoretical group velocity of the F(1,4) branch of 2600 m/s. Based on group velocity, the mode is attributed to the F(1,1) branch, which is the branch with the second largest normalized displacement magnitude of the modest that may be excited at the central frequency.

The attenuation coefficient per unit length can be computed from peaks A_1 and A_3 in both the 0-degree and 180-degree orientations because the peaks were attributed to the first pass and first return of the reflected wave of the mode on only one branch. The acceleration amplitudes, in Volts, of peaks A_1 and A_3 are presented on Table 7-11.

Table 7-11: Prototype pile C355-2430 (embedded), controlled frequency results for CF = 14000 Hz, peak Voltage value of select wave groups (longitudinal)

Peak	Acceleration at peak (Volts)	
	0-degree	180-degree
A_1	0.334	0.823
A_3	0.0380	0.0167

Peaks A_1 and A_3 represent u_1 and u_2, respectively in equation 7-4, and the travel distance, ΔL, in equation 7-4 is determined from Table 7-2 based on the assumed travel path. Peak A_3 was attributed to the first return of a reflected wave, for which ΔL is 4492 mm. The attenuation coefficients per unit length, in nepers/meter, computed by substituting the values from Table 7-11 and ΔL of 4492 mm into equation 7-4, are presented on Table 7-12.

Table 7-12: Prototype pile C355-2430 (embedded), controlled frequency results for CF = 14000 Hz, calculated attenuation coefficients (longitudinal)

Orientation	Attenuation coefficient per unit length (nepers/meter)
0-degree	-0.4839
180-degree	-0.8677

The average of the values presented on Table 7-12 is –0.6758, compared to the theoretical value of –0.6062 for the mode on the F(1,1) branch presented on Table 7-6.

The mode identified from the analysis of Peak A_3 is attributed to the F(1,1) branch based on group velocity, attenuation, and normalized displacement. Peaks A_2 on the 0-degree

orientation, could not be attributed to the F(1,1) branch, nor could peaks A_2 on the 180-degree orientation, suggesting they are spurious responses.

7.3.3 Comparison of Radial and Longitudinal Results

The analysis of the controlled frequency results indicate that a flexural wave is induced in the pile, and that a mode on the F(1,1) branch was excited for both the radial and longitudinal components and that a mode on the F(1,5) branch was also excited in the radial component.

The group velocity values determined from the analysis of the test results presented in the text of Sections 7.2.1 and 7.2.2, can be presented graphically by superimposing the group velocity – frequency data on the numerically-determined group velocity curves developed by the procedures in Sections 2.3 and 4.3, or by the mode identification method described in Section 3.5.2. The group velocity values calculated from the test results are summarized on Table 7-13.

Table 7-13: Prototype pile C355-2430 (embedded), controlled frequency results for CF = 14000 Hz, summary of group velocity values

Direction	Branch	Group velocity (m/s)		Attenuation coefficient per unit length (nepers/m)
		Average	Standard deviation	
Radial	F(1,1)	2240	170	N/I
	F(1,5)	1420	20	N/I
Longitudinal	F(1,1)	2500	200	-0.6758

Notes: N/I indicates that the quantity could not be computed.

The values presented on Table 7-13 are superimposed on the numerically-determined group velocity – frequency curve on Figure 7-6.

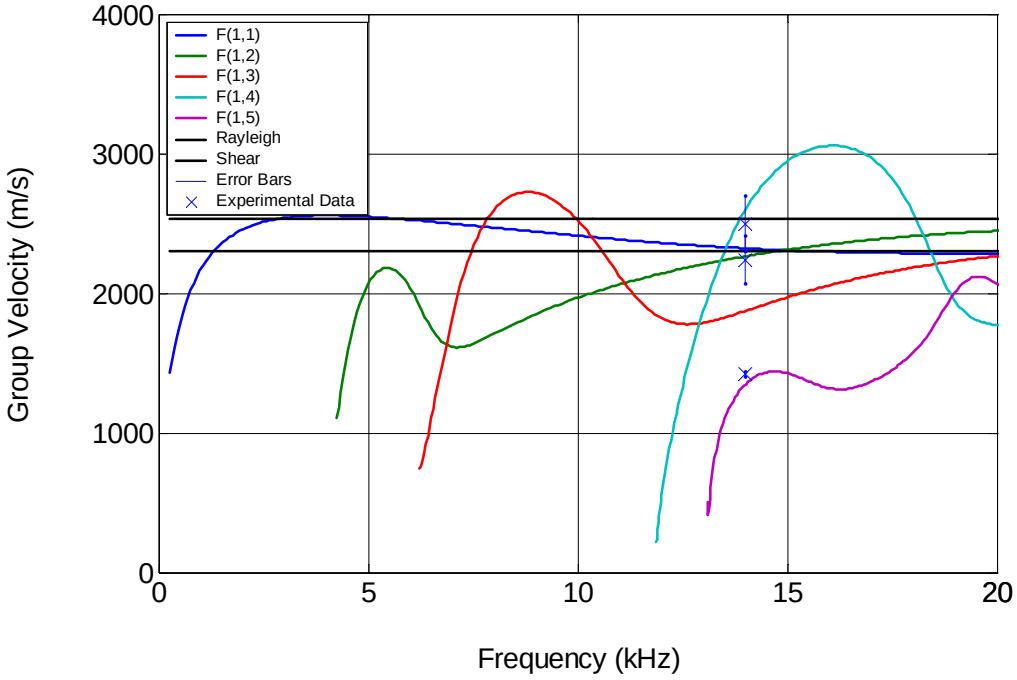

Figure 7-6: Prototype pile C355-2430 (embedded), controlled frequency results with CF = 14000 Hz, superimposed on numerically-determined group velocity – frequency curves of first five flexural branches for concrete with $\nu_c = 0.20$

The two data points corresponding to modes attributed to the F(1,1) branch are near the theoretical group velocity for the F(1,1) branch; however, given the uncertainty in the data and the range of theoretical group velocity values for the first four flexural branches, the experimental data crosses all four group velocity – frequency curves. The modes on the F(1,2) and F(1,3) branch have small normalized displacement values for both the radial and longitudinal components, and the F(1,4) branch has a small normalized displacement value for the radial

component, which strengthens the conclusion that the excited mode lies on the F(1,1) branch. Also, the controlled frequency results presented in Chapter 6 indicated that modes were excited on the F(1,1) branch.

The results of the radial response for the 180-degree orientation analyzed by the mode identification method described in Section 3.5.2 are presented on Figures 7-7 and 7-8, with modifications of the data to isolate returns of the reflected wave. The joint velocity frequency curve was generated using the start of the wave at the shaker and the return of the first reflection. The start of the wave at the shaker occurs at 0.93 ms, as presented on Table 7-7, and the travel length for the wave is 4876 mm, as presented on Table 7-2. The wave groups corresponding to the returns of the reflected wave were isolated by multiplying the acceleration – time history of the pile response by a rectangular window. The rectangular window is defined such that its value is zero prior to the start of the wave group corresponding to the return of the reflected wave and one after the start of the wave group corresponding to the return of the reflected wave. The windowing was applied to the pile response because the first pass of the wave is so much larger than the return of the reflected wave that joint time frequency analysis of the entire signal would be dominated by the first pass and the returns would not be identifiable.

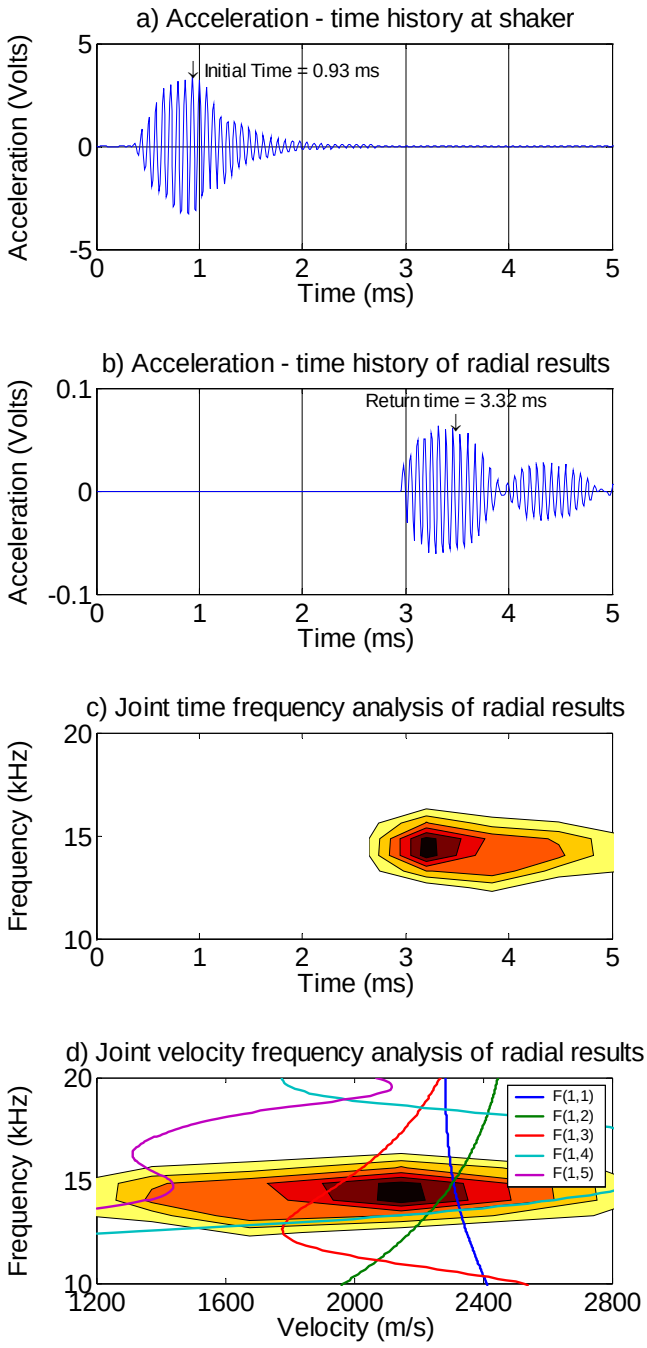

Figure 7-7: Prototype pile C355-2430 (embedded), controlled frequency results for CF = 14000 Hz, 180-degree orientation, radial direction mode identification method to identify first return of mode on F(1,1) branch

The largest contour on the joint velocity frequency analysis curve, shown on Figure 7-7d falls between the group velocity – frequency curve for the F(1,1) and F(1,3) branches and is close to the group velocity – frequency curve for the F(1,2) branch. The mode on the F(1,1) branch has a larger normalized displacement than the modes on the F(1,2) and F(1,3) branches. The results of the mode identification method indicate that the analyzed wave group corresponds to the return of the reflected wave on the F(1,1) branch, which is consistent with the results of the conventional time – frequency analysis presented on Figure 7-6.

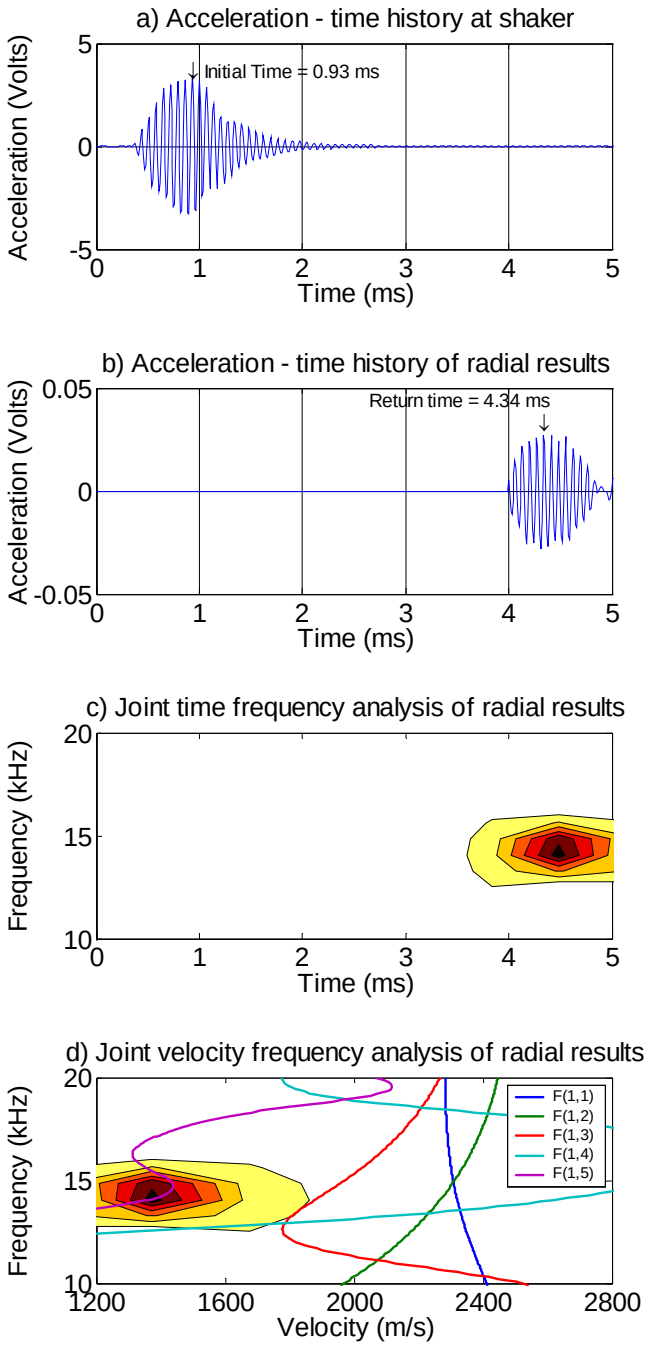

Figure 7-8: Prototype pile C355-2430 (embedded), controlled frequency results for CF = 14000 Hz, 180-degree orientation, radial direction mode identification method to identify first return of mode on F(1,5) branch

The largest contour on the joint velocity frequency analysis curve, shown on Figure 7-8d crosses the group velocity – frequency curve the F(1,5) branch. . The results of the mode identification method are consistent with the conventional time – frequency analysis for which results were presented on Figure 7-7.

7.4 Results for Prototype Pile B254-2220

Prototype pile B254-2220 has been embedded in the very loose fill sands at the NGES at Northwestern Univeristy, and evaluated nondestructively using the controlled frequency method. Tests were performed at several frequencies and those test results were evaluated by the criteria in Section 6.2 to identify useable test frequencies. Results are presented for controlled frequency tests performed at a central frequency of 14000 Hz, which was the only frequency that produced consistently useable results. The test results were filtered with a bandpass Butterworth filter of order 6, with a low cutoff frequency of 2000 Hz and a high cutoff frequency of 20000 Hz.

The controlled frequency tests performed at a central frequency of 14000 Hz could potentially excite modes on the first three flexural branches based on the cutoff frequencies presented in Section 5.3.1. The actual branches on which modes were excited in a test are identified by considering the group velocities, attenuation, and normalized displacement of each mode on the various branches at 14000 Hz.

The theoretical group velocity – frequency relationship for the first three flexural branches, as well as the theoretical values of attenuation and normalized displacement value at the test frequency were computed by the procedure presented in Section 7.2, using the values on Tables 7-3 and 7-4. The nondimensional frequency is 4.092, rounded to 4 significant digits, and the corresponding nondimensional wavenumber values for each active flexural branch are presented on Table 7-14.

Table 7-14: Prototype pile B254-2220 embedded in very loose sand, nondimensional wavenumber for the flexural branches at nondimensional frequency of 4.092

Branch	Nondimensional wavenumber	
	Real part	Imaginary part
F(1,1)	4.578	0.07361
F(1,2)	3.382	0.02773
F(1,3)	2.308	0.04271

For the 0-degree and 180-degree orientations, the normalized displacements were computed at the outer edge of the pile (R = 1) for the first three flexural branches using the procedures outlined in Section 2.3.8.2. The attenuation coefficients per unit length were computed by equation 7-7. The results are summarized on Table 7-15.

Table 7-15: Prototype pile B254-2220 (embedded), group velocities, attenuation coefficients per unit length & normalized displacement values at R = 1 for flexural branches at 14000 Hz for 0-degree and 180-degree orientations

Branch	Group velocity (m/s)	Attenuation coefficient per unit length (nepers/meter)	Normalized displacement values at R = 1	
			Radial Direction	Longitudinal Direction
F(1,1)	2610	-0.5796	0.39	0.23
F(1,2)	2030	-0.2183	0.17	0.08
F(1,3)	2940	-0.3363	0.08	0.20

Based on the attenuation and the normalized displacements, modes are most likely to be identified on the F(1,1) and F(1,2) branches in the radial direction and on the F(1,1) and F(1,3) branches in the longitudinal direction. Furthermore, if modes are excited on more than one branch, the returns of the reflected wave on different branches could be distinctly identified based on the group velocity. The group velocity of the mode on the F(1,1) branch is 1.29 times greater than the group velocity of the mode on the F(1,2) branch, and the group velocity of the mode on the F(1,3) branch is 1.13 times greater than the group velocity of the mode on the F(1,1) branch.

7.4.1 Analysis of Radial Direction Results

The acceleration – time histories for the response measured at the shaker and the radial component of the pile response are shown on Figure 7-9.

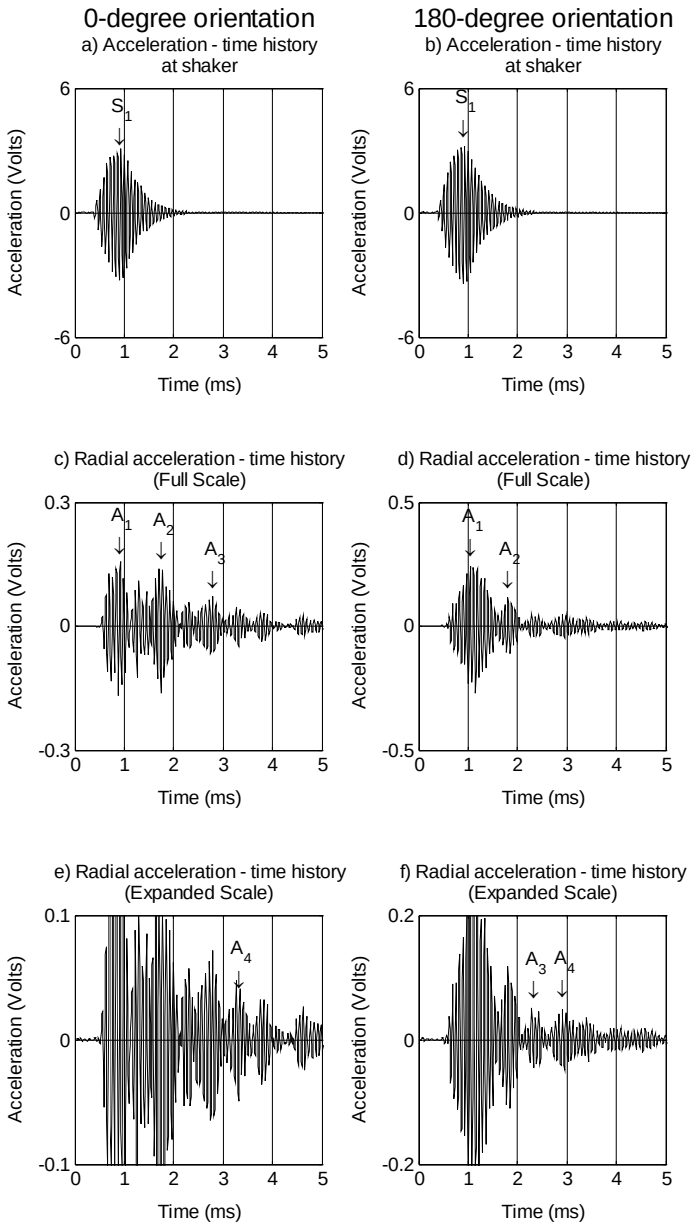

Figure 7-9: Prototype pile B254-2220 (embedded), controlled frequency test results with CF = 14000 Hz, radial acceleration – time histories for 0-degree and 180-degree orientations

The peaks designated S_1 and A_1 represent the start of the wave at the shaker and the first arrival at the triaxial accelerometer. The peaks designated A_2 through A_5 represent possible returns of the reflected wave. The times at which each peak occurred are presented on Table 7-16.

Table 7-16: Prototype Pile B254-2220 (embedded), controlled frequency results with CF = 14000 Hz, peaks in measured responses (radial)

Peak designation	Time at which peak occurred (ms)	
	0-degree orientation	180-degree orientation
S_1	0.86	0.93
A_1	0.92	1.11
A_2	1.71	1.81
A_3	N/I	2.35
A_4	2.79	2.91
A_5	3.27	3.39

N/I Peak not identified

The group velocity is computed from equation 7-2 using the assumed travel paths defined on Figure 7-2, the computed travel distances presented on Tables 7-3 and 7-4, and the recorded time values presented on Table 7-16. The calculated group velocities for selected peaks are presented on Table 7-17.

Table 7-17: Prototype pile B254-2220 (embedded), controlled frequency results with CF = 14000 Hz, group velocity values for reflected wave (radial)

Orientation	Combination of peaks	Expected travel path	Travel distance, *L* (mm)	Travel time Δt (ms)	Group velocity (m/s)	Branch
0-degree	$A_4 - A_1$	First reflection	3756	1.87	2010	F(1,2)
	$A_4 - S_1$		4058	1.92	2110	
	$A_5 - A_1$	Second pass	4440	2.36	1880	F(1,2)
	$A_5 - S_1$		4742	2.41	1970	
180-degree	$A_4 - A_1$	First reflection	3756	1.80	2090	F(1,2)
	$A_4 - S_1$		4222	2.05	2060	
	$A_5 - A_1$	Second pass	4440	2.28	1950	F(1,2)
	$A_5 - S_1$		4908	2.46	2000	

Notes: F(1,2) theoretical group velocity is 2010 m/s

Based on group velocity, modes were identified on the F(1,2) branch, which is the branch with the second largest normalized displacement values and lowest attenuation coefficient per unit length of the branches on which modes may be excited. The group velocity values range from 1880 to 2110 m/s with an average value of 2010 m/s and a standard deviation of 80 m/s or 4.0 % of the average value. The theoretical group velocity for the F(1,2) branch is 2030 m/s.

The attenuation coefficient presented on Table 7-15 can be evaluated from the analysis of peaks A_1 and A_4 in both the 0-degree and 180-degree orientations because the peaks attributed to the first pass and first return of the reflected wave were attributed to the a mode on only one branch. The acceleration amplitudes in volts of peaks A_1 and A_3 are presented on Table 7-18.

Table 7-18: Prototype pile B254-2220 (embedded), controlled frequency results for CF = 14000 Hz, peak voltage value of select wave groups (longitudinal)

Peak	Acceleration at peak (Volts)	
	0-degree	180-degree
A_1	0.1566	0.2458
A_4	0.04730	0.04748

The attenuation coefficients per unit length, in nepers/meter, presented on Table 7-19 were computed by Equation 7-4 using the acceleration values, in Volts, of Peaks A_1 and A_4 on Table 7-18, and a travel distance, ΔL, of 3756 mm. The travel distance is based on the assumed travel path on Table 7-17 and the distances on Table 7-2.

Table 7-19: Prototype pile B254-2220 (embedded), controlled frequency results for CF = 14000 Hz, calculated attenuation coefficients (radial)

Orientation	Attenuation coefficient per unit length (nepers/meter)
0-degree	-0.3187
180-degree	-0.4378

The average of the values presented on Table 7-19 is –0.6758, compared to the theoretical value of –0.2183 for the mode on the F(1,2) branch presented on Table 7-15. The experimental and theoretical values of attenuation do not compare very well; however, the amplitude of the reflected wave is much smaller than the amplitude of the incident wave. Some possible explanations of the poor match between the experimental and theoretical results are

- Uncertainties in the measurement of the acceleration values
- Uncertainties in the measurement of the input parameters required to develop the theoretical solution, and
- Limitations of the guided wave theory

The mode identified from the analysis of Peaks A_4 and A_5 is attributed to a mode on the F(1,2) branch. Peak A_2 in the 0-degree orientation and peaks A_2 and A_3 in the 180-degree orientation, could not be attributed to the F(1,2) branch, and a peak in the 0-degree orientation corresponding to peak A_3 in the 180-degree orientation was not identified, suggesting they are spurious responses.

7.4.2 Analysis of Longitudinal Direction Results

The acceleration – time histories for the response measured at the shaker and the longitudinal component of the pile response are shown on Figure 7-10.

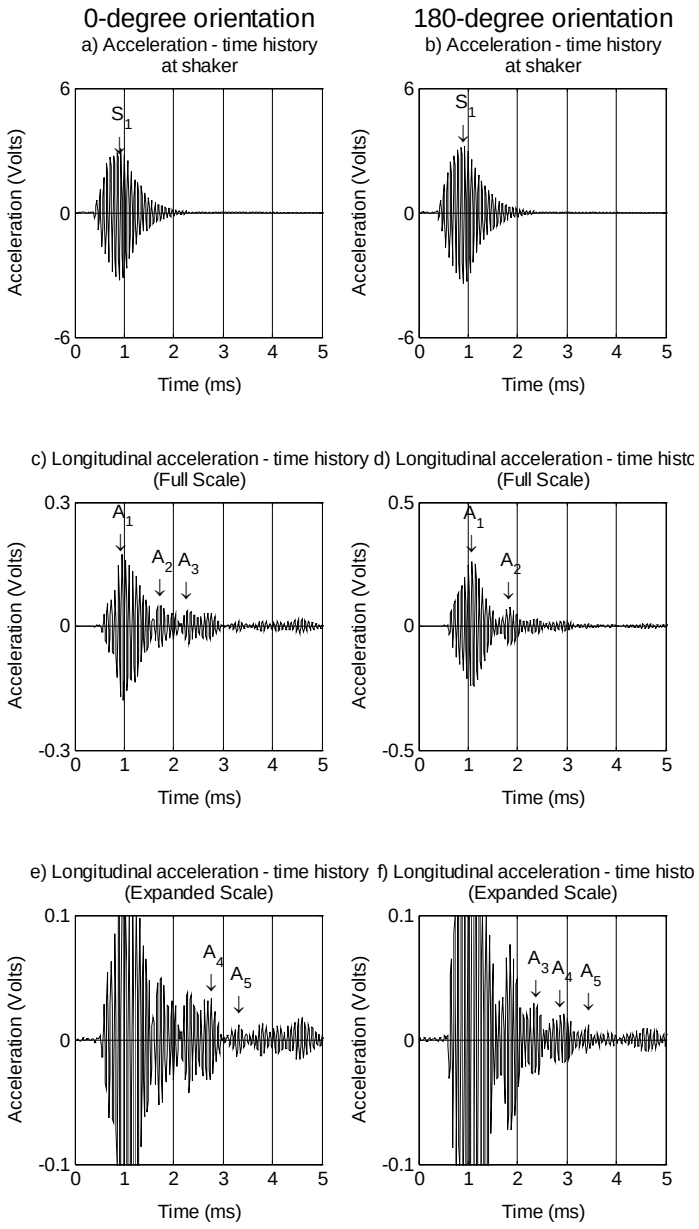

Figure 7-10: Prototype pile B254-2220 (embedded), controlled frequency test results with CF = 14000 Hz, longitudinal acceleration – time histories for 0-degree and 180-degree orientations

The peaks designated S_1 and A_1 represent the start of the wave at the shaker and the first arrival at the triaxial accelerometer, respectively. The peaks designated A_2 through A_4 represent possible returns of the reflected wave. The times at which each peak occurred are presented on Table 7-20.

Table 7-20: Prototype Pile B254-2220 (embedded), controlled frequency results with CF = 14000 Hz, peaks in measured responses (longitudinal)

Peak designation	Time at which peak occurred (ms)	
	0-degree orientation	180-degree orientation
S_1	0.86	0.93
A_1	0.96	1.08
A_2	1.74	1.85
A_3	2.28	2.33
A_4	2.79	2.87
A_5	3.27	3.37

N/I Peak not identified

The group velocity values were computed from various combinations of the start of the wave at the shaker, first arrival and return of the reflected wave at the triaxial accelerometer. The group velocity is computed from equation 7-2 using the assumed travel paths defined on Figure 7-2, the computed travel distances presented on Tables 7-3 and 7-4, and the recorded time values presented on Table 7-20. The calculated group velocities for selected peaks are presented on Table 7-21.

Table 7-21: Prototype pile B254-2220 (embedded), controlled frequency results with CF = 14000 Hz, group velocity values for reflected wave (longitudinal)

Orientation	Combination of peaks	Expected travel path	Travel distance, L (mm)	Travel time Δt (ms)	Group velocity (m/s)	Branch
0-degree	$A_3 - A_1$	First reflection	3756	1.32	2850	F(1,3)
	$A_3 - S_1$		4058	1.42	2860	
180-degree	$A_3 - A_1$	First reflection	3756	1.25	3000	F(1,3)
	$A_3 - S_1$		4222	1.49	3020	

Notes: F(1,3) theoretical group velocity is 2940 m/s

The group velocity values range from 2850 to 3000 m/s with an average value of 2930 m/s and a standard deviation of 90 m/s or 3.1 % of the average value. The experimentally-determined group velocity most closely matches the theoretical group velocity value for the F(1,3) branch, which is 2940 m/s.

The attenuation coefficient presented on Table 7-15 can be evaluated from the analysis of peaks A_1 and A_3 in both the 0-degree and 180-degree orientations because the peaks attributed to the first pass and first return of the reflected wave were attributed to the a mode on only one branch. The acceleration amplitudes in volts of peaks A_1 and A_3 are presented on Table 7-22.

Table 7-22: Prototype pile B254-2220 (embedded), controlled frequency results for CF = 14000 Hz, peak voltage value of select wave groups (longitudinal)

Peak	Acceleration at peak (Volts)	
	0-degree	180-degree
A_1	0.1748	0.2588
A_3	0.03818	0.02950

The attenuation coefficients per unit length, in nepers/meter, presented on Table 7-23 were computed by Equation 7-4 using the acceleration values, in Volts, of Peaks A_1 and A_4 on Table 7-22, and a travel distance, ΔL, of 3756 mm. The travel distance is based on the assumed travel path on Table 7-17 and the distances on Table 7-2.

Table 7-23: Prototype pile B254-2220 (embedded), controlled frequency results for CF = 14000 Hz, calculated attenuation coefficients (longitudinal)

Orientation	Attenuation coefficient per unit length (nepers/meter)
0-degree	-0.4050
180-degree	-0.5782

The average of the values presented on Table 7-23 is –0.4916, compared to the theoretical value of –0.2183 presented on Table 7-15. The experimental and theoretical values of attenuation do not compare very well for the reasons discussed in Section7.4.1; however, the amplitude of the reflected wave is much smaller than the amplitude of the incident wave.

The mode identified for the experimental results is attributed to the F(1,3) branch based on group velocity and normalized displacement. Peaks A_2 in the 0-degree orientation and 180-degree orientation could not be attributed to the F(1,3) branch, indicating they are spurious responses.

7.4.3 Comparison of Radial and Longitudinal Results

The analysis of the controlled frequency results indicate that a flexural wave is induced in the pile, and that a mode on the F(1,2) branch for the radial component and and that a mode on the F(1,3) branch was excited for the longitudinal component.

The group velocity values determined from the analysis of the test results presented in the text of Sections 7.2.1 and 7.2.2, can be presented graphically by superimposing the group velocity – frequency data on the numerically-determined group velocity curves, which were presented on Figure 7-4, or by the mode identification method described in Section 3.5.2. The group velocity values calculated from the test results are summarized on Table 7-24.

Table 7-24: Prototype pile B254-2220 (embedded), controlled frequency results for CF = 14000 Hz, summary of group velocity values

Direction	Mode	Group velocity (m/s)		Attenuation coefficient per unit length (nepers/m)
		Average	Standard deviation	
Radial	F(1,2)	2010	80	-0.6758
Longitudinal	F(1,3)	2930	90	-0.4916

The values presented on Table 7-24 are superimposed on the numerically-determined group velocity – frequency curve on Figure 7-11.

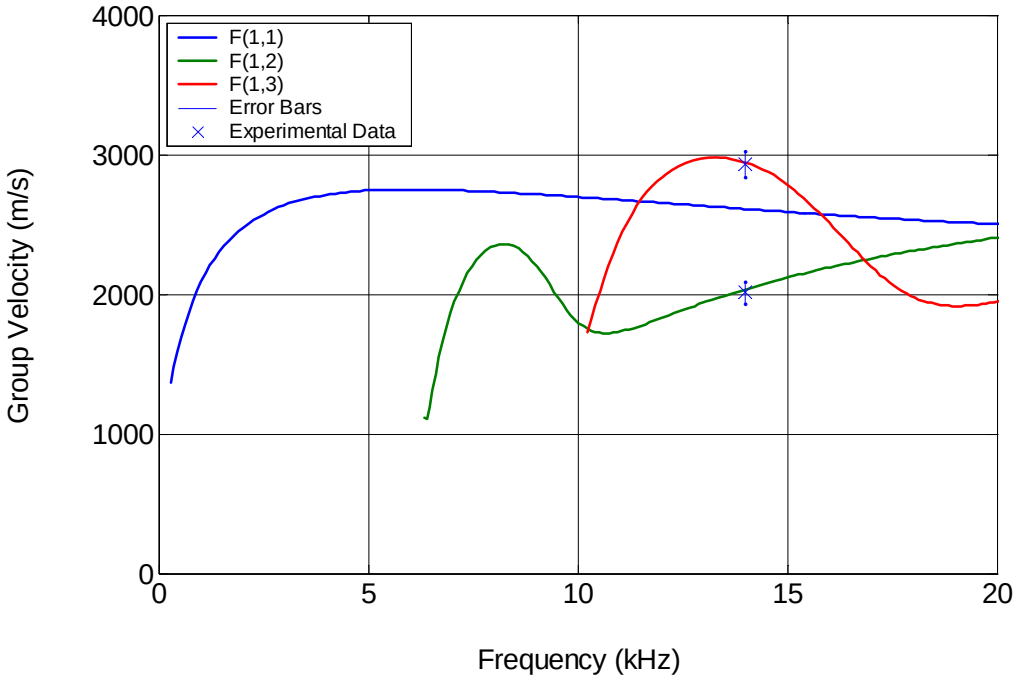

Figure 7-11: Prototype pile B254-2220 (embedded), controlled frequency results with CF = 14000 Hz, superimposed on numerically-determined group velocity – frequency curves of first three flexural branches for concrete with $\nu_c = 0.18$

The results of the radial response for the 180-degree orientation analyzed by the mode identification method described in Section 3.5.2 are presented on Figure 7-12. The joint velocity frequency curve was generated using the start of the wave at the shaker and the return of the first reflection. The start of the wave at the shaker occurs at 0.93 ms, as presented on Table 7-9, and the travel length for the wave is 4876 mm, as presented on Table 7-8.

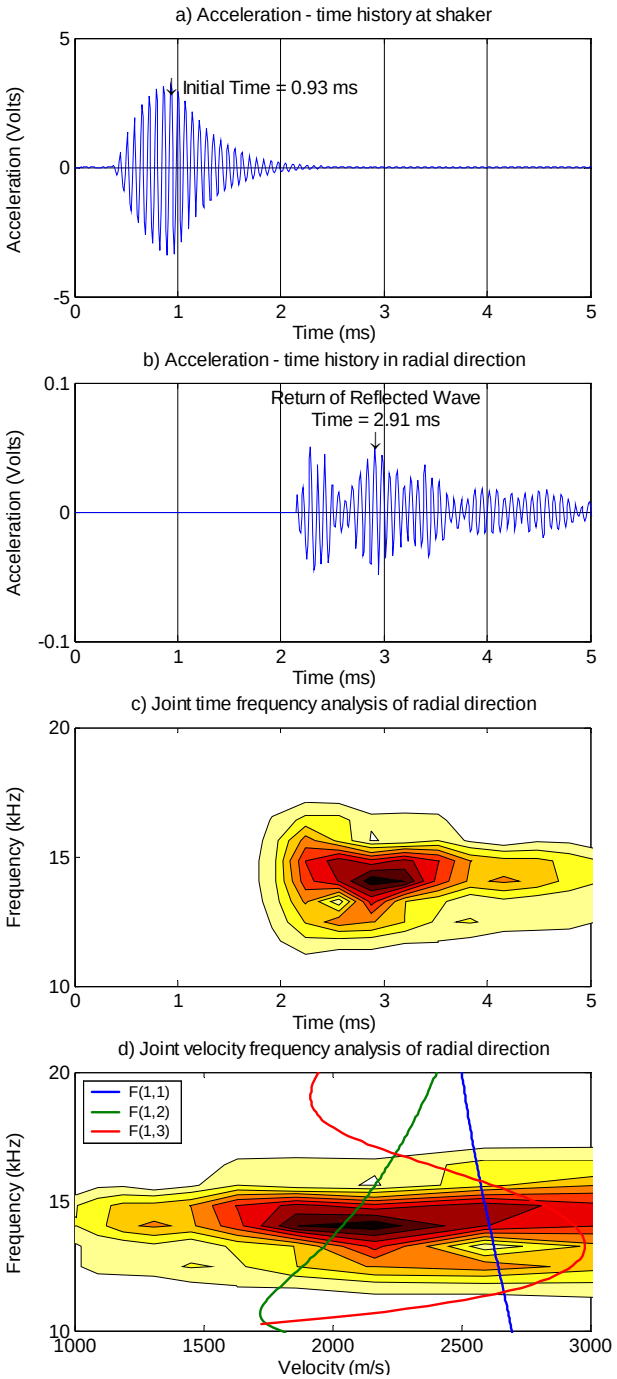

Figure 7-12: Prototype pile B254-2220 (embedded), controlled frequency results for CF = 14000 Hz, 180-degree orientation, radial direction mode identification method

The largest contour on the joint velocity frequency analysis curve, shown on Figure 7-12d crosses the group velocity – frequency curve for the F(1,2) branch, which is consistent with the results the conventional time – frequency analysis presented on Figure 7-11.

7.5 Results for Prototype Pile B308-2400

Prototype pile B308-2400 has been embedded in the very loose fill sands at the NGES at Northwestern Univeristy, and evaluated nondestructively using the controlled frequency method. Tests were performed at several frequencies and those test results were evaluated by the criteria in Section 6.2 to identify useable test frequencies. Results are presented for controlled frequency tests performed at a central frequency of 14000 Hz, which was the only frequency that produced consistently useable results. The test results were filtered with a bandpass Butterworth filter of order 6, with a low cutoff frequency of 2000 Hz and a high cutoff frequency of 20000 Hz.

The controlled frequency tests performed at a central frequency of 14000 Hz could potentially excite modes on the first three flexural branches based on the cutoff frequencies presented in Section 5.3.1. The actual branches on which modes were excited in a test are identified by considering the group velocities, attenuation, and normalized displacement of each mode on the various branches at 14000 Hz.

The theoretical group velocity – frequency relationship for the first three flexural branches, as well as the theoretical values of attenuation and normalized displacement value at the test frequency were computed by the procedure presented in Section 7.2, using the values on Tables 7-3 and 7-4. The nondimensional frequency is 4.873, rounded to 4 significant digits, and the corresponding nondimensional wavenumber values for each active flexural branch are presented on Table 7-25.

Table 7-25: Prototype pile B308-2400 embedded in very loose sand, nondimensional wavenumber for the flexural branches at nondimensional frequency of 4.873

Branch	Nondimensional wavenumber	
	Real part	Imaginary part
F(1,1)	5.300	0.07365
F(1,2)	4.323	0.02614
F(1,3)	3.089	0.05617

For the 0-degree and 180-degree orientations, the normalized displacements were computed at the outer edge of the pile (R = 1) for the first three flexural branches using the procedures outlined in Section 2.3.8.2. The attenuation coefficients were computed by equation 7-7. The results are summarized on Table 7-26.

Table 7-26: Prototype pile B308-2400 (embedded), group velocities, attenuation coefficients & normalized displacement values at R = 1 for flexural branches at 14000 Hz for 0-degree and 180-degree orientations

Branch	Group velocity (m/s)	Attenuation coefficient per unit length (nepers/meter)	Normalized displacement values at R = 1	
			Radial Direction	Longitudinal Direction
F(1,1)	2670	-0.4782	0.36	0.18
F(1,2)	2260	-0.1697	0.13	0.08
F(1,3)	2200	-0.3647	0.14	0.11

Based on the normalized displacements, modes are most likely to be identified on the F(1,1) branch in both the radial direction and the longitudinal direction; however, the mode on the F(1,1) branch has the largest attenuation coefficient per unit length of the active branches.

7.5.1 Analysis of Radial Direction Results

The acceleration – time histories for the response measured at the shaker and the radial component of the pile response are shown on Figure 7-13.

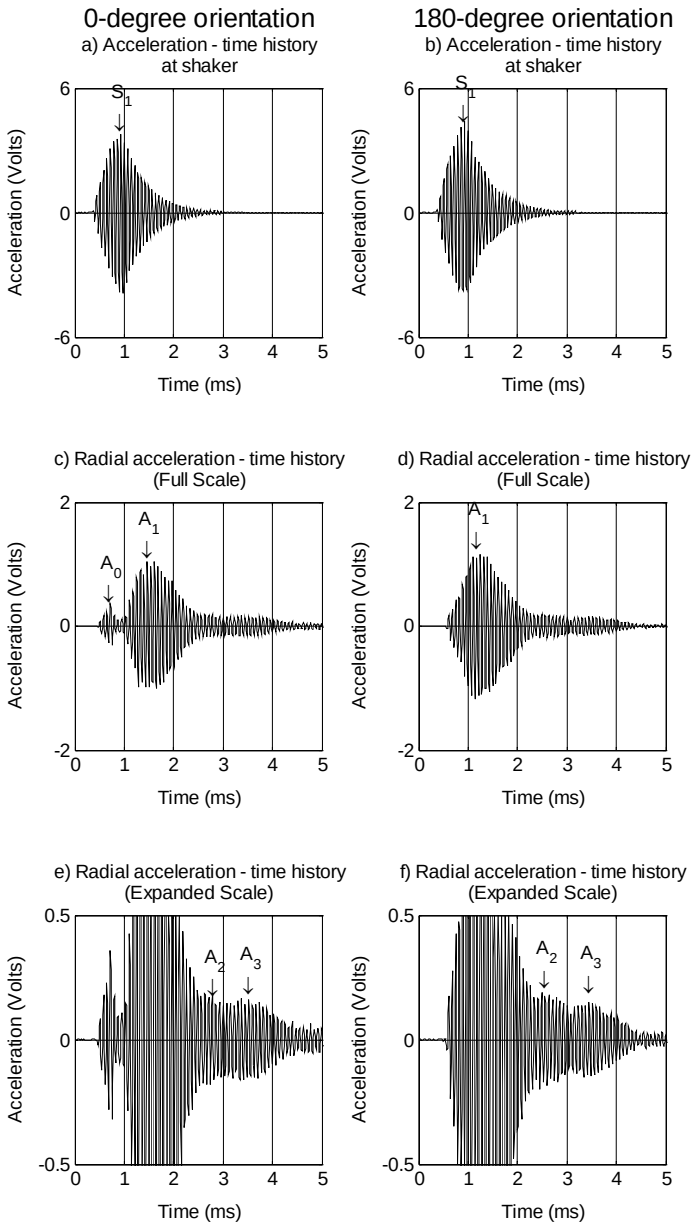

Figure 7-13: Prototype pile B308-2400 (embedded), controlled frequency test results with CF = 14000 Hz, radial acceleration – time histories for 0-degree and 180-degree orientations

The peaks designated S_1 and A_1 represent the start of the wave at the shaker and the first arrival at the triaxial accelerometer. The peak designated A_0 is a spurious peak that occurs in the response of the test performed at the 0-degree orientation prior to the start of the wave at the shaker. The peaks designated A_2 through A_5 represent possible returns of the reflected wave. The times at which each peak occurred are presented on Table 7-27.

Table 7-27: Prototype Pile B308-2400 (embedded), controlled frequency results with CF = 14000 Hz, peaks in measured responses (radial)

Peak designation	Time at which peak occurred (ms)	
	0-degree orientation	180-degree orientation
S_1	0.93	0.93
A_0	0.72	N/I
A_1	1.29	1.15
A_2	2.61	2.46
A_3	3.52	3.52

N/I Peak not identified

The group velocity is computed from equation 7-2 using the assumed travel paths defined on Figure 7-2, the computed travel distances presented on Tables 7-3 and 7-4, and the recorded time values presented on Table 7-27. The calculated group velocities for selected peaks are presented on Table 7-28.

Table 7-28: Prototype pile B308-2400 (embedded), controlled frequency results with CF = 14000 Hz, group velocity values for reflected wave (radial)

Orientation	Combination of peaks	Expected travel path	Travel distance, L (mm)	Travel time Δt (ms)	Group velocity (m/s)	Branch
0-degree	$A_2 - S_1$	First reflection	4510	1.68	2690	F(1,1)
180-degree	$A_2 - S_1$	First reflection	4670	1.53	3050	F(1,1)

Notes: F(1,1) theoretical group velocity is 2670 m/s

The average group velocity value 2870 m/s and a standard deviation of 250 m/s or 8.7 % of the mean value. The experimentally-determined group velocity most closely matches the theoretical group velocity value for the F(1,1) branch, which is 2670 m/s. Based on the normalized displacement values presented on Table 7-26, the mode on the F(1,1) branch has the largest normalized displacement but it also has the highest attenuation.

The calculation of group velocity based on peaks A_1 and A_2 was not consistent with the expected values based on theoretical considerations, nor was is consistent with the values computed from the analysis of peaks S_1 and A_2. Peaks A_1, particularly for the tests performed in the 0-degree orientation, did not fall within a wave group that was as well defined as for the tests performed on the other prototype piles. The controlled frequency tests designed for verification of the longitudinal branches (Chao, 2002) were analyzed using the start of the wave at the shaker and the return of the reflected wave to the accelerometer because the first pass of the accelerometer contained other modes of vibration and the longitudinal wave had not fully developed. The conditions observed on the verification of the longitudinal branches may

contribute to the difficulty in analyzing the data from controlled frequency tests designed to induce a flexural wave.

The attenuation coefficient could not be directly calculated because the first pass of the wave, peak A_1, was not included in the analysis. It can be observed, however, that the amplitude of the reflected wave, peak A_2, is smaller than the amplitude of the first pass.

The mode identified for the experimental results is attributed to the F(1,1) branch based on group velocity, and normalized displacement.

Peak A_3 in the 0-degree and 180-degree orientation could not be attributed to the F(1,1) branch, suggesting they are spurious responses.. Peak A_0 in the 0-degree orientation did not occur in the 180-degree orientation and occurred before the start of the wave at the shaker, suggesting it is a spurious response. Furthermore, peak A_0 in the 0-degree orientation did interfered with peak A_1, which is the first pass of the wave.

7.5.2 Analysis of Longitudinal Direction Results

The acceleration – time histories for the response measured at the shaker and the longitudinal component of the pile response are shown on Figure 7-14.

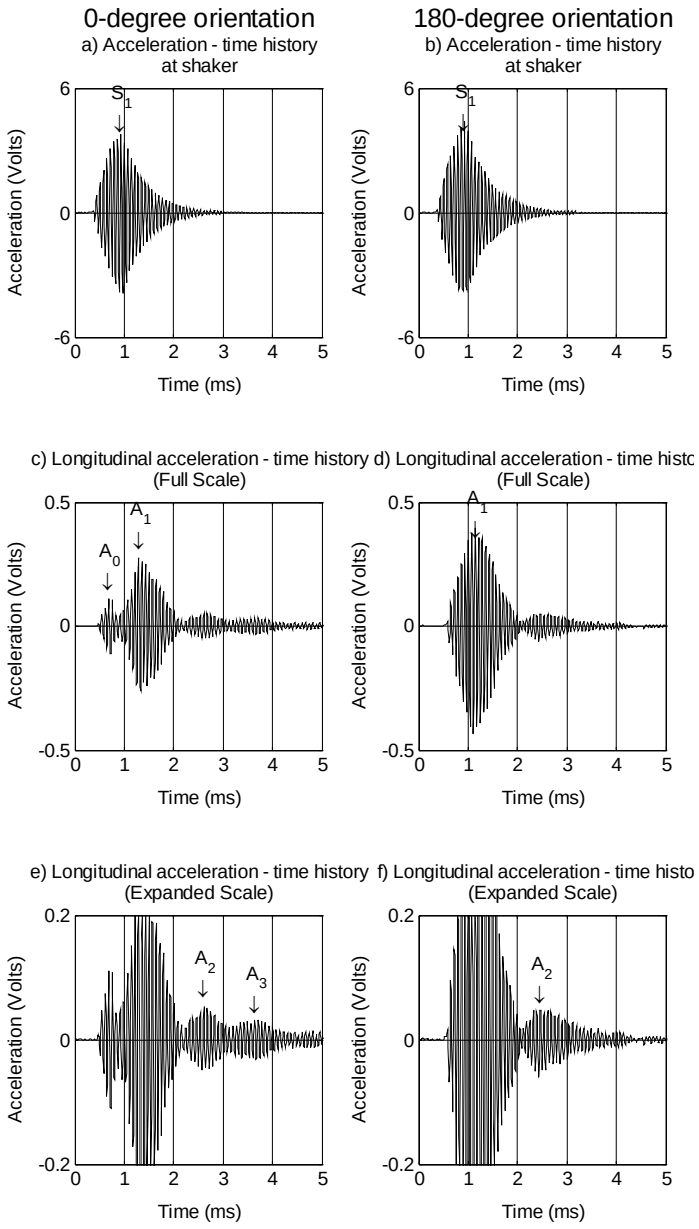

Figure 7-14: Prototype pile B308-2400 (embedded), controlled frequency test results with CF = 14000 Hz, longitudinal acceleration – time histories for 0-degree and 180-degree orientations

The peaks designated S_1 and A_1 represent the start of the wave at the shaker and the first arrival at the triaxial accelerometer. The peak designated A_0 is a spurious peak that occurs in the response of the test performed at the 0-degree orientation prior to the start of the wave at the shaker. The peaks designated A_2 through A_5 represent possible returns of the reflected wave. The times at which each peak occurred are presented on Table 7-29.

Table 7-29: Prototype Pile B308-2400 (embedded), controlled frequency results with CF = 14000 Hz, peaks in measured responses (longitudinal)

Peak designation	Time at which peak occurred (ms)	
	0-degree orientation	180-degree orientation
S_1	0.93	0.93
A_0	0.69	N/I
A_1	1.43	1.15
A_2	2.61	2.61
A_3	3.64	N/I

N/I Peak not identified

The group velocity is computed from equation 7-2 using the assumed travel paths defined on Figure 7-2, the computed travel distances presented on Tables 7-3 and 7-4, and the recorded time values presented on Table 7-29. The calculated group velocities for selected peaks are presented on Table 7-30.

Table 7-30: Prototype pile B308-2400 (embedded), controlled frequency results with CF = 14000 Hz, group velocity values for reflected wave (longitudinal)

Orientation	Combination of peaks	Expected travel path	Travel distance, ΔL (mm)	Travel time Δt (ms)	Group velocity (m/s)	Branch
0-degree	$A_2 - S_1$	First reflection	4510	1.68	2680	F(1,1)
180-degree	$A_2 - S_1$	First reflection	4670	1.68	2780	F(1,1)

Notes: F(1,1) theoretical group velocity is 2670 m/s

The experimentally-determined group velocity most closely matches the theoretical group velocity value for the F(1,1) branch. The average group velocity value is 2730 m/s with a standard deviation of 70 m/s or 2.6 % of the average value. Based on the normalized displacement values presented on Table 7-32, the mode on the F(1,1) branch has the largest normalized displacement of the modes that may be excited at the central frequency.

The calculation of group velocity based on peaks A_1 and A_2 was not consistent with the expected values based on theoretical considerations, nor was is consistent with the values computed from the analysis of peaks S_1 and A_2. Peaks A_1, particularly for the tests performed in the 0-degree orientation, did not fall within a wave group that was as well defined as for the tests performed on the other prototype piles. The controlled frequency tests designed for verification of the longitudinal branches (Chao, 2002) were analyzed using the start of the wave at the shaker and the return of the reflected wave to the accelerometer because the first pass of the accelerometer contained other modes of vibration and the longitudinal wave had not fully developed. The conditions observed on the verification of the longitudinal branches may

contribute to the difficulty in analyzing the data from controlled frequency tests designed to induce a flexural wave.

The attenuation coefficient could not be directly calculated because the first pass of the wave, peak A_1, was not included in the analysis. It can be observed, however, that the amplitude of the reflected wave, peak A_2, is smaller than the amplitude of the first pass.

The mode identified for the experimental results is attributed to the F(1,1) branch based on group velocity, and normalized displacement. Peak A_0 in the 0-degree orientation did not occur in the 180-degree orientation and occurred before the start of the wave at the shaker, suggesting it is a spurious response. Furthermore, peak A_0 in the 0-degree orientation did interfered with peak A_1, which is the first pass of the wave.

7.5.3 Comparison of Radial and Longitudinal Results

The analysis of the controlled frequency results indicate that a flexural wave is induced in the pile, and that a mode on the F(1,1) branch was excited for both the radial and longitudinal components.

The group velocity values determined from the analysis of the test results presented in the text of Sections 7.2.1 and 7.2.2, can be presented graphically by superimposing the group

velocity – frequency data on the numerically-determined group velocity curves, or by the mode identification method described in Section 3.5.2. The group velocity values calculated from the test results are summarized on Table 7-31.

Table 7-31: Prototype pile B308-2400 (embedded), controlled frequency results for CF = 14000 Hz, summary of group velocity values

Direction	Mode	Group velocity (m/s)		Attenuation coefficient per unit length (nepers/m)
		Average	Standard deviation	
Radial	F(1,1)	2870	250	N/I
Longitudinal	F(1,1)	2730	70	N/I

Notes: N/I indicates that the value could not be computed.

The values presented on Table 7-31 are superimposed on the numerically-determined group velocity – frequency curve on Figure 7-15.

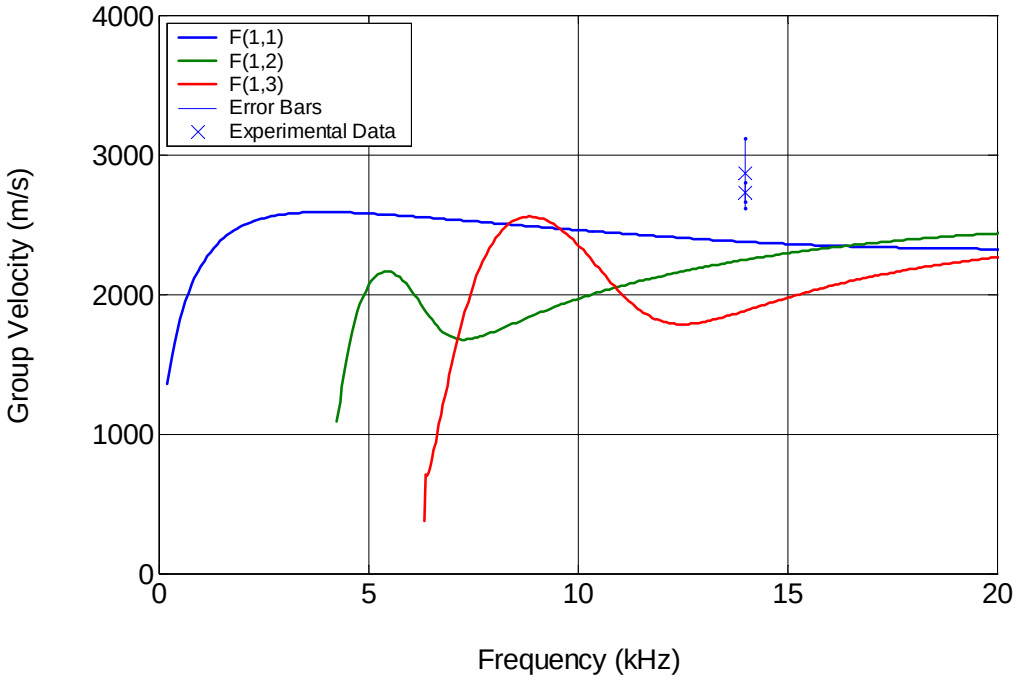

Figure 7-15: Prototype pile B308-2400 (embedded), controlled frequency results with CF = 14000 Hz, superimposed on numerically-determined group velocity – frequency curves of first three flexural branches for concrete with $\nu_c = 0.28$

The data points, with their error bars fall closest to the group velocity value for the F(1,1) branch, which is the branch with the largest normalized displacement .

The results of the radial response for the 180-degree orientation analyzed by the mode identification method described in Section 3.5.2 are presented on Figure 7-16. The joint velocity frequency curve was generated using the start of the wave at the shaker and the return of the first reflection. The start of the wave at the shaker occurs at 0.93 ms, as presented on Table 7-27, and the travel length for the wave is 4670 mm, as presented on Table 7-27.

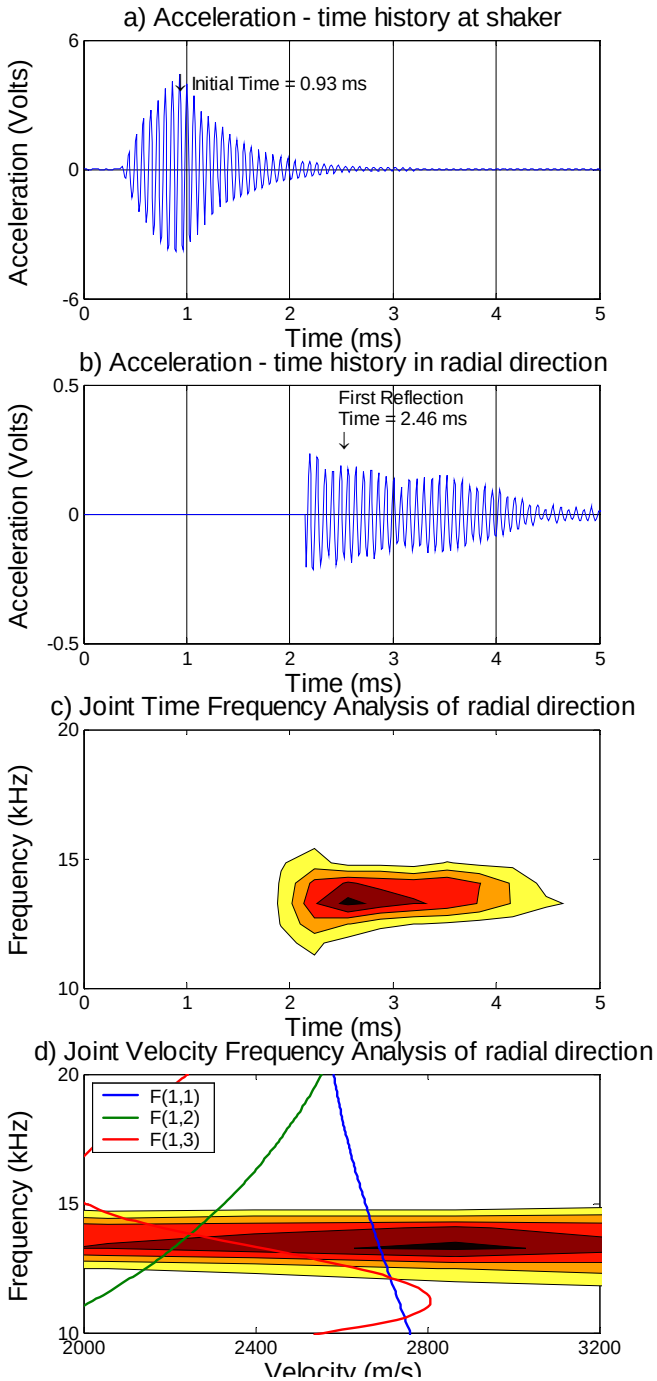

Figure 7-16: Prototype pile B308-2400 (embedded) controlled frequency results for CF = 14000 Hz, 180-degree orientation, radial direction mode identification method

The largest contour on the joint velocity frequency analysis curve, shown on Figure 7-16d crosses the group velocity – frequency curve for the F(1,1) branch, which is the mode identified by conventional time and frequency . The results of the mode identification method are consistent with the conventional time – frequency analysis for which results were presented on Figure 7-15.

7.6 Summary and Conclusions

Prototype pile C355-2430 and two Group B prototype piles were embedded in the loose sand fill at the NGES at Northwestern Univeristy, and were evaluated nondestructively with the controlled frequency method. The piles were evaluated at several central frequencies and those results were analyzed to identify suitable test frequencies. As with the evaluation of Prototype pile C355-2430 under traction-free conditions, a central frequency of 14000 Hz was identified as a suitable frequency, and the results those tests were analyzed to determine the group velocity. The group velocity values determined from the test results were compared to the theoretical results to identify the branch or branches on which modes were excited. The branch identified based on group velocity was compared to the normalized displacement magnitudes to determine if the mode should be identified on that branch. In addition to the analysis of group velocity and normalized displacement magnitude, attenuation was included in the analysis of tests performed on embedded prototype piles.

For the controlled frequency tests, the input and response were measured with the embedded transducer in the shaker with which the force was applied and with a triaxial accelerometer mounted on the side of the pile. Tests were performed at several central frequencies and those results were evaluated to identify suitable test frequencies.

The results of suitable test frequencies were analyzed to determine if the test induced a flexural wave and to identify the branch or branches on which modes were excited. The branches were identified based on group velocity, normalized displacement magnitude, and attenuation coefficient per unit length. The group velocity has been calculated for various combinations of first pass of the wave and return of the reflected wave. The computed group velocity values were compared to theoretical values of group velocity as part of the verification of the flexural guided wave theory.

The evaluation of Prototype pile C355-2430 indicated that modes were excited on the F(1,1) and F(1,5) branch, and that modes could be identified on both branches from the analysis of the radial response and on the F(1,1) branch from the analysis of the longitudinal response. The evaluation of Prototype pile B254-2220 indicated that modes were excited on the F(1,2) and F(1,3) branch, and that the mode on the F(1,2) branch was identified from the analysis of the radial response and on the F(1,3) branch from the analysis of the longitudinal response. The evaluation of Prototype pile B308-2400 indicated that a mode was excited on the F(1,1) branch, and that mode was identified from the analysis of both the radial and longitudinal responses.

Based on the evaluation of the piles prototype piles under embedded conditions, the controlled frequency method could potentially be used as a method for nondestructive evaluation of deep foundations.

Chapter 8: Summary and Conclusions

Two experimental methods, the lateral impact method and controlled frequency method, have been developed to verify the flexural guided wave theory (Wang, 2004) and to be used to nondestructively evaluate deep foundations. Both methods use a dynamic force applied to the side of a pile and one or more triaxial accelerometers mounted to the side of the pile. Depending on the test type and prototype pile geometry, the results can be analyzed to compute phase velocity, group velocity, geometric attenuation, and normalized displacement magnitude. The experimental results are compared to numerically-determined theoretical values as verification of the flexural guided wave theory and evaluation of the suitability of the methods to nondestructively evaluation deep foundations.

8.1 Summary

Conventional impact methods for nondestructive evaluation of deep foundations, such as the sonic echo method and the impulse response method, are performed with an impact hammer and one transducer. The impact is applied to, and the response is measured on, the top of the structure. Some limitations of the conventional methods for

nondestructive evaluation of deep foundations are their ability to identify small defects due to the long wavelengths associated with the low frequencies induced by a hammer impact and

insufficient measurement to determine the propagation velocity unless the exact location of a reflection source is known. Furthermore, the presence of an intervening structure limits the amount of energy transmitted to the deep foundation (Finno and Gassman, 1998). Two new methods, the lateral impact method and the controlled frequency method, were developed to overcome some of the limitations of the conventional methods for nondestructive evaluation of deep foundations. Both methods assume that a three-dimensional flexural wave is induced in the pile, compared to the one-dimensional longitudinal wave that is induced by the conventional methods.

A mathematical framework was proposed for a potential method for NDE of deep foundations based on three-dimensional wave propagation within a waveguide based on the theory of elasticity (Hannifah, 1998). The governing equation proposed by Hannifah (1998) describes all modes of longitudinal, flexural, and torsional waves. The governing equation has been solved numerically for the longitudinal modes (Hannifah, 1998), and the numerical solutions were verified experimentally (Chao, 2002). The governing equation proposed by Hannifah (1998) was solved for the flexural modes and was proposed as a potential method to evaluate deep foundations (Wang, 2004). An experimental program developed to verify the numerical solutions proposed for the flexural modes is presented in this thesis. This experimental program was developed to determine the experimental values of phase velocity, group velocity, displacement, and attenuation for the frequency or frequencies excited in a test, and to compare these experimental results with the theoretical predictions made by Wang (2004).

The general procedure for the verification of the guided wave theory is

1. Characterize the soil to determine its density and shear wave velocity. The Poisson's ratio is also required as an input, but it is estimated.
2. Characterize the concrete prototype pile to determine its density, shear wave velocity, and Poisson's ratio.
3. Compute the density ratio and shear modulus ratio from the properties determined in Steps 1 and 2.
4. Compute the nondimensional frequency – nondimensional wavenumber relationships of each active branch using the pile – soil properties from Step 3.
5. Compute the nondimensional group velocity – nondimensional frequency relationships and the nondimensional phase velocity – nondimensional frequency relationships from the results of Step 4.
6. Convert the nondimensional relationships in Step 5 to dimensional form based on the geometry of the pile and the properties of the concrete.
7. Perform the tests on the pile (impact or controlled frequency).
8. Analyze the test results to determine the group velocity – frequency data or the phase velocity – frequency data.
9. Compare the results of Step 8 to the results of step 7 to determine the branch on which the mode is excited.
10. If modes could potentially be excited on more than one branch, consider the normalized displacement to evaluate if the mode identified in Step 9 should be excited, i.e., it has a large normalized displacement.
11. For embedded piles, consider the geometric attenuation.

The soil characterization can be performed through field and laboratory tests. The concrete density is ideally determined from test cylinders cast from the same concrete as the prototype pile to be tested. The shear wave velocity and Poisson's ratio are determined from the analysis of nondestructive test results. The bar wave velocity is determined from sonic echo (SE) tests, and the shear wave velocity is determined from identification of the universal mode frequency (UMF) for the L(0,1) branch (Chao, 2002). The Poisson's ratio can be calculated from the relationship between shear wave velocity and bar wave velocity, or by the point matching method (Chao, 2002).

The governing equation is solved by separation of variables and, because the equation is solved in a cylindrical domain, the eigenfunctions are Bessel functions of order *m*, with $m \geq 0$. Each Bessel function has an infinite number of zero crossings and each zero crossing corresponds to a family of solutions, or branch. The branches are designated as F(m,n) where *F* indicates flexural, *m* is the order of the Bessel function, and *n* is the branch. Each branch has an infinite number of points defined by an ordered pair of the real-valued frequency and the complex-valued wavenumber. Each frequency – wavenumber pair on a selected branch for a selected Bessel function order, corresponds to a mode, which has a specific phase velocity, group velocity, displacement profile, and, for embedded piles, geometric attenuation, all of which are computed from the frequency – wavenumber results.

A new prototype pile, with a Group C designation, was cast for the verification of the flexural guided wave theory (Wang, 2004), summarized in Section 2.3, and to evaluate the applicability of the lateral impact method and the controlled frequency method for nondestructive evaluation of deep foundations. Two Group B prototype piles cast by Chao (2002) were also evaluated under embedded conditions with both the lateral impact and controlled frequency tests. A new prototype pile cast as part of this research is 355 mm in diameter by 2430 mm long. This new prototype pile was characterized by the sonic echo method, and those results can be found in Chapter 4. This new prototype pile has a bar wave velocity of 3900 m/s, a shear wave velocity of 2530 m/s, a density of 2350 kg/m^3, and a Poisson's ratio of 0.20. The results of the sonic echo tests performed on the Group B prototype piles can be found in Chao (2002). One Group B pile is 254 mm in diameter by 2220 mm long,

with a shear wave velocity of 2730 m/s, a density of 2400 kg/m^3, and a Poisson's ratio of 0.18. The other Group B pile is 308 mm in diameter by 2400 mm long, with a shear wave velocity of 2780 m/s, a density of 2365 kg/m^3, and a Poisson's ratio of 0.28. The shear wave velocity of the soil surrounding the piles is 105 m/s and its density is 1600 kg/m^3 (Finno and Gassman, 1998). The Poisson's ratio of the soil is assumed to be 0.30 (Hannifah, 1998; Chao, 2002, Wang, 2004).

The lateral impact method described in Section 3.1.1 was developed as a method to induce flexural waves with which to verify the flexural guided wave theory (Wang, 2004). Lateral impact tests were performed with a hammer impact applied to the side of the pile and the pile response was measured with a triaxial accelerometer mounted to the side of the pile. Based on the maximum frequency induced by a hammer impact, measured modes were expected to lie on the F(1,1) branch. The tests were performed at the 0-degree, 90-degree, 180-degree, and 270-degree orientations, where the orientation is defined by the angle between the impact location and the accelerometer location. The test results were analyzed in the radial and longitudinal directions for the 0-degree and 180-degree orientations and the longitudinal direction for the 90-degree and 270-degree orientations based on the displacement equations presented in Section 2.3.8.

The lateral impact results were analyzed to determine the phase velocity –frequency and the group velocity – frequency relationships, and those results were compared to the corresponding numerically-determined relationships for the F(1,1) branch. The experimental values of phase velocity were obtained from peaks identified on the acceleration spectra and the

frequencies were converted to phase velocity assuming the lowest frequency identified is the lowest harmonic of the pile. The experimental values of group velocity and the corresponding frequency were computed from the acceleration – time histories. The group velocity was computed by identifying the first pass and return of the wave on the time history and computing the group velocity as the travel length divided by the travel time. The frequency of the group was computed from the period of the wave.

To evaluate the applicability of the lateral impact method to evaluate deep foundations, the new prototype pile and two Group B prototype piles were evaluated by the lateral impact method under embedded conditions. As with the lateral impact tests performed on the prototype pile under traction-free conditions, the tests on the embedded piles were performed at the 0-degree, 90-degree, 180-degree, and 270-degree orientations. The results were analyzed to determine the phase velocity – frequency and group velocity –frequency relationships, and the experimental results were compared to the theoretical values determined by the procedures presented in Section 2.3.

The controlled frequency method was developed to induce a dynamic force with a higher frequency than can be generated in a conventional impact tests. The controlled frequency method was originally developed to induce an axial force, and was applied to prototype piles under traction-free and embedded conditions to verify the longitudinal guided wave theory (Chao, 2002). Controlled frequency tests are identified by the central frequency, which is user-defined through a virtual pulse generator. The digital signal from the virtual pulse generator is

converted to an analog signal and amplified. The amplified analog signal causes the piezoelectric crystal in the shaker to vibrate at the central frequency, thus inducing a propagating stress wave. The pile response is measured with accelerometers and the results are evaluated to identify the first pass and possible returns of the reflected wave. Group velocity values and geometric attenuation values, for embedded conditions, are computed for various combinations of the first pass and return of the reflected wave, and those values are compared to theoretical values.

The test configuration was for the controlled frequency methods developed by Chao (2002) was modified to induce a lateral force, as described in Section 3.1.2, and the test results were analyzed to determine if that test configuration induces flexural guided waves. The tests were performed with a piezoelectric shaker attached to the side of the pile, to generate the force, and with one or more accelerometers mounted to the side of the pile, to measure the response.

The tests were performed with different configurations and frequencies to identify suitable test configurations and frequencies. The results of suitable test configurations and frequencies were analyzed to determine if flexural guided waves were induced in a prototype pile. Tests were performed at the 0-degree, 90-degree, 180-degree, and 270-degree orientations. The initial set of test frequencies was between 4000 Hz and 20000 Hz, in 2000 Hz increments, and a test frequency of 5300 Hz was added. The need to evaluate the performance of the shaker as mounted to the prototype pile was added to the evaluation criteria based on the testing over a range of test frequencies.

In theory, the shaker vibrates at a single frequency equal to the central frequency, which would induce stress wave in the pile with the same single frequency. The ideal shaker response should be zero prior to the start of the signal and after the end of the signal, and should have a no-zero portion that contains a single frequency equal to the central frequency. The ideal pile response should have the same frequency content and shape as the input for the first pass and returns of the reflected wave. Preliminary evaluation of the acceleration – time histories and acceleration spectra of the test results indicates that while the shaker and pile did respond at the central frequency, they responded at other frequencies too. The evaluation of the test results to identify suitable test frequencies indicated three basic types of response:

1. The magnitude of the Fourier transform coefficient at the central frequency is large compared to the near-by peak (more than an order of magnitude larger) and any other large peaks can be removed through digital filtering.
2. The magnitude of the Fourier transform coefficient at the central frequency is moderate compared the near-by peaks (less than an order of magnitude larger) and any other large peaks can be removed through digital filtering.
3. Frequencies with large Fourier transform coefficients that are near the central frequency cannot be removed through digital filtering.

The Type 1 response provides results that can be analyzed to determine the group velocity and geometric attenuation values. Only one suitable test frequency, 14000 Hz was identified during the controlled frequency testing.

The Group C prototype pile was evaluated under traction-free conditions by the controlled frequency methods at a central frequency of 14000 Hz with the upper and lower triaxial accelerometers mounted in the 0-degree and 180-degree orientations. The radial and longitudinal components of the response were analyzed to determine the group velocity based on

the start of the wave at the shaker, first arrival of the wave at the upper and lower triaxial accelerometers, and possible returns of the reflected wave to the upper and lower triaxial accelerometers. The experimental values of group velocity were compared to the theoretical values of group velocity for the branches on which modes could be excited to identify if modes were excited on one or more flexural branch. The normalized displacement magnitude was also considered to identify the branches on which modes should be excited.

To evaluate the applicability of the controlled frequency method for NDE of deep foundations, the Group C and two Group B prototype piles were evaluated under embedded conditions. The test equipment and configuration for embedded conditions were the same as for traction-free conditions, except that only one triaxial accelerometer was used for embedded conditions compared to two triaxial accelerometers for traction-free conditions. The test results were initially analyzed to identify suitable test configurations and frequencies. As with the evaluation of the Group C prototype pile evaluated under traction-free conditions, a central frequency of 14000 Hz was the only suitable test frequency. The group velocity and geometric attenuation results of the suitable test configurations and frequencies were compared to theoretical values to identify the branch or branches on which modes were excited. The normalized displacement magnitude was also considered to evaluate the branches on which modes should be excited.

Whereas, tests performed at the 0-degree and 180-degree orientations provided suitable results, those performed at the 90-degree and 270-degree orientations did not provide suitable

results. The response of the prototype piles to tests performed at the 90-degree and 270-degree orientations did not contain well-defined wave groups that could be attributed to a first pass and possible returns of the reflected wave. A possible explanation is that the pile response at the 90-degree and 270-degree orientations contained modes other than flexural waves.

8.2 Conclusions

Based on the results and analyses of the experiments presented herein, the following conclusions are drawn:

- Lateral impact tests were found to induce flexural waves based on considerations of the phase velocity- frequency and group velocity – frequency relationships.
- Controlled frequency tests were found to induce flexural waves based on the consideration of the group velocity – frequency relationships and normalized displacement magnitudes.
- The lateral impact method and controlled frequency method could potentially be used for NDE of deep foundations.

An advantage of NDE methods based on flexural guided waves over those based on longitudinal waves is in the characterization of deep foundations for which the top of the deep foundation is not accessible but part of the side is accessible. The force of the lateral impact method described in Section 3.1.1 and the controlled frequency method described in Section 3.1.2 are applied directly to the deep foundation rather than to an intervening structure atop the deep foundation.

The results of the lateral impact performed on the Group C prototype pile under traction-free conditions were analyzed to compute the phase velocity – frequency relationship and the

group velocity – frequency relationship, and those results were compared to the numerically-determined theoretical results. The experimental results followed the trend of the numerically-determined curves, suggesting the lateral impact does induce flexural waves, and that those waves lie along the F(1,1) branch.

The analysis of the lateral impact tests performed on the Group C and two Group B prototype piles under embedded conditions indicate that the lateral impact method does induce flexural waves that lie along the F(1,1) branch, suggesting the lateral impact method can be used to nondestructively evaluate deep foundations.

The results of the controlled frequency tests performed on the Group C prototype pile under traction-free conditions were analyzed to compute the group velocity at the central frequency and those results were compared to the numerically-determined theoretical values. The normalized displacement magnitude was also considered because the controlled frequency tests were performed at a frequency high enough that modes could potentially be excited on more than one branch. The comparison of the experimental values of group velocity were compared to the theoretical values of group velocity and were found to lie along the F(1,1) branch. The mode on the F(1,1) branch has the largest theoretical value of normalized displacement magnitude of the branches on which modes may be excited for the longitudinal component and the second largest theoretical value of normalized displacement magnitude of the branches on which modes may be excited for the radial component. The results of the controlled frequency tests performed on the new prototype pile indicate that controlled frequency method

does induce flexural guided waves based on considerations of group velocity and normalized displacement magnitude.

The results of the controlled frequency tests performed on the Group C and Group B prototype piles under embedded conditions were analyzed to compute the group velocity at the central frequency and, where possible, the geometric attenuation. The normalized displacement magnitude was considered to identify the branches on which modes should be excited. Modes were identified on the F(1,1) and F(1,5) branches for the tests performed on Prototype pile C355-2430, on the F(1,2) and F(1,3) branches for the tests performed on Prototype pile B254-2220, and on the F(1,1) branch for the tests performed on Prototype pile C308-2400. The results of the controlled frequency tests performed on the prototype piles under embedded condition suggest that the controlled frequency method can potentially be used for NDE of deep foundations.

References

ASTM Standards

ASTM C31-03: Standard Practice for Making and Curing Test Specimens in the Field

ASTM C192-02: Standard Practice for Making and Curing Test Specimens in the Laboratory

ASTM C617-98: Standard Practice for Capping Cylindrical Concrete Secimens

ACI Reports

ACI 211.1-91: Standard Practice for Selecting Proportions for Normal, Heavyweight and Mass Concrete

ACI 308R-01: Standard Practice for Curing Concrete

ACI 309R-96: Guide for Consolidation of Concrete

Achenbach, J. D. (1973). Wave Propagation in Elastic Solids, North-Holland.

Bishop, R. H. (2001). Learning with LabVIEW 6i. Upper Saddle River, NJ, Prentice Hall.

Chao, H.-C. (2002). Experimental Model for Pile Integrity Evaluation using Guided Wave Approach. Civil & Environmental Engineering. Evanston, Northwestern University**:** 330.

Davis, A. G. and C. S. Dunn (1974). "From Theory to Field Experience with teh Nondestructive Vibration Testing of Piles." Proceedings of the Institution of Civil Engineers **57**: 571-593.

Davis, A. G. and S. A. Robertson (1975). "Economic Pile Testing." Ground Engineering **8**(3): 40-43.

Finno, R. J., H.-C. Chao, et al. (2001). Nondestructive Evaluation of In Situ Concrete Piles at the Advanced Waterfront Technology Test Site, Port Hueneme, California. Evanston, Northwestern University**:** 18.

Finno, R. J. and S. L. Gassman (1998). Impulse response evaluation of drilled shafts. Journal of Geotechnical and Geoenvironmental Engineering, ASCE,Reston,VA,USA. **124:** 965-975.

Gassman, S. L. and R. J. Finno (1999). Impulse response evaluation of foundations using multiple geophones. Journal of Performance of Constructed Facilities, American Society of Civil Engineers,Reston,VA,USA. **13:** 82-89.

Gassman, S. L. and R. J. Finno (2000). Cutoff frequencies for impulse response tests of existing foundations. Journal of Performance of Constructed Facilities, American Society of Civil Engineers,Reston,VA,USA. **14:** 11-21.

Graff, K. F. (1975). Wave Motion in Elastic Solids. New York, Dover Publications, Inc.

Hanifah, A. A. (1999). A Theoretical Evaluation of Guided Waves in Deep Foundations. Civil Engineering. Evanston, Northwestern University**:** 215.

Holman, J. P. (2001). Experimental Methods for Engineers. Boston, McGraw Hill.

Holt, J. D. (1995). Finding the Lengths of Installed Steel H-Piles by Dispersive Bending Wave Propagation Methods, Orlando.

Holt, J. D., S. Chen, et al. (1994). "Determining lengths of installed timber piles by dispersive wave propagation." Transportation Research Record(1447Oct): 110-115.

Hughes, M. L., G. J. Rix, et al. (1998). "Nondestructive Determination of Pile Tip Elevation using Modal Analysis." SPIE: The International Society for Optical Engineering **3400**: 522-530.

Ifeachor, E. C. and B. W. Jervis (2002). Digital Signal Processing. Harlow, Prentice Hall.

Jalinoos, F., M. F. Aouad, et al. (1995). Three Stress-wave Methods for the Determination of Unknown Pile Depths, Orlando.

Kline, S. J. and F. A. McClintock (1953). "Describing Uncertainties in Single-Sample Experiments." Mechanical Engineering: 3-8.

Krautkramer, J. and H. Krautkramer (1990). Ultrasonic Testing of Materials. Berlin, Spinger-Verlag.

Montgomery, D., C. and G. C. Runger (2003). Applied Statistics & Probability for Engineers. New York, John Wiley & Sons, Inc.

Nicholson, N. C. and W. N. McDicken (1991). "Mode Propagation of Ultrasound in Hollow Waveguides." Ultrasonics **29**: 411-416.

Nicholson, N. C., W. N. McDicken, et al. (1989). "Waveguides in Medical Ultrasonics: an Experimental Study of Mode Propagation." Ultrasonics **27**: 101-106.

O'Neil, P. V. (1991). Advanced Engineering Mathematics. Belmont, Wadworth.

Osborn, P. W. (1997). Parallel Seismic Evaluation of the NDE Test Section at th National Geotechnical Experimentation Site at Northwestern University. Civil Engineering. Evanston, IL, Northwestern University**:** 125.

Porat, B. (1997). A Course in Digital Signal Processing. New York, John Wiley & Sons, Inc.

Sansalone, M. and N. J. Carino (1986). Impact-Echo: A Method for Flaw Detection in Concrete using Transient Stress Waves, U.S. Department of Commerce, International Bureau of Standards.

Subramaniam, K. V., J. S. Popovics, et al. (2000). "Determining Elastic Properties of Concrete Using Vibration Resonance Frequencies of Standard Test Cylinders." Cement, Concrete, and Aggregates **22**(2): 81 - 89.

Timoshenko, S. P. and J. N. Goodier (1970). Theory of Elasticity. New York, McGraw-Hill.

Wang, H. (2004). Theoretical Evaluations of Embedded Plate-like and Solid Cylindrical Structures with Guided Waves. Civil and Environmental Engineering. Evanston, Northwestern University**:** 289.

Zemanek, J. (1971). "An experimental and Theoretical Investigation of Elastic Wave Propagation in a Cylinder." Journal of the Acoustical Society of America: 265-283.

Appendix A: Computer Codes

“Flexural_Dipserion.mws”

“modal_shape_flexural.m”

“mode_identification.m”

Code to solve the Frequency Equation (Maple ® worksheet)

```
> restart:
> nu1:=0.3317:
> nu2:=0.3:
> m:=3250.:
> r:=13.3:
> mu:=1./m:
> rho:=1./r:
> r1:=2.*nu1/(1.-2.*nu1):
> r2:=2.*nu2/(1.-2.*nu2):
> ds:=0.05:
> f:=proc(z,o)
  global m,r,mu,rho,r1,r2;
  local k11,k12,k21,k22,a11,a12,a21,a22,A,d,
  J111,J121,H112,H122,J011,J021,H012,H022;
  k21:=o^2;
  k22:=rho*o^2/mu;
  k11:=o^2/(2.+r1);
  k12:=rho*o^2/(mu*(2.+r2));
  a11:=sqrt(k11-z^2);
  a12:=sqrt(k12-z^2);
  a21:=sqrt(k21-z^2);
  a22:=sqrt(k22-z^2);
  A:=array(1..6,1..6):
  J111:=BesselJ(1,a11);
  J121:=BesselJ(1,a21);
  H112:=HankelH1(1,a12);
  H122:=HankelH1(1,a22);
  J011:=BesselJ(0,a11);
  J021:=BesselJ(0,a21);
  H012:=HankelH1(0,a12);
  H022:=HankelH1(0,a22);
  A[1,1]:=a11*J011;
  A[1,2]:=(-a21)*J021;
  A[1,3]:=a21*J021;
  A[1,4]:=a12*H012;
  A[1,5]:=(-a22)*H022;
  A[1,6]:=a22*H022;
  A[2,1]:=-J111;
  A[2,2]:=J121;
  A[2,3]:=(-a21)*J021+J121;
  A[2,4]:=-H112;
  A[2,5]:=H122;
```

```
 A[2,6]:=(-a22)*H022+H122;
 A[3,1]:=z*J111;
 A[3,2]:=(a21^2)*J121/z;
 A[3,3]:=0;
 A[3,4]:=z*H112;
 A[3,5]:=(a22^2)*H122/z;
 A[3,6]:=0;
 A[4,1]:=((-1.)*r1*((a11^2)+(z^2))-2.*(a11^2))*J111;
 A[4,2]:=2.*(a21^2)*J121;
 A[4,3]:=(-1.)*(a21^2)*J121;
 A[4,4]:=((-1.)*r2*mu*((a12^2)+(z^2))-2.*mu*(a12^2))*H112;
 A[4,5]:=2.*mu*(a22^2)*H122;
 A[4,6]:=(-1.)*mu*(a22^2)*H122;
 A[5,1]:=2.*(J111-(a11*J011-J111));
 A[5,2]:=2.*(-J121+(a21*J021-J121));
 A[5,3]:=2.*(a21*J021-J121)-J121*(2.-(a21^2));
 A[5,4]:=2.*mu*(H112-(a12*H012-H112));
 A[5,5]:=2.*mu*(-H122+(a22*H022-H122));
 A[5,6]:=mu*(2.*(a22*H022-H122)-H122*(2.-(a22^2)));
 A[6,1]:=2.*(a11*J011-J111);
 A[6,2]:=(((a21^2)/(z^2))-1.)*(a21*J021-J121);
 A[6,3]:=J121;
 A[6,4]:=2.*mu*(a12*H012-H112);
 A[6,5]:=mu*(((a22^2)/(z^2))-1.)*(a22*H022-H122);
 A[6,6]:=mu*H122;
 d:=linalg[det](A);
 RETURN(d);
 end:
> g:=diff(f(z,o),z):
> h:=diff(f(z,o),o):
> start:=fsolve({Re(f(x+I*y,6.56)=0,Im(f(x+I*y,6.56))=0},{x,y},{x=0.2..0.4,y=0.0..0.2});
> o0:=6.56;
> z0:=subs(start,x)+I*subs(start,y);
> f1:=f(z0,o0);
>
F:=[[Re(z0),Im(z0),o0,Re(f1),Im(f1)]];writedata[APPEND]("F15_n3317_Traction_Free.txt
",F);
> with(linalg):
> rpoints:=[[Re(z0),o0]];
> ipoints:=[[Im(z0),o0]];
> v0:=evalm(vector(3,[1.,0,1.])/sqrt(2.)):
> for j from 1 while Re(z0) < 20 do
d1:=eval(subs({z=z0,o=o0},g)):
d2:=eval(subs({z=z0,o=o0},h)):
```

```
B:=linalg[matrix](2,3,[Re(d1),-Im(d1),Re(d2),
Im(d1),Re(d1),Im(d2)]):
v:=op(1,nullspace(B)):
w:=evalm(v*1./norm(v,2)):
if (innerprod(v0,w)<0) then w:=evalm(-1*w) fi:
print (w);
z1:=z0:
o1:=o0:
for i from 1 to 30 do
    f0:=f(z1,o1):
    d1:=eval(subs({z=z1,o=o1},g)):
    d2:=eval(subs({z=z1,o=o1},h)):
    b:=vector(3,[-Re(f0),-Im(f0),
      ds-Re(z1-z0)*w[1]-Im(z1-z0)*w[2]-(o1-o0)*w[3]]):
    J:=array(1..3,1..3,[[Re(d1),-Im(d1),Re(d2)],
            [Im(d1),Re(d1),Im(d2)],
            [w[1],w[2],w[3]]]):
    dx:=linsolve(J,b):
    z1:=z1+(dx[1]+I*dx[2]):
    o1:=o1+dx[3]:
    if (norm(dx,2)<.0000001) then break fi:
    od:
print
(i,z1,o1,f0);F:=[[Re(z1),Im(z1),o1,Re(f0),Im(f0)]];writedata[APPEND]("F15_n3317_Tracti
on_Free.txt",F);
rpoints:=[op(rpoints),[Re(z1),o1]]:
ipoints:=[op(ipoints),[Im(z1),o1]]:
z0:=z1:
o0:=o1:
od:
> plot(rpoints);
> plot(ipoints);
END
>
```

Code to compute Displacements Profile (Matlab ® script file)

```
function modal_shape_flexural
%Program to compute displacement profiles for guided waves
warning off MATLAB:divideByZero
format long;

    %Initialize variables for frequency and wavenumber
        o0 = 2.336326711;
        zr = 0.901501395;
        zi = 0.041619535;
        z0 = zr + zi*i;
    %Initialize variables for soil and concrete properties
        properties.nu1 = 0.20;
        properties.nu2 = 0.30;
        properties.m = 825;
        properties.r = 1.5;
        properties.mu = 1/properties.m;
        properties.rho = 1/properties.r;
        properties.r1 = 2*properties.nu1/(1-2*properties.nu1);
        properties.r2 = 2*properties.nu2/(1-2*properties.nu2);
    %Define angle for displacement profile
        Central_Frequency = '20';
        Poisson = '20';
        Branch = 'F12';
        td = 0;
        t = td * pi / 180;
    %Find Nullspace Vector
        NS = null_space(o0, z0, properties);
    %Compute normalizing constant
        R = 1.;
        [u, sigma] = compute_quantities(o0, z0, t, NS, properties, R);
        Prr = sigma.rr*conj(u.r);
        Prt = sigma.rt*conj(u.t);
        Prz = sigma.rz*conj(u.z);
        g = sqrt(abs(4.*imag(z0)/(pi*o0*(imag(Prr)+imag(Prt)+imag(Prz)))));
        check = (g^2)*pi*o0*(imag(Prr)+imag(Prt)+imag(Prz))/(4.*imag(z0));
    %Compute stresses, displacements, and power profiles
        for index = 1:100
            R = 0.01 * index;
            [u, sigma] = compute_quantities(o0, z0, t, NS, properties, R);
                u.r = g * u.r;
                u.z= g * u.z;
                u.t = g * u.t;
```

```
U(index, :) = [R real(u.r) imag(u.r) real(u.t) imag(u.t) real(u.z) imag(u.z)];
                end
        %Write output
filename = ['CF_' Central_Frequency '_n' Poisson '_Disp_' num2str(td) '_' Branch '.txt'];
                dlmwrite(filename, U, '\t');
%End of main program

function NS = null_space(o, z, properties);
        %Compute coefficient matrix
        %Define input parameters
                k21 = o^2;
                k22 = properties.rho * o^2 / properties.mu;
                k11 = o^2 / (2+properties.r1);
                k12 = properties.rho * o^2 / (properties.mu*(2+properties.r2));
                a11 =sqrt(k11 - z^2);
                a12 = sqrt(k12 - z^2);
                a21 = sqrt(k21 - z^2);
                a22 = sqrt(k22 - z^2);
        %Simplify bessel functions
                J111 = besselj(1,a11);
                J121 = besselj(1, a21);
                H112 = besselh(1,2,a12);
                H122 = besselh(1,2,a22);
                J011 = besselj(0,a11);
                J021 = besselj(0,a21);
                H012 = besselh(0,2,a12);
                H022 = besselh(0,2,a22);
        %Create first row of matrix
                A(1,1) = a11 * J011;
                A(1,2) = (-a21) * J021;
                A(1,3) = a21 * J021;
                A(1,4) = a12 * H012;
                A(1,5) = (-a22) * H022;
                A(1,6) = a22 * H022;
        %Create second row of matrix
                A(2,1) = -J111;
                A(2,2) = J121;
                A(2,3) = (-a21) * J021 + J121;
                A(2,4) = -H112;
                A(2,5) = H122;
                A(2,6) = (-a22) * H022 + H122;
        %Create third row of matrix
                A(3,1) = z * J111;
                A(3,2) = (a21^2) * J121 / z;
```

```
                A(3,3) = 0;
                A(3,4) = z * H112;
                A(3,5) = (a22^2) * H122 / z;
                A(3,6) = 0;
        %Create fourth row of matrix
                A(4,1) = ((-1)*properties.r1*((a11^2)+(z^2)) - 2*(a11^2))*J111;
                A(4,2) = 2 * (a21^2) * J121;
                A(4,3) = (-1)*(a21^2)*J121;
A(4,4) = ((-1)*properties.r2*properties.mu*((a12^2)+(z^2)) - 2*properties.mu*(a12^2))*H112;
                A(4,5) = 2*properties.mu*(a22^2)*H122;
                A(4,6) = (-1)*properties.mu*(a22^2)*H122;
        %Create fifth row of matrix
                A(5,1) = 2*(J111 - (a11*J011-J111));
                A(5,2) = 2*(-J121 + (a21*J021-J121));
                A(5,3) = 2*(a21*J021-J121) - J121*(2-(a21^2));
                A(5,4) = 2*properties.mu*(H112 - (a12*H012-H112));
                A(5,5) = 2*properties.mu*(-H122 + (a22*H022-H122));
                A(5,6) = properties.mu*(2*(a22*H022-H122) - H122*(2-(a22^2)));
        %Create sixth row of matrix
                A(6,1) = 2*(a11*J011-J111);
                A(6,2) = (((a21^2)/(z^2))-1) * (a21*J021-J121);
                A(6,3) = J121;
                A(6,4) = 2*properties.mu*(a12*H012-H112);
                A(6,5) = properties.mu*(((a22^2)/(z^2))-1) * (a22*H022-H122);
                A(6,6) = properties.mu*H122;
        %Find null space and rearrange entires
                [L, U] = lu(A);
                U(6,6) = 0;
                NS = null(U);
                swap = 1 / NS(1);
                NS = NS * swap;
%End of function

function [u, sigma] = compute_quantities(o, z, t, ns, properties, R);
%Compute bessel function arguments
        a11 = sqrt(((o^2)/(2.+properties.r1))-(z^2));
        a21 = sqrt((o^2)-(z^2));
%Compute displacements
        u.r = cos(t)/R * ((a11*R*besselj(0,a11*R) - besselj(1,a11*R))*ns(1) - (z/a21) *
                (a21*R*besselj(0,a21*R) - besselj(1,a21*R))*ns(2) + besselj(1,a21*R)*ns(3));
        u.t = sin(t)/R * (-besselj(1,a11*R)*ns(1) + (z/a21)*besselj(1,a21*R)*ns(2)
                - (a21*R*besselj(0,a21*R) - besselj(1,a21*R))*ns(3));
        u.z = cos(t)*i*(z*besselj(1,a11*R)*ns(1) + a21*besselj(1,a21*R)*ns(2));
%Compute stresses
```

```
        sigma.rr = cos(t)*(((-properties.r1*((a11^2)+(z^2)) + 2.*((1./(R^2)) –
                (a11^2)))*besselj(1,a11*R) - (2./(R^2))*(a11*R*besselj(0,a11*R) –
                besselj(1,a11*R)))*ns(1) + (2.*z)*(besselj(1,a21*R)*(a21 - (1./(a21*R)))
                + (1./(a21*R))*(a21*R*besselj(0,a21*R) - besselj(1,a21*R)))*ns(2) +
                (2./(R^2))*(a21*R*besselj(0,a21*R) - besselj(1,a21*R) –
                besselj(1,a21*R))*ns(3));
        sigma.rt = sin(t)*((2./(R^2))*(besselj(1,a11*R) - (a11*R*besselj(0,a11*R) –
                besselj(1,a11*R)))*ns(1) + (2.*z/R)*(-besselj(1,a21*R)/(a21*R) +
                (1./(a21*R))*(a21*R*besselj(0,a21*R) - besselj(1,a21*R)))*ns(2) +
                ((2./(R^2))*(a21*R*besselj(0,a21*R) - besselj(1,a21*R)) –
                besselj(1,a21*R)*((2./(R^2)) - (a21^2)))*ns(3));
        sigma.rz = cos(t)*i*(((2.*z/R)*(a11*R*besselj(0,a11*R) –
                besselj(1,a11*R)))*ns(1) –
                ((((z^2)-(a21^2))/(a21*R))*(a21*R*besselj(0,a21*R) –
                besselj(1,a21*R)))*ns(2) + (z/R*besselj(1,a21*R))*ns(3));
        sigma.zz = -cos(t)*((properties.r1*((a11^2)+(z^2)) +
                2.*(a11^2))*besselj(1,a11*R)*ns(1) + (2*z*a21*besselj(1,a21*R))*ns(2));
        sigma.zt = sin(t)*i*(-((2.*z/R)*besselj(1,a11*R))*ns(1) +
                ((-(a21/R)+((z^2)/(a21*R)))*besselj(1,a21*R))*ns(2) ...
                - (z/R*(a21*R*besselj(0,a21) - besselj(1,a21*R)))*ns(3));
        sigma.tt = cos(t)*((-properties.r1*((a11^2) + (z^2))*besselj(1,a11*R) –
                2./(R^2)*besselj(1,a11*R)+ (2./(R^2))*(a11*R*besselj(0,a11*R) –
                besselj(1,a11*R)))*ns(1) + ((2.*z/a21/(R^2))*besselj(1,a21*R) –
                (2.*z/a21*(R^2))*(a21*R*besselj(0,a21*R) - besselj(1,a21*R)))*ns(2)
                + ((2./(R^2))*besselj(1,a21*R) - (2./(R^2))*(a21*R*besselj(0,a21*R) –
                besselj(1,a21*R)))*ns(3));
%End of function
```

Code for Mode Identification Method (Matlab ® script file)

```
clear;
%Obtain data
	Data_Source = questdlg('What type of data is source', 'Select file type for source data', ...
		'Excel', 'Text', 'Excel');
	if strcmp(Data_Source, 'Excel');
		[filename pathname] = uigetfile('*.xls', 'Select file to read');
			full_name = [pathname filename];
		if filename ~= 0
			U = xlsread(full_name);
		end
	else
		[filename pathname] = uigetfile('*.txt', 'Select file to read');
			full_name = [pathname filename];
		if filename ~= 0
			U = dlmread(full_name);
		end
	end

%Obtain time parameters
numpoints = length(U(:,1));
dt = U(2,1) - U(1,1);

%Determine frequency parameters
samp_freq = 1000 / dt;
nyquist_freq = samp_freq / 2;
df = samp_freq / numpoints;

%Filter the data
cutoff_freq = [2000 20000];
cutoff_norm = cutoff_freq / nyquist_freq;
filter_order = 6;
[b, a] = butter(filter_order, cutoff_norm);
UF(:,1) = U(:,1);
UF(:,2:7) = filter(b, a, U(:,2:7));

%Compute the spectrogram
num_fft = 128;
window_time = dt * num_fft;
num_overlap = 64;
num_offset = num_fft - num_overlap;
[B f t] = specgram(UF(:,4), num_fft, samp_freq, [], num_overlap);
	B = abs(B);
```

```
%Create mesh
df = f(2) - f(1);
fmax = max(f);
dt = 1000 * (t(2) - t(1));
tmax = 1000 * max(t);
B_Size = size(B);
        num_row = B_Size(1);
        num_col = B_Size(2);
[X, Y] = meshgrid(0:dt:tmax, 0:df:fmax);

%Create joint velocity frequency array
travel_length = 4058;
initial_time = 1.024;
vel_min = 900;
vel_max = 3500;
index = 0;
for k = 1:length(t);
        velocity = travel_length / (1000*t(k) - initial_time);
        if (velocity>vel_min) & (velocity<vel_max)
                index = index + 1;
                for m = 1:num_row
                        Velocity_One(m,index) = velocity;
                end
                B_One(:,index) = B(:,k);
                Freq_One(:,index) = Y(:,k);
        end
end

%Graph results
font_size = 16;
figure(1);
datalabel on;
set(gcf, 'PaperSize', [8.5 17], 'PaperOrientation', 'portrait', 'PaperPosition', [1.25 1 6 15]);
subplot(4,1,1); plot(UF(:,1)-window_time/2, UF(:,3), 'Linewidth', 1); grid on; %datalabel on;
        hndl = title('Time history of input', 'Fontsize', font_size);
                set(hndl, 'Units', 'normalized', 'Position', [0.5 1.05 0]);
        hndl = xlabel('Time (ms)', 'Fontsize', font_size);
                set(hndl, 'Units', 'normalized', 'Position', [0.5 -0.15 0]);
                xlim([0 5]);
        hndl = ylabel('FFT Amplitude', 'Fontsize', font_size);
                set(hndl, 'Units', 'normalized', 'Position', [-0.125 0.5 0]);
        set(gca, 'FontSize', font_size, 'GridLineStyle', '-', 'Position', [0.15 0.8 0.75 0.15]);
subplot(4,1,2); plot(UF(:,1)-window_time/2, UF(:,4), 'Linewidth', 1); grid on;
```

```
        hndl = title('Time history of response', 'Fontsize', font_size);
                set(hndl, 'Units', 'normalized', 'Position', [0.5 1.05 0]);
        hndl = xlabel('Time (ms)', 'Fontsize', font_size);
                set(hndl, 'Units', 'normalized', 'Position', [0.5 -0.15 0]);
                xlim([0 5]);
        hndl = ylabel('FFT Amplitude', 'Fontsize', font_size);
                set(hndl, 'Units', 'normalized', 'Position', [-0.125 0.5 0]);
        set(gca, 'FontSize', font_size, 'GridLineStyle', '-', 'Position', [0.15 0.55 0.75 0.15]);
subplot(4,1,3); contourf(X, Y/1000, B);
        hot_array = colormap(hot);
                hot_array_reverse(:,:) = hot_array(length(hot_array):-1:1,:);
        colormap(hot_array_reverse);
        hndl = title('Spectrogram of response', 'Fontsize', font_size);
                set(hndl, 'Units', 'normalized', 'Position', [0.5 1.05 0]);
        hndl = xlabel('Time (ms)', 'Fontsize', font_size);
                set(hndl, 'Units', 'normalized', 'Position', [0.5 -0.15 0]);
                xlim([0 5]);
        hndl = ylabel('Frequency (kHz)', 'Fontsize', font_size);
                set(hndl, 'Units', 'normalized', 'Position', [-0.125 0.5 0]);
                ylim([0 20]);
        set(gca, 'FontSize', font_size, 'GridLineStyle', '-', 'Position', [0.15 0.3 0.75 0.15]);
subplot(4,1,4); contourf(Velocity_One, Freq_One/1000, B_One);
        hot_array = colormap(hot);
                hot_array_reverse(:,:) = hot_array(length(hot_array):-1:1,:);
        colormap(hot_array_reverse);
        hndl = title('Spectrogram of response', 'Fontsize', font_size);
                set(hndl, 'Units', 'normalized', 'Position', [0.5 1.05 0]);
        hndl = xlabel('Velocity (m/s)', 'Fontsize', font_size);
                set(hndl, 'Units', 'normalized', 'Position', [0.5 -0.15 0]);
                xlim([1000 3000]);
        hndl = ylabel('Frequency (kHz)', 'Fontsize', font_size);
                set(hndl, 'Units', 'normalized', 'Position', [-0.125 0.5 0]);
                ylim([0 20]);
        set(gca, 'FontSize', font_size, 'GridLineStyle', '-', 'Position', [0.15 0.05 0.75 0.15]);
```

Appendix B: Lateral Impact Results, Phase Velocity Calculations and Verification

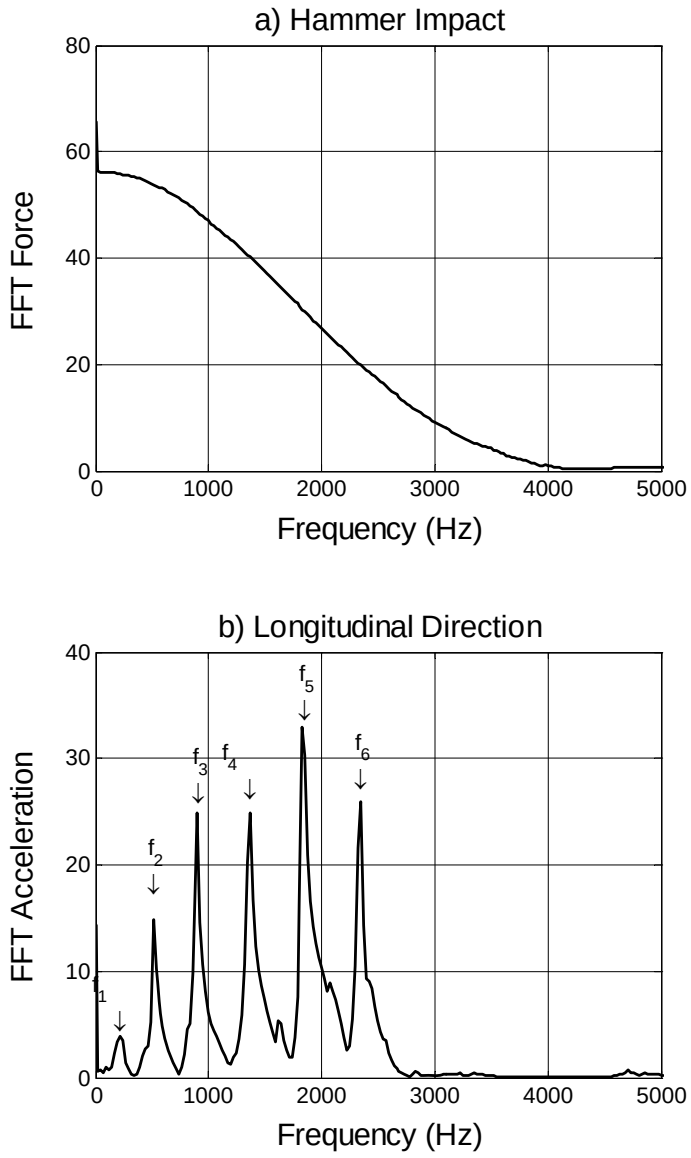

Figure B-1: Prototype Pile C355-2430, lateral impact results for 0-degree orientation, longitudinal direction

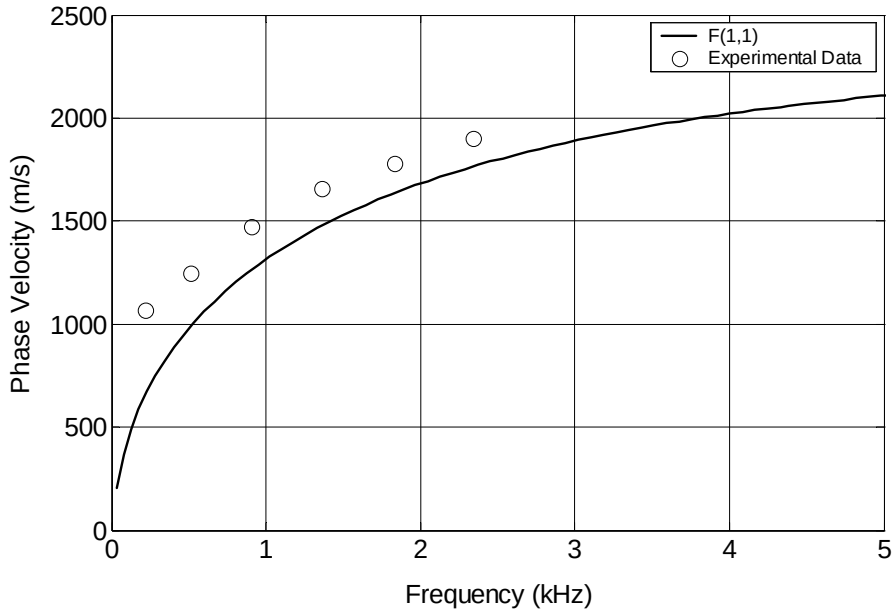

Figure B-2: Prototype Pile C355-2430, lateral impact results for 0-degree orientation, longitudinal phase velocity - frequency data superimposed on numerically-determined F(1,1) branch

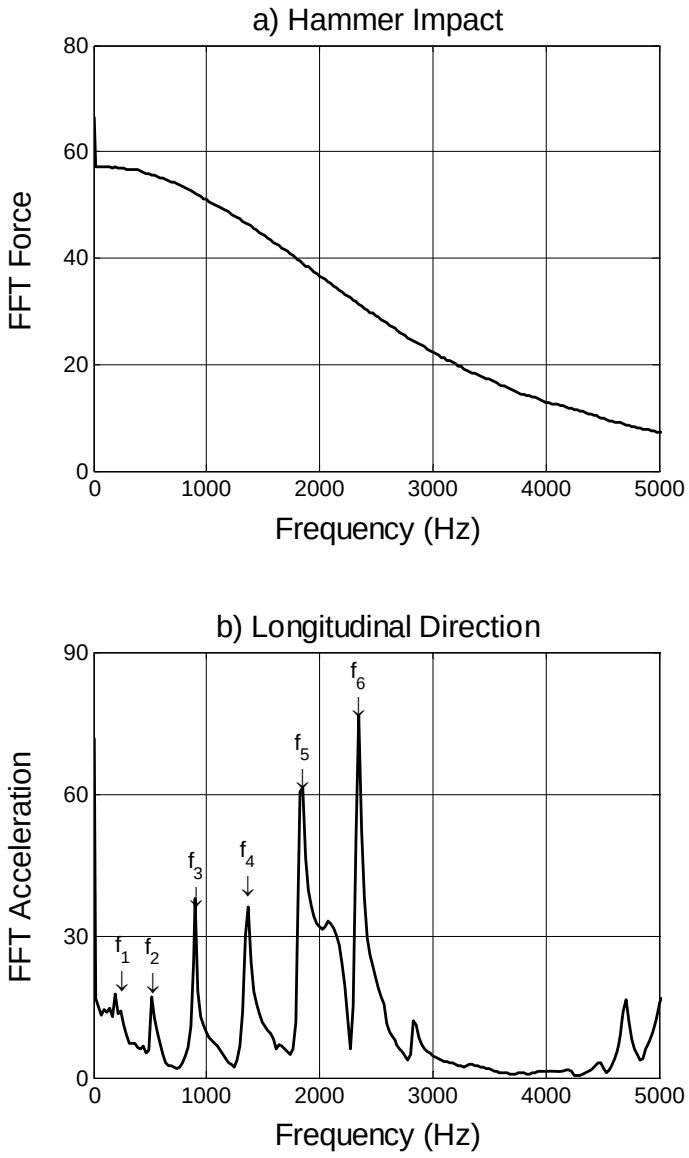

Figure B-3: Prototype Pile C355-2430, lateral impact results for 180-degree orientation, longitudinal direction

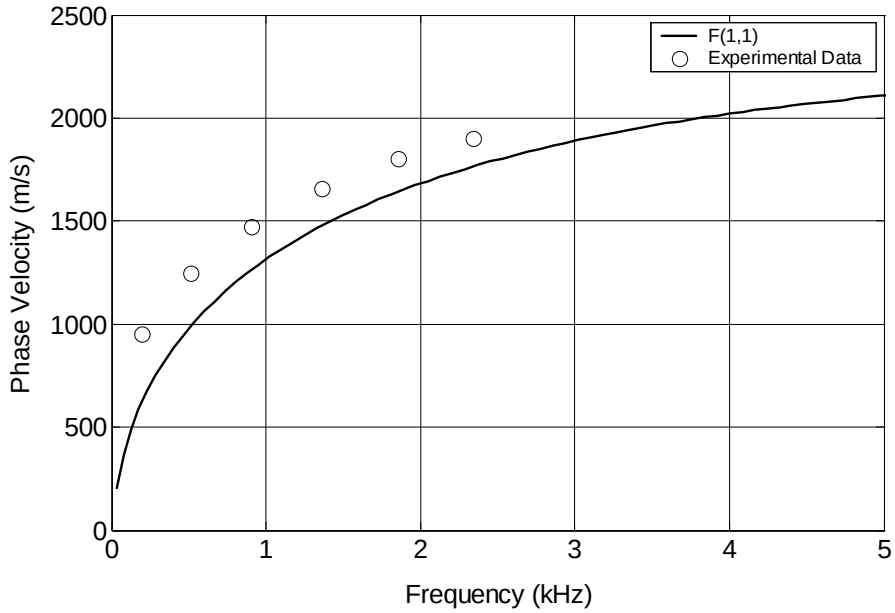

Figure B-4: Prototype Pile C355-2430, lateral impact results for 180-degree orientation, longitudinal phase velocity - frequency data superimposed on numerically-determined F(1,1) branch

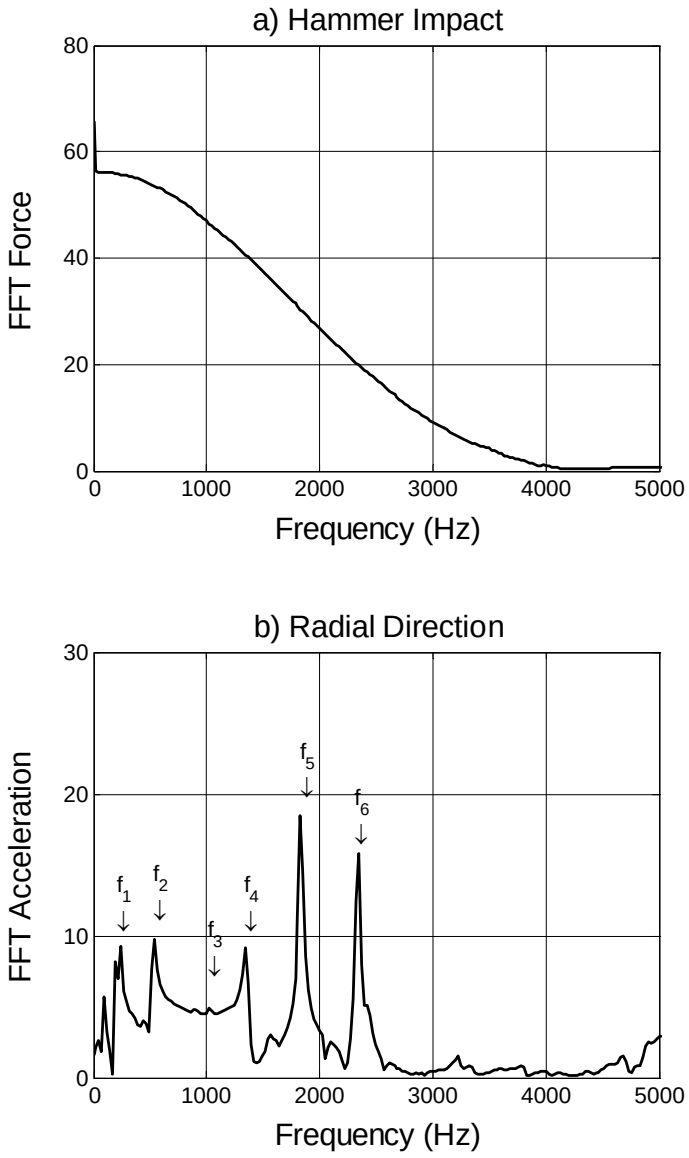

Figure B-5: Prototype Pile C355-2430, lateral impact results for 0-degree orientation, radial direction

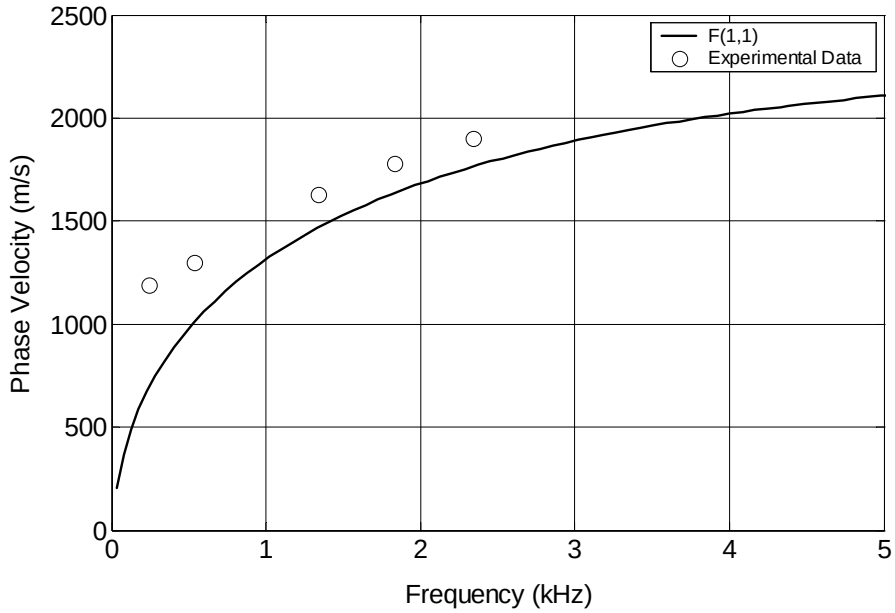

Figure B-6: Prototype Pile C355-2430, lateral impact results for 0-degree orientation, radial phase velocity - frequency data superimposed on numerically-determined F(1,1) branch

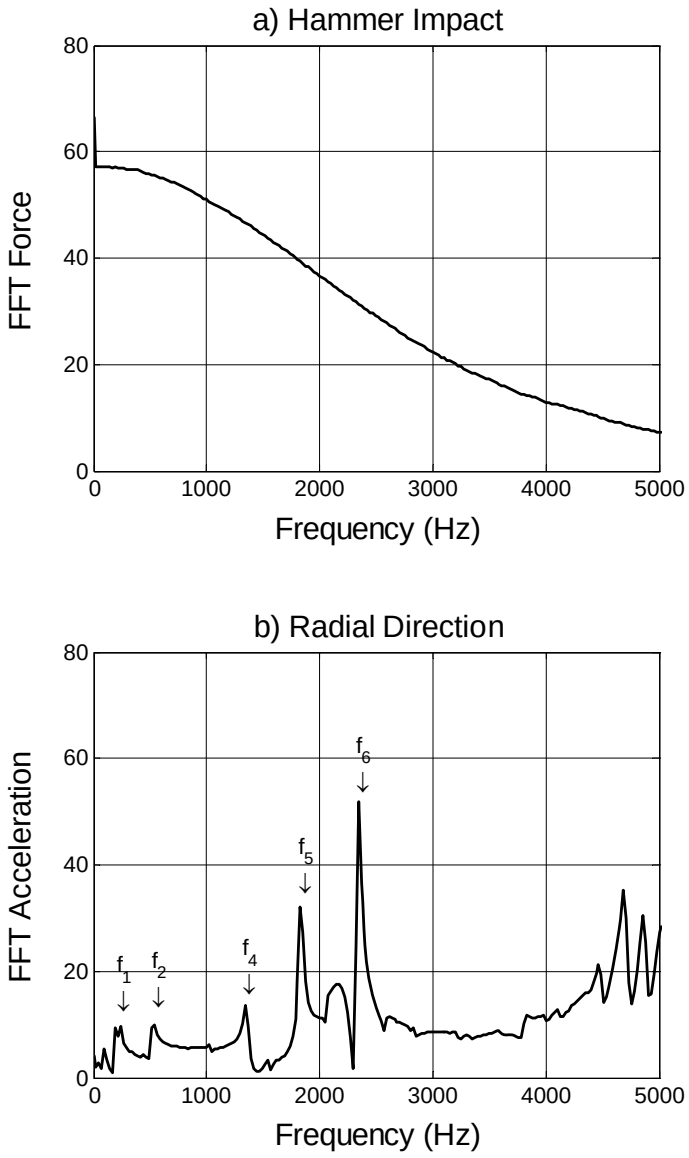

Figure B-7: Prototype Pile C355-2430, lateral impact results for 180-degree orientation, radial direction

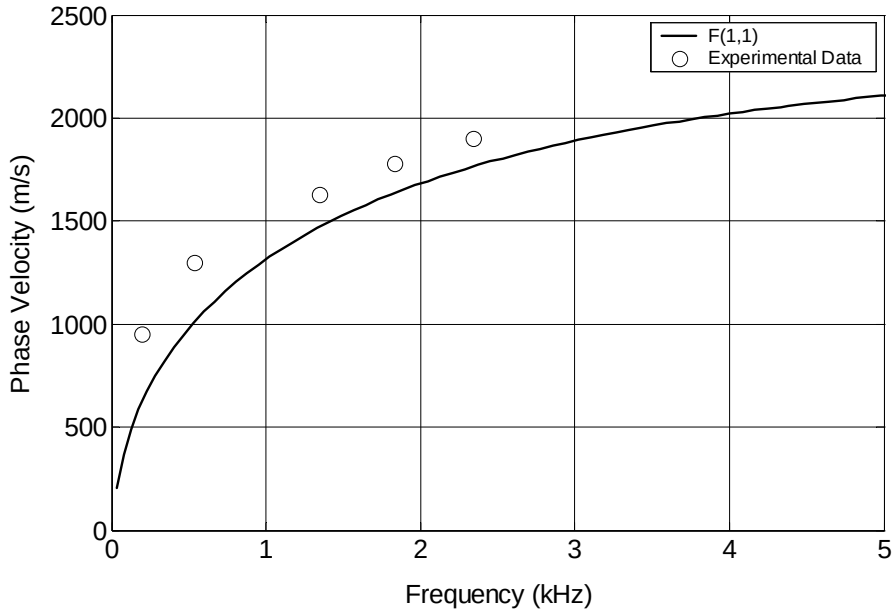

Figure B-8: Prototype Pile C355-2430, lateral impact results for 180-degree orientation, radial phase velocity - frequency data superimposed on numerically-determined F(1,1) branch

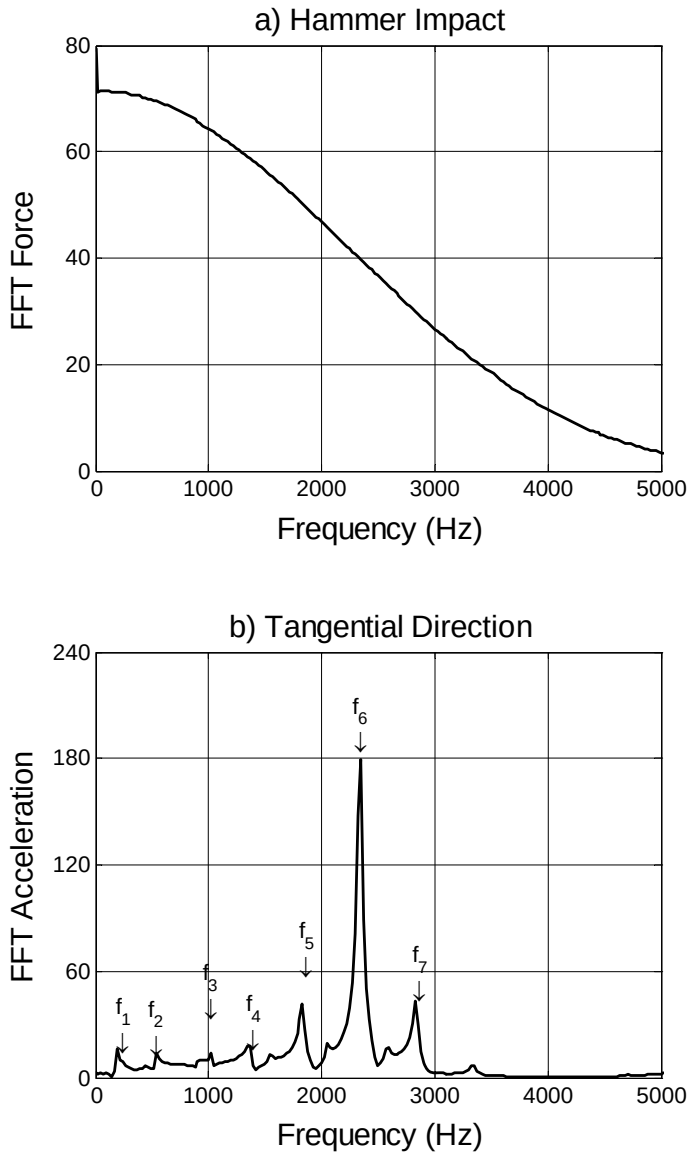

Figure B-9: Prototype Pile C355-2430, lateral impact results for 90-degree orientation, tangential direction

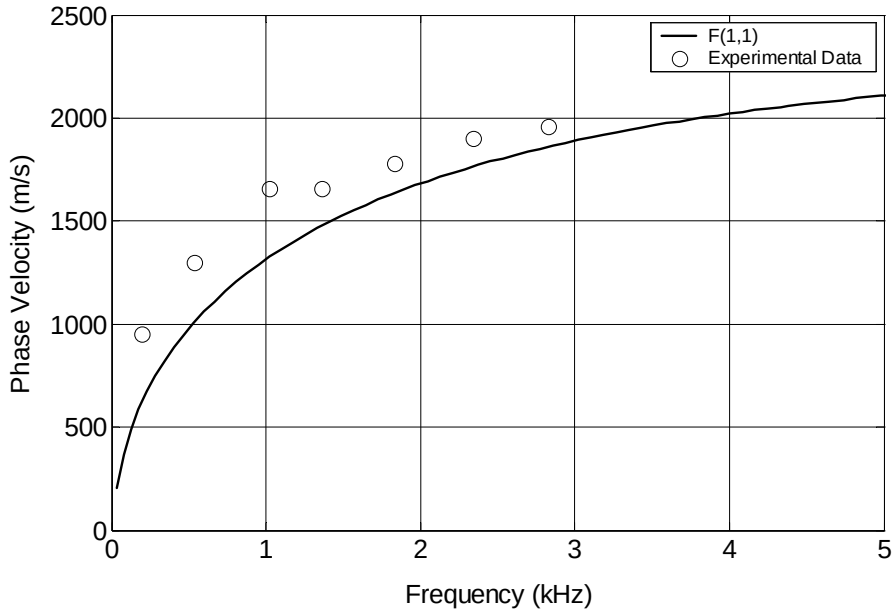

Figure B-10: Prototype Pile C355-2430, lateral impact results for 90-degree orientation, tangential phase velocity - frequency data superimposed on numerically-determined F(1,1) branch

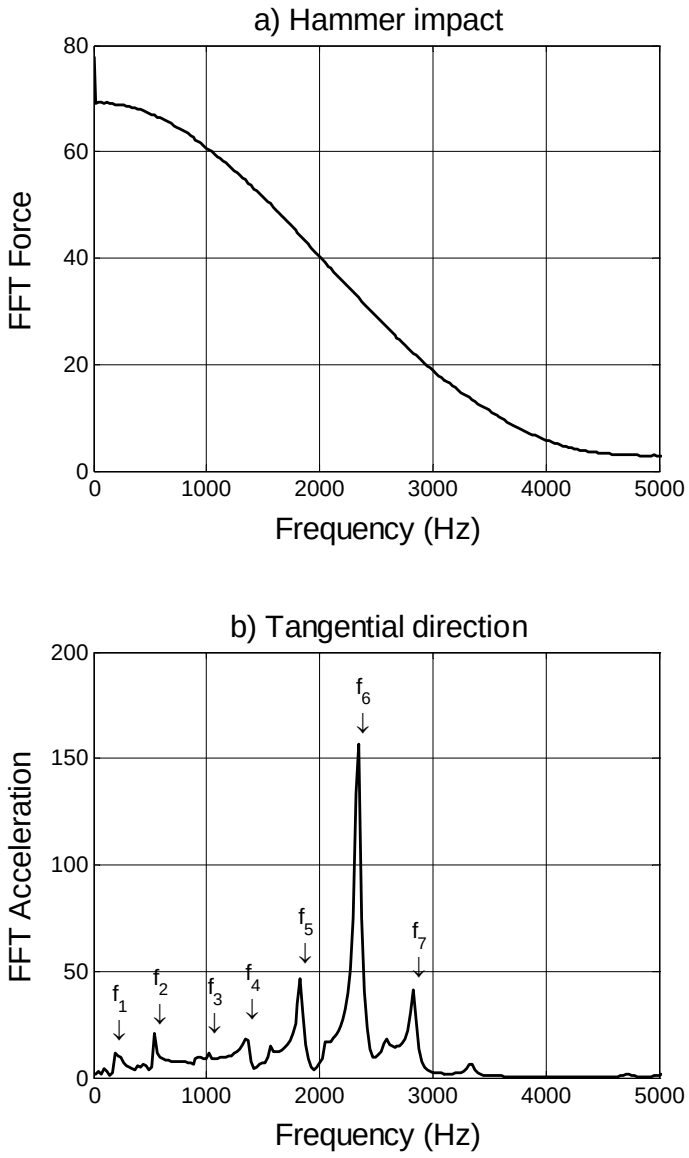

Figure B-11: Prototype Pile C355-2430, lateral impact results for 270-degree orientation

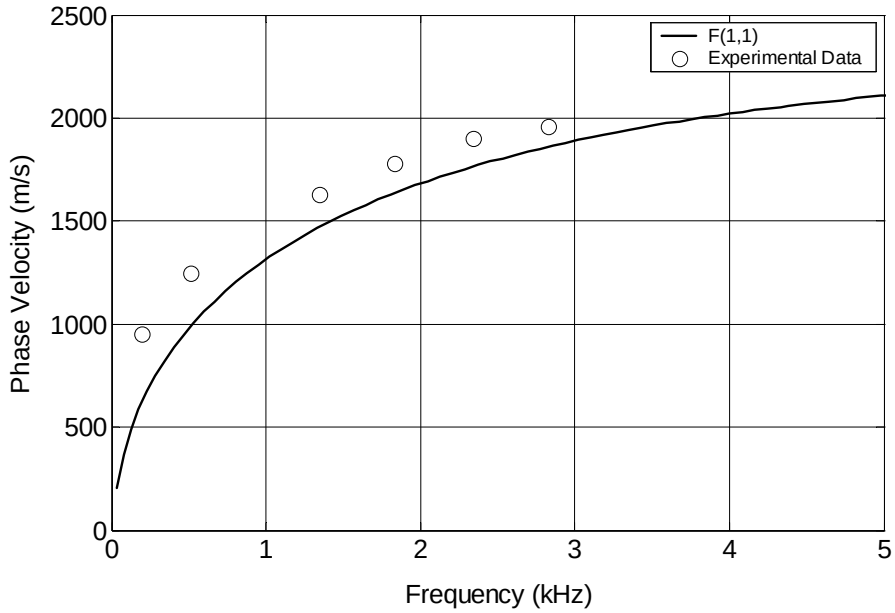

Figure B-12: Prototype Pile C355-2430, lateral impact results for 270-degree orientation, tangential phase velocity - frequency data superimposed on numerically-determined F(1,1) branch

Table B-1: Prototype Pile C355-2430, frequencies and phase velocities determined from lateral impact tests

Longitudinal direction				Radial direction				Tangential direction			
0-degree face		180-degree face		0-degree face		180-degree face		90-degree face		270-degree face	
f (Hz)	c_p (m/s)	f (Hz)	c_p (m/s)	f (Hz)	c_p (m/s)	f (Hz)	c_p (m/s)	f (Hz)	c_p (m/s)	f (Hz)	c_p (m/s)
220	1070	195	950	245	1190	245	1190	195	950	195	950
515	1250	515	1250	535	1300	535	1300	535	1300	535	1300
905	1470	905	1470	1025	1660	N/I	N/I	1025	1660	1025	1660
1365	1660	1365	1660	1345	1630	1345	1630	1365	1660	1345	1630
1830	1780	1855	1800	1830	1780	1830	1780	1830	1780	1830	1780
2345	1900	2345	1900	2345	1900	2345	1900	2345	1900	2345	1900
N/I	N/I	N/I	N/I	N/I	N/I	N/I	N/I	2830	1960	2830	1960

Note: N/I indicates that the harmonic was not identified in the specified test and measurement direction.

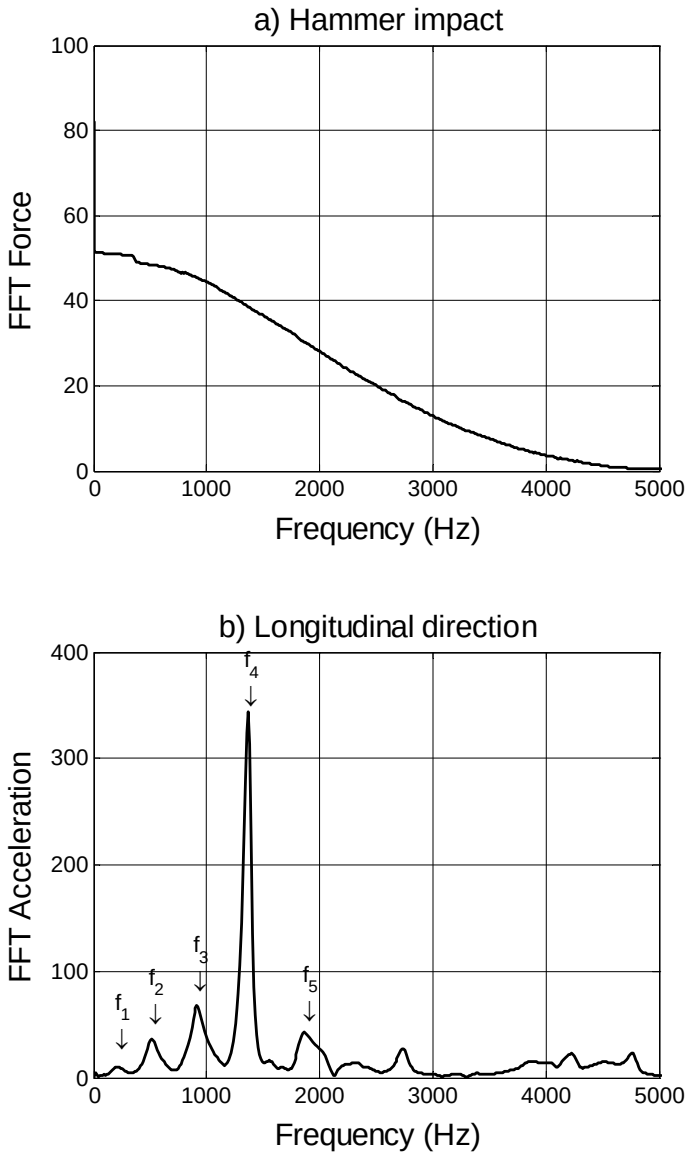

Figure B-13: Prototype Pile C355-2430, lateral impact results for 0-degree orientation, longitudinal direction

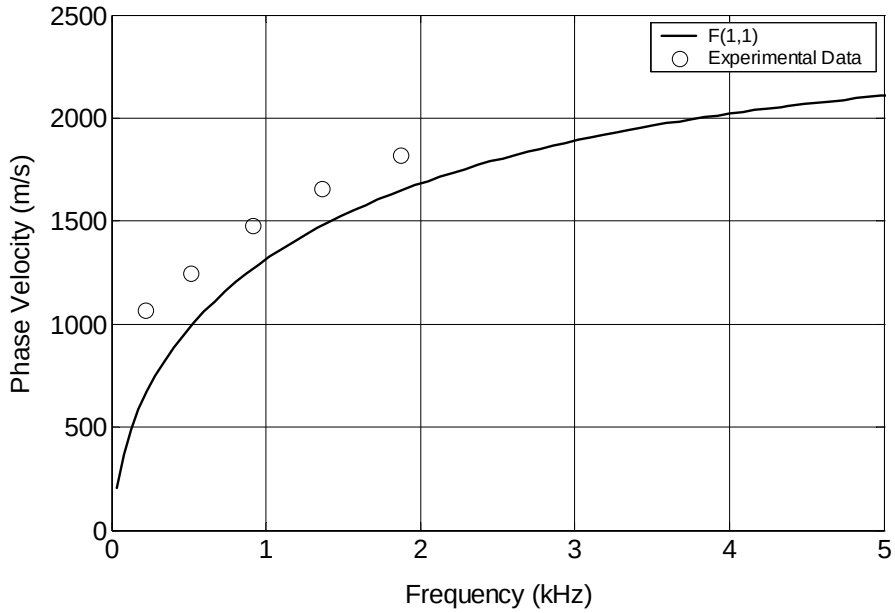

Figure B-14: Prototype Pile C355-2430, lateral impact results for 0-degree orientation, longitudinal phase velocity - frequency data superimposed on numerically-determined F(1,1) branch

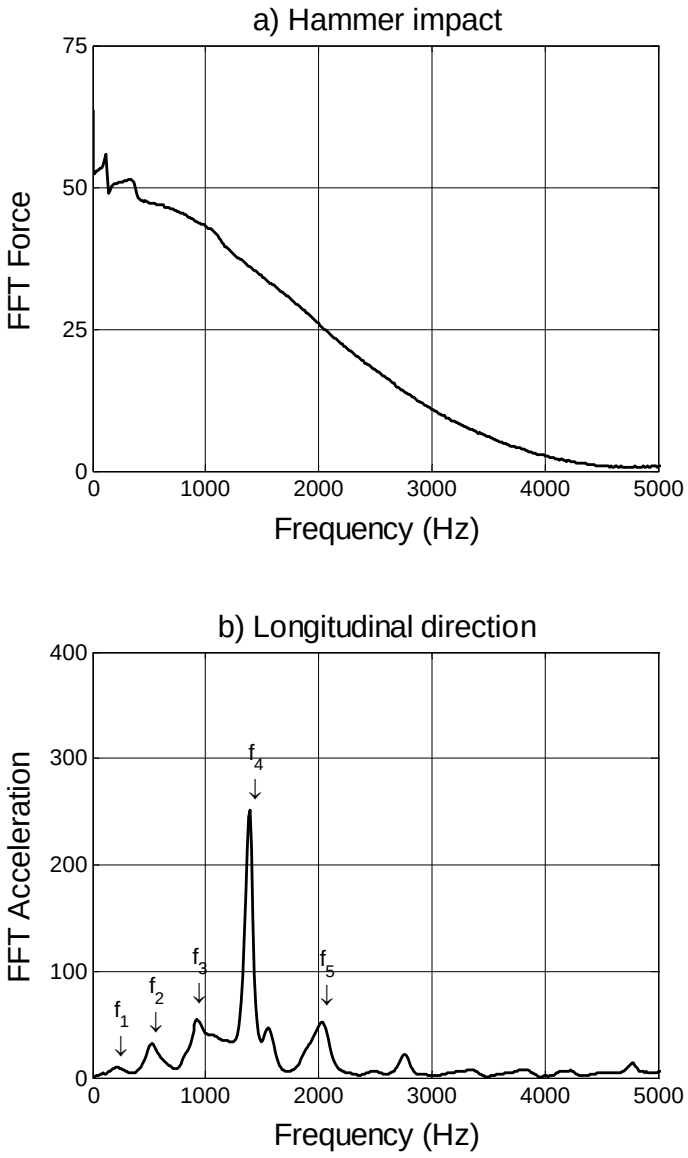

Figure B-15: Prototype Pile C355-2430, lateral impact results for 180-degree orientation, longitudinal direction

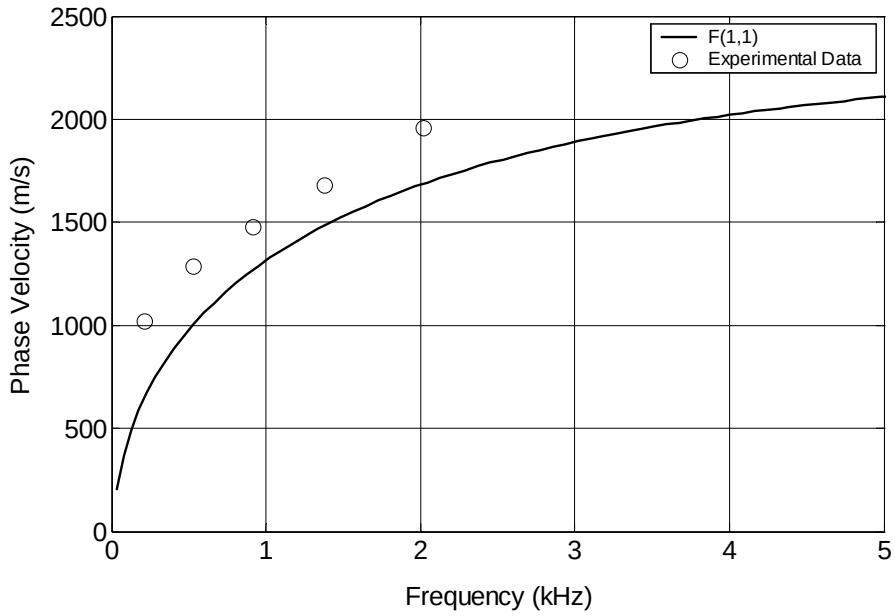

Figure B-16: Prototype Pile C355-2430, lateral impact results for 180-degree orientation, longitudinal phase velocity - frequency data superimposed on numerically-determined F(1,1) branch

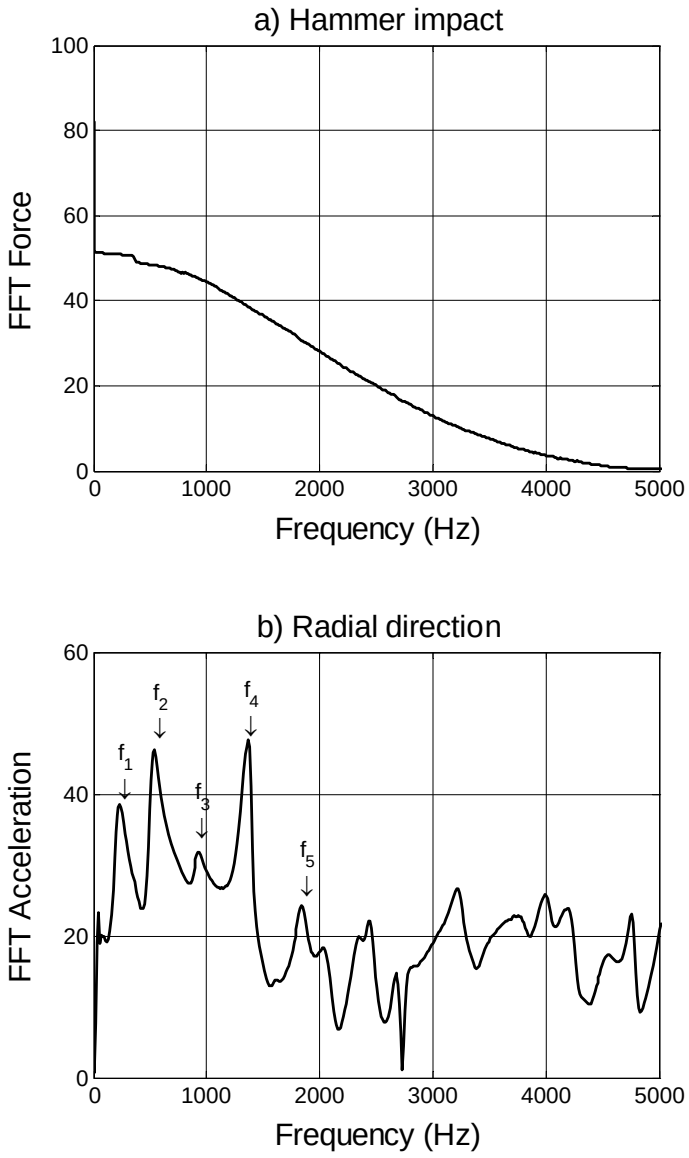

Figure B-17: Prototype Pile C355-2430, lateral impact results for 0-degree orientation, radial direction

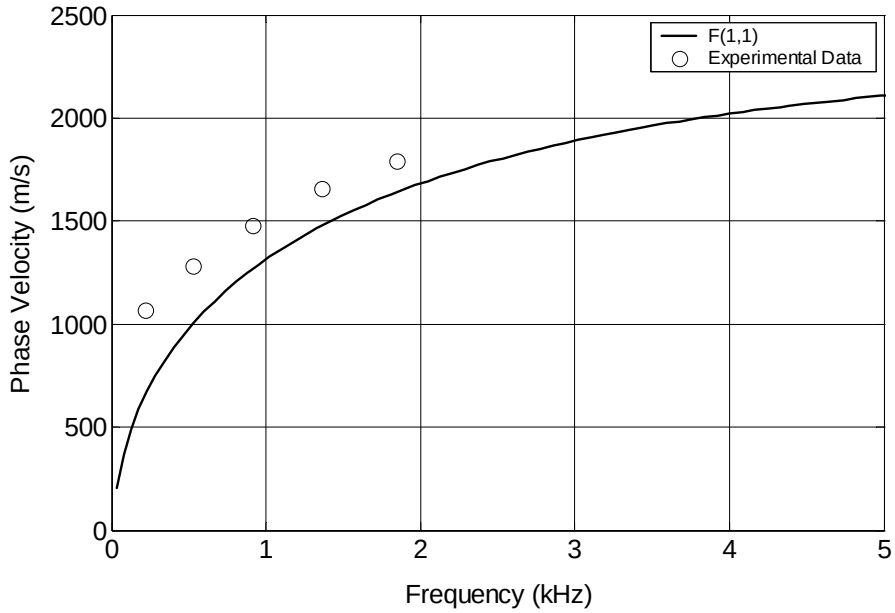

Figure B-18: Prototype Pile C355-2430, lateral impact results for 0-degree orientation, radial phase velocity - frequency data superimposed on numerically-determined F(1,1) branch

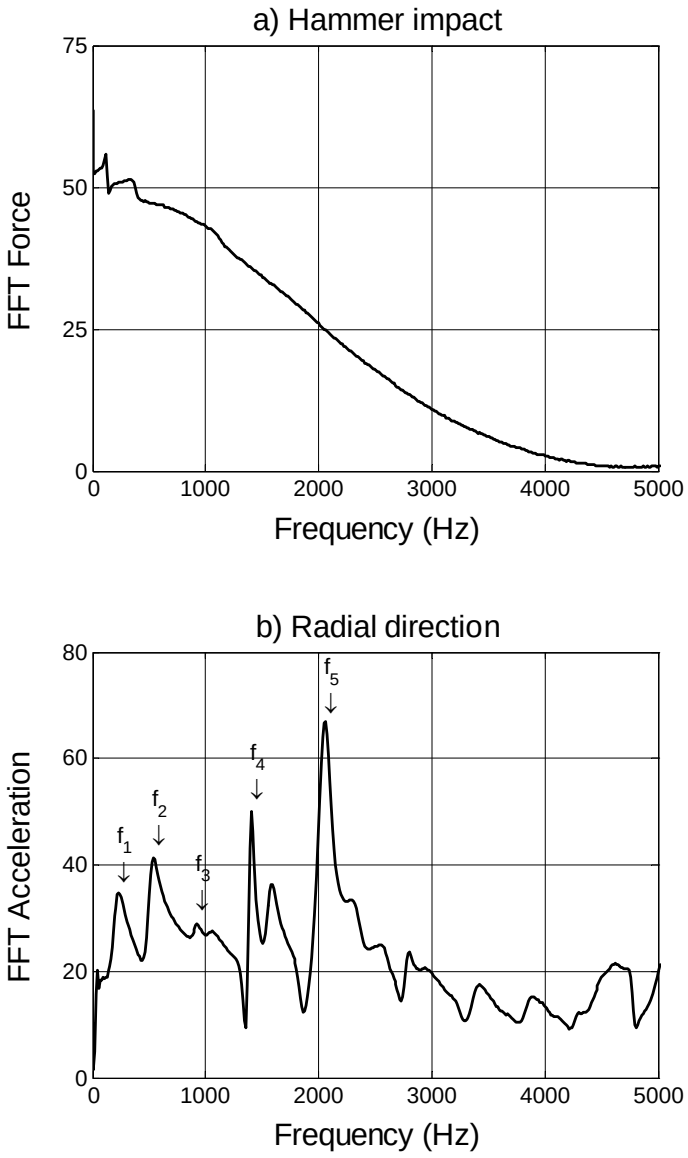

Figure B-19: Prototype Pile C355-2430, lateral impact results for 180-degree orientation, radial direction

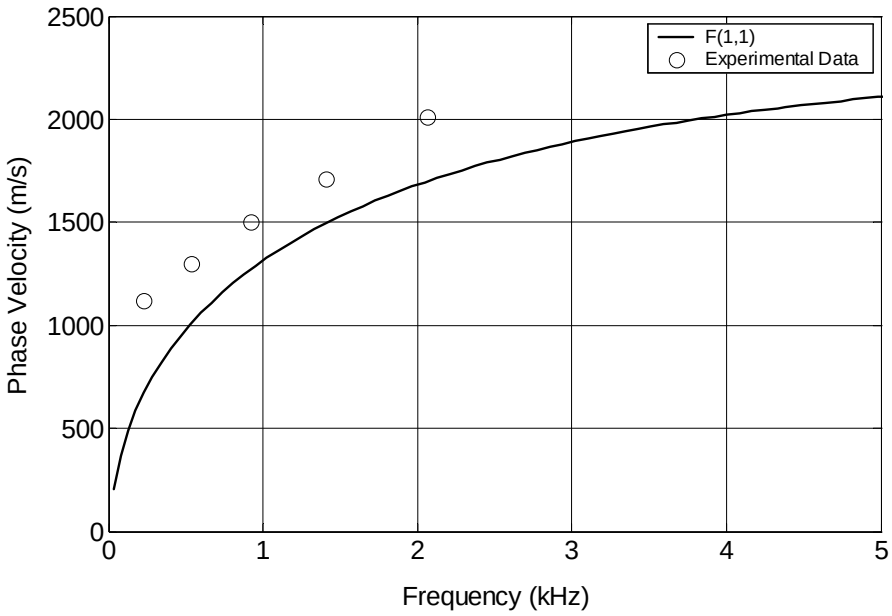

Figure B-20: Prototype Pile C355-2430, lateral impact results for 180-degree orientation, radial phase velocity - frequency data superimposed on numerically-determined F(1,1) branch

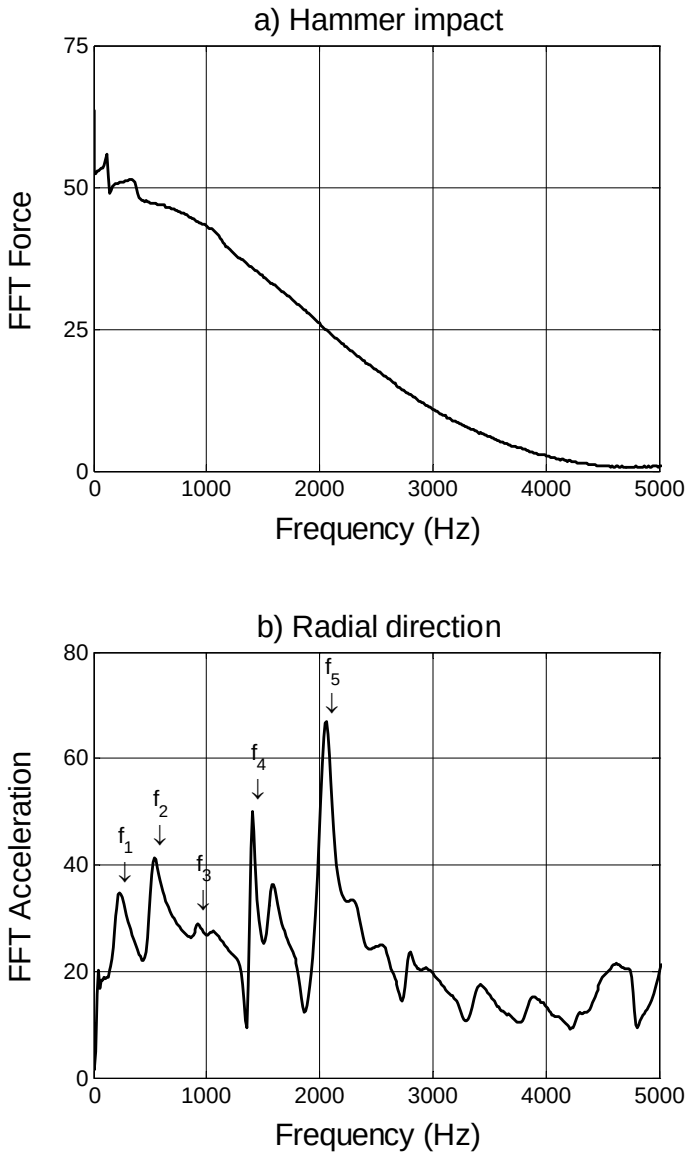

Figure B-21: Prototype Pile C355-2430, lateral impact results for 90-degree orientation, tangential direction

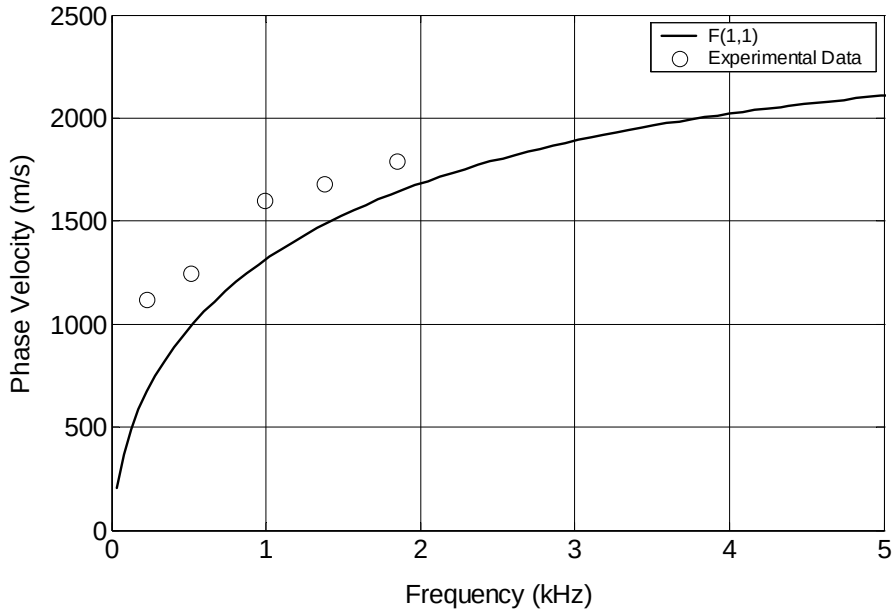

Figure B-22: Prototype Pile C355-2430, lateral impact results for 90-degree orientation, tangential phase velocity - frequency data superimposed on numerically-determined F(1,1) branch

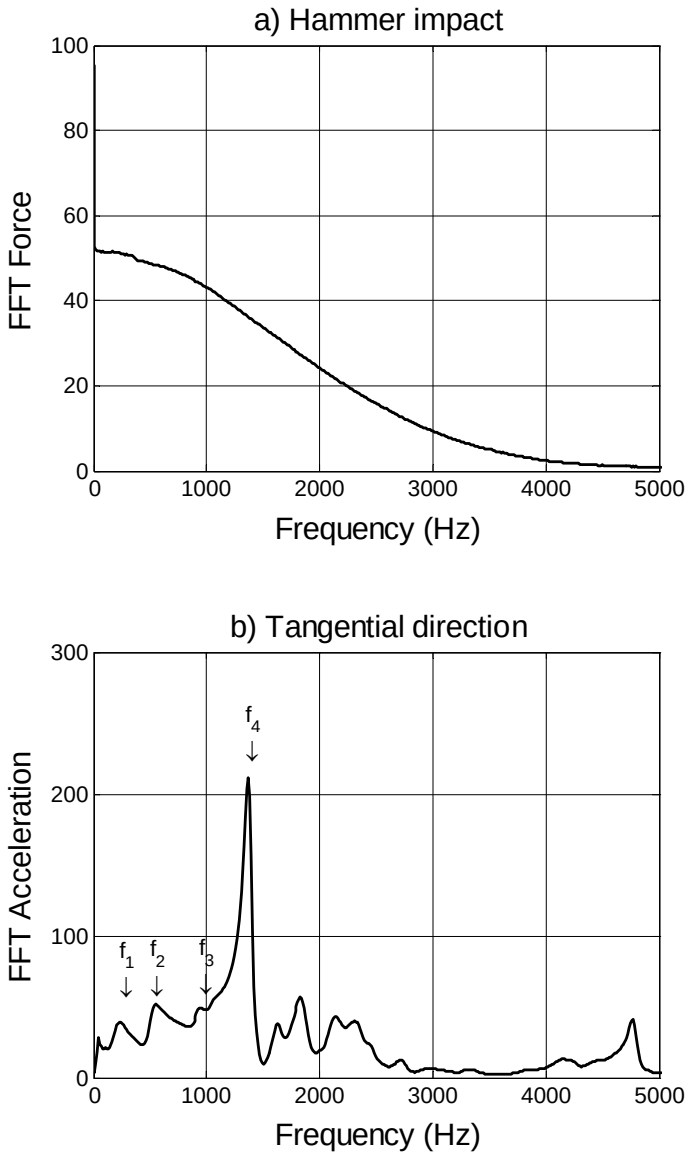

Figure B-23: Prototype Pile C355-2430, lateral impact results for 90-degree orientation, tangential direction

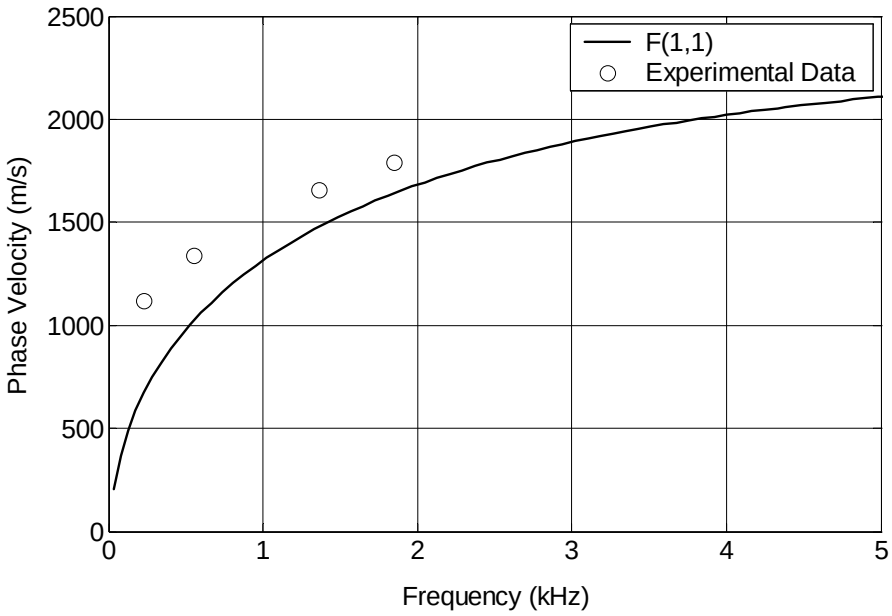

Figure B-24: Prototype Pile C355-2430, lateral impact results for 270-degree orientation, tangential phase velocity - frequency data superimposed on numerically-determined F(1,1) branch

Table B2: Prototype Pile C355-2430, frequencies and phase velocities determined from lateral impact tests

Longitudinal direction				Radial direction				Tangential direction			
0-degree face		180-degree face		0-degree face		180-degree face		90-degree face		270-degree face	
f (Hz)	c_p (m/s)	f (Hz)	c_p (m/s)	f (Hz)	c_p (m/s)	f (Hz)	c_p (m/s)	f (Hz)	c_p (m/s)	f (Hz)	c_p (m/s)
220	1070	210	1020	220	1070	230	1120	230	1120	230	1120
515	1250	530	1290	525	1280	535	1300	515	1250	550	1340
915	1480	915	1480	915	1480	925	1500	990	1600	N/I	N/I
1365	1660	1380	1680	1365	1660	1405	1710	1380	1680	1365	1660
1870	1820	2015	1960	1845	1790	2065	2010	1845	1790	1845	1790
N/I	N/I	N/I	N/I	N/I	N/I	N/I	N/I	2830	1960	2830	1960

Note: N/I indicates that the harmonic was not identified in the specified test and measurement direction.

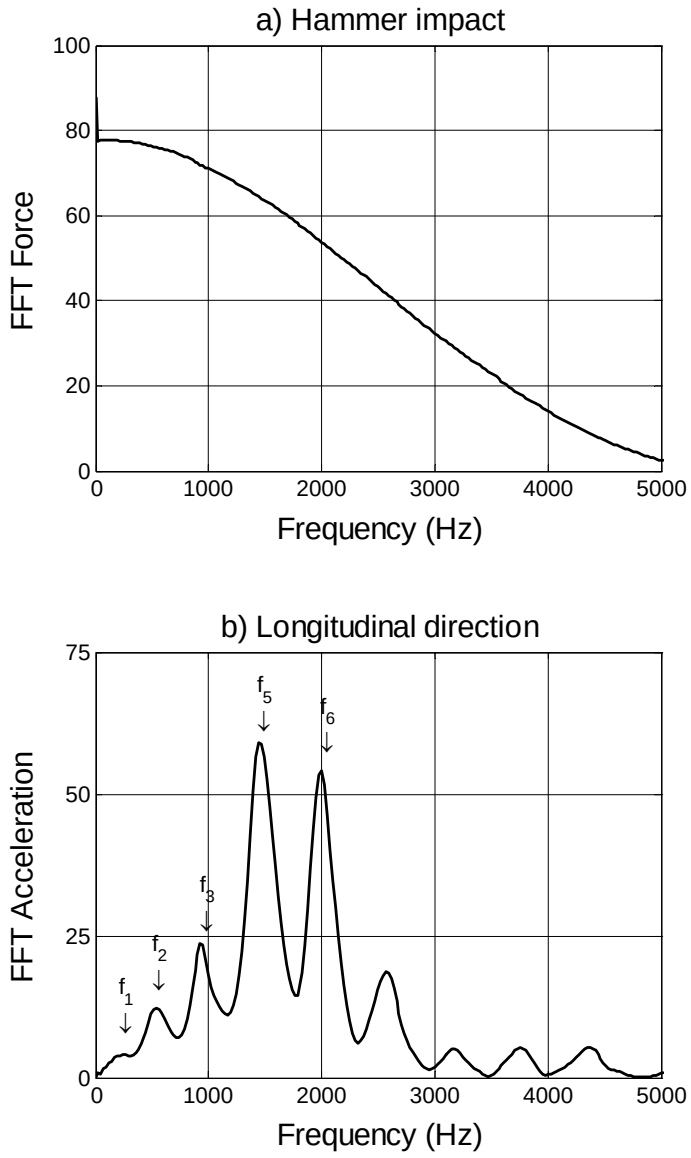

Figure B-25: prototype pile B254-2220, lateral impact results for 0-degree orientation, longitudinal direction

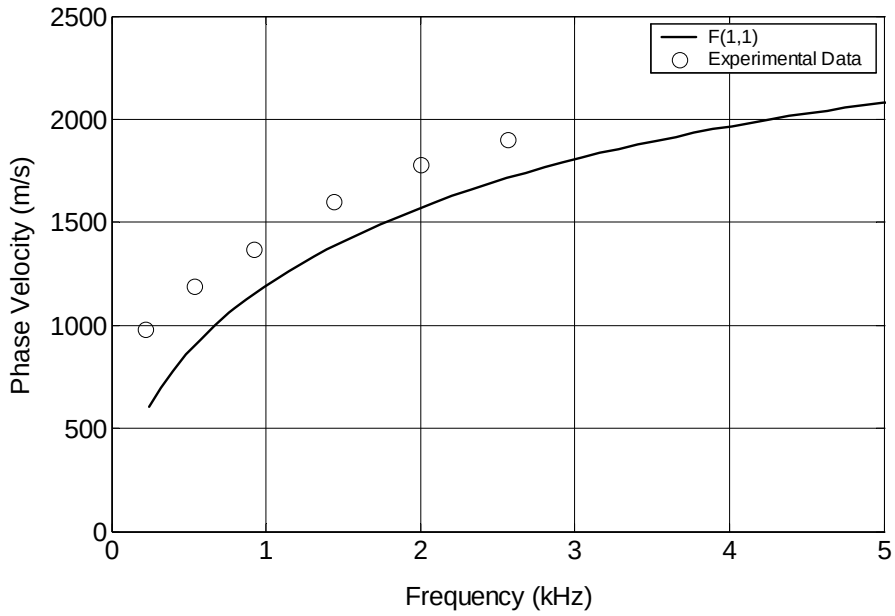

Figure B-26: Prototype Pile B254-2220, lateral impact results for 0-degree orientation, longitudinal phase velocity - frequency data superimposed on numerically-determined F(1,1) branch

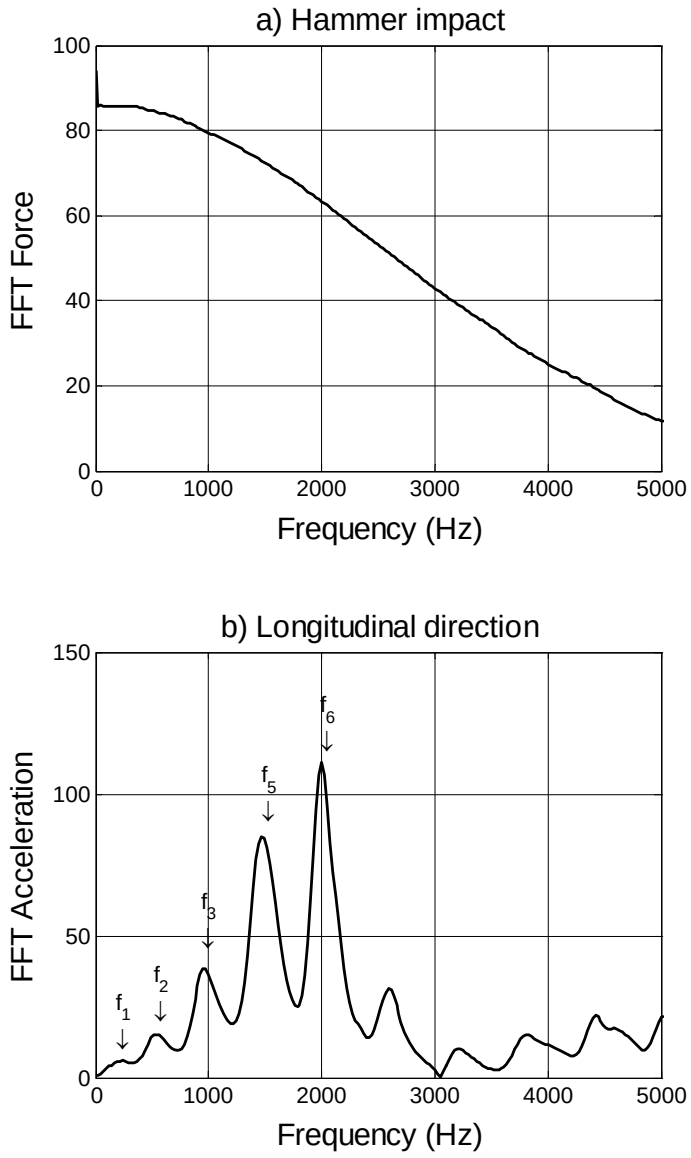

Figure B-27: prototype pile B254-2220, lateral impact results for 180-degree orientation, longitudinal direction

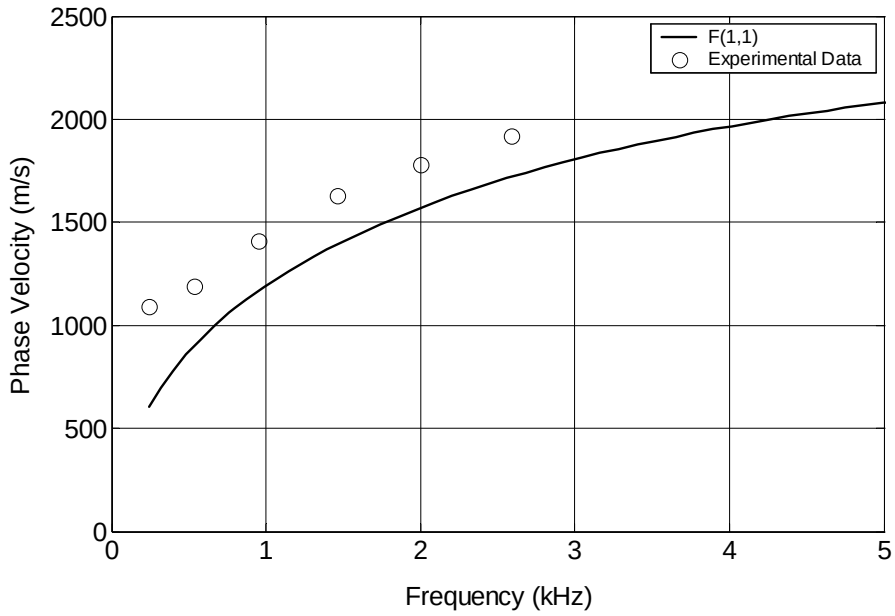

Figure B-28: Prototype Pile B254-2220, lateral impact results for 180-degree orientation, longitudinal phase velocity - frequency data superimposed on numerically-determined F(1,1) branch

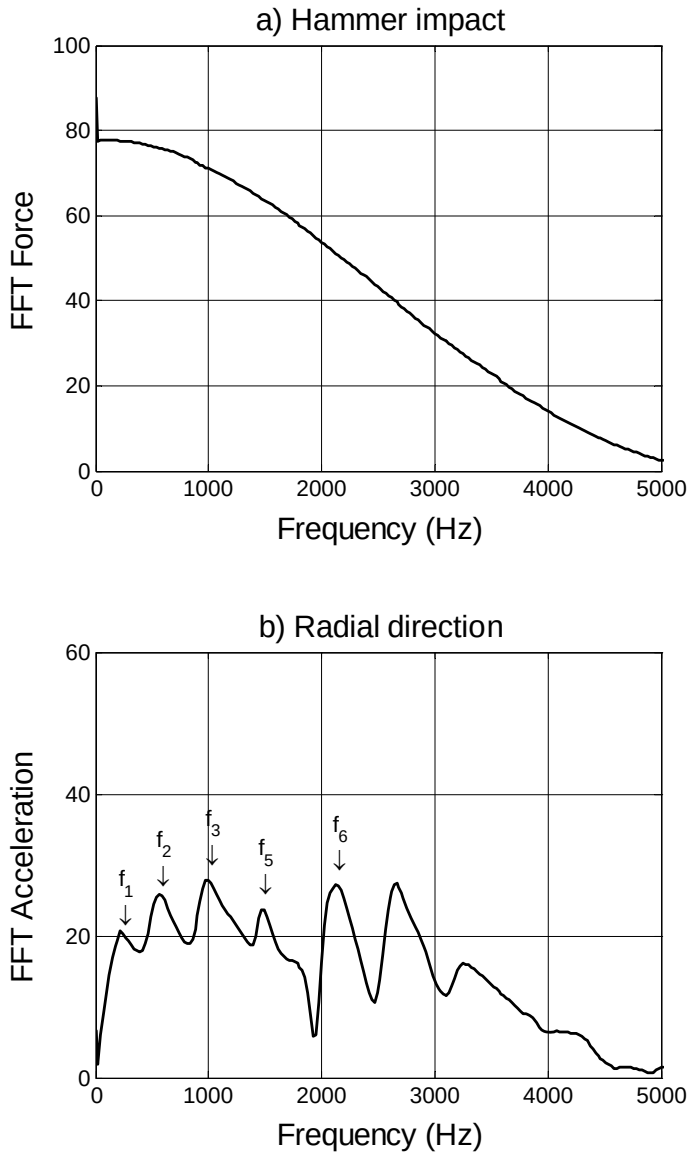

Figure B-29: prototype pile B254-2220, lateral impact results for 0-degree orientation, radial direction

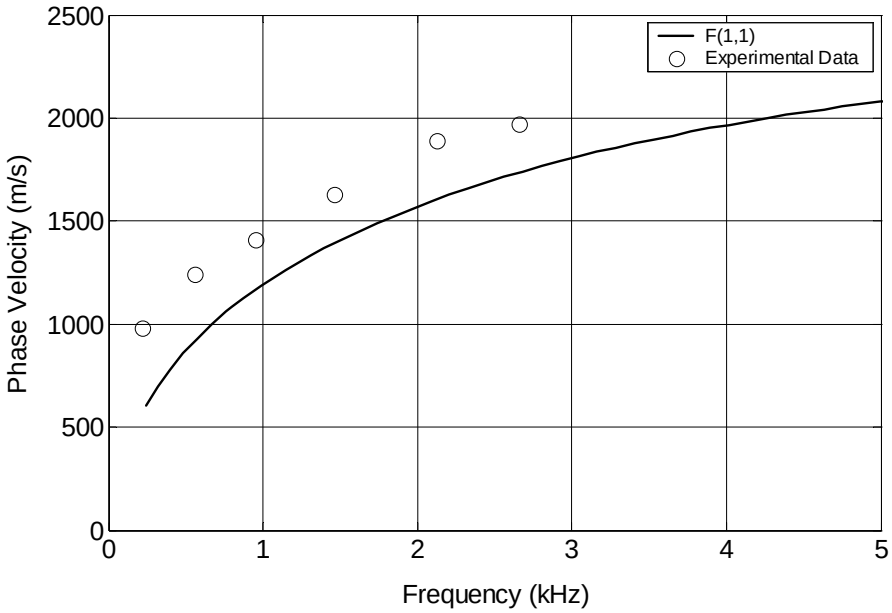

Figure B-30: Prototype Pile B254-2220, lateral impact results for 0-degree orientation, radial phase velocity - frequency data superimposed on numerically-determined F(1,1) branch

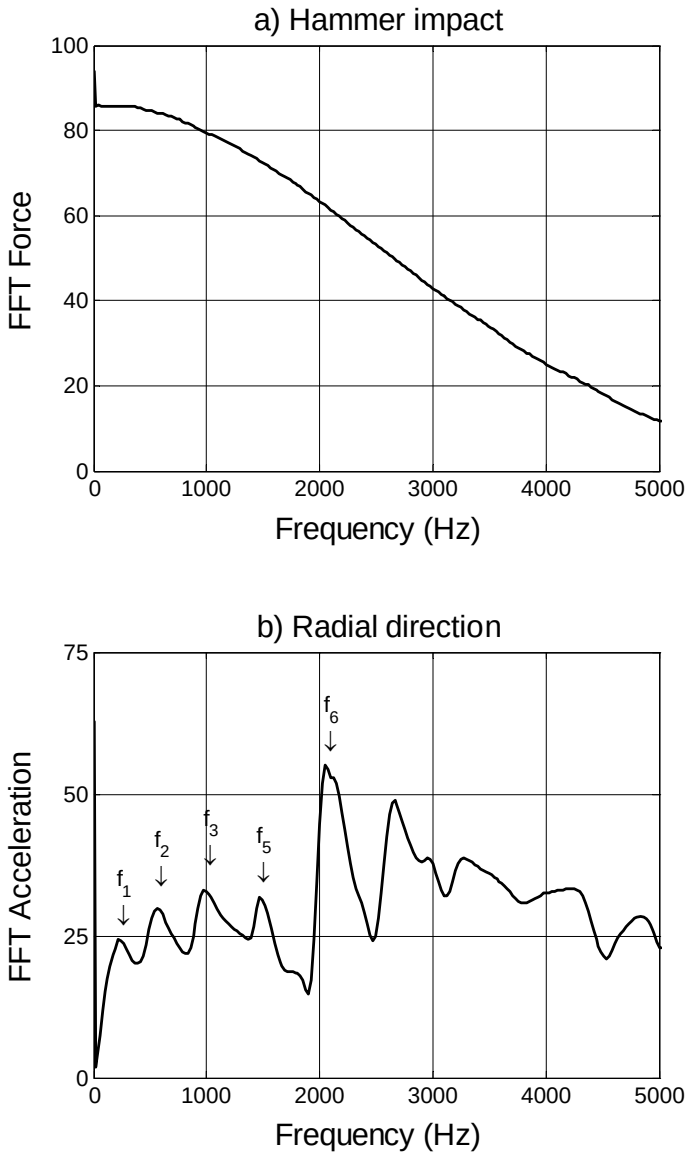

Figure B-31: prototype pile B254-2220, lateral impact results for 180-degree orientation, radial direction

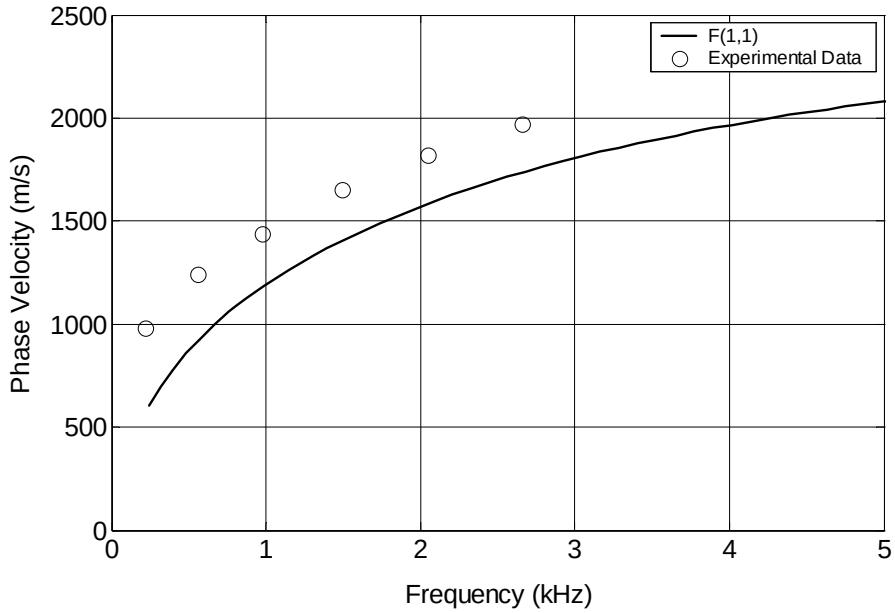

Figure B-32: Prototype Pile B254-2220, lateral impact results for 180-degree orientation, radial phase velocity - frequency data superimposed on numerically-determined F(1,1) branch

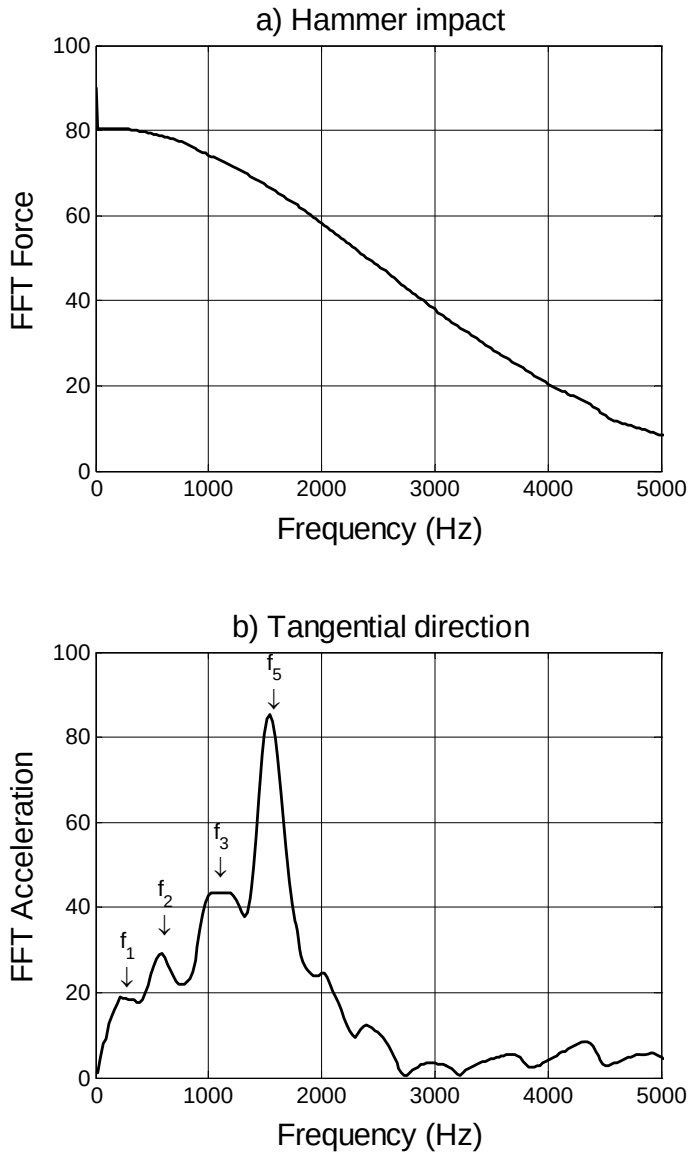

Figure B-33: prototype pile B254-2220, lateral impact results for 90-degree orientation, tangential direction

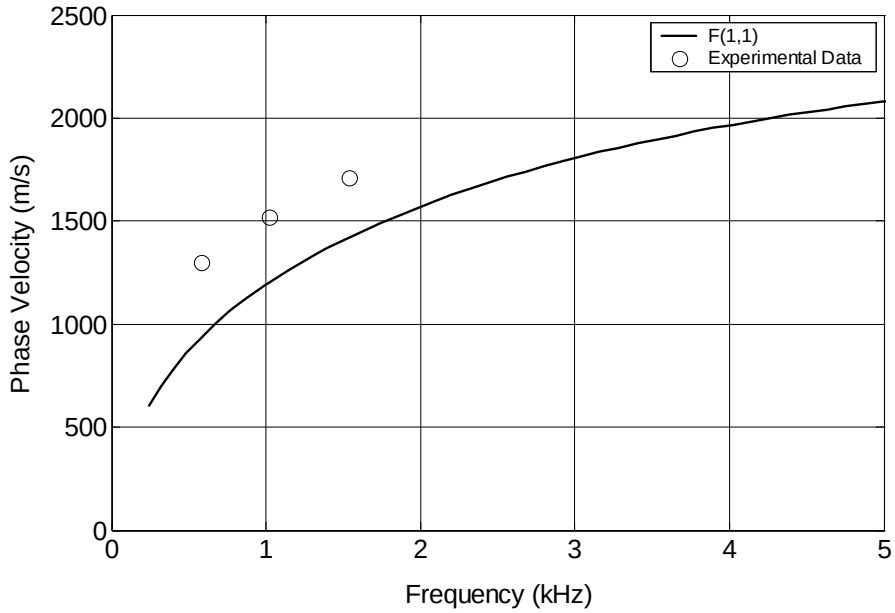

Figure B-34: Prototype Pile B254-2220, lateral impact results for 90-degree orientation, tangential phase velocity - frequency data superimposed on numerically-determined F(1,1) branch

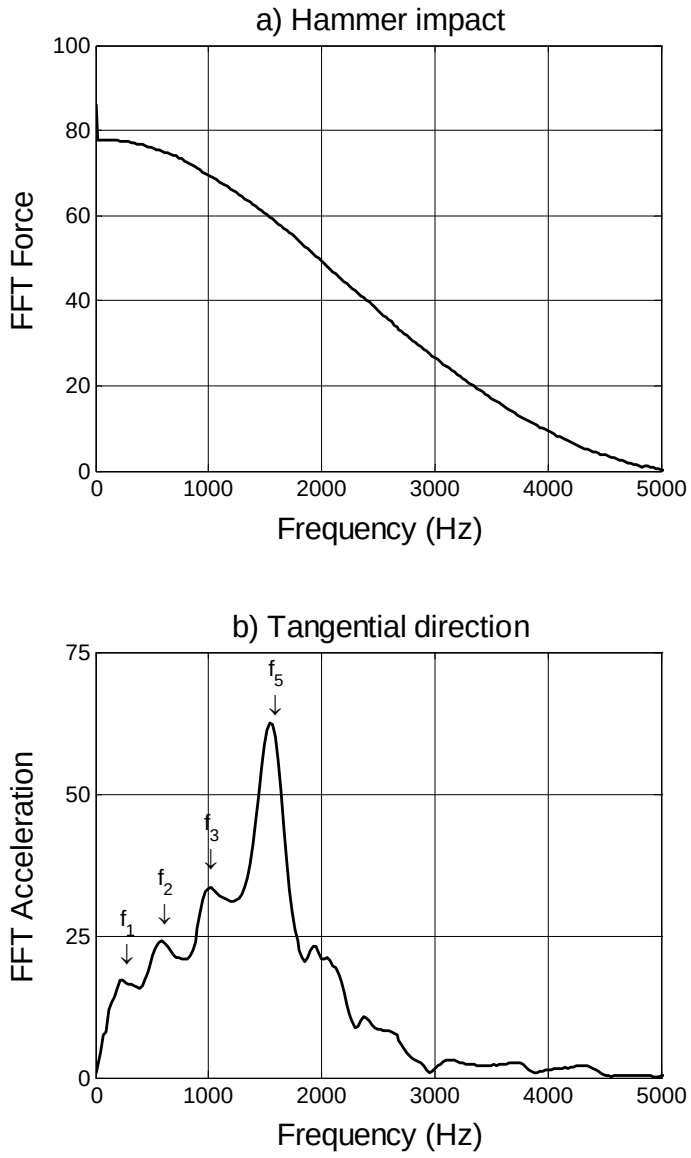

Figure B-35: prototype pile B254-2220, lateral impact results for 270-degree orientation, tangential direction

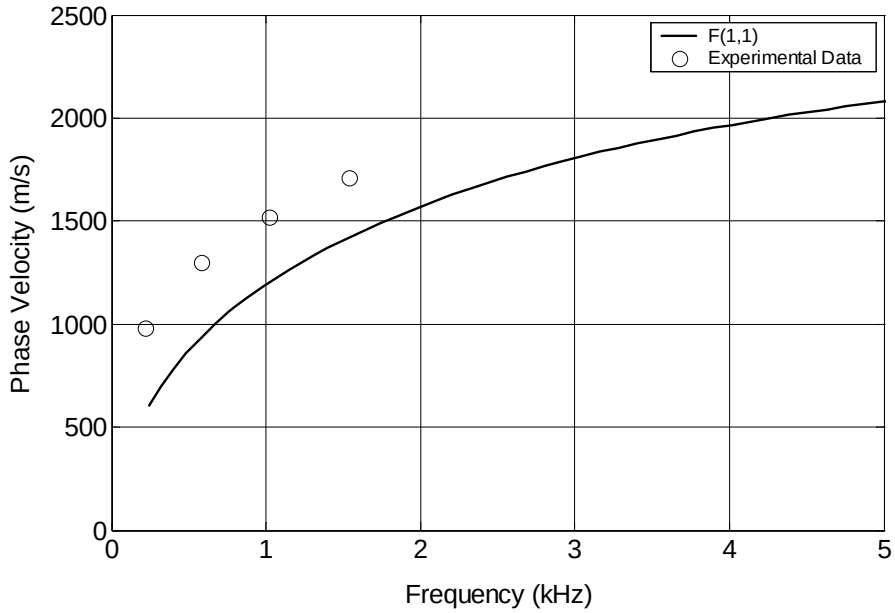

Figure B-36: Prototype Pile B254-2220, lateral impact results for 270-degree orientation, tangential phase velocity - frequency data superimposed on numerically-determined F(1,1) branch

Table B-3: Prototype pile B254-2220, frequencies and phase velocities determined from lateral impact tests

Longitudinal direction				Radial direction				Tangential direction			
0-degree face		180-degree face		0-degree face		180-degree face		90-degree face		270-degree face	
f (Hz)	c_p (m/s)	f (Hz)	c_p (m/s)	f (Hz)	c_p (m/s)	f (Hz)	c_p (m/s)	f (Hz)	c_p (m/s)	f (Hz)	c_p (m/s)
220	980	245	1090	220	980	220	980	N/I	N/I	220	980
535	1190	535	1190	560	1240	560	1240	585	1300	585	1300
925	1370	950	1410	950	1410	975	1440	1025	1520	1025	1520
1440	1600	1465	1630	1465	1630	1490	1650	1540	1710	1540	1710
2000	1780	2000	1780	2125	1890	2050	1820	N/I	N/I	N/I	N/I
220	980	245	1090	220	980	220	980	N/I	N/I	220	980
2565	1900	2590	1920	2660	1970	2660	1970	N/I	N/I	N/I	N/I

Note: N/I indicates that the harmonic was not identified in the specified test and measurement direction.

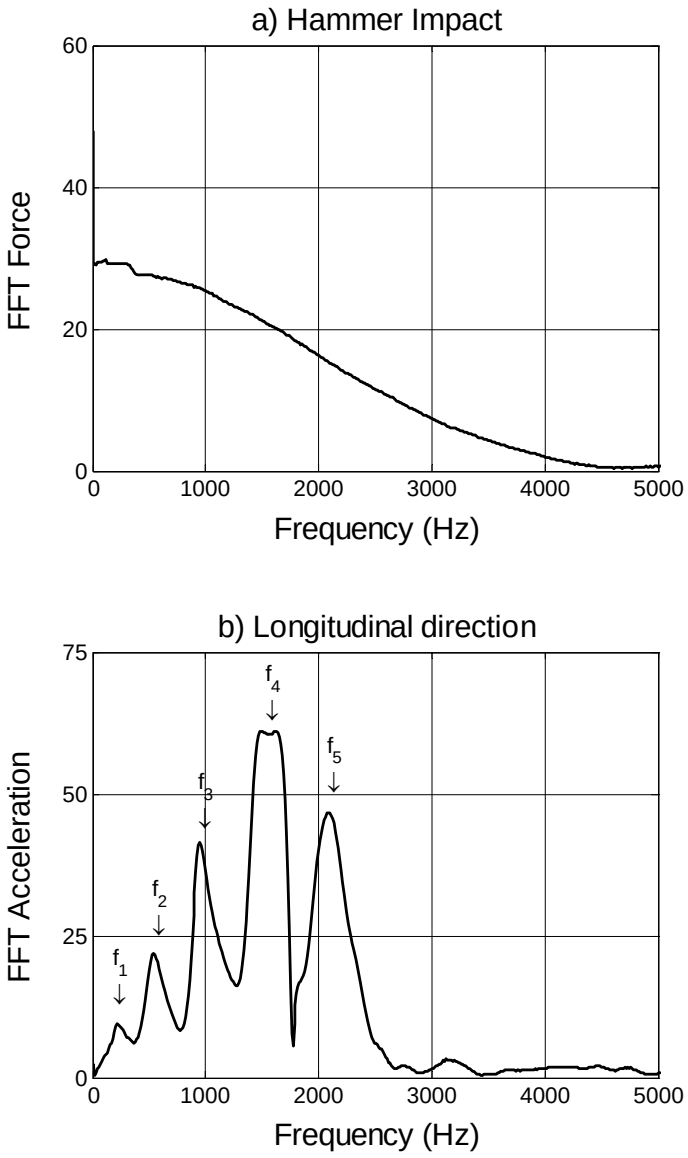

Figure B-37: prototype pile B308-2400, lateral impact results for 0-degree orientation, longitudinal direction

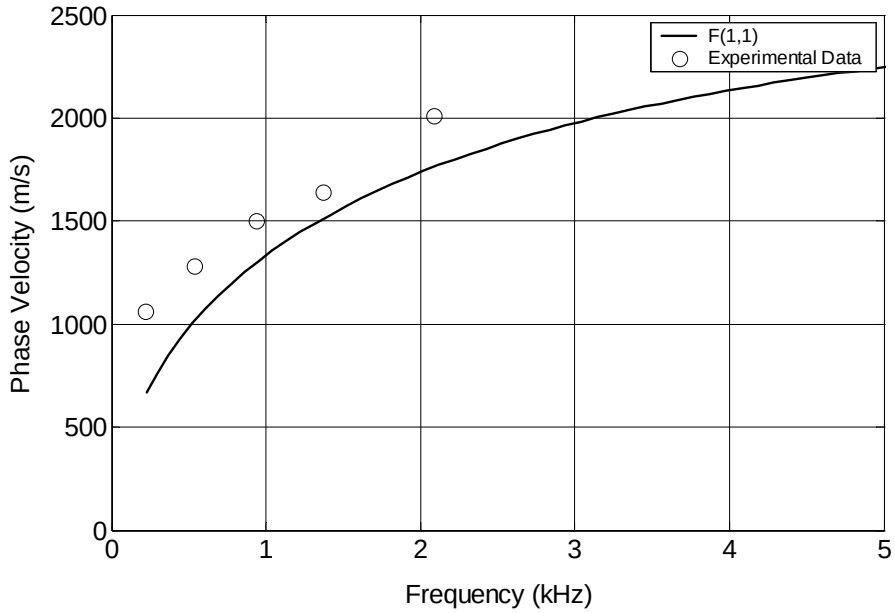

Figure B-38: Prototype Pile B308-2400, lateral impact results for 0-degree orientation, longitudinal phase velocity - frequency data superimposed on numerically-determined F(1,1) branch

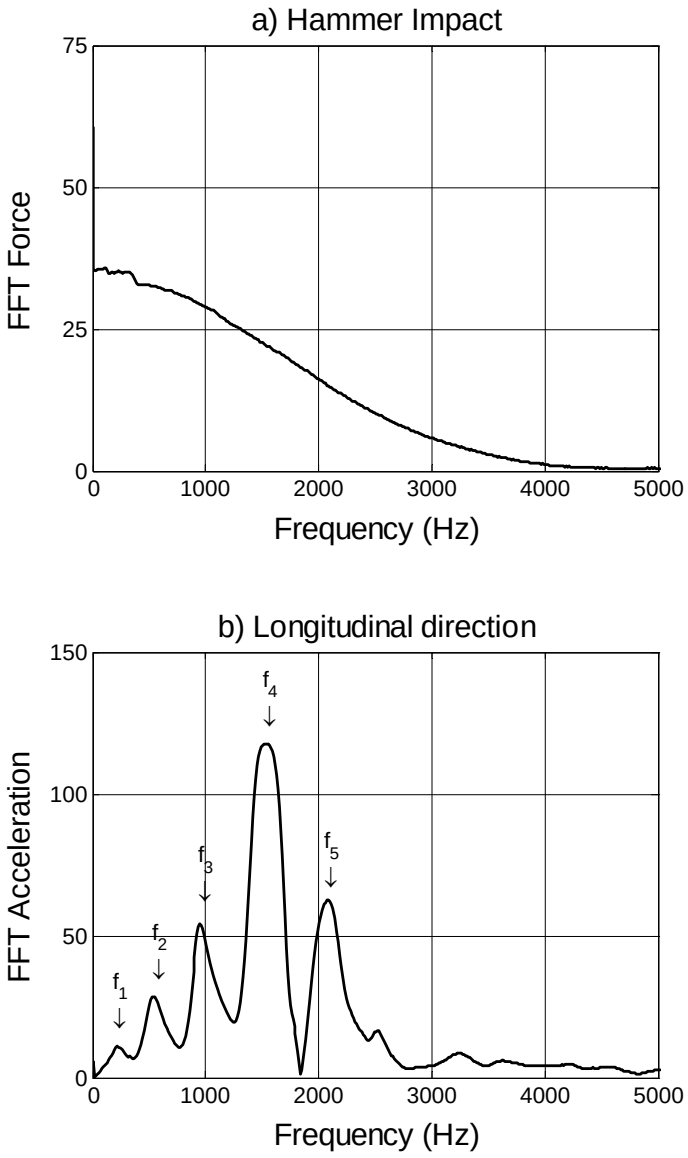

Figure B-39: prototype pile B308-2400, lateral impact results for 180-degree orientation, longitudinal direction

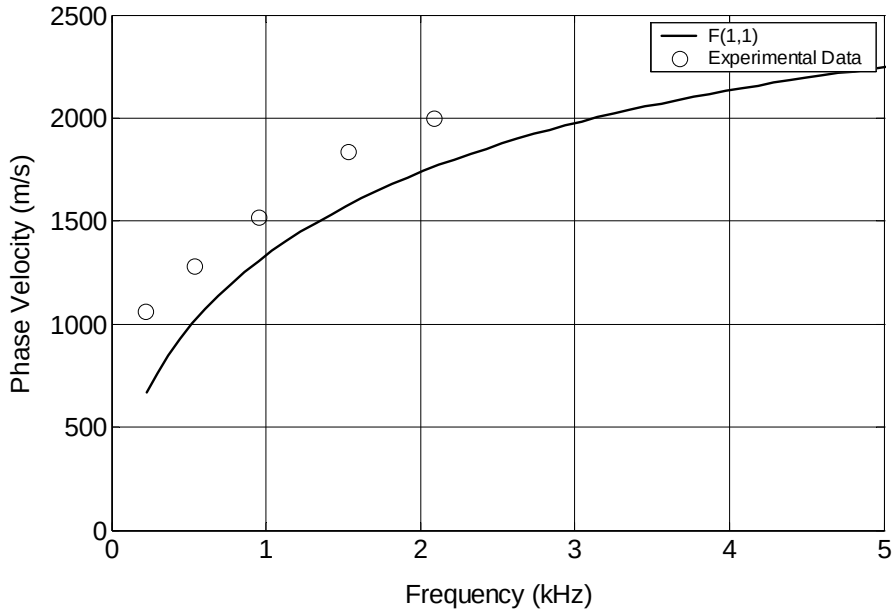

Figure B-40: Prototype Pile B308-2400, lateral impact results for 180-degree orientation, longitudinal phase velocity - frequency data superimposed on numerically-determined F(1,1) branch

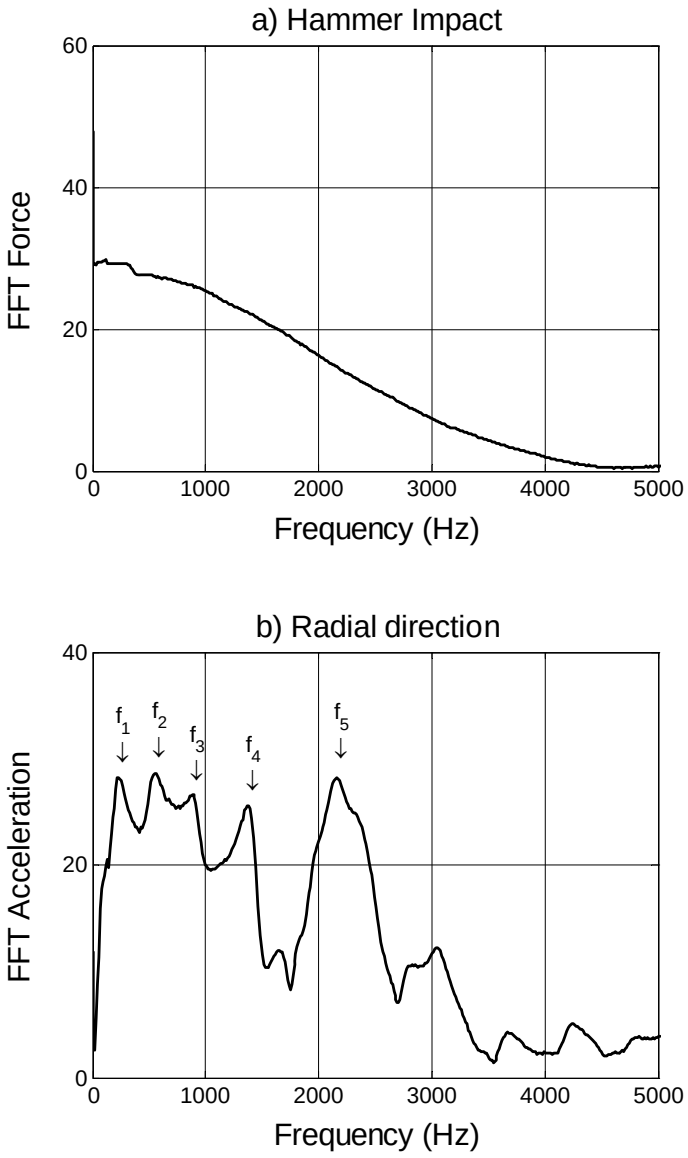

Figure B-41: prototype pile B308-2400, lateral impact results for 0-degree orientation, radial direction

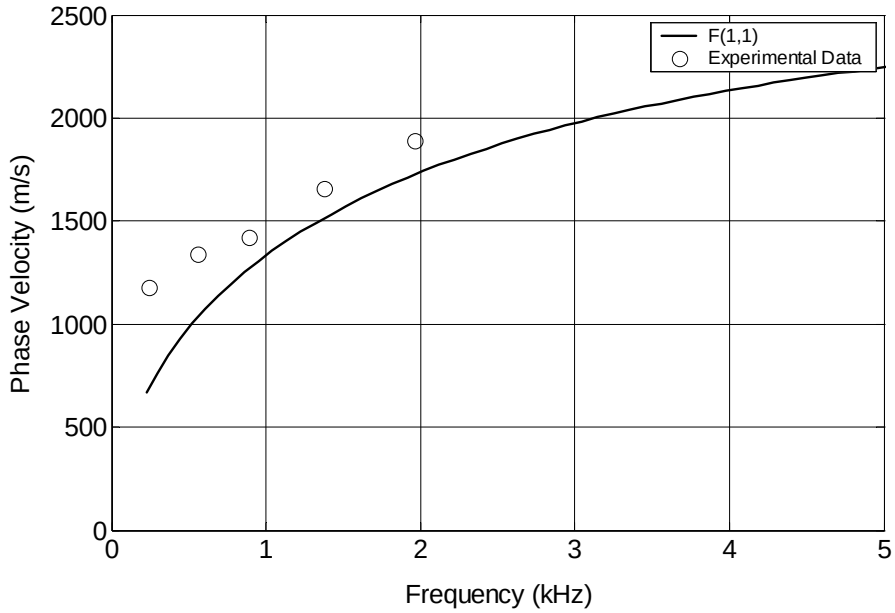

Figure B-42: Prototype Pile B308-2400, lateral impact results for 0-degree orientation, radial phase velocity - frequency data superimposed on numerically-determined F(1,1) branch

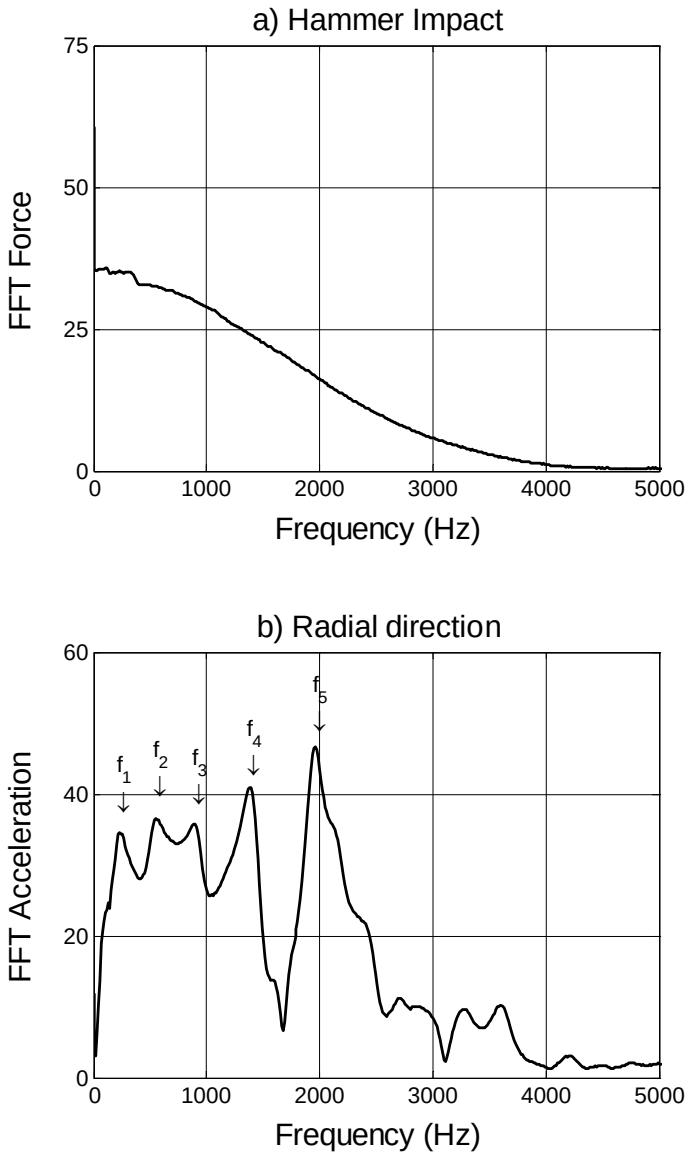

Figure B-43: prototype pile B308-2400, lateral impact results for 180-degree orientation, radial direction

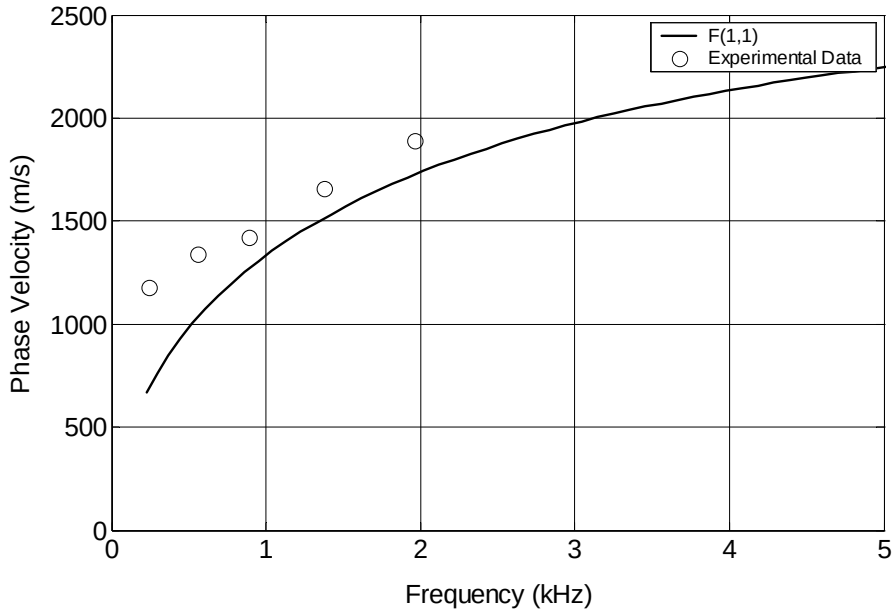

Figure B-44: Prototype Pile B308-2400, lateral impact results for 180-degree orientation, radial phase velocity - frequency data superimposed on numerically-

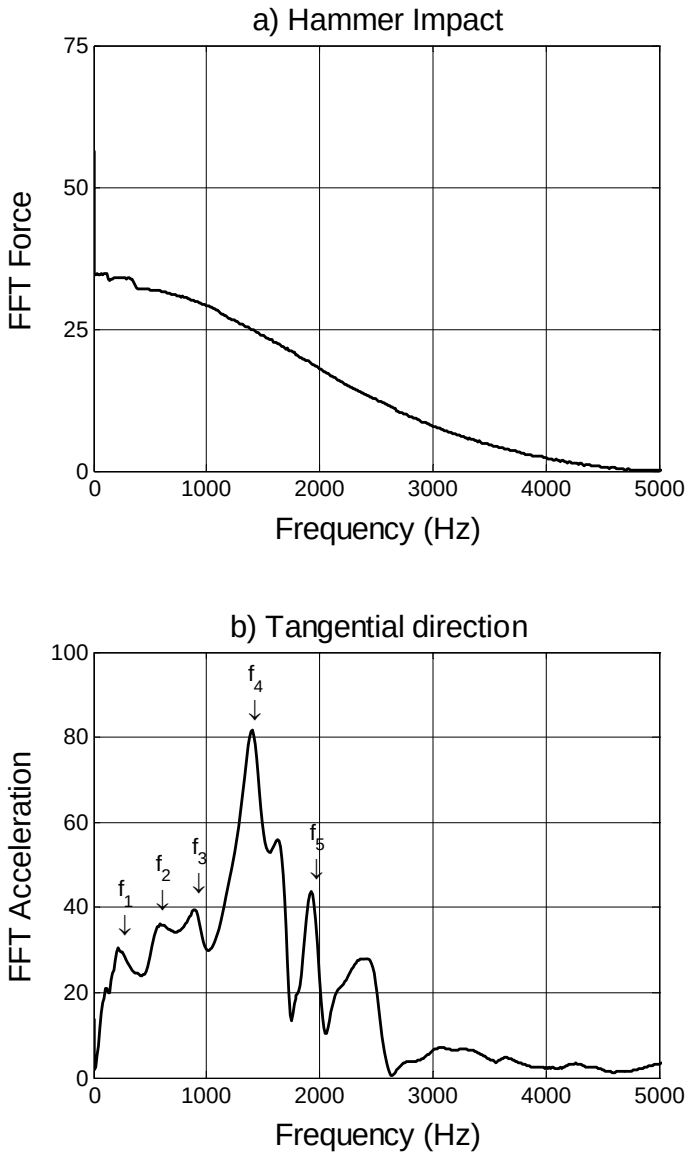

Figure B-45: prototype pile B308-2400, lateral impact results for 90-degree orientation, tangential direction

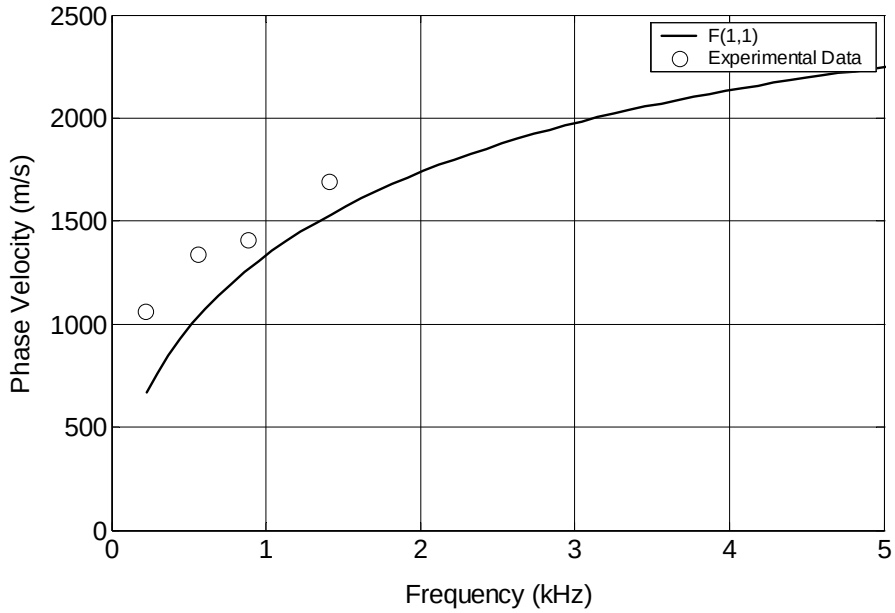

Figure B-46: Prototype Pile B308-2400, lateral impact results for 90-degree orientation, tangential phase velocity - frequency data superimposed on numerically-determined F(1,1) branch

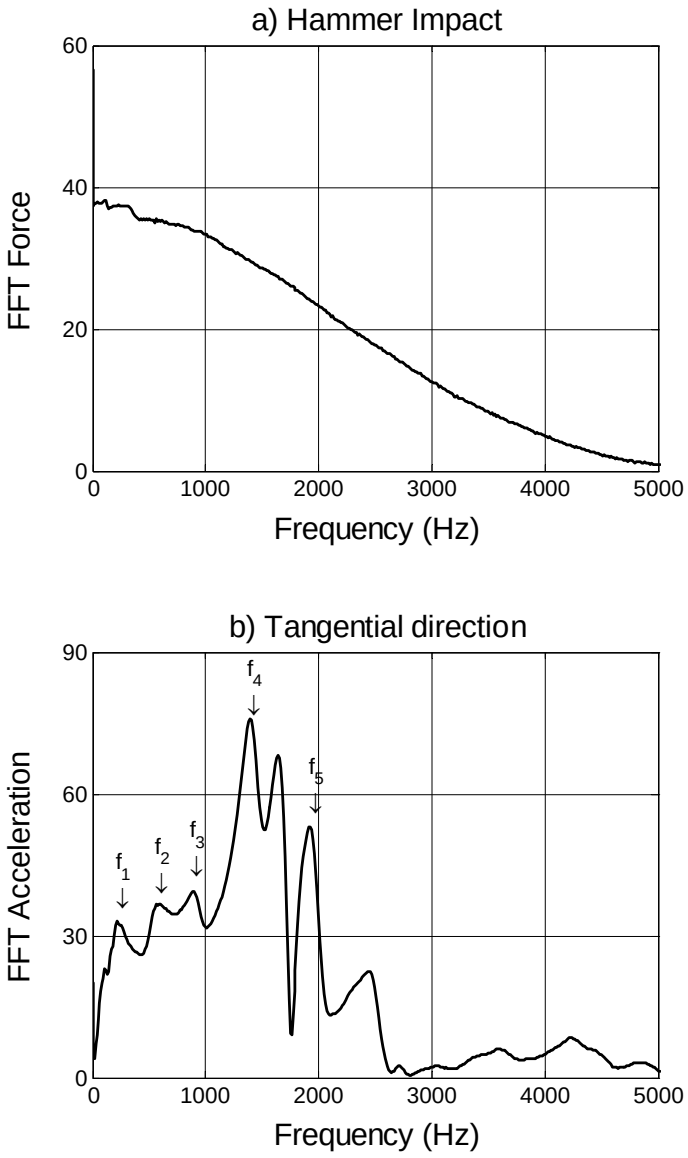

Figure B-47: prototype pile B308-2400, lateral impact results for 270-degree orientation, tangential direction

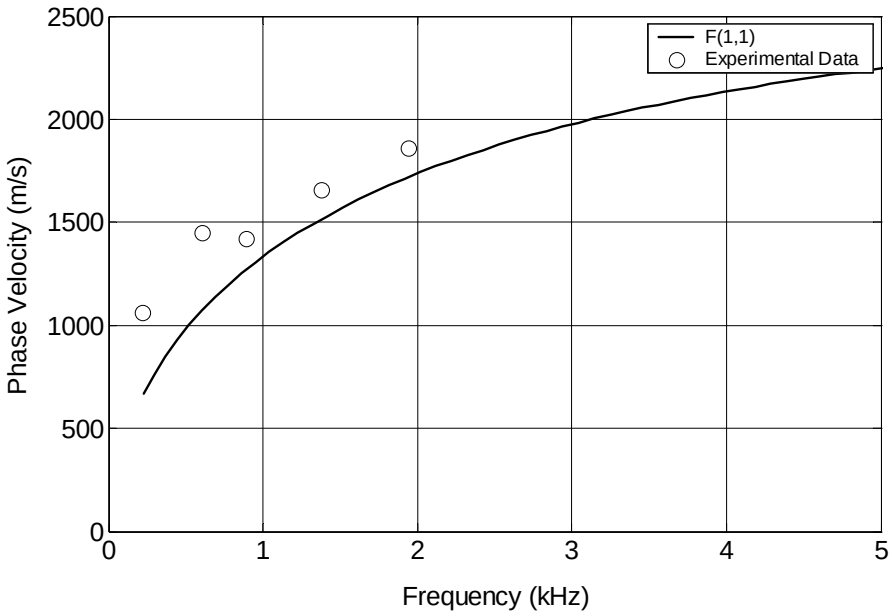

Figure B-48: Prototype Pile B308-2400, lateral impact results for 270-degree orientation, tangential phase velocity - frequency data superimposed on numerically-determined F(1,1) branch

Table B-4: Prototype pile B308-2400, frequencies and phase velocities determined from lateral impact tests

Longitudinal direction				Radial direction				Tangential direction			
0-degree face		180-degree face		0-degree face		180-degree face		90-degree face		270-degree face	
f (Hz)	c_p (m/s)	f (Hz)	c_p (m/s)	f (Hz)	c_p (m/s)	f (Hz)	c_p (m/s)	f (Hz)	c_p (m/s)	f (Hz)	c_p (m/s)
220	1060	220	1060	195	940	245	1180	220	1060	220	1060
525	1260	535	1280	550	1320	560	1340	560	1340	605	1450
940	1500	950	1520	940	1500	890	1420	880	1410	890	1420
1450	1740	1530	1840	1450	1740	1380	1660	1405	1690	1380	1660
2090	2010	2085	2000	1950	1870	1095	1050	N/I	N/I	1940	1860

Note: N/I indicates that the harmonic was not identified in the specified test and measurement direction.

Appendix C: Lateral Impact Results, Group Velocity – Frequency Calculations and Verification

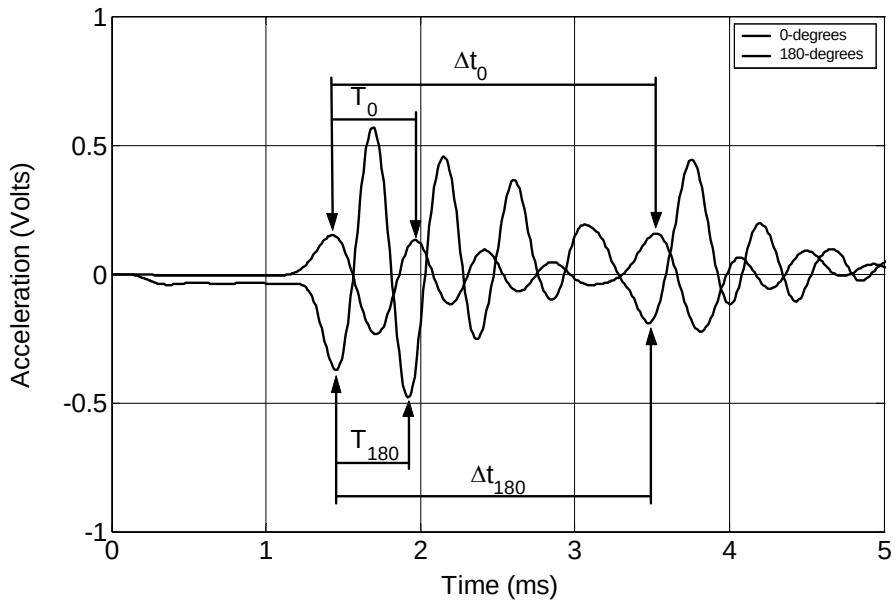

Figure C-1: Prototype pile C355-2430 (traction-free), filtered longitudinal acceleration – time histories for lateral impact results for impacts at 0-degree and 180-degree orientations

Table C-1: Prototype pile C355-2430 (traction-free), longitudinal results of lateral impact results for impacts at 0-degree and 180-degree orientations

Test orientation	Start of first peak (ms)	End of first peak (ms)	Start of return (ms)
0-degree	1.43	1.96	3.52
180-degree	1.47	1.92	3.48

Table C-2: Prototype pile C355-2430 (traction-free), group frequency and group velocity for longitudinal results of lateral impact results for impacts at 0-degree and 180-degree orientations

Test orientation	Duration of first peak (ms)	Frequency of first peak (Hz)	Travel time (ms)	Group velocity (m/s)
0-degree	0.43	2325	2.09	2170
180-degree	0.45	2130	2.01	2250

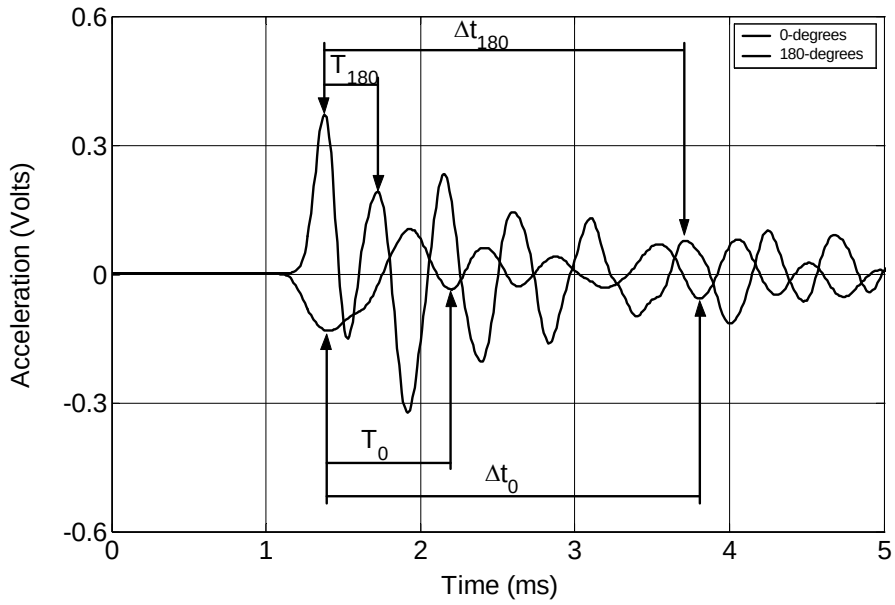

Figure C-2: Prototype pile C355-2430 (traction-free), filtered radial acceleration – time histories for lateral impact results for impacts at 0-degree and 180-degree orientations

Table C-3: Prototype pile C355-2430 (traction-free), radial results of lateral impact results for impacts at 0-degree and 180-degree orientations

Test orientation	Start of first peak (ms)	End of first peak (ms)	Start of return (ms)
0-degree	1.40	2.20	3.79
180-degree	1.38	1.72	3.71

Table C-4: Prototype pile C355-2430 (traction-free), group frequency and group velocity for radial results of lateral impact results for impacts at 0-degree and 180-degree orientations

Test orientation	Duration of first peak (ms)	Frequency of first peak (Hz)	Travel time (ms)	Group velocity (m/s)
0-degree	0.80	1250	2.39	1900
180-degree	0.34	2940	2.33	1940

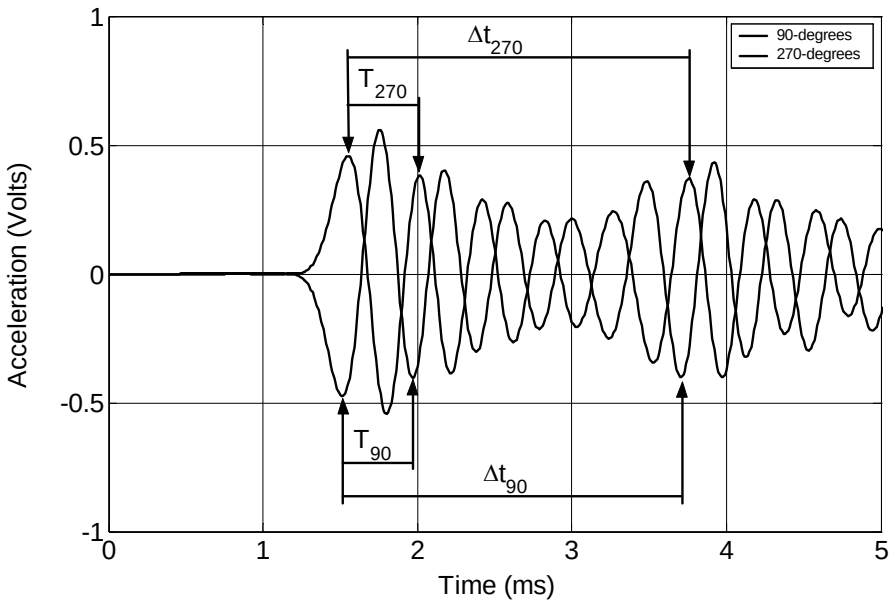

Figure C-3: Prototype pile C355-2430 (traction-free), filtered tangential acceleration – time histories for lateral impact results for impacts at 90-degree and 270-degree orientations

Table C-5: Prototype pile C355-2430 (traction-free), tangential results of lateral impact results for impacts at 90-degree and 270-degree orientations

Test orientation	Start of first peak (ms)	End of first peak (ms)	Start of return (ms)
0-degree	1.51	1.96	3.72
180-degree	1.55	2.03	3.76

Table C-6: Prototype pile C355-2430 (traction-free), group frequency and group velocity for tangential results of lateral impact results for impacts at 90-degree and 270-degree orientations

Test orientation	Duration of first peak (ms)	Frequency of first peak (Hz)	Travel time (ms)	Group velocity (m/s)
0-degree	0.45	2220	2.21	2050
180-degree	0.48	2080	2.21	2050

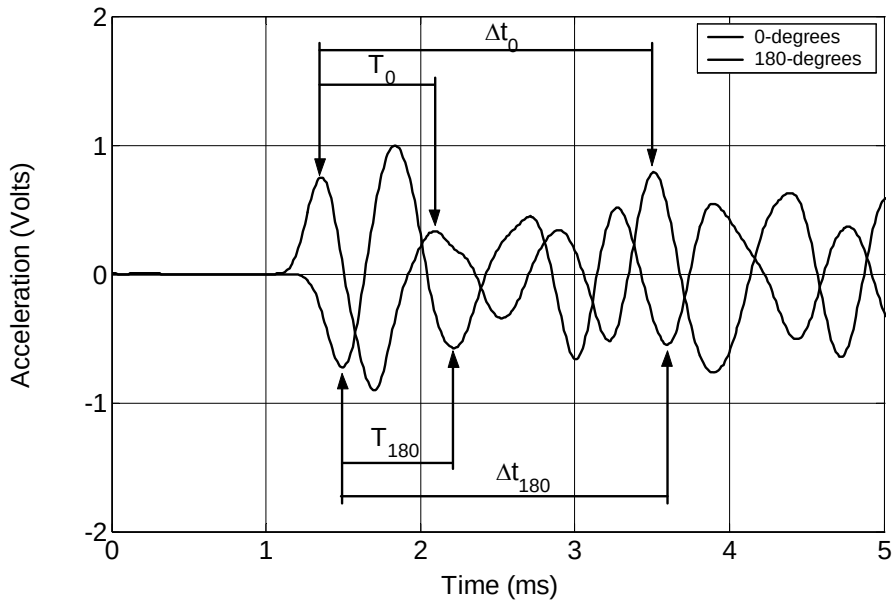

Figure C-4: Prototype pile C355-2430 (embedded), filtered longitudinal acceleration – time histories for lateral impact results for impacts at 0-degree and 180-degree orientations

Table C-7: Prototype pile C355-2430 (embedded), longitudinal results of lateral impact results for impacts at 0-degree and 180-degree orientations

Test orientation	Start of first peak (ms)	End of first peak (ms)	Start of return (ms)
0-degree	1.37	2.08	3.22
180-degree	1.49	2.22	3.27

Table C-8: Prototype pile C355-2430 (embedded), group frequency and group velocity for longitudinal results of lateral impact results for impacts at 0-degree and 180-degree orientations

Test orientation	Duration of first peak (ms)	Frequency of first peak (Hz)	Travel time (ms)	Group velocity (m/s)
0-degree	0.71	1410	1.85	2430
180-degree	0.73	1370	1.78	2520

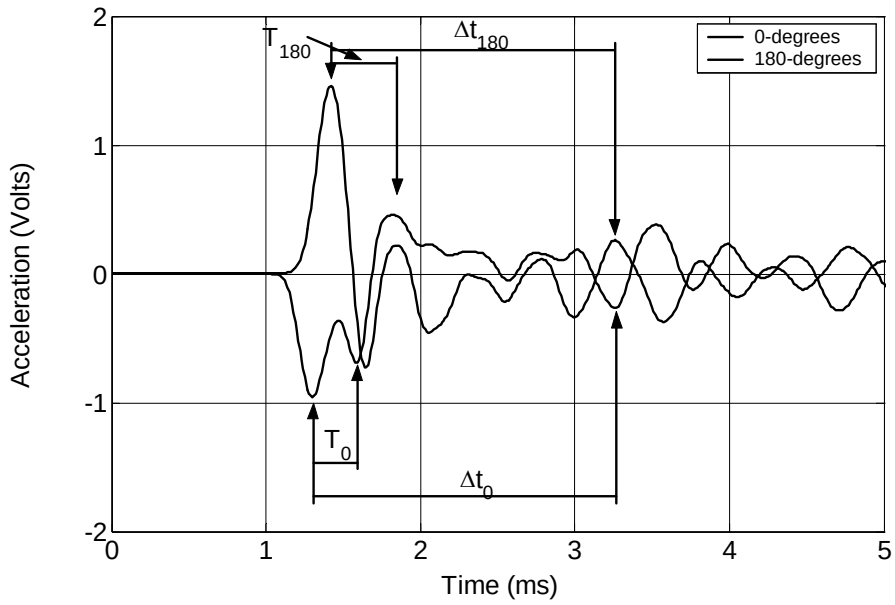

Figure C-5: Prototype pile C355-2430 (embedded), filtered radial acceleration – time histories for lateral impact results for impacts at 0-degree and 180-degree orientations

Table C-9: Prototype pile C355-2430 (embedded), radial results of lateral impact results for impacts at 0-degree and 180-degree orientations

Test orientation	Start of first peak (ms)	End of first peak (ms)	Start of return (ms)
0-degree	1.30	1.60	3.26
180-degree	1.41	1.84	3.26

Table C-10: Prototype pile C355-2430 (embedded), group frequency and group velocity for radial results of lateral impact results for impacts at 0-degree and 180-degree orientations

Test orientation	Duration of first peak (ms)	Frequency of first peak (Hz)	Travel time (ms)	Group velocity (m/s)
0-degree	0.30	3330	1.96	2290
180-degree	0.43	2330	1.85	2430

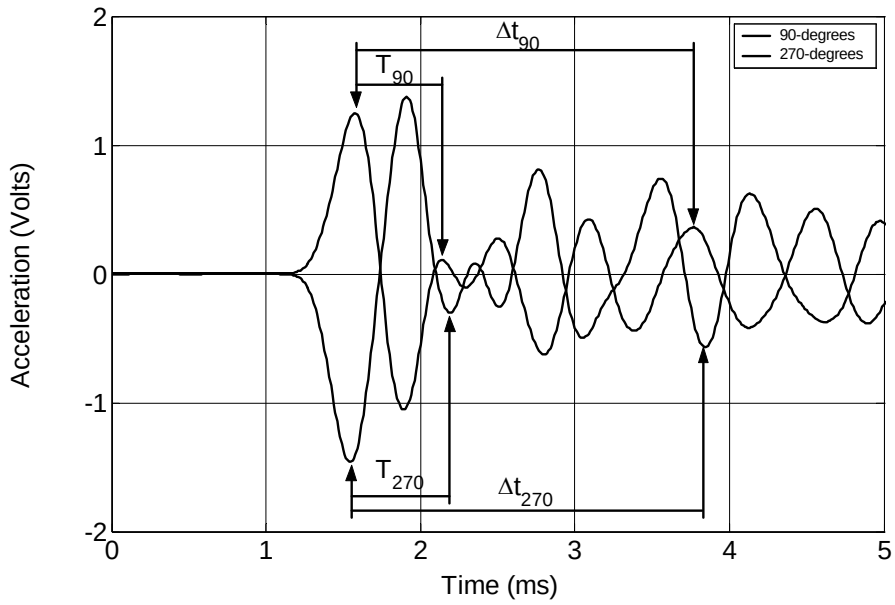

Figure C-6: Prototype pile C355-2430 (embedded), filtered tangential acceleration – time histories for lateral impact results for impacts at 90-degree and 270-degree orientations

Table C-11: Prototype pile C355-2430 (embedded), tangential results of lateral impact results for impacts at 90-degree and 270-degree orientations

Test orientation	Start of first peak (ms)	End of first peak (ms)	Start of return (ms)
0-degree	1.58	2.16	3.77
180-degree	1.55	2.19	3.84

Table C-12: Prototype pile C355-2430 (embedded), group frequency and group velocity for tangential results of lateral impact results for impacts at 90-degree and 270-degree orientations

Test orientation	Duration of first peak (ms)	Frequency of first peak (Hz)	Travel time (ms)	Group velocity (m/s)
0-degree	0.55	1820	2.19	2050
180-degree	0.64	1560	2.29	1960

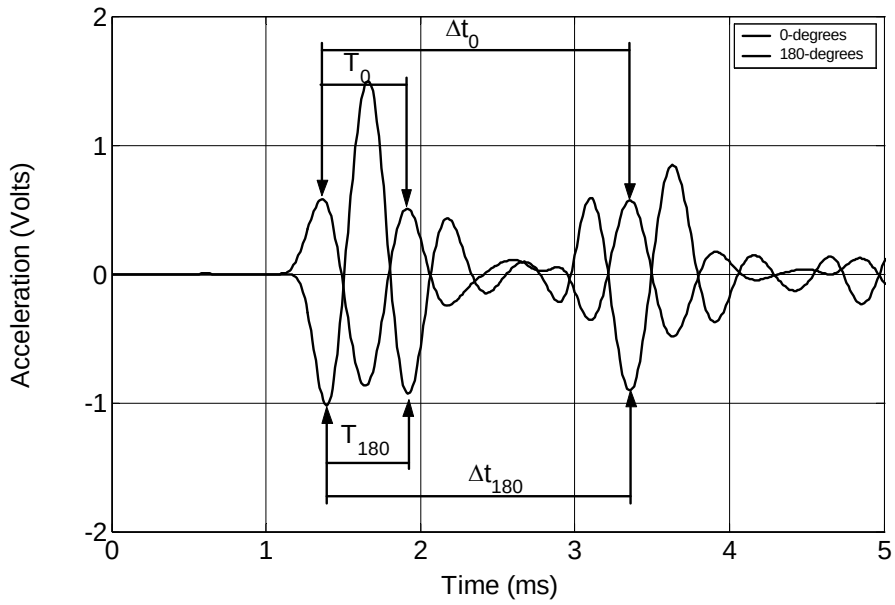

Figure C-7: Prototype pile B254-2220 (embedded), filtered longitudinal acceleration – time histories for lateral impact results for impacts at 0-degree and 180-degree orientations

Table C-13: Prototype pile B254-2220 (embedded), longitudinal results of lateral impact results for impacts at 0-degree and 180-degree orientations

Test orientation	Start of first peak (ms)	End of first peak (ms)	Start of return (ms)
0-degree	1.36	1.91	3.35
180-degree	1.39	1.92	3.36

Table C-14: Prototype pile B254-2220 (embedded), group frequency and group velocity for longitudinal results of lateral impact results for impacts at 0-degree and 180-degree orientations

Test orientation	Duration of first peak (ms)	Frequency of first peak (Hz)	Travel time (ms)	Group velocity (m/s)
0-degree	0.55	1820	1.99	1890
180-degree	0.53	1890	1.97	1910

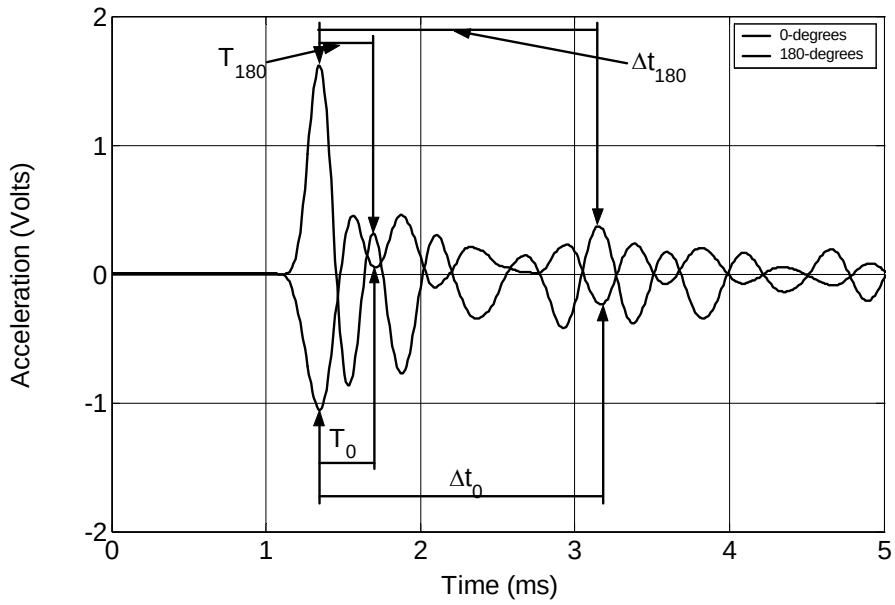

Figure C-8: Prototype pile B254-2220 (embedded), filtered radial acceleration – time histories for lateral impact results for impacts at 0-degree and 180-degree orientations

Table C-15: Prototype pile B254-2220 (embedded), radial results of lateral impact results for impacts at 0-degree and 180-degree orientations

Test orientation	Start of first peak (ms)	End of first peak (ms)	Start of return (ms)
0-degree	1.35	1.71	3.17
180-degree	1.35	1.70	3.16

Table C-16: Prototype pile B254-2220 (embedded), group frequency and group velocity for radial results of lateral impact results for impacts at 0-degree and 180-degree orientations

Test orientation	Duration of first peak (ms)	Frequency of first peak (Hz)	Travel time (ms)	Group velocity (m/s)
0-degree	0.36	2780	1.82	2060
180-degree	0.35	2860	1.81	2080

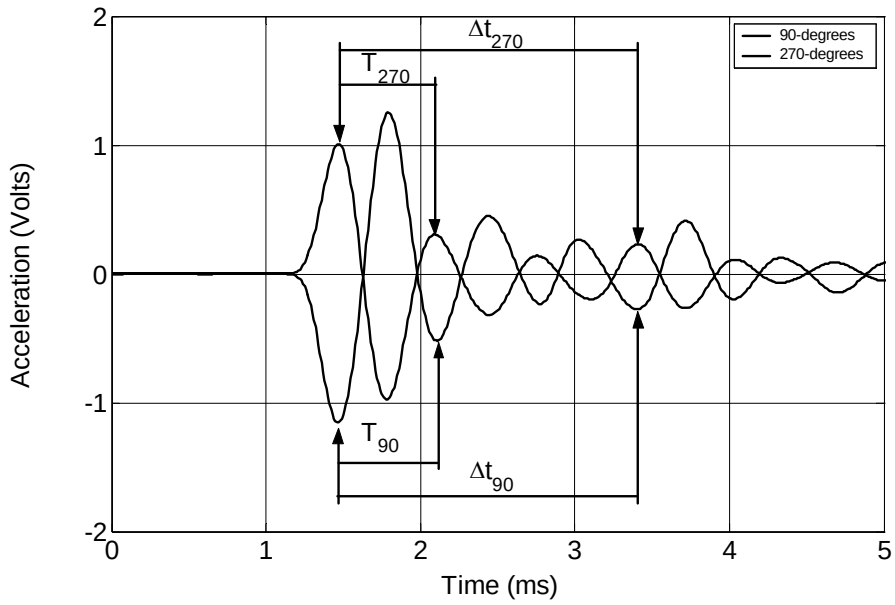

Figure C-9: Prototype pile B254-2220 (embedded), filtered tangential acceleration – time histories for lateral impact results for impacts at 90-degree and 270-degree orientations

Table C-17: Prototype pile B254-2220 (embedded), tangential results of lateral impact results for impacts at 90-degree and 270-degree orientations

Test orientation	Start of first peak (ms)	End of first peak (ms)	Start of return (ms)
0-degree	1.47	2.11	3.40
180-degree	1.47	2.09	3.43

Table C-18: Prototype pile B254-2220 (embedded), group frequency and group velocity for tangential results of lateral impact results for impacts at 90-degree and 270-degree orientations

Test orientation	Duration of first peak (ms)	Frequency of first peak (Hz)	Travel time (ms)	Group velocity (m/s)
0-degree	0.64	1560	1.93	1950
180-degree	0.62	1610	1.96	1920

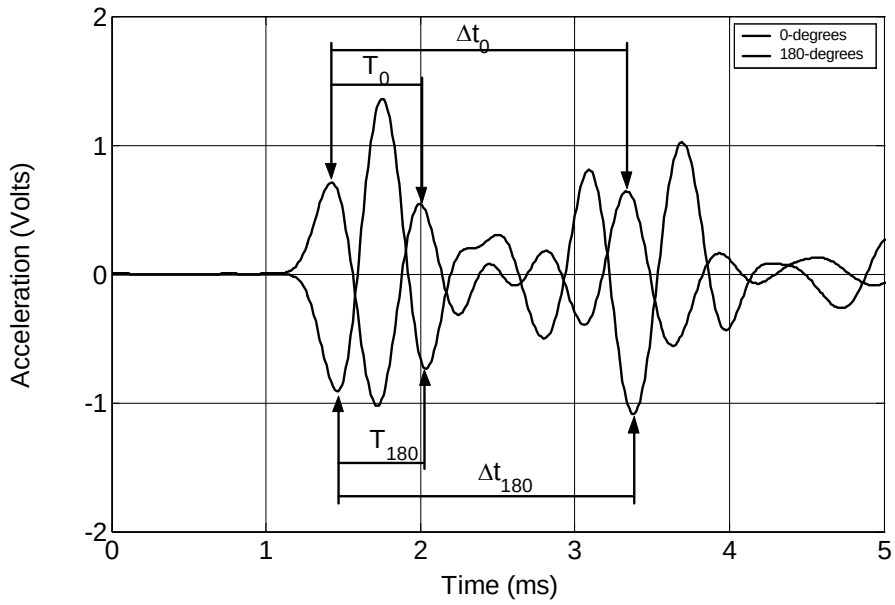

Figure C-10: Prototype pile B308-2400 (embedded), filtered longitudinal acceleration – time histories for lateral impact results for impacts at 0-degree and 180-degree orientations

Table C-19: Prototype pile B308-2400 (embedded), longitudinal results of lateral impact results for impacts at 0-degree and 180-degree orientations

Test orientation	Start of first peak (ms)	End of first peak (ms)	Start of return (ms)
0-degree	1.42	1.99	3.33
180-degree	1.46	2.04	3.38

Table C-20: Prototype pile B308-2400 (embedded), group frequency and group velocity for longitudinal results of lateral impact results for impacts at 0-degree and 180-degree orientations

Test orientation	Duration of first peak (ms)	Frequency of first peak (Hz)	Travel time (ms)	Group velocity (m/s)
0-degree	0.57	1750	1.91	2250
180-degree	0.58	1720	1.92	2240

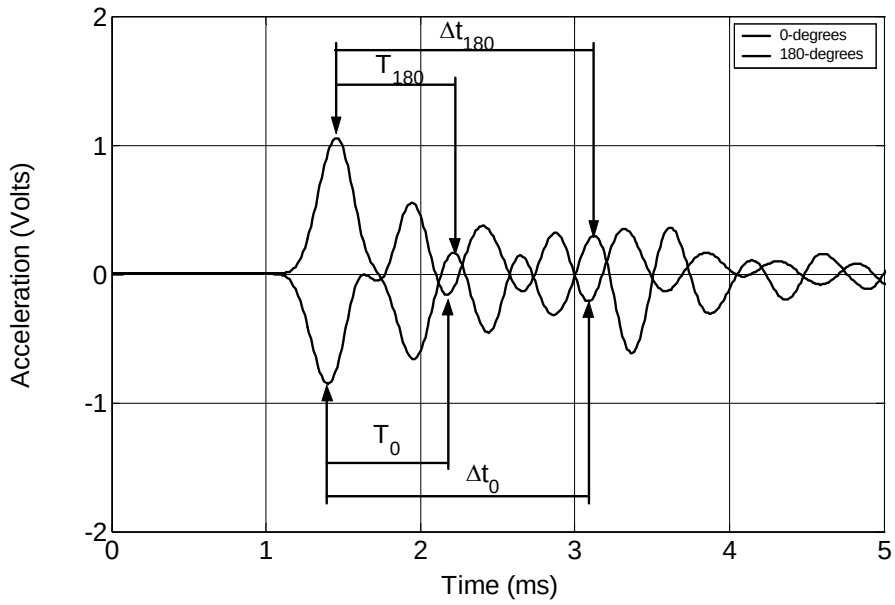

Figure C-11: Prototype pile B308-2400 (embedded), filtered radial acceleration – time histories for lateral impact results for impacts at 0-degree and 180-degree orientations

Table C-21: Prototype pile B308-2400 (embedded), radial results of lateral impact results for impacts at 0-degree and 180-degree orientations

Test orientation	Start of first peak (ms)	End of first peak (ms)	Start of return (ms)
0-degree	1.40	2.17	3.12
180-degree	1.47	2.21	3.09

Table C-22: Prototype pile B308-2400 (embedded), group frequency and group velocity for radial results of lateral impact results for impacts at 0-degree and 180-degree orientations

Test orientation	Duration of first peak (ms)	Frequency of first peak (Hz)	Travel time (ms)	Group velocity (m/s)
0-degree	0.77	1300	1.72	2500
180-degree	0.74	1350	1.62	2650

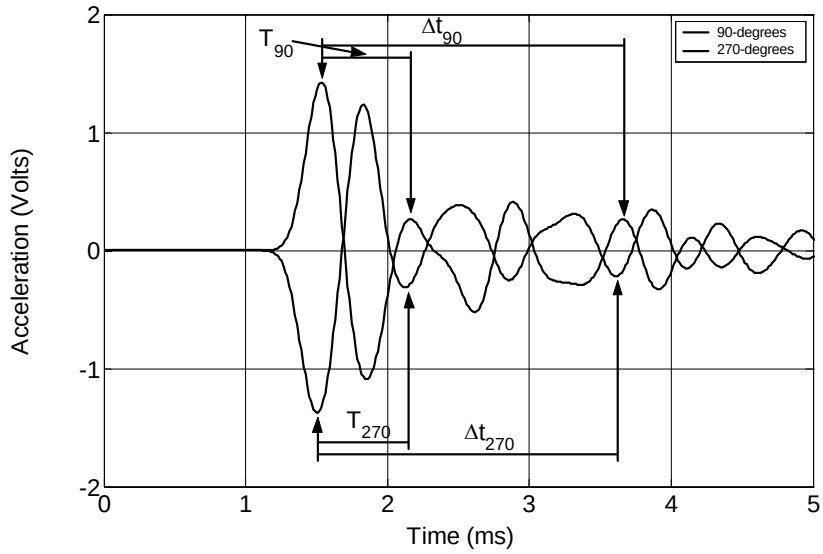

Figure C-12: Prototype pile B308-2400 (embedded), filtered tangential acceleration – time histories for lateral impact results for impacts at 90-degree and 270-degree orientations

Table C-23: Prototype pile B308-2400 (embedded), tangential results of lateral impact results for impacts at 90-degree and 270-degree orientations

Test orientation	Start of first peak (ms)	End of first peak (ms)	Start of return (ms)
0-degree	1.53	2.16	3.66
180-degree	1.50	2.14	3.61

Table C-24: Prototype pile B308-2400 (embedded), group frequency and group velocity for tangential results of lateral impact results for impacts at 90-degree and 270-degree orientations

Test orientation	Duration of first peak (ms)	Frequency of first peak (Hz)	Travel time (ms)	Group velocity (m/s)
0-degree	0.63	1590	2.13	2020
180-degree	0.64	1560	2.11	2040